The role of SPARK-I receptor-like kinases in the arbuscular mycorrhizal symbiosis

Héctor Albert Montero Sommerfeld

Department of Plant Sciences

University of Cambridge - St John's College

This thesis is submitted for the degree of Doctor of Philosophy

July 2020

Declaration

This thesis is the result of my own work and includes nothing which is the outcome of work done in collaboration except as declared in the Preface and specified in the text. It is not substantially the same as any that I have submitted, or, is being concurrently submitted for a degree or diploma or other qualification at the University of Cambridge or any other University or similar institution except as declared in the Preface and specified in the text. I further state that no substantial part of my thesis has already been submitted, or, is being concurrently submitted for any such degree, diploma or other qualification at the University of Cambridge or any other University or similar institution except as declared in the Preface and specified in the text. It does not exceed the prescribed word limit for the Faculty of Biology Degree Committee

The role of SPARK-I receptor-like kinases in the arbuscular mycorrhizal symbiosis

Hector Albert Montero Sommerfeld

Summary

The nutritional mutualism formed between land plants and arbuscular mycorrhizal (AM) fungi involves intracellular accommodation of the fungal symbiont and relies on concerted cellular reprograming. Maximal physical interaction is achieved during the emergence and development of the arbuscules, creating a hub for nutrient exchange and potentially for plant-fungal communication. Receptor-like kinases (RLKs) allow plant cells to sense and respond to their environment and are crucial for signalling during biotic interactions. A rice RLK, ARBUSCULAR RECEPTOR-LIKE KINASE 1 (OsARK1), had earlier been found to localize specifically to the symbiotic interface of arbusculated cells and its orthologues are present only among AM-competent plant species. In this dissertation, the symbiotic role of OsARK1 was studied using genetics, phylogenetics and cell biology approaches.

Mutation in *OsARK1* resulted in normal arbuscule development but reduced colonization levels that could be rescued in the presence of a wild-type AM fungal mycelium indicating OsARK1 regulates AM symbiosis after arbuscule formation by maintaining fungal fitness. Phylogenetic analyses of the *OsARK1* RLK subfamily showed *ARK* and *SIMILAR PROTEIN TO ARK 1* (*SPARK1*) as the two members present in non-vascular plants while the paralogues *ARK1* and *ARK2* arose early in the evolution of tracheophytes. The pattern of occurrence of the newly discovered SPARK domain in the extracellular region of members of this RLK subfamily, named SPARK-I, argues for *ARK1* and *ARK2* to have coevolved. A rice *ark2* mutant displayed a reduced colonization phenotype which was quantitatively different compared to *ark1*. Global transcriptional signatures of the mutants showed several putative components of common as well as distinctive signalling pathways being regulated by OsARK1 and OsARK2. A global downregulation of hydrolytic enzymes in the mutant backgrounds and alterations in lipid distribution in arbusculated cells suggest these RLKs to be part of an ancient signalling pathway directing post-arbuscule development processes to sustain AM symbiosis.

Acknowledgments

The work presented in this dissertation was carried out in the Department of Plant Sciences, University of Cambridge and I acknowledge all the people that keep this institution running as a friendly and collaborative environment. Vital in this project was Uta Paszkowski whose fine balance between pragmatism and open mindedness benefited to a great degree the achievements here presented. Scientific feedback was always flowing opportunely and her ability to run a lab in a positive and proactive way made the experience truly remarkable. Being part of the Cereal Symbiosis laboratory was fun and provided a constant wealth of advice and help from past and present members. Ronelle Roth was especially important for guidance in the early stages of the PhD by introducing me to the world of confocal microscopy and to ARK1. Several skilled undergraduate students under my supervision were of great help. Jen McGaley assisted in the characterization of the GFP-OsSCAMP *ark1* cross, Gabriel García helped in the molecular characterization of Golden Gate cloning lines and Gabriel Ferreras grew the rice experiment subsequently used for RNA-seq assays. I would also like to say thank you to the many collaborators that helped in different stages of this work. Peter Eastmond (Rothamsted Research) received me in his laboratory and showed me how to perform lipid assays. Tak Lee (Sainsbury Laboratory-Cambridge) helped during RNA-seq data analyses. Boas Pucker (Department of Plant Sciences, University of Cambridge) contributed in the early stages of the characterization of the SPARK domain by performing a pattern search across genome databases. Rob Finn (European Bioinformatics Institute) curated the SPARK domain and incorporated it into the Pfam database. Nathan Zaccai (Cambridge Institute for Medical Research) was very helpful advising on the cloning of the SPARK domain for future crystallography work. Rice transformation was performed by Emma Wallington and Sarah Bowden (NIAB-Cambridge). Akio Miyao (Institute of Crop Science, National Agriculture and Food Research Organization, Japan) provided seed from Tos17 insertional rice mutants and Amy Cartwright (DOE Joint Genome Institute, California) provided seed from the *ark1* T-DNA insertional *Brachypodium distachyon* mutant. I also acknowledge the Agencia

Nacional de Investigación y Desarrollo (ANID-Chile) and Cambridge Trust for financial support during my PhD.

Contents

Chapter 1

Introduction

1.1. The arbuscular mycorrhizal association

Many of the abundant microorganisms in the rhizosphere have evolved to live in association with plants forming root endosymbioses, where a microbial symbiont lives inside root tissues for part or the entirety of its life cycle. Among them, the association between plants and arbuscular mycorrhizal (AM) fungi from the subphylum Glomeromycotina is considered the most important root endosymbiosis attending to its ancient origin and widespread occurrence (Parniske, 2008). The AM symbiosis is a nutritional mutualism of global distribution and has been prevalent over millions of years of plant diversification (Brundrett and Tedersoo, 2018). A recent compilation of plant mycorrhizal status showed 85% of plant genera being able to host AM fungi in their roots or thalli (Soudzilovskaia et al., 2020). Fossils of early land plants exhibit fungal structures remarkably similar to those from extant AM fungi inside their tissues (Remy et al., 1994; Strullu-Derrien et al., 2014) and recent time-calibrated phylogenies place the origin of the AM symbiosis to circa 480 million years ago, close to the onset of embryophytes (Lutzoni et al., 2018). The first plants living above the primitive soil crust in the early Devonian had no roots and AM fungi resided in their aerial axes, perhaps exerting part of the function modern roots have by accessing soil nutrients (reviewed in Strullu-Derrien et al., 2018). This would be reminiscent to the AM-like mutualism occurring in extant liverworts whose rhizoids are used by AM fungi to access and profusely colonize the aerial thalli (Ligrone et al., 2007; Humphreys et al., 2010). According to the fossil record, around 100 million years elapsed until true mycorrhizas, with roots hosting AM fungi, appeared in the Carboniferous (Strullu-Derrien et al., 2009; Krings et al., 2011). Hence, crucial events in land plant evolution; the transition from

water to land and the development of roots are believed to have taken place aided by AM fungi (Brundrett, 2002; Martin et al., 2017; Rensing, 2018).

Some plant clades have lost AM competence during evolution, a process that had been facilitated as plants partnered with alternative symbionts or evolved environmental adaptations for resource acquisition (Werner et al., 2018). Other non-AM mycorrhizal associations include ectomycorrhizas, orchid mycorrhiza and ericoid mycorrhiza. These symbioses are established between some plant groups and fungi from the Basidiomycota and Ascomycota. While ectomycorrhizas are common in gymnosperms, orchid and ericoid mycorrhizas are restricted to the Orchidaceae and Ericaceae families respectively (Smith and Read, 2008). Only a few plant clades are not able to establish mycorrhizas (around 6% of plant genera, Soudzilovskaia et al., 2020). These usually correspond to plant groups exhibiting particular nutritional or environmental lifestyles, such as epiphytes, parasites or aquatic plants (Lambers and Teste, 2013). The model species *Arabidopsis thaliana* is also not able to form mycorrhizal associations (Veiga et al., 2013; Fernández et al., 2019), perhaps as a reflection of the Brassicaceae being adapted to live in disturbed habitats where low competition renders soil nutrient availability not limiting for plant performance (Lambers and Teste, 2013).

The trade of nutrients is the basis of the AM symbiosis. Plants supply AM fungi with carbon in the form of carbohydrates and lipids and in return receive soil nutrients accessible by AM fungi beyond the root depletion zone (reviewed in Roth and Paszkowski, 2017; Lanfranco et al., 2018). AM-mediated symbiotic nutrient acquisition, particularly inorganic phosphate (Pi), is highly efficient and consequently of major interest for agriculture (reviewed in Chiu and Paszkowski, 2019; Kobae, 2019). This becomes especially relevant taking into account that rock Pi deposits used for commercial fertilizers are being depleted, their access is subjected to geopolitical constrains and their use often results in water pollution (Gross, 2017). Besides nutrient acquisition, AM symbioses benefit plants by maintaining soil structure (Mardhiah et al., 2016), by inducing resistance to pathogens (Cameron et al., 2013) and by helping plants to cope with abiotic stresses such as drought, heat and salinity (Jayne et al., 2014; Begum et al., 2019). The AM association can also be employed to reduce soil nutrient loss (Cavagnaro et al., 2015) and for heavy metal bioremediation (Göhre and

Paszkowski, 2006). In ecosystem scales, AM symbioses have an influence on plant biodiversity and productivity (Van Der Heijden et al., 1998) and contribute to the sequestration of plant fixed carbon in the rhizosphere (Bago et al., 2000; Rillig et al., 2001). Its ubiquitous nature together with its benefits for plant performance places the understanding of the AM association central to modern sustainable practices in agroecology (Chen et al., 2018; Ferrol et al., 2019).

1.2. The successive stages of AM colonization

1.2.1. AM fungi in the rhizosphere

AM fungi are obligate symbionts that need to interact with plants for the completion of their life cycle. Normally, part of their biomass inhabits root tissues while AM fungal mycelia also populate the rhizosphere serving as a physiological extension of roots. Asexual AM fungal spores are generated in the rhizosphere and can be found detached or in connection with AM fungal hyphae. These serve as AM fungal propagules ensuring continuity of the association in plant communities over time. Nuclei can move along the coenocytic AM fungal hyphae and nuclei numbers per spore may reach the thousands (reviewed in Kokkoris et al., 2020). AM fungal hyphae in the rhizosphere can fuse (Giovannetti et al., 2015) forming a network and given that hyphae from a common mycelium can colonize multiple plants, the term common mycorrhizal network has been coined. These networks connect plants underground and play important ecological roles in natural ecosystems (Simard et al., 2012). For example, common mycorrhizal networks can mobilize phosphorus (P) from rich to poor patches in the soil (Whiteside et al., 2019), or facilitate mycoheterotrophy where highly specialized non-photosynthetic plants obtain their carbon from common mycorrhizal networks (Merckx, 2013).

1.2.2. AM fungal entry into host roots

As a first step in a typical AM fungal colonization process, a chemical dialog is established thanks to the release of root and spore exudates (Nadal and Paszkowski,

2013; Bonfante and Genre, 2015). Following spore germination, AM fungal hyphae will branch and elongate to eventually reach the surface of a plant root (Fig. 1). Upon contact with the root epidermis, the fungal hypha swells forming a hyphopodium. Contrary to the situation seen in interactions between plants and diverse fungal pathogens, from this point onwards the plant is physically assisting the fungus to invade. This is first manifested by the generation of a pre-penetration apparatus (PPA) by means of organelle reorganization in root epidermal cells (Genre et al., 2005). The PPA creates an intracellular route that will guide hyphae to the root cortex. Once there, AM fungal hyphae spreads longitudinally along the root length and form intracellular structures that hallmark the association, the arbuscules.

1.2.3. Arbuscule development

The formation of tree-shaped arbuscules is a widespread feature of the AM association, reflecting the functional importance of this structure. Arbuscules are formed by iterative branch dichotomy of terminal hyphae inside plant host cells. To facilitate this, loosening of the plant cell wall needs to occur, a process that plants must orchestrate as no plant cell wall degrading components have been detected among AM genomes (Morin et al., 2019). The course of arbuscule development continuously transits from an initial arbuscule trunk, first order coarse arbuscule branches, high order branching hallmarking arbuscule maturity and arbuscule degeneration (Gutjahr and Parniske, 2013). Arbuscule formation concurs with important cytological changes from the plant side. The host cell experiences compartmentalization and likely fractionation of the vacuole (Pumplin and Harrison, 2009), cytoskeleton rearrangements (Blancaflor et al., 2001; Genre et al., 2008), mitochondria and plastid proliferation (Lohse et al., 2005) and stimulation of increases in nuclear size and ploidy (Balestrini et al., 1992; Carotenuto et al., 2019).

During arbuscule formation, a distinctive symbiotic interface from plant origin continuous to the plasma membrane is formed to surround every single arbuscule branch. This membrane is called the periarbuscular membrane (PAM) and in cells hosting fully developed arbuscules its surface area surpasses by far that of the plasma membrane. The assembly of symbiotic interfaces surrounding AM fungal hyphae are

believed to be mediated by the cell plate formation machinery as a protein mediating cell plate anchoring, TPLATE, accumulates at sites around intracellular AM fungal structures (Russo et al., 2019). In addition, genetics and cell biological studies point towards the involvement of specialized exocytotic processes in PAM formation (reviewed in Harrison and Ivanov, 2017). The PAM has two domains, the trunk domain and the branch domain (Pumplin and Harrison, 2009). The branch domain of the PAM is a specialized membrane as it contains proteins not found in the plasma membrane. Transporters for Pi, the most well characterized, have been described to localize exclusively at the branch domain of the PAM in monocots and dicots (Harrison et al., 2002; Pumplin and Harrison, 2009; Kobae and Hata, 2010; Tamura et al., 2012). Ammonium transporters have also been described to have PAM localization (Kobae et al., 2010; Koegel et al., 2013; Breuillin-Sessoms et al., 2015). The existence of these nutrient transporters at the PAM supports the notion of the arbusculated cell being at the core of symbiotic nutrient exchange (Luginbuehl and Oldroyd, 2017).

Between the PAM and the fungal cell wall, the periarbuscular space (PAS) represents an apoplastic site of communication and nutrient exchange between the symbionts. Ultrastructural studies on this interface have revealed it to be immensely complex and rich in distinctive plant and fungal membrane compartments (Ivanov et al., 2019; Roth et al., 2019). Much less is known about the arbuscule membrane, which should have analogue nutrient transporters releasing nutrients to the PAS for the subsequent uptake by the PAM transporters mentioned above. For AM fungal Pi transporters, candidates have been identified based on comparative genomics and transport activity in heterologous systems but their putative functions in AM fungal efflux are yet to be addressed (Plassard et al., 2019).

1.2.4. Arbuscule collapse and the post-arbuscule development stage

Although arbuscule formation occurs constantly throughout plant ontogeny, arbuscules as units are ephemeral. Ultrastructural studies have showed that at the start of arbuscule degeneration, cellular contents and organelles are emptied from terminal branches followed by hyphal septation and collapse of AM fungal cell walls. Loss of arbuscular cytoplasmic and membrane integrity leads to a progressive reduction in

arbuscule size and organization (Bonfante-Fasolo, 1984). This is accompanied by the arising of lipid droplets in host cells (Kobae et al., 2014). Eventually, amorphous remnants of arbuscule bodies are gradually metabolized by unknown mechanisms and the host cell regains its pre-arbuscule development appearance.

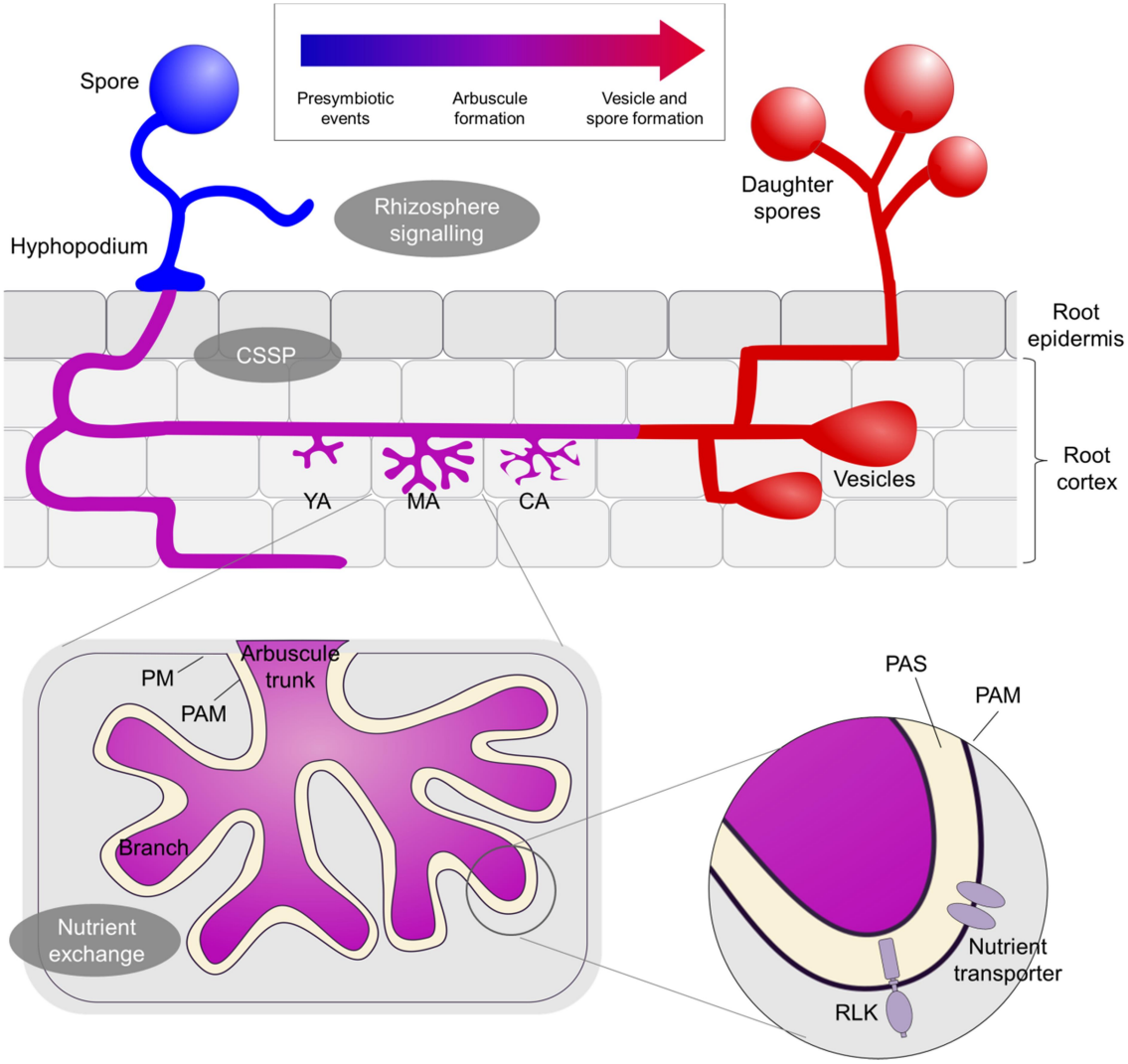

Figure 1. AM colonization in plant roots. Extraradical hyphae from germinated spores form a hyphopodium to enter roots, which is assisted by a common symbiosis signalling pathway (CSSP). Intraradical hyphae form arbuscules in cortical cells. Young arbuscules (YA) consist in a trunk and a few dichotomous branches. Mature arbuscules (MA) fill the host cell. A periarbuscular membrane (PAM) continuous to the plasma membrane (PM) surrounds the arbuscule. Nutrient transporters localize to the PAM. Genes coding for receptor-like kinases (RLKs) are induced in arbusculated cells and one RLK, OsARK1, is known to localize to the PAM. Collapsing arbuscules (CA) reduce in size and have amorphous shapes. Vesicles appear after arbuscules and hyphae eventually leave the root to form daughter spores.

Many AM fungal species produce globular fungal structures termed vesicles inside root tissues which are packed with lipids (Jabaji-Hare et al., 1984). The arising of fungal vesicles usually occurs after arbuscules and their presence hallmarks mature stages of the symbiosis. The subsequent proliferation of hyphae along the root length is accompanied by hyphal growth outside roots where daughter spores are formed. This marks the completion of the fungal life cycle and these daughter spores can germinate to initiate new colonization cycles in the same or neighbouring plants.

1.3. Signalling events sustaining AM symbiosis

To regulate the different symbiotic stages of the intimate association between plants and AM fungi, the two partners need to sense each other and elaborate appropriate cellular responses. In general, much of the knowledge gained on AM symbiosis signalling mechanisms derives from work on the plant partner as AM fungi are not amenable for stable genetic transformation and mutagenesis. Signalling in the AM symbiosis occur in the rhizosphere, prior to symbiosis establishment (the presymbiotic stage) and also in the intraradical stage of the association, where the development of symbiotic interfaces gives rise to maximized physical proximity between plants and AM fungi. Many of the molecular components needed for AM regulation have been lost in plant clades unable to form AM (Bravo et al., 2016; Radhakrishnan et al., 2020) highlighting their specialized function.

1.3.1. Presymbiotic signalling events

Entry and accommodation of AM fungi in plant tissues depends on appropriate signalling events first occurring using the rhizosphere as a communication route. The carotenoid-related plant hormone strigolactone (SL) plays a predominant role at this stage. SLs are released by roots through dedicated ABCG transporters (Kretzschmar et al., 2012; Banasiak et al., 2020) and stimulate spore germination and hyphal branching (Akiyama et al., 2005; Besserer et al., 2006; Yoneyama et al., 2007). SLs are labile compounds and their degradation upon release by roots may create a concentration gradient that serves as a positional cue for soil AM fungal hyphae to be guided towards

roots (Nadal and Paszkowski, 2013). AM colonization or high environmental Pi trigger a negative CLAVATA3/ESR-related (CLE) peptide-mediated feedback loop pathway that reduces SL production levels and modulates AM colonization (Müller et al., 2019; Karlo et al., 2020), highlighting the importance of SLs for AM fungal accommodation in roots. Besides SLs, other compounds from root exudates may play a role in rhizosphere communication. For example, AM hyphal tip elongation and hyphal branching of germinated AM fungal spores can be stimulated by root-released flavonoids and 2-hydroxy fatty acids respectively (Bécard et al., 1992; Nagahashi and Douds, 2011). In response to SL treatment, several predicted small secreted peptide-coding genes are transcriptionally induced in germinated spores of the model AM fungus *Rhizophagus irregularis* (Tsuzuki et al., 2016). One of those, *SL-INDUCED PUTATIVE SECRETED PROTEIN 1* (*SIS1*), appears to have a symbiotic role as suggested by the colonization depression phenotype when knocking-down the gene through host-induced gene silencing (HIGS) (Tsuzuki et al., 2016).

Plant roots are also able to respond to spore exudates by for example triggering nitric oxide bursts (Martínez-Medina et al., 2019). In addition, plants activate a signalling pathway enabling fungal accommodation by perceiving as-yet-unknown butenolide compounds by a receptor complex likely sharing the same evolutionary origin than that dedicated for the perception of SLs (Gutjahr et al., 2015a; Choi et al., 2020). This complex is formed by the α/β-hydrolase DWARF14 LIKE (D14L) and the F-box domain-containing protein DWARF3 (D3), which are essential for AM fungal accommodation in roots (Gutjahr et al., 2015a). Activation of D14L causes the removal of SUPPRESSOR OF MAX2 1 (SMAX1) resulting in downstream symbiotic signalling activation (Choi et al., 2020).

1.3.2. Myc factor perception by plant RLKs

The polysaccharide chitin is a major constituent of fungal cell walls and is formed by *N*-acetylglucosamine monomers. A plant *N*-acetylglucosamine transporter, NO PERCEPTION 1 (NOPE1) is required for AM fungal entry in roots (Nadal et al., 2017) and an AM fungal homologue is transcriptionally induced in the intraradical mycelium of

R. irregularis (Kobae et al., 2015) suggesting chitin derivatives being important for symbiotic communication and functioning.

A class of diffusible chitinaceous AM fungal molecules termed Myc factors stimulate AM formation. These consist in lipo-chitooligosaccharides (LCOs) and COs, the later devoid of an *N*-acyl moiety (Kosuta et al., 2003; Maillet et al., 2011). As chitin and its derivatives are also present in pathogenic fungi, the means by which plants can distinguish and respond to beneficial or detrimental fungal groups has been a long-standing question. Recognition of long chain COs, particularly *N*-acetyl chitooctaose (CO8), has been regarded as a primary activator of immunity signalling while short chain COs have been associated with symbiosis (Cao et al., 2017). However, recent work has demonstrated that recognition of both short and long chain COs can induce symbiosis signalling and that the combination of LCOs and COs conditions enhancement of symbiosis signalling and dampening of immunity (Feng et al., 2019). Activation of LCO and CO-mediated symbiotic signalling outcomes is also thought to be determined by specific interaction dynamics of their receptors (Zipfel and Oldroyd, 2017).

LCO and CO perception is mediated by complexes of members of the lysin motif (LysM) receptor-like kinase (RLK) subfamily, many of which are transcriptionally induced during AM colonization (reviewed in Buendia et al., 2018). These RLKs have three LysM domains stabilized by disulphide bonds in their extracellular region with affinity for *N*-acetylglucosamine (Liu et al., 2016). LCO and CO perception is mediated by the LysM RLKs NOD FACTOR RECEPTOR 5 (NFR5) and CHITIN ELICITOR RECEPTOR KINASE 1 (CERK1) (Carotenuto et al., 2017; He et al., 2019). NFR5 harbours a dysfunctional kinase domain and mutants in *Parasponia andersonii*, solanaceous species and rice *NFR5* orthologues display reduced AM fungal penetration sites which in some cases hinders arbuscule formation (Op den Camp et al., 2011; Buendia et al., 2016; Girardin et al., 2019; He et al., 2019). Unlike NFR5, CERK1 in addition participates in the perception of compounds that do not contain *N*-acetylglucosamine such as glucans (Desaki et al., 2018) and lipopolysaccharides (Mélida et al., 2018) and its involvement in both symbiosis and immunity signalling suggest it to be a more multifaceted co-receptor. The reduced or delayed colonization phenotype of mutants of CERK1 orthologues in several plant species (reviewed in Chiu and Paszkowski, 2020) suggest it to mediate

early stages of AM fungal penetration akin to NFR5. An *nfr5 cerk1* double mutant in *Medicago truncatula* displayed less colonization levels than the *cerk1* single mutant (He et al., 2019). These additive effects may be a reflection of an NFR5 and CERK1 concerted function that is, however, not essential for AM symbiosis as colonization still occurs. However, the LysM RLKs subfamily has been importantly expanded in land plants and particularly in legumes (Buendia et al., 2018). Therefore, other uncharacterized members of the subfamily may potentially assist in Myc factor perception.

1.3.3. The common symbiosis signalling pathway (CSSP)

Following Myc factor perception, signal transduction events take place in root tissues in the form of calcium oscillations (Gough and Cullimore, 2011; Sun et al., 2015). Both the AM symbiosis and the root nodule symbiosis share part of the molecular repertoire decoding these calcium oscillations into cellular responses. The root nodule symbiosis co-opted this pathway from the evolutionary more ancient AM symbiosis and it has been accordingly termed common symbiosis signalling pathway (CSSP) (Kistner et al., 2005). The components of this pathway are mentioned below using the gene/protein nomenclature of the rice orthologues. At the top of this pathway, a malectin domain leucine-rich repeat (LRR) RLK, SYMBIOSIS RECEPTOR KINASE (SYMRK), is essential for AM symbiosis development (Stracke et al., 2002). It is not known what SYMRK perceives. Work in the root nodule symbiosis in legumes suggests SYMRK to associate to LysM receptors, maybe to perceive as-yet-unknown compounds of microbial origin (Antolín-Llovera et al., 2014; Ried et al., 2014). Other CSSP components downstream of SYMRK initially identified in legumes are also essential for AM symbiosis. These include the nuclear Ca^{2+} channels CASTOR and POLLUX (Ané et al., 2004; Imaizumi-Anraku et al., 2005; Kim et al., 2019), the nuclear pore complex proteins NUCLEOPORIN85 (NUP85) (Saito et al., 2007), NUP133 (Kanamori et al., 2006) and NENA (Groth et al., 2010) and a CALCIUM AND CALMODULIN-DEPENDENT PROTEIN KINASE (CCaMK, Lévy et al., 2004). These CSSP components mediate nuclear and perinuclear calcium oscillations and decode calcium responses into transcriptional activation outputs. This is achieved as CCaMK activates the coiled-coil domain-containing transcription factor CYCLOPS through phosphorylation (Yano et al., 2008; Singh et al.,

2014). Mutants of most of these CSSP genes are impaired in fungal penetration into epidermal cells which has also been confirmed to occur in rice orthologues (Gutjahr et al., 2008). The most downstream component of the pathway, CYCLOPS, is an exception. Mutation in *CYCLOPS* allows AM penetration and hyphal spread inside roots but either without arbuscule formation or displaying quantitative defects in AM colonization depending on the plant species (Gutjahr et al., 2008; Yano et al., 2008; Horváth et al., 2011; Jin et al., 2018; Lindsay et al., 2019).

1.3.4. Regulation of intraradical stages of the AM symbiosis is directed by GRAS proteins

CYCLOPS activates the transcription factors REQUIRED FOR ARBUSCULAR MYCORRHIZA 1 (RAM1) with the aid of the gibberellic acid (GA) regulator DELLA (Pimprikar et al., 2016). These transcriptional regulators function after AM entry in roots has occurred and are part of a set of several GRAS proteins regulating AM symbiosis (reviewed in Pimprikar and Gutjahr, 2018). These also include NODULATION SIGNALLING PATHWAY 1 (NSP1), NSP2, DELLA INTERACTING PROTEIN 1 (DIP1), REQUIRED FOR ARBUSCULE DEVELOPMENT (RAD1) and MYCORRHIZA INDUCED GRAS 1 (MIG1). Mutants of *DIP1*, *NSP1* and *NSP2* have quantitative defects in AM colonization (Maillet et al., 2011; Delaux et al., 2013; Takeda et al., 2013; Yu et al., 2014) and NSP1 and NSP2 have been linked to SL biosynthesis (Liu et al., 2011). Based on the arbuscule morphology defects of the respective mutants, a role in arbuscule development has been demonstrated for RAM1, RAD1 and MIG1 (Park et al., 2015; Rich et al., 2015; Xue et al., 2015; Heck et al., 2016; Pimprikar et al., 2016).

There are several other molecular components of the AM association that when mutated display quantitative or qualitative alterations in AM colonization. Included are those involved in quantitative dynamics *MILDEW LOCUS O 1* (*MLO1*, Jacott et al., 2020), *LOST MERISTEMS 1* (*LOM1*, Couzigou et al., 2017) and the putative MEDIATOR complex subunit *LACK OF SYMBIONT ACCOMMODATION* (*LAN*, Suzaki et al., 2019). On the other hand, a Major Sperm Protein (MSP) domain-ankyrin repeat protein, VAPYRIN, is involved in intracellular development of AM fungal hyphae (Feddermann et al., 2010;

Pumplin et al., 2010; Murray et al., 2011). The knowledge on the mechanisms and molecular processes regulated by the different protein products is limited.

1.3.5. Regulation of nutrient exchange in arbusculated cells

The formation of arbuscules involves substantial changes in cellular homeostasis and reprograming which is supported by the important volume of genes transcriptionally altered in arbusculated cells (Hogekamp and Küster, 2013). Many of these encode nutrient transporters, some of which operate exclusively at the PAM. PAM acquisition of AM fungal-derived Pi occurs through transporters from the PHOSPHATE TRANSPORTER 1 (PHT1) family. Orthologues of the rice PHOSPHATE TRANSPORTER 11 (OsPT11) are responsible for Pi uptake at the PAM and their mutants display aberrant arbuscule development (Javot et al., 2007; Yang et al., 2012; Xie et al., 2013). In rice, another Pi transporter, OsPT13, regulates Pi homeostasis in arbusculated cells and its mutant phenotype is similar to *pt11* in terms of arbuscule development arrest (Yang et al., 2012). These phenotypes indicate that arbuscule development is linked to symbiotic Pi acquisition, and also that Pi acquisition occurs as arbuscules develop and not only in arbusculated cells hosting fully formed arbuscules. Aberrant arbuscule development is also seen when genetically disrupting proton gradients energizing transport of Pi at the PAM (Krajinski et al., 2014; Wang et al., 2014; Liu et al., 2020). Work in *M. truncatula* has shown that in low nitrogen conditions, arbuscule development is not arrested in Pi transporter mutants, a process that depends on PAM ammonium transporters (Javot et al., 2011; Breuillin-Sessoms et al., 2015). Thus, it appears that the arrest in arbuscule development is in great part executed by the plant as they sense Pi not been acquired and that scarcity of additional nutrients (in this case nitrogen) prompts the plant to maintain arbuscule development to boost their acquisition. However, genetically disrupting the symbiotic acquisition of nutrients other than Pi, such as ammonium, nitrate or potassium, results in depressed AM symbiosis without alterations in arbuscule development (Breuillin-Sessoms et al., 2015; Liu et al., 2019; Wang et al., 2020a). This suggests nutrient acquisition dynamics in arbusculated cells are dominated by Pi but more studies are needed focusing on the symbiotic acquisition of other nutrients. It is not known how nutrients acquired in arbusculated cells are

sensed. It has been hypothesised that dedicated symbiotic sensors exist (Wang et al., 2017) and also that the symbiotic transporters may in addition function as receptors (Yang and Paszkowski, 2011).

In return for inorganic nutrients, plants deliver photosynthates to the AM fungal symbiont in the form of sugars and lipids. The SWEET (Sugar Will Eventually be Exported Transporter) family of transporters are the main plant efflux transporters of hexoses and sucrose while other sucrose transporter (SUT) or monosaccharide transporter (MST) families are mainly involved in sugar influx (reviewed in Chen et al., 2015; Eom et al., 2015). A *M. truncatula* glucose transporter specifically localizing at the trunk and branch domains of the PAM, MtSWEET1b, is involved in arbuscule development as overexpression of dominant negative *MtSWEET1b* alleles led to more frequency of degenerating arbuscules (An et al., 2019). Also, early senescent arbuscules were observed when knocking-down a highly arbusculated cell-induced cytoplasmic sucrose synthase that converts sucrose to glucose, MtSucS1 (Baier et al., 2010). AM fungal uptake of monosaccharides from the PAS is likely mediated by a *R. irregularis* monosaccharide transporter, RiMST2, which is highly expressed in arbuscules. Downregulation of *RiMST2* by HIGS also resulted in malformed arbuscules (Helber et al., 2011).

Although AM fungi are primarily oleaginous microorganisms, they are fatty acid auxotrophs with no capability for *de novo* fatty acid synthesis (Wewer et al., 2014). Plants transfer fatty acids directly to the AM fungus (Jiang et al., 2017; Keymer et al., 2017; Luginbuehl et al., 2017) and a recently described pathway has been proposed for lipid nourishment to the AM fungus. This pathway includes several fatty acid biosynthesis enzymes that operate specifically in arbusculated cells including FatM, REQUIRED FOR ARBUSCULAR MYCORRHIZA 2 (RAM2) and DISORGANIZED ARBUSCULES (DIS). The fatty acid products of these enzymes have been hypothesised to be transferred to the PAS by the PAM-localized half-size ABC transporters STUNTED ARBUSCULE (STR) and STR2 (Bravo et al., 2017; Jiang et al., 2017; Keymer et al., 2017; Luginbuehl et al., 2017; Brands et al., 2018; Jiang et al., 2018). This lipid biosynthesis-transport pathway is regulated by RAM1 and some members of the WRINKLED (WRI) family of transcription factors (Gobbato et al., 2012; Park et al., 2015; Luginbuehl et al., 2017; Jiang et al., 2018; Xue et al., 2018). This pathway is also required for arbuscule

development as mutation of its components results in alterations in arbuscule morphology. Therefore, both plant acquisition of AM-derived soil nutrients and AM fungal acquisition of plant-derived carbon appear to be involved in arbuscule development.

As arbuscules mature and collapse, nutrient exchange and the associated consequent physiological changes in the two partners takes place. In *M. truncatula*, arbuscule collapse is executed by a repertoire of plant hydrolytic enzymes which are under the transcriptional regulation of a MYB-like transcription factor, MtMYB1, which may in turn be regulated by the GRAS proteins MtDELLA and MtNSP1 (Floss et al., 2017). The subsequent appearance of lipid-packed AM fungal vesicles inside root tissues marks mature stages of the symbiosis although is currently unknown which molecular events trigger their formation or the metabolic processing of the lipids stored.

1.3.6. An AM symbiosis-dedicated RLK specifically localizing at the PAM

To coordinate the important changes arbusculated cells experience during the ephemeral stages of arbuscule development, precise signalling events must take place. In arbusculated cells, the PAM is a symbiotic interface directly facing the symbiotic AM fungus and therefore an ideal place for perception of AM fungal-derived signals. Very little is known about RLKs operating in arbusculated cells. Some members of the LysM RLK subfamily are transcriptionally induced in arbusculated cells such as the rice *OsLYK1* (Roth et al., 2018) and the *NFR5* orthologues in solanaceous species (Girardin et al., 2019). Although several nutrient transporters have been characterized to specifically localize to the PAM (see section 1.3.5), no RLK had been described to function at the PAM.

From transcriptional work focusing on laser capture micro dissected arbusculated cells in conjunction with proteomics, one RLK from rice, ARBUSCULAR RECEPTOR-LIKE KINASE 1 (ARK1), was found to be a prevalent component of arbusculated cells (Roth et al., 2018). OsARK1 specifically localized to the PAM surrounding mature to collapsing arbuscules (Roth et al., 2018) and its orthologues are only present in plant species that engage in AM symbiosis (Bravo et al., 2016). These observations suggest ARK1 to be an

evolutionary conserved signalling component regulating AM symbiosis in arbusculated cells.

1.4. Research objectives

The work presented in this dissertation aims to better understand the role of the RLK ARK1 in AM symbiosis using rice as the main model system. General research objectives can be individualized as follows:

-To evaluate the stage of AM symbiosis development where *OsARK1* operates through detailed phenotypic assessment of the phenotype of *ark1* mutants, by documenting the differences in symbiotic structures in the mutants grown in monoculture and in nurse plant systems and by analysing arbuscule development in *ark1* mutants using chitin staining and subcellular marker lines (Chapter 3).

-To conduct a phylogenetic survey in order to understand *ARK1* relationship with its close homologues and the features of the currently unknown RLK subfamily *ARK1* belongs to (Chapter 4).

-To assess a possible symbiotic role of *OsARK1* closest homologue *OsARK2*, by phenotypically characterizing single and double mutant alleles in terms of their AM colonization dynamics, lipid profiling and lipid distribution in arbusculated cells (Chapter 5).

-To conduct a transcriptional survey of mutants of *OsARK1*, *OsARK2* and the double mutant to identify genes under the potential transcriptional regulation of the two RLKs and to determine commonalities and differences in their functions (Chapter 6).

Chapter 2

Materials and methods

2.1. Plant-AM fungal material and growth conditions

2.1.1. Plant genotypes

All rice experiments were conducted using *Oryza sativa* subsp. japonica cv. Nipponbare as a background genotype. Segregating seed from two Tos17 (Transposon of *Oryza sativa* 17) insertional mutant alleles for *OsARK1*, NF1782 (*ark1-1*) and NF4582 (*ark1-2*) and one for *OsARK2*, NG0028 (*ark2*) were obtained from the National Institute of Agrobiological Sciences (NIAS, Japan). These alleles are part of a large collection of rice insertional mutants generated using the Tos17 property of transposable induction in tissue culture (Miyao et al., 2003). The 4,114 base pair (bp) long Tos17 element resides naturally as two genomic copies in chromosomes 7 and 10 (Hirochika et al., 1996). In this study, the *ark1 ark2* double knockout (DKO) was generated by crossing the *ark1-2* and *ark2* alleles used as female and male respectively.

The rice line pSCAMP:GFP-SCAMP was generated in a previous study (Kobae and Fujiwara, 2014) and crossed with the *ark1-2* allele in the Cereal Symbiosis laboratory.

Lines where O*sARK1* expression is driven by the constitutive rice ubiquitin promoter or the mycorrhizal specific 3,000 bp promoter region of the rice *OsPT11* (*LOC_Os01g46860*, Paszkowski et al., 2002) were generated through Golden Gate cloning (Table 1 and Fig. 2). Individual level 0 modules are listed in Appendix table 1.

Experiments involving *Brachypodium distachyon* were carried out using a T-DNA insertional mutant for *BdARK1* (ID: JJ27771) in the Bd21 background genotype obtained from the *Brachypodium* T-DNA Collection (DOE Joint Genome Institute, USA, Bragg et al., 2012).

Assays involving the liverwort *Marchantia paleacea* were carried out using propagules derived from specimens originally collected in a temperate forest in Veracruz, Mexico (Humphreys et al., 2010).

Table 1. Transgenic fluorescent reporter lines generated in this study through Golden Gate cloning. Codes for Level 0 modules are indicated.

Line	Construct	Background genotype	Promoter	Coding sequence	Fluorescent tag	Terminator
UP106	pUBI:*OsARK1*-GFP	wild-type	pUBI	*OsARK1*	TagGFP	Actin
			EC15328	EC85087	EC85022	EC4430
UP110	pUBI:*OsARK1*-GFP	*ark1-2*	pUBI	*OsARK1*	TagGFP	Actin
			EC15328	EC85087	EC85022	EC4430
UP123	pPT11:*OsARK1*-GFP	wild-type	pPT11	*OsARK1*	TagGFP	Actin
			EC85017	EC85087	EC85022	EC4430
UP113	pPT11:*OsARK1*-GFP	*ark1-2*	pPT11	*OsARK1*	TagGFP	Actin
			EC85017	EC85087	EC85022	EC4430

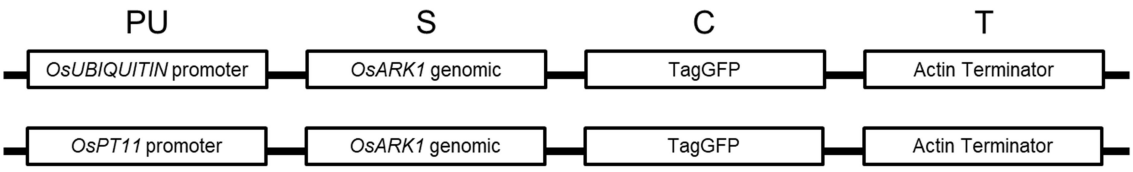

Figure 2. Constructs generated through Golden Gate cloning. Different level 0 modules are boxed. PU, promoter + 5' untranslated region (UTR); S, coding sequence; C, 3' terminal tag; T, terminator.

2.1.2. Seed sterilization and germination

O. sativa seeds were dehusked and surface-sterilized in 3% (v/v) sodium hypochlorite solution for 15 min, rinsed with sterile deionized water (diH_2O) and germinated in petri dishes sealed with Micropore™ tape containing 0.7% (w/v) Bacto™ Agar in a 30°C incubator in the dark.

After awn removal from *B. distachyon* florets, seed sterilization took place as described for rice and stratified in 0.7% (w/v) Bacto™ Agar petri dishes at 4°C for seven days followed by four days of germination at 24°C in the dark. Germinated seedlings were planted once coleoptiles and seminal roots had emerged.

2.1.3. Fungal inoculum and plant inoculation procedure

The AM fungal model species *R. irregularis* (DAOM197198) was employed for all inoculation assays. The source of spore inoculum was for most experiments from *Agrobacterium rhizogenes* transformed carrot hairy root cultures (Bécard and Fortin, 1988). For spore extraction, carrot roots that had grown in agarose plates under 25°C in the dark for several weeks were mixed with citrate buffer at a 1:3 ratio (g:mL). After stirring in a magnetic plate, the mixture was sieved through a 45 µM metal mesh to retrieve spores. A small aliquot of diH_2O diluted spores was inspected under a GXM-L2800 microscope (GT Vision, Stanfield, United Kingdom) to quantify spores and calculate their concentrations.

For colonization experiments involving *OsARK1* driven by different promoters, commercially available *R. irregularis* aseptic spores in suspension (Mycorise® ASP, Premier Tech Biotechnologies, Rivière-du-loup, Canada) were used.

Aliquoted inoculum was applied onto the substrate of half-filled containers, after which substrate was replenished and germinated seedlings transferred to the containers. For nurse plant experiments, inoculum was applied to holes made in the sand substrate. Seedlings were placed on top of each hole and sand was replenished. The amount of spore inoculum applied varied across experiments and is therefore specified in the relevant results sections.

2.1.4. Plant-fungal growth conditions

O. sativa colonization experiments were carried out in a phytochamber with photoperiod of 12-hour day-night cycle at a fluctuating temperature of 28/20°C day-night and 65% relative humidity under fluorescent lamp illumination with a light intensity of 400 µmol/µm^{2}s. Colonization assays of *B. distachyon* and *M. paleacea* were carried out in a phytochamber with photoperiod and temperature conditions of 16/8-hour day-night cycle at constant 20°C and 60% relative humidity under a light intensity of 150 µmol/µm^{2}s.

For *O. sativa* colonization experiments, plants were grown in either black petri dishes (4 cm diameter), grey cones (12 cm depth, 2.5 cm diameter), black falcon tubes (12 cm depth, 3 cm diameter) or pots (10 cm diameter) using autoclaved sand as substrate. For *B. distachyon* colonization experiments, plants were grown in cones as above in a 2:1 mixture of sand and Terra-Green®. *M. paleacea* was grown in 5 cm diameter pots with sand. Hi-Loft Polyester was applied at the bottom of cones and pots to prevent leaking of substrate.

For the nurse plant experiments, two tester plants were positioned in the middle of a pot and were surrounded by six wild-type nurse plants in a set-up resembling that of Gutjahr et al., (2012). This way, tester plants were equally exposed to the common mycorrhizal network. Both nurse and tester plants were inoculated.

Plants were watered every second day, the first two weeks post inoculation (wpi) with reverse osmosis water (R-O H_2O) followed by low Pi fertilization every other watering day with half-strength Hoagland solution containing 25 µM KH_2PO_4.

2.1.5. Crossing rice plants

Flowers from around three-months-old rice plants selected as females were cut at a 45° angle above the anthers and vacuum-emasculated in the morning of the day of crossing. Plants whose anthers were protruding from the flowers by midday were selected as males and gently tapped over female panicles to facilitate pollen release. The procedure was repeated over 30 min intervals for two hours. For the next two days female panicles were manually pollinated with male plant stamens using metal tweezers. Upon maturation, seeds were harvested and left to dry at 50°C for three weeks in a laboratory oven (model GP-OV-120-CLAD-F-100-HYD, Leader Engineering, St Helens, United Kingdom).

2.2. Microscopy

2.2.1. Quantification of fungal colonization

To stain AM fungal structures, root pieces were incubated at 95°C in 10% (w/v) KOH for 30 min. After rinsing with diH_2O, roots were incubated in 0.3 M HCl for 30 min at room temperature. HCl was removed and 0.1% (w/v) trypan blue (Sigma-Aldrich, St. Louis, USA) diluted in a 2:1:1 lactic acid/glycerol/diH_2O solution was added. Roots in trypan blue solution were incubated for 8 min at 95°C. Trypan blue was removed and roots were washed in 50% v/v acidic glycerol. Ten 2-cm root pieces per biological replicate were mounted in a glass microscope slide. Quantification of fungal colonization took place by recording the presence of extraradical hyphae, intraradical hyphae, hyphopodia, arbuscules, vesicles and spores along 100 different visual fields under a 20× magnification objective using a GXM-L2800 microscope (GT Vision, Stanfield, United Kingdom) and expressed as percentage of the total root length scored.

2.2.2. Visualization of lipids in AM fungal vesicles

Rice roots were stained with Sudan Red IV (Abcam, Cambridge, United Kingdom) by modifying a protocol originally developed to stain lipids of dark septate fungal endophytes (Barrow and Aaltonen, 2001). Root pieces were incubated in microcentrifuge tubes at 95°C in 10% (w/v) KOH for 30 min. After rinsing with diH_2O, roots were incubated in 0.3 M HCl for two hours at room temperature. HCl was removed and roots were rinsed with diH2O. Freshly made Sudan Red IV solution (3 mg mL^{-1} dissolved in 70% ethanol) was applied and tubes were incubated for 10 min in a 95°C heat block shaking at 150 rpm. Root pieces were rinsed in 50% v/v acidic glycerol, mounted in microscope slides and visualized using a GXM-L2800 microscope (GT Vision, Stanfield, United Kingdom) under a 20× magnification objective.

2.2.3. Imaging of fungal chitin and lipids in arbusculated cells

To visualize AM fungal structures using confocal laser scanning microscopy (CLSM), roots or thalli were treated with fluorophore-conjugated Wheat Germ Agglutinin (WGA), a lectin that binds to *N*-acetylglucosamine, the monomeric unit of chitin. WGA-Alexa Fluor™ 488 and WGA-Alexa Fluor™ 633 (Invitrogen, Carlsbad, USA) exhibiting green and far-red fluorescence respectively were used in this study. Roots or thalli sections were

excised and incubated in 50% (v/v) ethanol for one hour. Ethanol was removed and 20% (w/v) KOH solution added. After two days, KOH was removed and roots were rinsed with diH_2O after which samples were incubated for two hours in 0.1 M HCl. Roots were rinsed with 1× phosphate-buffered saline (PBS, pH 7.4) solution. A 0.2 µg mL^{-1} WGA-Alexa Fluor™ 488/633 solution in 1× PBS was added and samples were incubated at 4°C in the dark for at least one week before imaging. Roots treated with WGA conjugated with the far-red fluorophore Alexa Fluor™ 633 were counter-stained with the recently developed blue lipophilic fluorochrome Ac-201 (Avicor, Szeged, Hungary) (Kuntam et al., 2015). 5 µg mL^{-1} of Ac-201 was used for one hour incubation of roots at room temperature prior to imaging.

Visualization of roots and thalli took place using CLSM on a Leica TCS SP8 (Leica Microsystems, Wetzlar, Germany). To detect WGA-Alexa Fluor™ 488, white light laser (WLL) was used with an excitation wavelength of 488 nm (20% laser power), and emitted wavelengths collected at 492-533 nm. To detect autofluorescence, an excitation wavelength of 442 nm was used (5% laser power) and emitted wavelengths collected at 770-790 nm. One image per arbusculated cell was taken at the point of maximal arbuscule expansion at a line average of 2 and dimension of 2048 × 2048 pixels. Roots and thalli sections were observed using a 63× or 25× water immersion objectives.

For the simultaneous imaging of fungal chitin and lipids, WGA-Alexa Fluor™ 633 was detected using WLL with an excitation wavelength of 630 nm (5.6% laser power), and emitted wavelengths collected at 650-730 nm. To detect Ac-201, UV laser was used with an excitation wavelength of 405 nm (5.6% laser power) and emitted wavelengths collected at 410-510 nm. One image per arbusculated cell was taken at the point of maximal arbuscule expansion at a line average of 2 and dimension of 2048 × 2048 pixels. Roots were observed using a 63× or 25× water immersion objective.

Image processing was carried out using the Fiji package under the ImageJ software license (Schindelin et al., 2012). For arbuscule size quantification, the areas of arbuscules and their host cells were measured using the freehand selection tool and their ratios were calculated. To measure Ac-201 fluorescence intensity, arbusculated cells were individualized using the freehand selection tool in the blue channel images. Blue pixel to grayscale conversion was applied and Mean Grey Values were measured

on the selection area, corresponding to the sum of the grey values of all pixels in the selection area divided by the number of pixels.

2.2.4. Live cell imaging

To investigate the dynamics of translational fluorescent reporter in rice roots, CLSM was carried out using a Leica TCS SP8 (Leica Microsystems, Wetzlar, Germany). Roots were washed in diH_2O to remove substrate, mounted in diH_2O on a microscope slide and covered with a coverslip.

For visualization of the GFP-SCAMP *ark1-2* line, GFP was detected using the WLL with an excitation wavelength of 488 nm (20% laser power), and emitted wavelengths collected at 492-533 nm. To detect autofluorescence, an excitation wavelength of 442 nm was used (30% laser power) and emitted wavelengths collected at 593-700 nm. Z-stacks of up to 30 slices were taken (0.5 µm step size) at a line average of 4 and dimension of 1024 × 1024 pixels. Image processing was carried out using the Fiji package under the ImageJ software license (Schindelin et al., 2012).

For inspections of the fluorescent reporter lines generated through Golden Gate cloning, TagGFP was detected using the WLL with an excitation wavelength of 488 nm (20% laser power), and emitted wavelengths collected at 492-533 nm. To detect autofluorescence, an excitation wavelength of 442 nm was used (5% laser power) and emitted wavelengths were collected at 770-790 nm. Roots were observed using a 63× water immersion objective. Images were acquired at a line average of 2 and dimension of 2048 × 2048 pixels. Image processing was carried out using the Fiji package of ImageJ as above.

2.3. Molecular biology techniques

2.3.1. gDNA extraction and PCR genotyping

Genomic DNA (gDNA) extraction for genotyping was carried out following a modified sucrose solution extraction protocol originally developed for *A. thaliana* tissues (Berendzen et al., 2005). Briefly, a 1 cm-piece of rice leaf was collected and frozen in

liquid nitrogen. Leaf pieces were lysed in 2 mL safe-lock microcentrifuge tubes with glass beads using a Qiagen TissueLyser II (Hilden, Germany) and mixed with 200 µL sucrose gDNA extraction buffer containing 50 mM Tris-HCl, pH 7.5; 300 mM NaCl and 300 mM sucrose. Samples were incubated in a heat block for 10 min at 95°C and centrifuged at 14,000 rpm for 2 min. Supernatant containing extracted gDNA was used as a template for PCR genotyping with recombinant *Taq* DNA Polymerase (Invitrogen, Carlsbad, USA) in a PTC-225 Peltier thermal cycler (Watertown, USA). PCR conditions were: 94°C initial denaturation, 35 cycles of 3 min denaturation at 94°C, 40 s annealing at 56°C, 40 s elongation at 72°C followed by 2 min of final elongation at 72°C. 1 µg mL^{-1} ethidium bromide agarose gel electrophoresis (1% agarose) was carried out over PCR products. Gels were visualized under UV light and images were acquired using a GBox Chemi 16 Bio Imaging System (Syngene, Cambridge, United Kingdom). Oligonucleotides for genotyping are listed in Appendix Table 2.

2.3.2. DNA purification and Sanger sequencing

Either PCR products, agarose gel electrophoresis bands or plasmid DNA were subjected for DNA purification and Sanger sequencing analysis. For purification of PCR products and purification of excised electrophoresis bands the NucleoSpin® Gel and PCR Clean-up kit (Macherey-Nagel, Düren, Germany) was used following manufacturer's instructions. Plasmid DNA purification was carried out using the NucleoSpin® Plasmid kit (Macherey-Nagel, Düren, Germany) following manufacturer's instructions. 5 µL of 10 ng $µL^{-1}$ of DNA and 3.2 pmol $µL^{-1}$ of gene or vector-specific oligonucleotides were submitted for an external Sanger sequencing service (Source BioScience, Cambridge, United Kingdom).

2.3.3. Golden Gate cloning and rice transformation

Constructs in this dissertation were generated using Golden Gate cloning (Engler et al., 2009; Weber et al., 2011). Level 0 modules were designed using Geneious v11.1 software (https://www.geneious.com/home/). Nucleotide sequences for modules were domesticated to remove *Bsa*I or *Bpi*I restriction sites considering codon usage for rice

during nucleotide substitutions. Linkers containing restriction sites for Golden Gate cloning were added to the 5' and 3' end of the domesticated sequences. Golden Gate cloning was carried out *in silico* using Geneious prior to module synthesis to confirm correct module design. Gene module synthesis was carried out using GeneArt™ Gene Synthesis (Invitrogen, Carlsbad, USA) and transformed into level 0 vectors containing either kanamycin (Kan) or spectinomycin (Spec) antibiotic selection cassettes. Level 0 modules were assembled into the EC47732_pL1V-F1 vector backbone in a level 1 reaction containing 20 U of *Bsa*I-HF (NEB, Hitchin, United Kingdom), 1× of CutSmart™ Buffer (NEB, Hitchin, United Kingdom), 400 U of T4 DNA ligase (NEB, Hitchin, United Kingdom) and 10 mM of ATP (NEB, Hitchin, United Kingdom). Enzymatic digestion and ligation reactions took place using a PTC-225 Peltier thermal cycler (Watertown, USA) with the following cycling conditions: 3 cycles of 10 min at 40°C and 10 min at 16°C followed by 10 min at 50°C and 20 min at 80°C. 5 µL of Golden Gate level 1 reaction were used for transformation into One Shot® TOP10 competent *E. coli* cells (Invitrogen, Carlsbad, USA). Cells were heat-shocked in a water bath at 42°C for 45 s and transferred to ice for five min after which 250 µL of S.O.C medium (Invitrogen, Carlsbad, USA) was added. Samples were incubated at 37°C for one hour in a heat block shaking at 400 rpm. Samples were streaked out on 100 µg mL^{-1} ampicillin (Amp) resistance Luria-Bertani (LB) plates containing 40 µg $µL^{-1}$ X-gal (5-bromo-4-chloro-3-indolyl-β-D-galactopyranoside, Melford) and 0.1 mM IPTG (Isopropyl β-d-1-thiogalactopyranoside, Melford) for blue/white selection and incubated at 37°C overnight. White colonies were sub cultured in liquid LB media supplied with 100 µg mL^{-1} Amp and incubated overnight in a 37°C shaker at 150 rpm. Plasmid DNA was subsequently purified ahead of Golden Gate level 2 reactions.

For level 2 reactions, level 1 modules were assembled into the EC60606_pL2V-GW level 2 vector backbone flanked by Gateway attL1 and L2 sites and the end linker Golden Gate vector EC41722_ELE1. The level 2 reaction contained 10 U of *Bpi*I (ThermoFisher, Waltham, USA), 1× of Buffer G (ThermoFisher, Waltham, USA), 400 U of T4 DNA ligase (NEB, Hitchin, United Kingdom) and 10 mM of ATP (NEB, Hitchin, United Kingdom). Enzymatic digestion and ligation reactions took place as above with the following cycling conditions: 3 cycles of 10 min at 37°C and 10 min at 16°C followed by 10 min at 37°C and 20 min at 65°C. 5 µL of the Golden Gate level 2 reaction products were used for

bacterial transformation as above. Samples were streaked out on 50 µg mL^{-1} Kan resistance LB plates and incubated at 37°C overnight for red/white selection. White colonies were subcultured in liquid LB media supplied with 50 µg mL^{-1} Kan and incubated overnight in a 37°C shaker at 150 rpm. Plasmid DNA was subsequently purified. Confirmation of correct assembly of level 2 modules through Sanger sequencing was followed by recombination into the binary destination vector pEW343-R1R2 containing a hygromycin (Hyg) selection cassette. This final destination vector was used for *Agrobacterium tumefaciens*-mediated rice callus transformation which was performed in the Crop Transformation laboratory in NIAB (National Institute for Agricultural Botany, Cambridge, United Kingdom).

2.3.4. Cloning the SPARK domain for protein expression

M. paleacea thalli inoculated with *R. irregularis* (10 wpi, 500 spores) were harvested upon confirmation of colonization through WGA staining (as in section 2.2.3). RNA was extracted and cDNA synthesised (as in section 2.3.7). The 1,292 bp long *MpARK* cDNA was amplified using Phusion High-Fidelity DNA Polymerase (Thermo Scientific™, Waltham, USA) with Phusion HF Buffer in a PTC-225 Peltier thermal cycler (Watertown, USA). PCR conditions were: 98°C initial denaturation, 35 cycles of 10 s denaturation at 98°C, 30 s annealing at 58°C, 2 min elongation at 72°C followed by 5 min of final elongation at 72°C. 1 µg mL^{-1} ethidium bromide agarose gel electrophoresis (1.5% agarose) was carried out over PCR products. The gel was visualized under UV light and images were acquired using a GBox Chemi 16 Bio Imaging System (Syngene, Cambridge, United Kingdom). Purified PCR products were confirmed through Sanger sequencing and used as templates for a nested Phusion PCR with oligonucleotides amplifying the predicted cDNA sequence coding for the 609 bp long *MpARK* SPARK domain, devoid of the flanking signal peptide in the 5' end and transmembrane region in the 3' end. These primers were compatible for In-Fusion® cloning to the pET-20b(+) vector (Novagen, Darmstadt, Germany) carrying a C-terminal His Tag® sequence. The purified PCR product was cloned into pET-20b(+) vector linearized with *XhoI* and *NdeI* (NEB, Hitchin, United Kingdom) using the In-Fusion® HD Cloning Kit (Takara Bio, Kusatsu, Japan) following manufacturer's instructions. The In-Fusion® product was

transformed into One Shot® TOP10 competent *E. coli* cells (Invitrogen, Carlsbad, USA) and streaked out on 100 µg mL^{-1} Amp resistance LB plates. Colony PCR followed by Sanger sequencing of PCR products confirmed *MpARK* SPARK domain cloned in frame to pET-20b(+) vector. Plasmid DNA was subsequently used for transformation into BL21(DE3)pLysS competent cells (Promega, Madison, USA) followed by culturing into 100 µg mL^{-1} Amp resistance solid and liquid LB media.

2.3.5. Fatty acid quantification by gas chromatography

Using root material that had been frozen at -80°C (100-300 mg FW), fatty acid methyl esters (FAMEs) were prepared by transmethylation in 5 mL of methanol/HCL at 80°C for two hours. 50 µL of heptadecanoic acid (17:0) was added as internal standard. 250 µL KCl (0.9% w/v) and 500 µL hexane were added and mixed by vortexing. Samples were centrifuged for five min at 4000 rpm and the upper hexane phase was collected into a fresh vial. Hexane extraction was repeated and the extracts pooled. The FAMEs were analysed by gas chromatography (GC) in a 6890N Network GC System (Agilent Technologies, Santa Clara, USA).

2.3.6. RNA extraction and cDNA synthesis

For *O. sativa* and *B. distachyon* roots and *M. paleacea* thalli, tissues were immediately frozen in liquid nitrogen after collection and stored at -80°C until used for RNA extraction. Frozen tissues were ground using mortar and pestle in liquid nitrogen and 100 mg were used for RNA extraction following a TRIzol reagent-based method as described in Roth et al., (2018). After testing for RNA integrity under 1.5% agarose gel electrophoresis and quantifying RNA concentrations in a NanoDrop™ 2000 spectrophotometer (ThermoFisher, Waltham, USA), 1 µg of RNA was treated with DNase I (Invitrogen, Carlsbad, USA) to remove genomic contamination following manufacturer's guidelines. First-strand cDNA synthesis was carried out using SuperScript™ II reverse transcriptase (Invitrogen, Carlsbad, USA) according to manufacturer's instructions.

2.3.7. Reverse transcription (RT)-PCR assays

RT-PCR gene expression assays over *O. sativa* and *B. distachyon* roots were carried out using recombinant *Taq* DNA Polymerase (Invitrogen, Carlsbad, USA) in a PTC-225 Peltier thermal cycler (Watertown, USA). PCR conditions were: 94°C initial denaturation, 35 cycles of 3 min denaturation at 94°C, 40 s annealing at 56°C, 40 s elongation at 72°C followed by 2 min of final elongation at 72°C. 1 µg mL^{-1} ethidium bromide agarose gel electrophoresis (1.5% agarose) was carried out over PCR products. Gels were visualized under UV light and images were acquired using a GBox Chemi 16 Bio Imaging System (Syngene, Cambridge, United Kingdom). Gene expression of the housekeeping genes *OsGAPDH* (*LOC_Os08g03290*) and *BdGAPDH* (*Bradi3g14120*) was measured in parallel to the target genes.

2.3.8. RNAseq library preparation and sequencing

RNA extraction and DNase I treatment was conducted as in section (2.3.6). RNA integrity was monitored on 1% agarose gels, using the NanoPhotometer® spectrophotometer (IMPLEN, Los Angeles, USA) and the RNA Nano 6000 Assay Kit of the Bioanalyzer 2100 system (Agilent Technologies, Santa Clara, USA). 1 µg RNA per sample was used for library preparation generated using NEBNext® Ultra™ RNA Library Prep Kit for Illumina® (NEB, Hitchin, United Kingdom) following manufacturer's instructions. Library quality was monitored on the Agilent Bioanalyzer 2100 system. After cluster generation on a cBot Cluster Generation System using PE Cluster Kit cBot-HS (Illumina, San Diego, USA), the library preparations were sequenced on an Illumina platform and paired-end reads were generated. RNAseq library preparation and sequencing were performed by Novogene (Cambridge, United Kingdom).

2.4. Bioinformatics and phylogenetics

2.4.1. Identification and characterization of protein motifs and domains

Signal peptides and transmembrane regions were predicted using Phobius (http://phobius.sbc.su.se/, Käll et al., 2004). Glycosylphosphatidylinositol (GPI) anchored proteins were predicted using PredGPI (http://gpcr.biocomp.unibo.it/predgpi/, Pierleoni et al., 2008). Kinase domains were predicted using ScanProsite (https://prosite.expasy.org/scanprosite/, De Castro et al., 2006). Individual motifs and regions from kinase domains were identified by homology to the vertebrate cAMP-dependent Protein Kinase catalytic subunit (PKA-ca, Hanks and Hunter, 1995). Protein domain sequence logos were created using WebLogo v.2.8.2 (https://weblogo.berkeley.edu/, Crooks et al., 2004).

The SPARK domain was initially identified by aligning the extracellular domains of members of the OsARK1 RLK subfamily using the built-in MUSCLE tool (Edgar, 2004) in Jalview v2.10.5 (Waterhouse et al., 2009). Conservation of individual residues was identified by using the Taylor colour scheme (Taylor, 1997) applied above different percentage identity thresholds. Determination of SPARK domain occurrence was carried out using sequence pattern searches against a database of 121 plant species genomes (Pucker and Brockington, 2018) employing the following sequence formula: C×(18-27)CC(26-32)C×(15-23)C×(8-15)C×(22-26)C×(7-10)C×(2)C, where C corresponds to cysteine, '×' corresponds to any residue except cysteine and numbers in parentheses indicate the number of residues '×' allowed in between cysteines. A multiple protein sequence alignment of the SPARK domain was used to build a Hidden Markov Model (HMM)-based profile generated with HMMER3 (http://hmmer.org/) as described in El Gebali et al., (2019) and a Pfam entry for the SPARK domain was created.

2.4.2. Databases used for orthologue searches

Orthologues of the different proteins under investigation were retrieved from the iTAK database (http://itak.feilab.net/cgi-bin/itak/index.cgi, Zheng et al., 2016). In addition, orthologue searches among non-flowering plants and basal angiosperms were carried out using the One Thousand Plant Transcriptomes (1KP) database (Leebens-Mack et al., 2019). The built-in tools BLASTP (https://db.cngb.org/blast/blast/blastp/) and TBLASTN (https://db.cngb.org/blast/blast/tblastn) were employed. Orthology was established by reciprocal BLAST of the best hit. When sequences were incomplete or had low quality,

the following resources were used to find better quality sequences; NCBI standard protein BLAST (https://blast.ncbi.nlm.nih.gov/Blast.cgi?PAGE=Proteins), NCBI translated BLAST (https://blast.ncbi.nlm.nih.gov/Blast.cgi?PROGRAM=tblastn&PAGE_TYPE=BlastSearch&LINK_LOC=blasthome), UniProt BLAST (https://www.uniprot.org/blast/) or Phytozome v12.1 BLAST (https://phytozome.jgi.doe.gov/pz/portal.html#!search?show=BLAST). Appendix Table 3 and 4 list the source of all individual protein sequences.

2.4.3. Phylogenetic analyses

The amino acid sequences of predicted kinase domains from the protein subfamilies under investigation were aligned using the built-in MUSCLE alignment tool (Edgar, 2004) in Jalview v2.10.5 (Waterhouse et al., 2009) and curated manually. Phylogenetic analyses were conducted in MEGA X software (Kumar et al., 2018). The evolutionary history of SPARK-I subfamily members was inferred by using the Maximum Likelihood method and JTT matrix-based model (Jones et al., 1992). A discrete Gamma distribution was used to model evolutionary rate differences among sites. All positions from the total 103 sequences with less than 95% site coverage were eliminated resulting in a total of 263 positions in the final dataset. A consensus tree was built from 1,000 bootstrap replicates. The evolutionary relationship between the SPARK-I, URK-1 and RKF3 subfamilies was inferred as before employing 447 amino acid sequences and resulting in 197 positions in the final dataset after removing those with less than 95% site coverage. A *Chlamydomonas reinhardtii* protein kinase (UniProt ID: A8IVV6) was used as outgroup.

2.4.4. RNAseq data analysis

Raw RNAseq reads of FASTQ format were processed to remove low quality reads and reads containing adapter and poly-N sequences. Q20, Q30 and GC content of the clean data were calculated. Paired-end clean reads were mapped to the *O. sativa* Nipponbare reference genome (Os-Nipponbare-Reference-IRGSP-1.0, Kawahara et al., 2013) using STAR v2.7.3a software (Dobin et al., 2013). The expression levels of genes were

calculated in raw counts and FPKM (Fragments Per Kilobase of exon model per Million reads mapped) with featureCounts in R package Rsubread (version 2.0.0) (Liao et al., 2014). TPM (Transcripts Per Million) values were calculated from raw counts using a custom Python script. Genes with CPM (Counts Per Million) values (calculated from R package edgeR 3.26.8, Robinson et al., 2010) lower than 0.5 in more than 10 samples were filtered out to avoid confounding results in differential expression analysis due to small expression changes. The remaining 27,498 genes were subjected to pairwise differential expression analysis between three genotypes (*ark1*, *ark2*, DKO) in relation to expression levels in the wild-type (ten biological replicates per genotype) using the R package DESeq2 v1.26.0 (Love et al., 2014) employing the raw count numbers. Genes with log2 fold changes greater than 1 or less than −1 that had the significance of Benjamini-Hochberg false discovery rate (FDR) corrected p value < 0.05 were classified as differentially expressed. The correlation between the expression level of genes (TPM) in the different genotypes and percentage of arbuscule colonization was determined with Spearman correlation coefficient using p value of 0.05 as a significance cut-off. The annotations of the genes were collected from three different sources: Gene Ontology (GO, Ashburner et al., 2000) terms used in Choi et al., (2020), GO slim (Mi et al., 2019) terms (http://rice.plantbiology.msu.edu/) and Kyoto Encyclopedia of Genes and Genomes (KEGG) pathways (Kanehisa and Goto, 2000). Functional gene annotations derived from experimental work were retrieved from the dataset of Yao et al., (2018) and rice orthologues of AM conserved genes were identified in a previous study (Choi et al., 2020) based on orthology with *M. truncatula* genes in the dataset of Bravo et al., (2016).

Chapter 3

OsARK1 functions in the post-arbuscule development stage

3.1. Introduction

The establishment and development of the AM association relies on constant communication between the plant and fungal partners. Plant and AM fungal compounds are reciprocally sensed resulting in progression of symbiosis. Mediating plant perception of AM fungal-derived compounds (e.g. chitin derivatives), RLKs from the LysM subfamily have been well described (reviewed in Chiu and Paszkowski, 2020). As chitinaceous cell walls are property of fungi in general, symbiotic outcomes by perception of chitin derivatives are likely conditioned by downstream signalling mechanisms specific for AM symbiosis. Another RLK, SYMRK, harbouring LRR and malectin domains in its extracellular region, is required for AM fungal penetration in roots (Stracke et al., 2002) although its mechanism of action remains unclear. *SYMRK* is a CSSP gene also functioning in the legume root nodule symbiosis (Endre et al., 2002; Stracke et al., 2002) and phylogenomics work has showed it to be present in genomes of plants engaging with diverse endosymbioses other than AM such as ericoid and orchid mycorrhiza (Radhakrishnan et al., 2020).

In its fully functional form, arbuscules populate root tissues facilitating nutrient exchange. Most of the proteins described to function in the arbusculated cell are nutrient transporters and proteins participating in membrane dynamics (Luginbuehl and Oldroyd, 2017). Besides nutrient transport, the PAM constitutes an ideal interface for plant-AM fungal communication, RLKs being primary candidates for inter-kingdom perception. Although no RLK functioning at the PAM had been described, several RLK-coding genes had been known to be transcriptionally induced in AM symbiosis stages

where arbuscule abundance prevails. One of such genes in rice, *LOC_Os11g26140*, first named *OsAM14* was identified as one of the most induced during AM symbiosis (Güimil et al., 2005). Later, *OsAM14* was described to exhibit temporally progressive high gene induction in AM symbiosis, prompting its use as a transcriptional marker of the association (Gutjahr et al., 2008). A proteomics approach also showed the maize orthologue, ZmAM14, to be abundantly present in AM colonized roots (Roth et al., 2018). Finally, laser capture microdissection (LCM) transcriptomics showed *OsAM14* to be transcriptionally induced in arbusculated cells and GUS reporter assays evidenced this cell type as the only site where *OsAM14* is transcriptionally active. The generation of a translational reporter allowed studying OsAM14 subcellular localization which was confined to the PAM surrounding mature to collapsing arbuscules (Roth et al., 2018). *OsAM14* encodes a RLK with a predicted active kinase domain belonging to an uncharacterized RLK subfamily and was renamed *ARBUSCULAR RECEPTOR-LIKE KINASE 1* (*OsARK1*, Roth et al., 2018). These findings suggest OsARK1 to function in a signalling pathway at the plant-fungal symbiotic interface.

Mutation of components known to operate in arbusculated cells such as AM-specific nutrient transporters interferes with arbuscule development and functioning (reviewed in Lanfranco et al., 2018), creating the notion that if nutrient delivery is impaired arbuscules will not fully form. To determine if *OsARK1* has a similar role relative to previously described arbusculated cell-specific proteins, a phenotypic characterisation was carried out of *ark1* insertional mutants. It was found that in the *ark1* mutants although colonization drops as plant-AM fungal co-cultivation progresses, arbuscules develop normally. These colonization defects could be rescued by a common mycorrhizal network formed with wild-type plants, revealing that OsARK1 has a post-arbuscule development function that relates to AM fungal fitness maintenance.

3.2. Results

3.2.1. Molecular characterization of two Tos17 *ark1* mutant alleles in rice

Two rice Tos17 insertional mutant alleles for *OsARK1* were available in a public collection (Miyao et al., 2003); *ark1-1* (ID: NF1782) and *ark1-2* (ID: NF4582). PCR

genotyping followed by Sanger sequencing of the purified electrophoresis band confirmed the insertions to be in exon IV for *ark1-1* (1,561 bp from first nucleotide of ATG) and exon VI for *ark1-2* (2,087 bp from first nucleotide of ATG). In the two cases, the Tos17 element is inserted in the kinase domain-coding region (Fig. 3a).

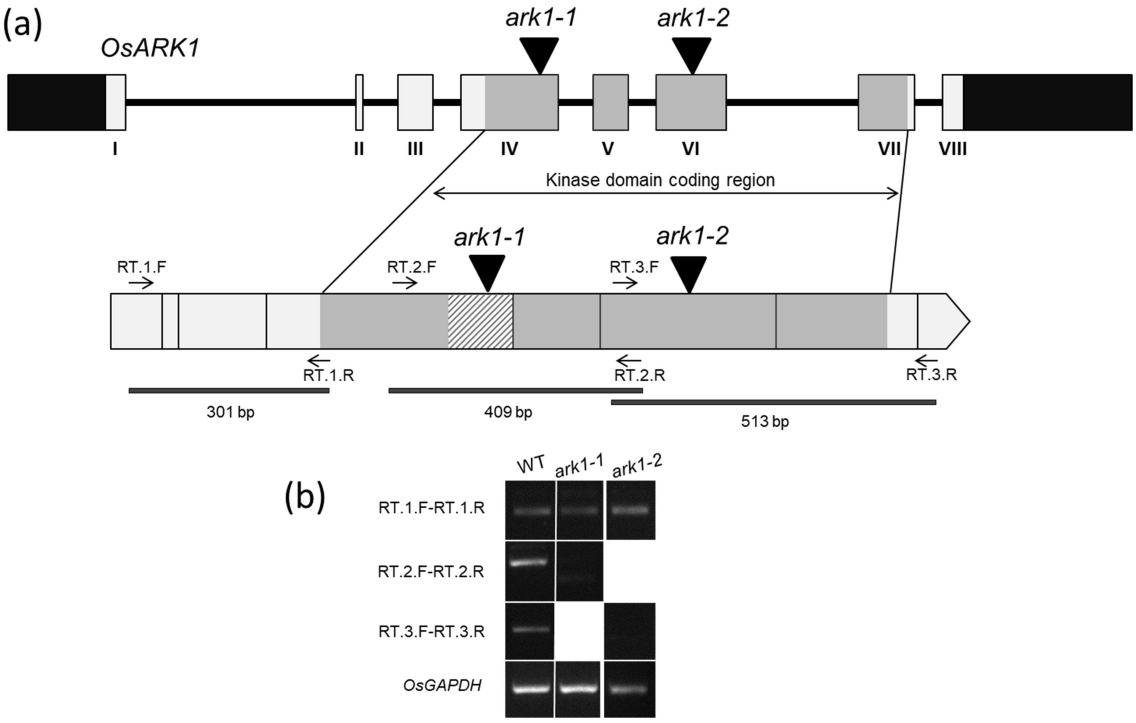

Figure 3. Molecular characterization of *ark1* mutant alleles. (a) Gene structure schematic depicting exons in roman numerals. Sites of Tos17 insertion are shown as triangles. Black boxes correspond to untranslated regions. Arrows correspond to sites of oligonucleotide hybridization for RT-PCR. (b) RT-PCR amplifying *OsARK1* cDNA upstream and flanking the Tos17 insertion (35 PCR cycles). Region with diagonal pattern shows 109 nucleotides spanning the Tos17 insertion missing in the small population of *OsARK1* transcripts detected in the *ark1-1* allele. *GAPDH*, *GLYCERALDEHYDE 3-PHOSPHATE DEHYDROGENASE*, WT, wild-type.

In order to confirm perturbation of the *OsARK1* transcript in the two mutant alleles, RNA was extracted from wild-type and mutant roots of plants inoculated with 300 *R. irregularis* spores and grown in cones for five weeks. cDNA was synthesised for RT-PCR assays. Oligonucleotides employed were designed to hybridize in regions upstream and spanning the Tos17 insertions. For the two alleles, transcripts were detected when employing oligonucleotides upstream of the insertion. When using oligonucleotides spanning the insertion for the *ark1-1* allele, there was a faint ~100 bp smaller PCR product compared to the band present in the wild-type. This band was

purified and sequenced revealing that the product amplified corresponded to the wild-type fragment but with a stretch of 109 bp missing. This missing portion corresponds to the *OsARK1* sequence flanking the Tos17 element and ends with the 3' end of exon IV (Fig. 3a). This suggest that in the *ark1-1* allele, the intron between exons IV and V is spliced out along with the Tos17 element carrying in the process a portion of exon IV flanking the Tos17 element. If transcribed, this would result in a frameshift starting from the site of deletion. As the electrophoresis band was rather faint, this event should be rare. In the case of the *ark1-2* allele, there was no PCR product detected when employing oligonucleotides spanning the insertion (Fig. 3b). Overall, these results indicate that in the two alleles the Tos17 insertion perturbs *OsARK1* transcription.

3.2.2. Reduced colonization phenotype in *ark1* can be rescued by a wild-type common mycorrhizal network

Prior observations indicated *ark1* mutants to have a reduced colonization phenotype (Roth et al., 2018). These reduced colonization levels may be explained by either roots being less receptive for the AM fungus or due to the AM fungus not been able to grow properly. To distinguish the nature of this phenotype, a nurse plant experiment was conducted where mutant plants were grown in pots alongside wild-type plants in sand substrate with low Pi fertilization regime. In nurse plant systems, a common mycorrhizal network is formed allowing nutrient fluxes to be established between AM fungi colonizing different plants. Controls where pots had only wild-type and only mutant plants were included. This experiment was carried out using the two *ark1* mutant alleles in parallel. It was found that at 7 wpi, control pots containing only *ark1* mutant plants had reduced percentage of extraradical hyphae, intraradical hyphae, arbuscules, vesicles and spores compared to plants grown in pots containing only wild-type plants. In contrast, mutant plants from the two alleles that were grown surrounded by wild-type plants had fully restored colonization levels of all symbiotic structures. These colonization levels did not differ either with the surrounding wild-type plants or with wild-type plants grown in monoculture (Fig. 4a-b). Representative pots are shown in Fig. 4c to illustrate that in the system used, there were no evident genotype-dependent alterations in plant growth in line with the situation occurring in

other growth conditions used throughout this dissertation. These results show that *ark1* plants are not impeded in AM fungal proliferation as long as hyphae are supplied with nutrients and/or signals from wild-type plants.

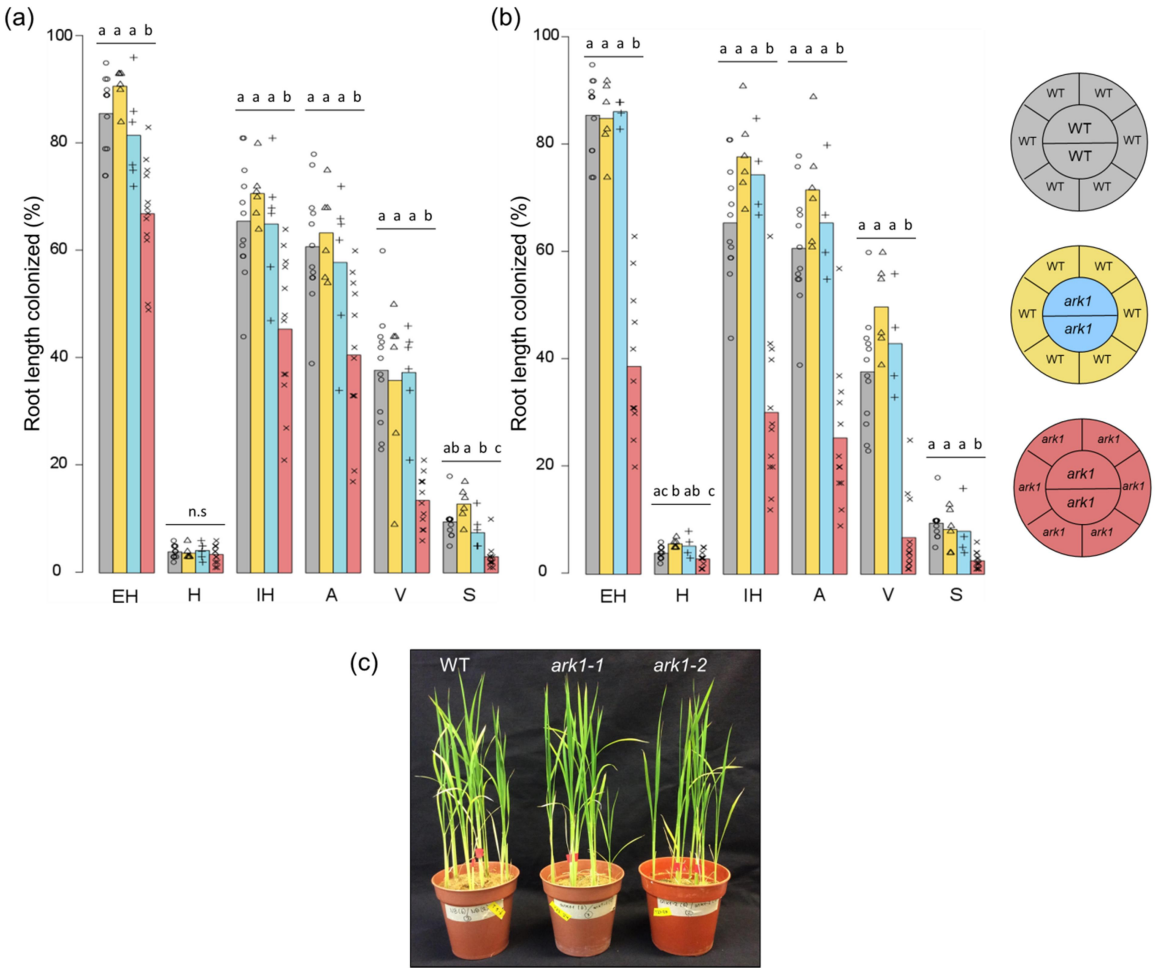

Figure 4. *ark1* phenotype can be rescued by wild-type nurse plants. (a) Colonization levels of 7 wpi *ark1-1* and (b) *ark1-2* alleles grown in a nurse plant system. Pot arrangement shown on the right. 15 pots in total were grown in this experiment (three per arrangement). Different letters denote statistically significant differences (p < 0.05, Kruskal-Wallis test with post hoc Dunn test using Benjamini-Hochberg multiple comparison correction). Bars represent means. EH, extraradical hyphae; H; hyphopodia; IH, intraradical hyphae; A, arbuscules; V, vesicles; S, spores; n.s, not significant; WT, wild-type.

3.2.3. Arbuscule development is not compromised in *ark1* mutants

In order to determine whether the phenotype of *ark1* mutants relates to the development of arbuscules, a CLSM approach was implemented for imaging of fixed root tissues and also via live cell imaging. Wild-type and *ark1-1* allele plants were

inoculated with 300 spores of *R. irregularis* and grown in sand substrate in black petri dishes for six weeks. At this time point, percentage of vesicles and spores had started decreasing in *ark1-1* but abundance of arbuscules was not different to the wild-type (Fig. 5a). This likely indicates that the mutant phenotype was starting to manifest. This early stage of the *ark1* phenotype also allowed for visual inspection of equivalent numbers of arbuscules in mutant and wild-type plants. Roots were fixed and stained with fluorophore-conjugated WGA and imaged in a Leica SP8 confocal microscope. The ratio between the area of arbuscules and their host cells was measured over the images acquired. Arbuscule size distribution was not different between genotypes (Fig. 5b) suggesting that a similar proportion of arbuscules of the different developmental stages are present in the *ark1* mutant. Representative confocal images are shown in Fig. 5c.

In order to observe arbuscule development dynamics in live root tissues, an AM fluorescent reporter line was used. *OsAM42* (*LOC_Os03g38600*) is a gene induced in AM symbiosis in rice (Güimil et al., 2005). This gene encodes a Secretory Carrier Membrane Protein (OsSCAMP) and a translational reporter GFP-OsSCAMP has been shown to localize to arbusculated cells throughout arbuscule lifespan (Kobae and Fujiwara, 2014). The specific subcellular localization and function of OsSCAMP are not known but SCAMP proteins are integral membrane proteins functioning in membrane trafficking (Hubbard et al., 2000) and OsSCAMP may localize to the endomembrane system and/or the PAM to mediate secretory or endocytic processes throughout arbuscule development (Kobae and Fujiwara, 2014). A cross between this GFP-OsSCAMP subcellular reporter line and the *ark1-2* allele was used to monitor arbuscule development. Plants were inoculated with 500 spores of *R. irregularis* and grown in sand substrate with low Pi fertilization treatment. After 6 and 14 wpi, three plants per genotype were selected for screening under a Leica SP8 confocal microscope. At 6 wpi, all the different arbuscule developmental stages (developing, mature and collapsing arbuscules) were found in the mutant background with no evident morphological differences to the wild-type (Fig. 6a). At 14 wpi, although percentage of arbuscules was low averaging 20% in the mutant background plants selected for imaging, patches with arbuscules still showed normal morphology (Fig. 6b). Together, these results suggest *OsARK1* not to be required for the formation of fully developed arbuscules.

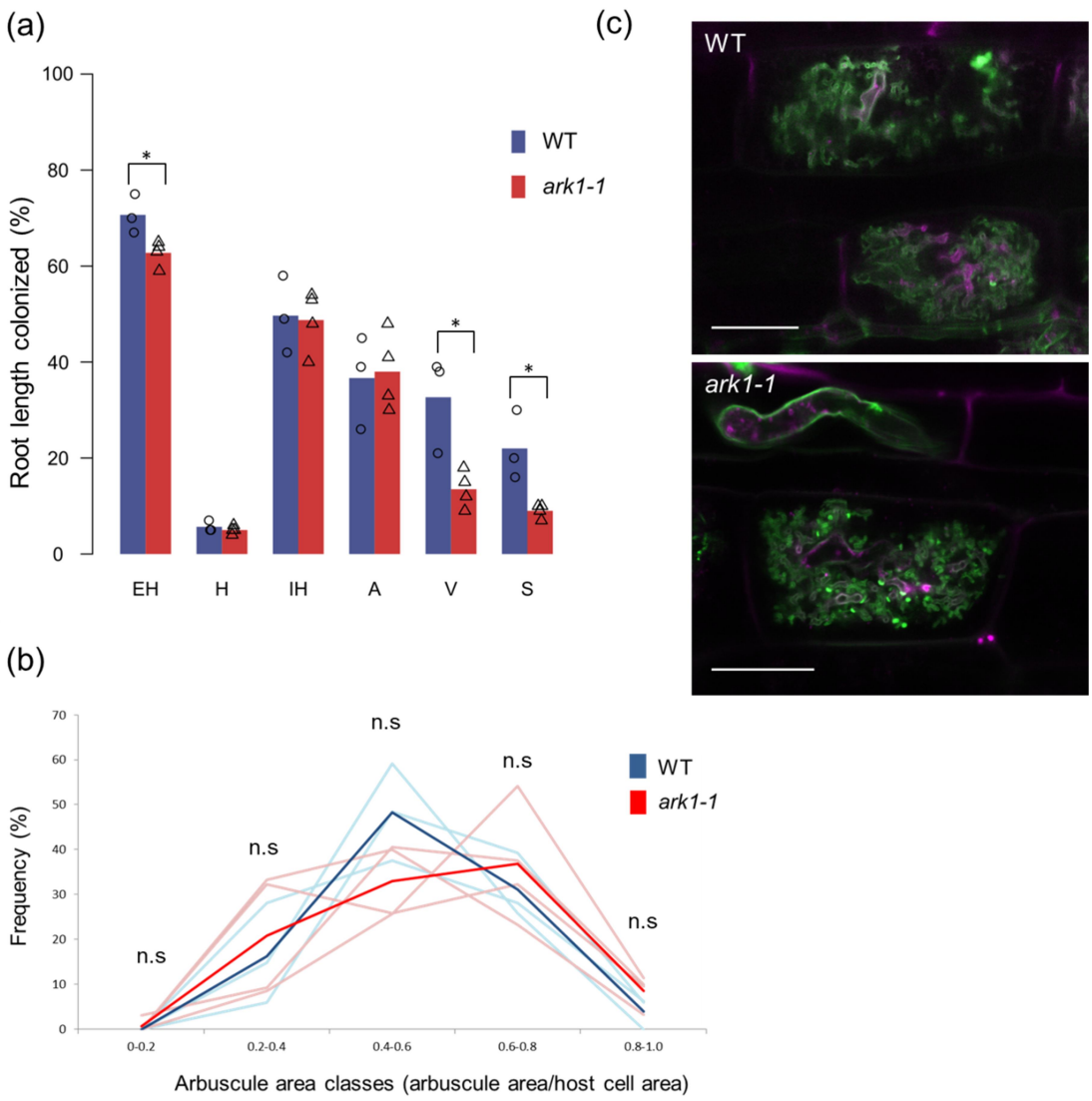

Figure 5. Arbuscule size class distribution is not perturbed in the *ark1* mutant. (a) Colonization levels at 6 wpi. *, statistically significant differences (Wilcoxon test, $p < 0.05$). (b) Frequencies of arbuscule area classes in the *ark1* mutant are comparable to that of wild-type. Averages from individual plants are shown light-coloured and total averages in bold colours. Around 30 arbuscules per plant were screened. n.s, not significant differences (Wilcoxon test, $p < 0.05$). (c) Representative images of Wheat germ agglutinin-Alexa Fluor™ 488-stained mature arbuscules. Host cells boundaries can be seen thanks to cell wall autofluorescence. Scale bar: 20 µm. EH, extraradical hyphae; H; hyphopodia; IH, intraradical hyphae; A, arbuscules; V, vesicles; S, spores. WT, wild-type.

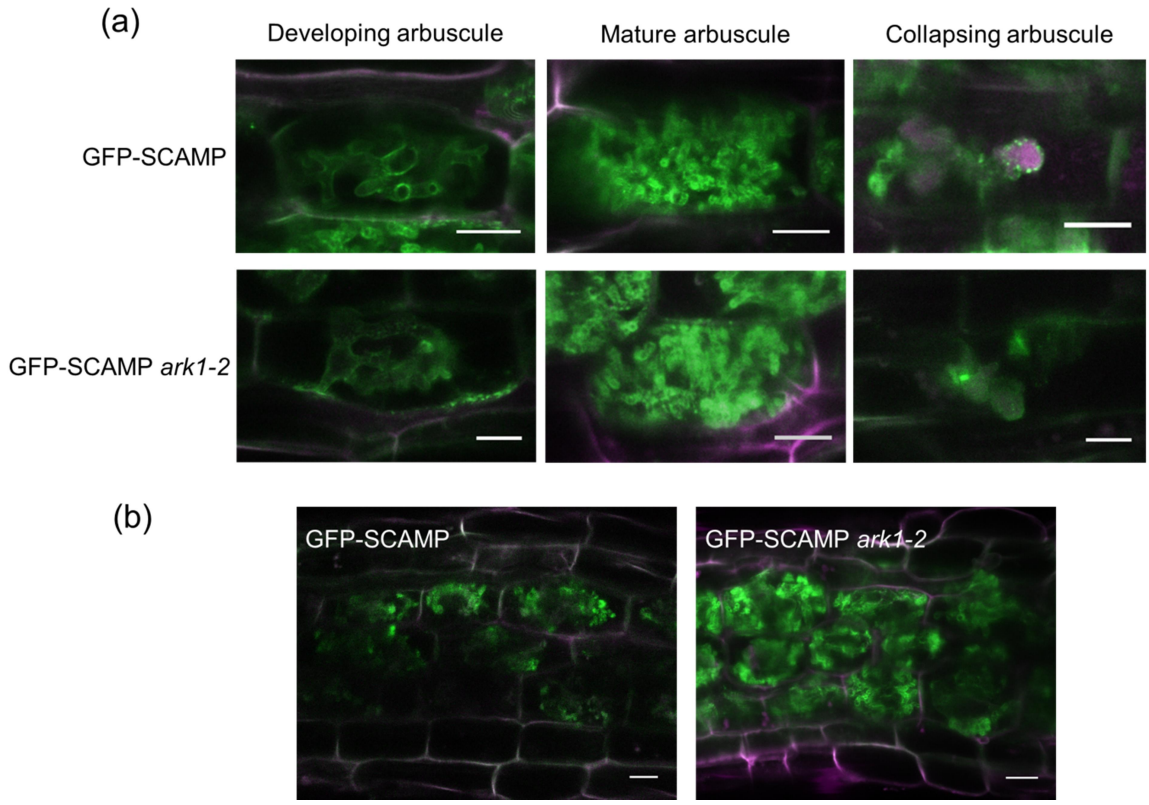

Figure 6. Live cell imaging of GFP-OsSCAMP *ark1-2* cross. Representative images are shown corresponding to stack projections of five slices. Three plants per genotype were screened per time point. (a) 6 wpi arbuscules of different developmental stages. Young arbuscules have coarse hyphae and low autofluorescence. Mature arbuscules display bright GFP-OsSCAMP signal. Autofluorescent collapsing arbuscules are amorphous and GFP-OsSCAMP accumulates in bright spots. (b) 14 wpi colonization patches show abundant GFP-OsSCAMP signal localizing to arbusculated cells hosting fully developed arbuscules. Scale bar: 10 µm.

3.3. Discussion

The transcriptional induction of *OsARK1* in mature stages of the AM symbiosis (Gutjahr et al., 2008) first suggested OsARK1 to be a signalling component operating in coincidence with the emergence and proliferation of arbuscules. As OsARK1 was found to localize specifically to the PAM surrounding fully developed to collapsing arbuscules (Roth et al., 2018), its putative signalling function conceivably centres on the plant-fungal symbiotic interface of arbusculated cells. *ark1* mutants have a reduced colonization phenotype with the most evident reduction being in vesicle numbers (Roth et al., 2018). Given that vesicle formation usually follows the formation of arbuscules and precedes the formation of new extraradical hyphae and daughter spores, it could be possible that *ark1* mutants harbour AM fungi unable to appropriately

complete their life cycle. The reduced colonization could be due to a disruption in the transfer of nutrients or signals to the fungus or impairment in intrinsic processes occurring in the plant cells harbouring arbuscules. As vesicles are lipid storage structures, it was hypothesised that nutrient dynamics are disrupted in the mutant. To dissect this, a nurse plant experiment was set up where a common mycorrhizal network was established between wild-type and *ark1* mutant plants. Colonization levels were fully restored in mutants growing alongside wild-type plants suggesting that the ultimate phenotypic consequence of *OsARK1* impairment is the plant been unable to transfer either nutrients or signals to the AM fungus affecting its fitness.

Interestingly, arbuscule morphology is not affected in *ark1* mutants. A mutant of the *ARK1* orthologue in *M. truncatula*, *KINASE 3* (*MtKIN3*, *Medtr7g116650*) was similarly shown to display reduced colonization levels when inoculated with the AM fungus *Diversispora epigaea* (Bravo et al., 2016). No defects in arbuscule development were reported for *kin3* suggesting ARK1 to have similar AM symbiosis functions in monocots and eudicots. The *ark1* phenotype contrasts with that seen in mutants of known genes functioning in nutrient dynamics in arbusculated cells, which usually display aberrant arbuscules. This is for example the case of mutants involved in Pi transfer (Javot et al., 2007; Yang et al., 2012), lipid nourishment (reviewed in Keymer and Gutjahr, 2018) and sugar transfer to the symbiotic fungus (An et al., 2019). The molecular components conditioning these processes are likely required for arbuscule development. OsARK1 in contrast, functions post-arbuscule development, probably by controlling processes related to arbuscule collapse or in novel nutrient delivery pathways different to the ones described so far. If OsARK1 conditions alternative nutrient delivery pathways, the metabolic destination of such nutrients would be to fuel subsequent colonization as opposed to nourishing arbuscules for their own development. AM colonization in *ark1* mutants is not abolished but reduced and a plausible scenario to explain this would be that the lipids contained in the spores used as inoculum have the capability of fuelling initial colonization. As this carbon supplement gets exhausted and in the absence of adequate nourishment to the symbiotic fungus in the mutants, this could lead to the observed depression in colonization levels over time.

The two *ark1* mutant alleles are predicted to result in a dysfunctional kinase domain which has otherwise all hallmarks of active kinases. Specifically, the mutations are

predicted to result in a lack of the F helix in the C-lobe which has been regarded as the organizing element of the entire kinase core, stabilizing the catalytic and regulatory spines of active kinases (Taylor and Kornev, 2011). In the absence of any discernible extracellular region, it is likely that OsARK1 functions as a co-receptor at the PAM relying on partnership with other signalling components and that its primary role might be to phosphorylate a substrate triggering an as-yet-unknown downstream symbiotic signalling transduction cascade.

Chapter 4

Identification of the novel SPARK domain revealed that *ARK1* coevolved with its paralogue *ARK2*

4.1. Introduction

A common feature of RLKs as hubs for signal transduction is their operation at complexes, often at highly compartmentalized membrane domains (Jaillais and Ott, 2020). While in some cases oligomerization is required for extracellular ligand binding, in others perception and signal transduction are uncoupled relying on specialized RLKs that then activate co-receptors to allow for intracellular signal transduction (Gou and Li, 2020). From work in the symbiosis and immunity fields, RLK complexes sensing microorganisms have mostly been described to carry LysM or LRR domains in their extracellular regions (Zipfel and Oldroyd, 2017). For undescribed types of RLKs such as *OsARK1*, studying the phylogenetic relationships and commonalities with other RLKs may help understand its role in symbiotic signalling circuits.

The symbiotic RLK *OsARK1* belongs to an uncharacterized group of receptor-like kinases, the Unknown Receptor Kinase-2 (URK-2) subfamily (Lehti-Shiu and Shiu, 2012). Two other rice genes besides *OsARK1* belong to this subfamily; *LOC_Os04g39180* and *LOC_Os07g12480*. The closest homologue of *OsARK1* corresponds to *LOC_Os04g39180*. A recent LCM dataset in rice shows this gene to be transcriptionally induced in arbusculated cells similarly to *OsARK1* (Roth et al., 2018). A broad transcriptomic study identified rice genes induced upon *R. irregularis* colonization and named them according to the level of upregulation compared to mock-inoculated plants (e.g. *OsAM1* is the most upregulated gene). While *OsARK1* was the 14th most highly induced gene of over 200 (*OsAM14*), *LOC_Os04g39180* (*OsAM124*) was upregulated to a lower degree

(Güimil et al., 2005). Both, *OsARK1* and *LOC_Os04g39180* have been described via phylogenomics approaches to be present in AM competent plant species and absent in plant clades that have lost the ability to establish symbiosis with AM fungi (Bravo et al., 2016). In *M. truncatula*, the closest homologue of *MtARK1/KIN3* corresponds to *MtKIN6* (*Medtr6g007690*) (Bravo et al., 2016), which according to the transcriptome dataset of Luginbuehl et al., (2017) is induced in AM conditions albeit to a lower degree than *MtARK1/KIN3* (fold change values AM vs non-AM conditions of 43 and 19 respectively at 4 wpi). The other URK-2 subfamily member in rice, *LOC_Os07g12480*, has no known AM colonization-dependent gene induction.

In this chapter, bioinformatics-based protein domain inspections coupled with phylogenetic analyses were performed to further understand the relationship between the members of the URK-2 subfamily. It was found that *OsARK1* and *LOC_Os04g39180* are paralogues and that the occurrence of an undescribed domain across their orthologues traces an ancient path of parallel evolution.

4.2. Results

4.2.1. *ARK1* and *ARK2* are ancient paralogues

OsARK1 shares a 40% identity at the protein sequence level with its closest homologue LOC_Os04g39180. Both proteins are predicted to lack an extracellular domain (ED) and LOC_Os04g39180 is predicted to lack a predicted signal peptide for secretion. The other URK-2 subfamily member, *LOC_Os07g12480*, is predicted to encode a protein harbouring a 250 amino acid-long ED (Fig. 7).

To compare the three RLKs belonging to the URK-2 subfamily, protein sequences from OsARK1, LOC_Os04g39180 and LOC_Os07g12480 orthologues were retrieved from the iTAK database (Zheng et al., 2016). This database classifies protein kinases from publicly available plant genomes into the different subfamilies established by Lehti-Shiu and Shiu (2012). A phylogenetic tree was constructed using the kinase domain protein sequences for the alignment. URK-2 RLKs from one plant species per order were chosen to achieve a balanced representation. Given the underrepresentation of non-flowering plants and basal angiosperms in sequenced genomes, orthologues in

these groups were surveyed across the One Thousand Plant Transcriptomes (1KP) database (Leebens-Mack et al., 2019) and included in the tree.

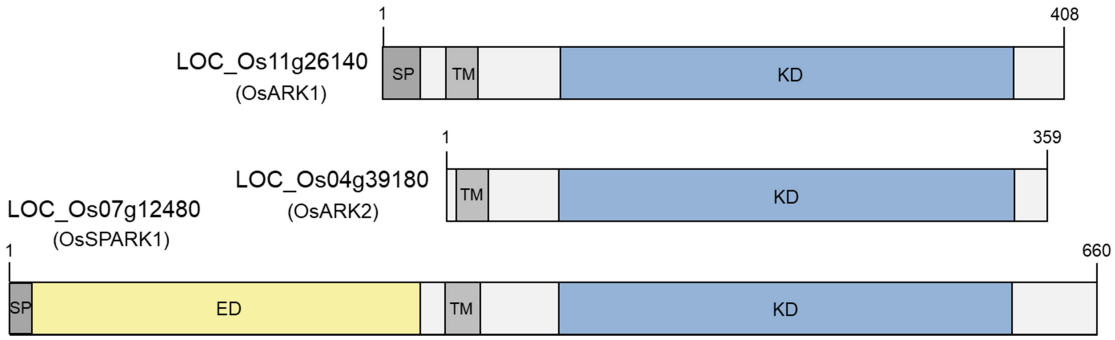

Figure 7. Predicted protein domain architecture of rice URK-2 subfamily members. Signal peptides and transmembrane regions were predicted with Phobius (http://phobius.sbc.su.se/) and kinase domains with ScanProsite (https://prosite.expasy.org/scanprosite/). SP, signal peptide; TM, transmembrane region; KD, kinase domain; ED, extracellular domain.

The phylogenetic analysis confirmed the close relationship between *OsARK1* and *LOC_Os04g39180*, the two occurring in most flowering plants (Fig. 8a). However, in non-flowering plants a single protein equally similar to OsARK1 and LOC_Os04g39180 occurs. For instance, the *M. paleacea* orthologue has 40 and 46% protein sequence identity to OsARK1 and LOC_Os04g39180 respectively. Thus, *OsARK1* and *LOC_Os04g39180* define two ancient paralogue groups arising from duplication before or early in angiosperm evolution. Accordingly, the single representative found in non-flowering plants was named *ARK* while the *OsARK1* paralogue, *LOC_Os04g39180*, was named *OsARK2*. Interestingly, *ARK2* duplicated in eudicots giving rise to a distinctive gene, *ARK2-LIKE*. Orthologues of the other URK-2 member in rice, *LOC_Os07g12480*, were present in non-flowering plants (Fig. 8A). This gene was named *OsSPARK1* which stands for *SIMILAR PROTEIN TO ARK 1*.

Further retrieval of protein sequences extended to one plant species per genus enabled to map the RLKs occurrence across different plant clades (species inspected are listed in Appendix Table 3). A synthesis of the findings is displayed in Fig. 8b and detailed in the following paragraphs.

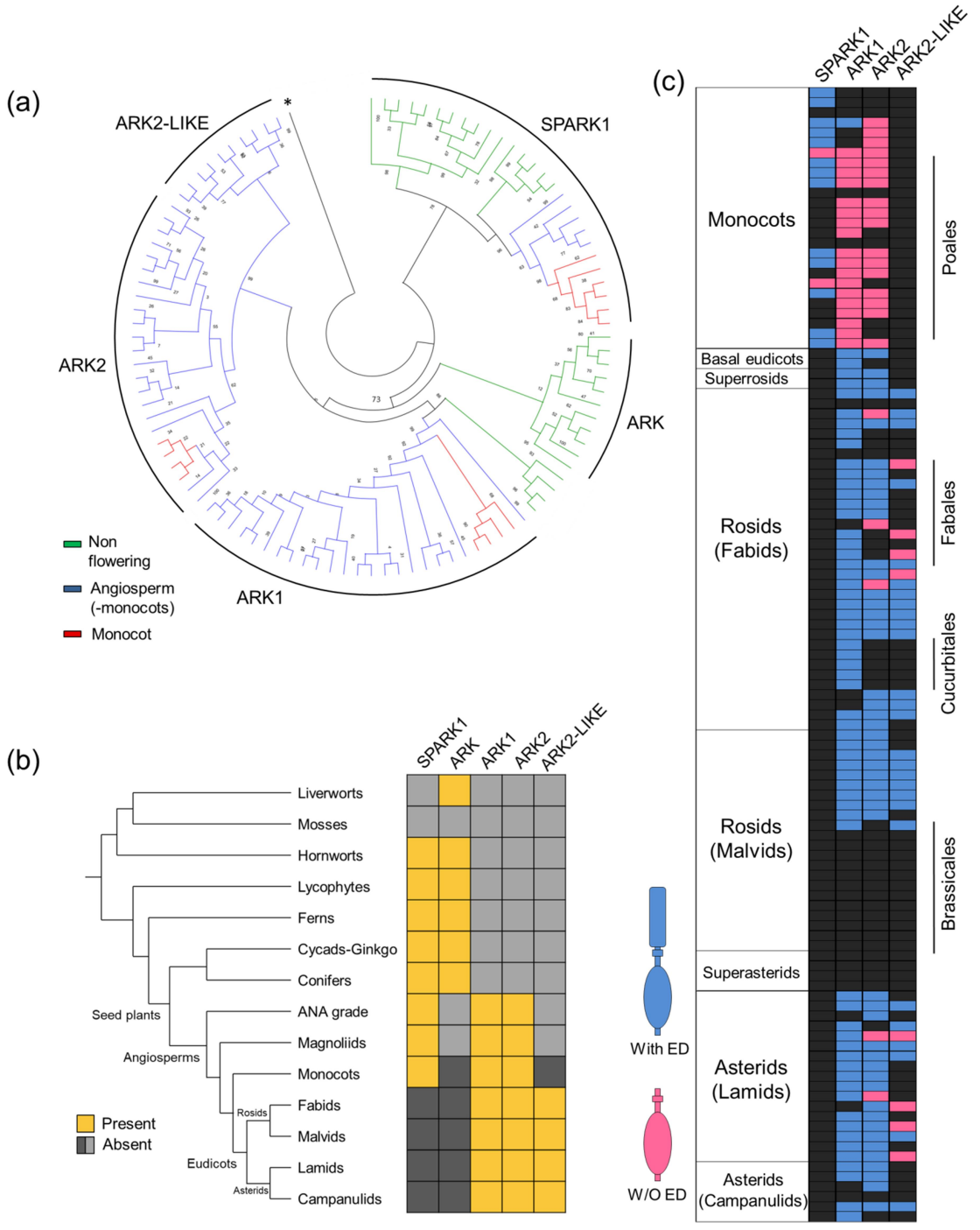

Figure 8. Occurrence of URK-2 RLK subfamily members and their extracellular domains in land plants. (a) ARK clade occurs only in non-flowering plants and it is phylogenetically distinct from the clade supporting ARK1, ARK2 and ARK2-LIKE (bootstrap value 73). Phylogenetic analysis was carried out using maximum likelihood method and 1000 bootstrap replicates over a kinase domain alignment (*, outgroup, a *Chlamydomonas reinhardtii* protein kinase (UniProt ID: A8IVV6). (b) Consensus pattern of occurrence of URK-2 subfamily members in different plant groups. When a given protein was not found in a clade represented by two or less fully sequenced genomes, light grey shade was used to account for uncertainty of absence. (c) One plant species per genus was selected over the angiosperms genomes to record the presence (blue) or absence (pink) of the extracellular domain (ED) on members of the URK-2 RLK subfamily. Black squares, protein not found. A detailed version of this figure with species names can be found in Appendix Table 3.

In bryophytes that do not form AM symbioses such as *Marchantia polymorpha*, *Physcomitrella patens* and *Sphagnum fallax*, no URK-2 member was found. In the AM competent liverwort *M. paleacea*, *ARK* was present. In hornworts, both *ARK* and *SPARK1* were detected. In ferns and lycophytes both *ARK* and *SPARK1* were found but non-AM ferns from the Salviniales only had *SPARK1*. The occurrence of *ARK* and *SPARK1* was also detected in gymnosperms.

The basal angiosperm *Amborella trichopoda* (Amborellales) and the magnoliid *Cinnamomum micranthum* (Laurales) are the basalmost plant species where *ARK* is not found, but is instead replaced by the paralogues *ARK1* and *ARK2*. In these species *SPARK1* also occurs.

In the basal eudicots *Aquilegia coerulea* and *Macleaya cordata* (Ranunculales) no *SPARK1* orthologue was found. However, through 1KP database searches a *SPARK1* orthologue was identified in *Hibbertia grossulariifolia* from the Dilleniales, a sister group of superrosids and superasterids and therefore basal among core eudicots. *ARK1* and *ARK2* are also present in basal eudicots. *ARK2-LIKE* does not occur in basal eudicots such as *Aquilegia coerulea* (Ranunculales) but it is present in the derived clades rosids and asterids suggesting *ARK2-LIKE* to appear early in the evolution of core eudicots. Thus, *SPARK1* and *ARK2-LIKE* do not co-occur in extant land plants as the former is absent in core eudicots and the later first appeared in this group.

AM competent core eudicots from the rosids and asterids have *ARK1*, *ARK2* and *ARK2-LIKE*. On the other hand, non-AM clades such as the Brassicales lack the three genes (papaya being the exception as it is AM competent, Khade et al., 2010). Curiously, neither *ARK2* nor *ARK2-LIKE* were found among the Cucurbitaceae (represented by five AM competent species) while *ARK1* was always present in this family. In addition, a particular scenario was found in legumes where the Phaseoloids *Cajanus cajan*, *Vigna angularis* and *Phaseolus vulgaris* had lost *ARK2-LIKE* and retained *ARK2*. The opposite situation occurred in members of the Inverted repeat-lacking clade (IRLC) such as *Cicer arietinum* and *M. truncatula* which had lost *ARK2* and retained *ARK2-LIKE*. Thus, *MtKIN6*, although the closest orthologue of *OsARK2* actually corresponds to *ARK2-LIKE* which is not present in monocots.

Among monocots, *ARK1* is present in AM and absent in non-AM monocot species in line with the findings of Bravo et al., (2016). *ARK2* is similarly present among AM

monocots and absent in non-AM monocots. However, an exception was found in orchids which engage in an alternative non-AM type of fungal endosymbiosis (Dearnaley et al, 2016). Here, *ARK2* but not *ARK1* was found in *Dendrobium officinale* and *Phalaenopsis equestris*. *SPARK1* tends to be generally present in monocots but some groups inside the Poales such as the Pooideae subfamily where *B. distachyon* belongs have lost this gene. In addition, *SPARK1* occurrence seems to be independent of the AM competence of the plant species (e.g. it is present in non-AM Alismatales such as duckweed (*Lemna minor*) and orchids).

In summary, angiosperm *ARK1*, *ARK2* and *ARK2-LIKE* seem to derive from a homologous *ARK* which is present among basal plants and their occurrence is associated with AM-competent plant clades. *SPARK1* on the other hand was lost in eudicots and its occurrence does not follow a plant clade AM competence pattern.

4.2.2. The occurrence of an ED-coding region among *ARK1* and *ARK2* orthologues suggest their parallel evolution

It was noted that the absence of a predicted ED in OsARK1 and OsARK2 is not a general property among their orthologues in land plants. Surveying for the presence or absence of the ED across URK-2 subfamily members revealed that ARK orthologues generally have an ED. With the emergence of *ARK1*, *ARK2* and *ARK2-LIKE*, however, the ED was found to be lost in distinctive patterns (Fig. 8c). Monocots in general lack an ED in ARK1 and ARK2. However, ARK1 was found to harbour an ED in *Xerophyta viscosa* (Pandanales) which is basal compared to the other monocots lacking the ED. As the arising of *ARK1* and *ARK2* occurred before the split of monocots from the rest of angiosperms, the finding of ARK1 harbouring an ED in basal monocots indicates this ED-coding region had been lost in *ARK1* and *ARK2* in independent evolutionary events. Contrary to the situation seen in ARK1 and ARK2 in monocots, SPARK1 mostly carries an ED (Fig. 8c).

In general, eudicot ARK1 orthologues always harboured an ED. Most ARK2 and ARK2-LIKE orthologues in eudicots were found to have an ED but in a minority of species the ED was absent (Fig. 8c). For example, MtKIN6/ARK2-LIKE along with its related

orthologue in *C. arietinum* are among the few ARK2-LIKE members that do not have an ED.

Altogether, although it seems that the duplication generating *ARK2* and *ARK2-LIKE* in the eudicots gave evolutionary plasticity to the retention or loss of the ED in the protein products, among AM monocots both *ARK1* and *ARK2* are consistently present and consistently lacking an ED-coding region. The independent losses of this ED-coding region in monocot *ARK1* and *ARK2* suggest them to be coevolving RLKs.

4.2.3. Identification of the ancient SPARK domain

Angiosperm genomes have an average of approximately 900 RLKs which harbour diverse ED configurations (Dievart et al., 2020). The ED present in URK-2 subfamily members has neither been defined nor predicted to exist as a domain of unknown function (DUF) by bioinformatics approaches. An alignment of the EDs of all URK-2 orthologues evidenced this domain to have a highly conserved signature arrangement of cysteine residues (Fig. 9a-c). This arrangement consists of two tandem cysteines close to the N-terminal region of the domain and a C××C motif towards the C-terminal region (Fig. 9d). The other eight cysteine residues are sparsely arranged and residues other than cysteines are lowly conserved. This newly described ED was named SPARK domain as SPARK1 is the only URK-2 subfamily member that consistently harbours it across its orthologues. Accordingly, the RLK subfamily URK-2 was renamed SPARK-I.

A sequence pattern search of the SPARK domain across public protein databases showed it to be present as an ED in other RLKs outside of the SPARK-I subfamily. These RLK subfamilies are seemingly unrelated to SPARK-I and correspond to the URK-1 (Unknown Receptor Kinase-1) and RKF3 (Receptor Kinase in Flowers 3). Members of these subfamilies are found across land plants regardless of their AM competence status. In rice, the URK-1 subfamily has three proteins, two of which harbour the SPARK domain. The third, devoid of extracellular and transmembrane regions has been regarded as a receptor-like cytoplasmic kinase (RLCK) according to a classification by Vij et al., (2008). All three RKF3 subfamily members in rice have the SPARK domain. No functional role was found to be described in the publically available literature for any of

the gene products. These five SPARK domain-containing rice RLKs were named OsSPARK2 to OsSPARK6. Table 2 lists them along with their *A. thaliana* homologues.

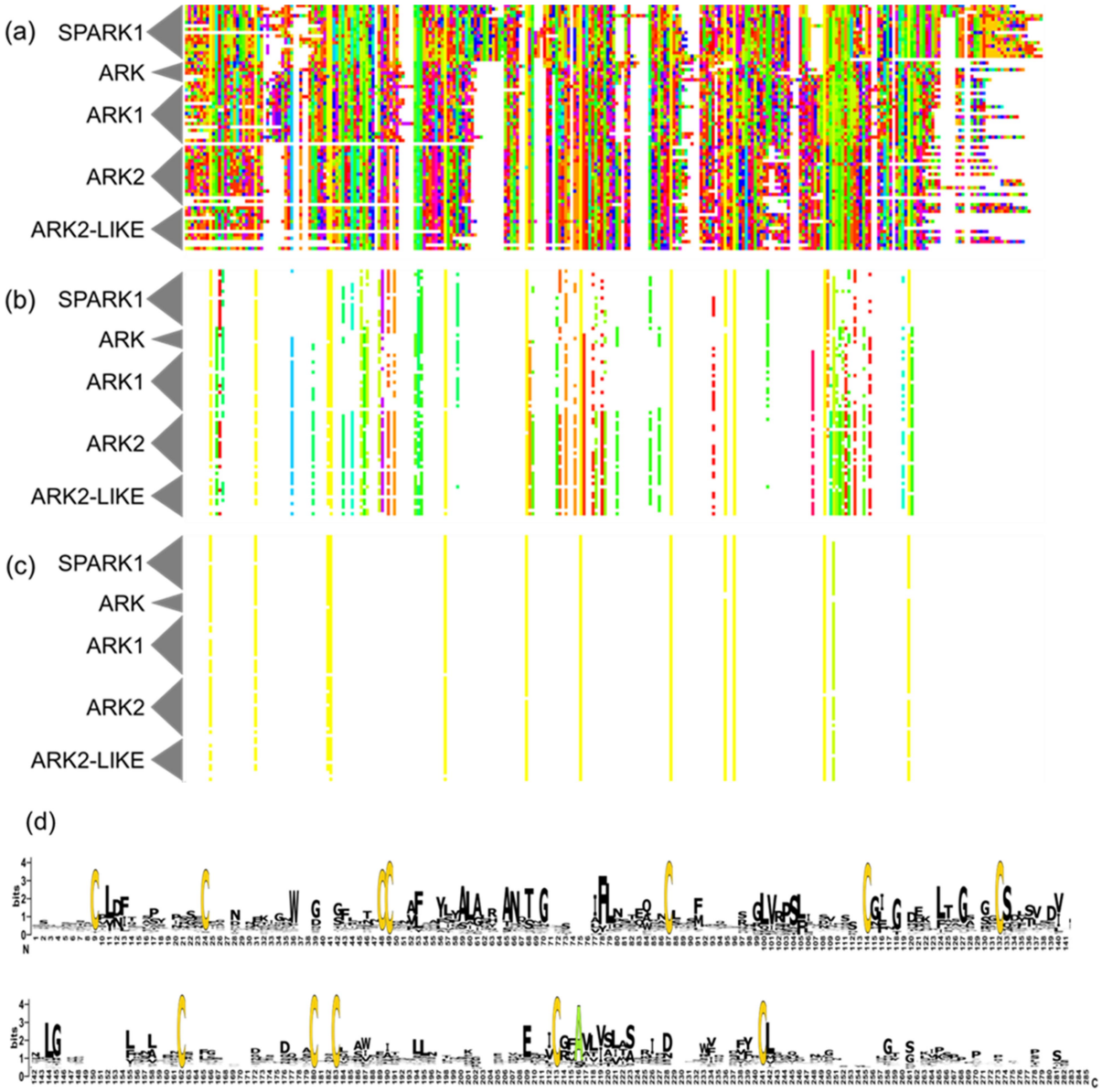

Figure 9. The SPARK domain. (a) Alignment of the extracellular domains of URK-2 (=SPARK-I) subfamily members. Amino acids are colour coded according to Taylor scheme in Jalview. (b) Residues conserved in 40% of the sequences are colour coded as before. (c) Residues conserved in 80% of the sequences are colour coded as before. (d) Sequence logo of the SPARK domain. Conserved residues in 80% of the sequences are coloured, most of them being cysteines.

Table 2. Members of the RLK subfamilies containing the SPARK domain in rice and Arabidopsis. Genes encoding proteins harbouring the SPARK domain are shaded in blue. Pink shading indicates absence of the SPARK domain.

RLK subfamily	Gene	*Oryza sativa* ID	*Arabidopsis thaliana* ID
SPARK-I (Ex URK-2)	*ARK1*	*LOC_Os11g26140*	no orthologue
	ARK2	*LOC_Os04g39180*	no orthologue
	SPARK1	*LOC_Os07g12480*	no orthologue
URK-1	*SPARK2*	*LOC_Os04g59320*	*AT1G49730 AT3G19300*
	SPARK3	*LOC_Os04g35114*	no orthologue
	RLCK223	*LOC_Os07g06570*	*AT5G22050*
RKF3	*SPARK4*	*LOC_Os05g34950*	*AT1G11050*
	SPARK5	*LOC_Os01g66020*	
	SPARK6	*LOC_Os01g28730*	*AT2G48010*

A SPARK domain multiple sequence alignment was used to build a HMM and search homologous sequences against the UniProt reference proteomes database as described in El Gebali et al., (2019). A Pfam entry was subsequently created for the SPARK domain (Pfam ID: PF19160, available in https://pfam.xfam.org/family/PF19160). The average length of the domain is 168 amino acids and is present in a total of 1,758 protein sequences in UniProt (accessed on June 2020). The SPARK domain was confirmed to occur only in streptophytes (embryophytes and charophytes). 896 of these proteins were RLKs. Surprisingly, more than 10% of the small repertoire of around 90 RLKs of the charophyte algae *Klebsormidium nitens* had the SPARK domain. Based on kinase domain homology, these *K. nitens* RLKs appeared to be unrelated to land plant SPARK domain-containing RLKs (Fig. 10). Interestingly, the domain architecture of the majority of these *K. nitens* RLKs consist in two tandemly arranged SPARK domains (Fig. 10). This is a unique feature not found in land plants with the exception of one *Physcomitrella patens* RLK (UniProt ID: A0A2K1JMC3).

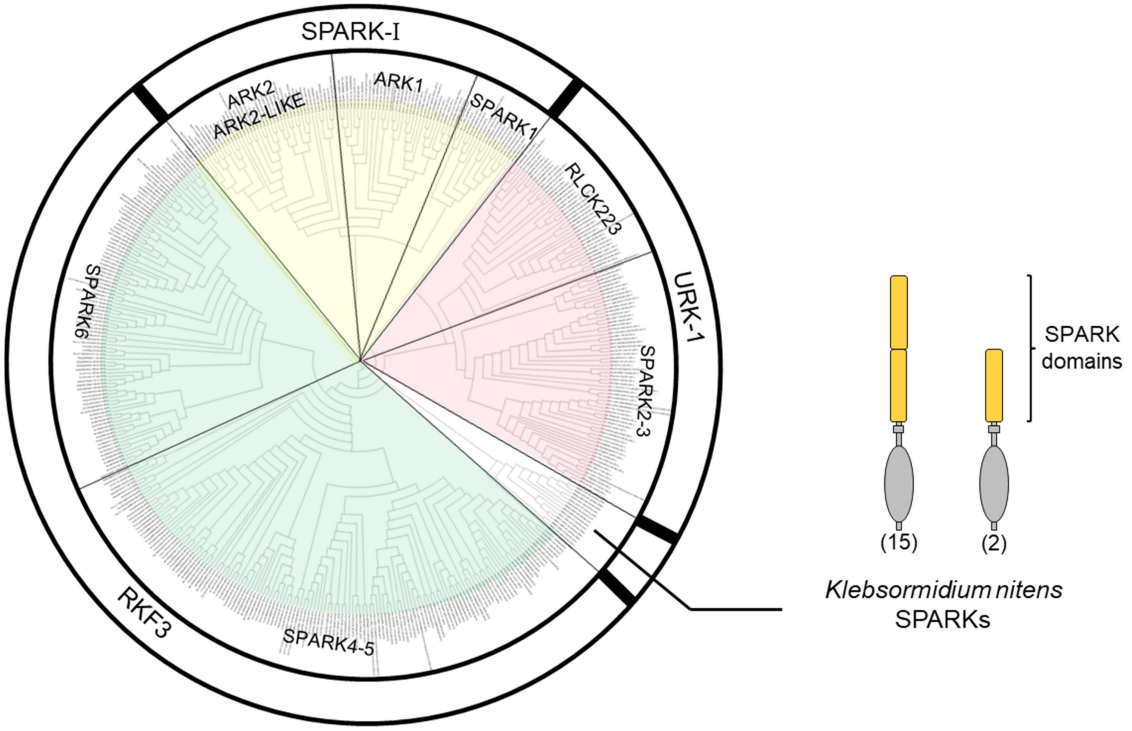

Figure 10. Phylogenetic tree of SPARK domain-containing RLKs. The RLK subfamilies SPARK-I, URK-1 and RKF3 in addition to RLKs from the charophyte algae *Klebsormidium nitens* are included. Phylogenetic analysis was carried out using maximum likelihood method and 1000 bootstrap replicates over a kinase domain alignment. Numbers in parentheses indicate the number of RLKs found to harbour one or two SPARK domains.

Besides constituting the ED of RLKs, 826 proteins had the SPARK domain as its sole domain. In the majority of these cases, the SPARK domain was flanked by a signal peptide and a GPI anchor site but without an intracellular kinase domain, matching the configuration of receptor-like proteins (RLPs). This domain architecture was found only in angiosperms and was represented by five rice members, named OsSPARK7 to OsSPARK11 (Fig. 11). Of these, OsSPARK9 (LOC_Os07g01240) has been previously characterized and corresponds to SEMI-ROLLED LEAF1 (OsSRL1, also known as CURLED LEAF AND DWARF 1, OsCLD1) (Xiang et al., 2012; Li et al., 2017). *OsSRL1* is a ubiquitously expressed gene whose mutation results in decreased cellulose and lignin contents accompanied by defects in cell wall formation (Xiang et al., 2012; Li et al., 2017).

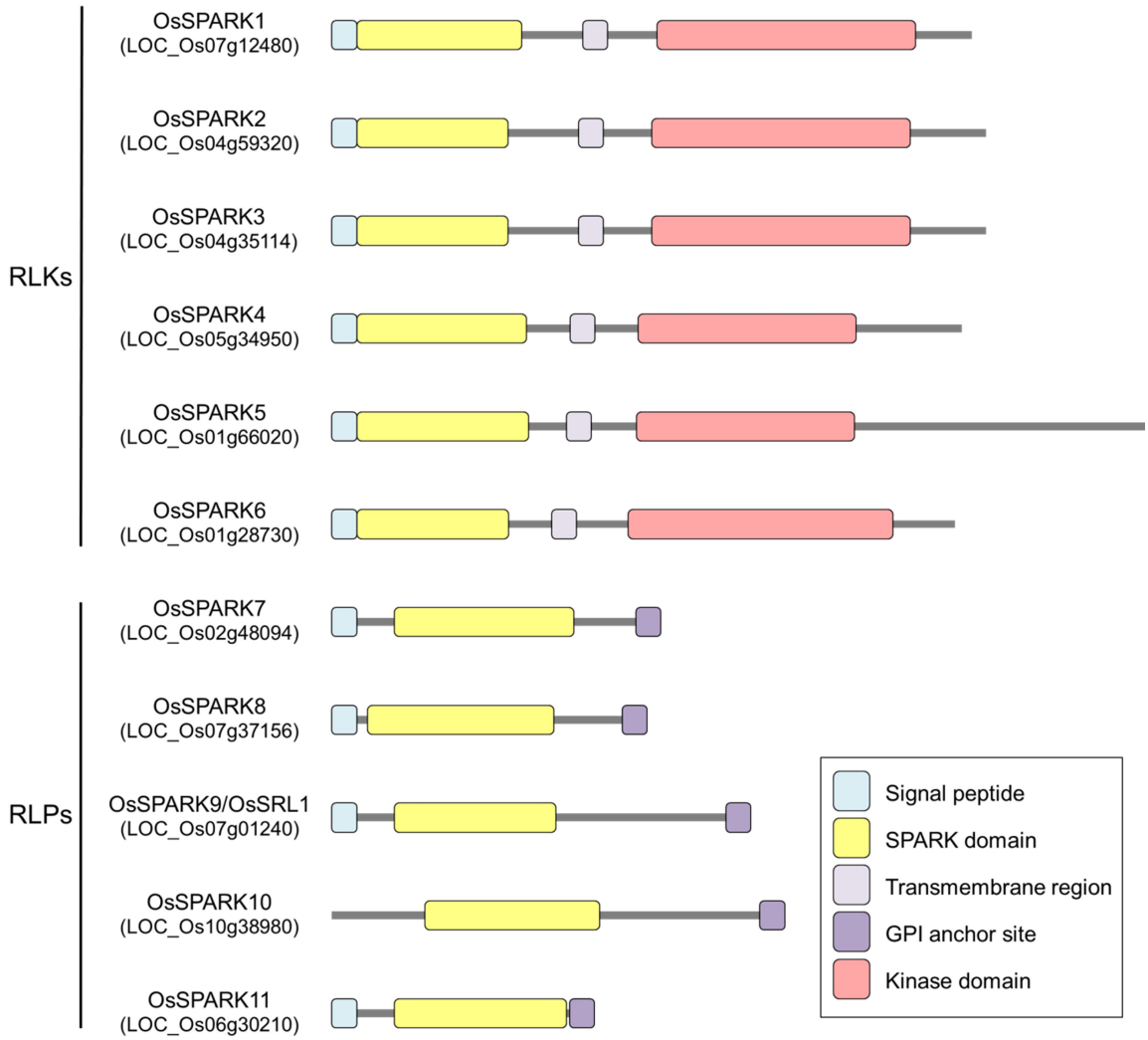

Figure 11. Protein domain architecture of SPARK domain-containing proteins in rice. Protein IDs are shown in parenthesis. Domain architectures are reproduced from Pfam. Differences in length of protein domains occur as some sections of the protein sequences are below the identity threshold of the consensus Pfam protein domain sequence. Motifs (signal peptides, transmembrane regions and Glycosylphosphatidylinositol (GPI) anchor sites) were predicted using Phobius and PredGPI. RLKs, receptor-like kinases; RLPs, receptor-like proteins.

M. paleacea is the basalmost AM plant species with genome sequenced (Radhakrishnan et al., 2020) and has one member in the SPARK-I subfamily, MpARK, which has a SPARK domain. To confirm the predicted cDNA sequence of *MpARK*, colonized *M. paleacea* thalli (Fig. 12a-c) were used for RNA extraction and cDNA synthesis. High-fidelity PCR and electrophoresis showed a band amplifying the 1,926 bp fragment corresponding to *MpARK* cDNA, which was confirmed by Sanger sequencing

(Fig. 12d). This product was used to clone the *MpARK* SPARK domain into a vector suitable for future crystallography work and pull down assays.

Altogether, these findings demonstrate the SPARK domain to be ancient and that it has been retained in a few RLK subfamilies in angiosperms, including those belonging to the symbiosis related SPARK-I subfamily. The pattern of occurrence of the SPARK domain among plant clades and SPARK-I subfamily members suggest their differential plant clade-dependent regulatory processes operating during AM symbiosis.

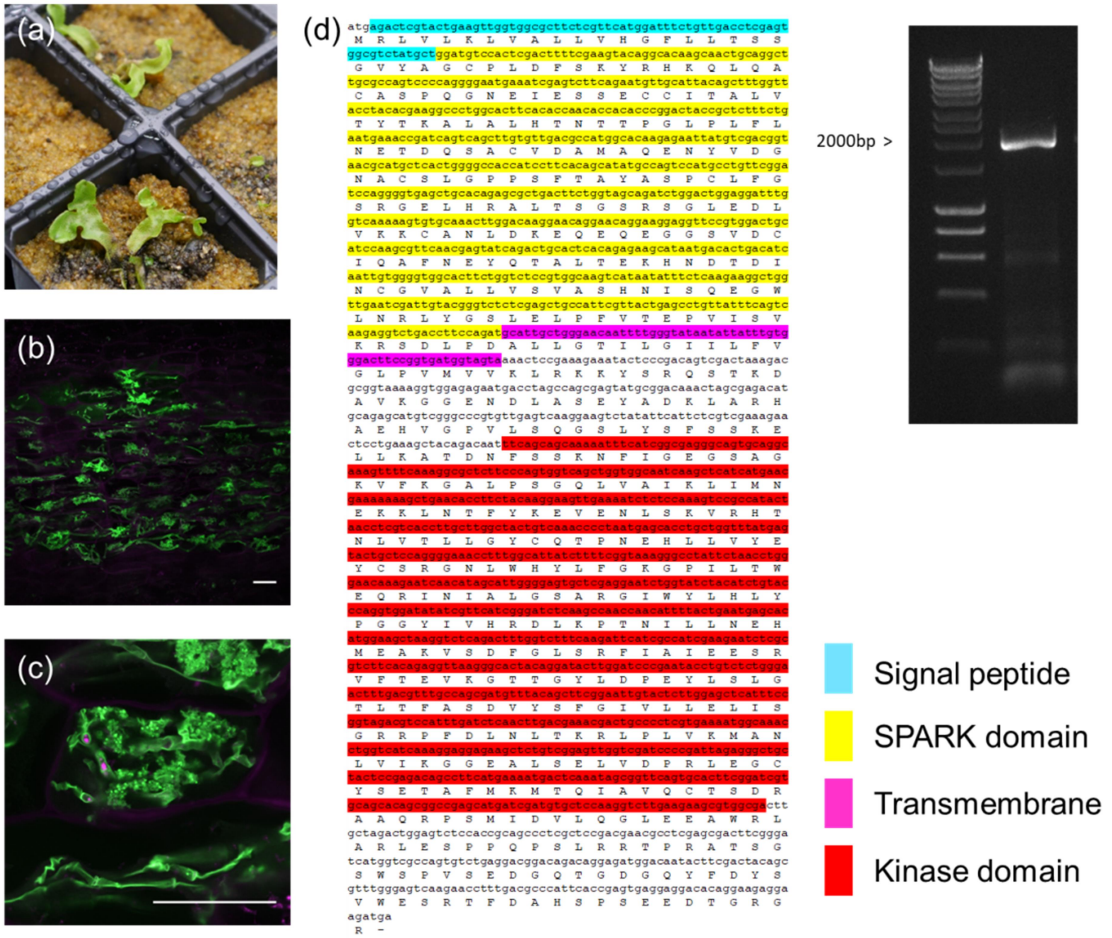

Figure 12. cDNA sequencing of *Marchantia paleacea ARK*. (a) Ten weeks post inoculation *M. paleacea* thalli. (b) Wheat germ agglutinin-Alexa Fluor™ 488-stained *M. paleacea* thalli displaying profuse colonization by the AM fungus *Rhizophagus irregularis*. (c) Detail of a fungal arbuscule in a thalloid cell (Scale bars in b-c: 50 µm). (d) Sequence of *MpARK* cDNA (1,926 bp length) confirmed by Sanger sequencing. Alignment to the amino acid sequence and agarose gel electrophoresis are shown.

4.2.4. Features in the kinase domains of SPARK-I subfamily members suggest differential roles

While the SPARK domain has been lost among SPARK-I subfamily members in some plant clades, transmembrane and kinase domains are ubiquitous. By inspecting conservation of kinase domain sequences, all features of active kinases could be found. Fig. 13 shows conserved residues among all SPARK-I subfamily orthologues, displayed as a function of the rice representatives. The HDR motif of the catalytic loop, DFG motif from the Mg^{2+} binding loop and APE motif were all highly conserved. In addition, four positions were found to be uniquely present in one or two of the paralogues. Most of those positions are in the catalytic and activation loops. The kinase domain of ARK2-LIKE differentiated from ARK2 and the other paralogues in that it invariably carries a proline three residues downstream of the gatekeeper residue (Fig. 14). This position is occupied by diverse residues in the other paralogues but ARK2 never harbours a proline in that position. These findings suggest SPARK-I subfamily members to be active kinases differentially functioning at the level of phosphorylation.

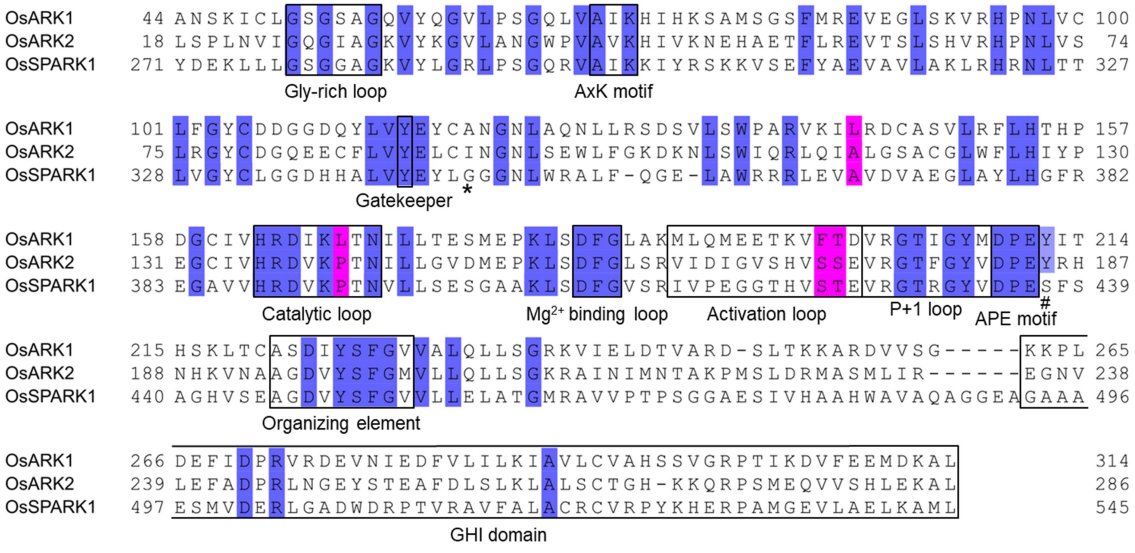

Figure 13. Kinase domain alignment of SPARK-I subfamily members in rice. Important kinase motifs are boxed. Blue coloured residues are shared among ≥ 90% of ARK1, ARK2 and SPARK1 orthologues collectively (using all orthologue sequences found in this study). Purple coloured residues denote those conserved among ≥ 90% of ARK1, ARK2 and SPARK1 orthologues separately and differing across at least one of the other two paralogues. *, position occupied by an invariable proline among ARK2-LIKE orthologues (see Fig. 14). #, Serine is invariable at this position among monocot SPARK1 but tyrosine prevails in other plant clades.

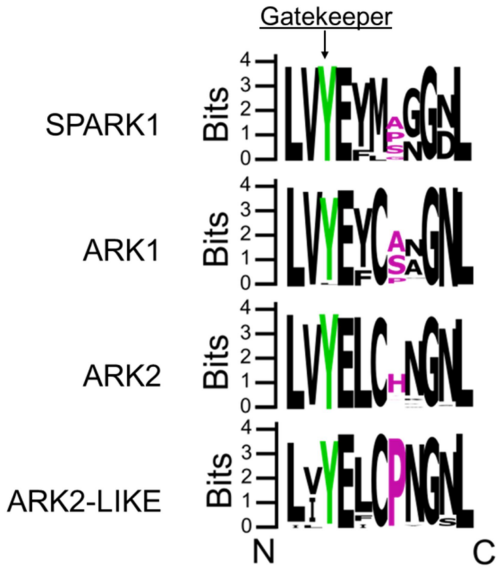

Figure 14. Sequence logo of kinase domain hinge region of SPARK-I subfamily members. Sequence logo was created using all orthologue sequences found in this study. The hinge region contains the gatekeeper tyrosine residue (shown in green). Position with invariable proline in ARK2-LIKE is shown in purple.

4.3. Discussion

The closest homologue of *OsARK1* is *OsARK2*. They are both predicted to be functional RLKs and both are transcriptionally induced in arbusculated cells (Roth et al., 2018). They also have some differences. *OsARK2* is transcriptionally induced in AM conditions at a lower extent than *OsARK1* (Güimil et al., 2005) and *OsARK2* does not have a signal peptide for secretion. *ARK1* and *ARK2* are both described to be conserved across AM competent plant clades and absent in non-AM clades (Bravo et al., 2016). However in the study of Bravo et al., (2016) *ARK2* and *ARK2-LIKE* were not distinguished as separated genes and in some cases only one of the paralogues is present (e.g. in some legumes). It is therefore more exact to indicate that in general, AM competent eudicots either have *ARK2* and/or *ARK2-LIKE*. An exception for this was detected, however, in the AM competent Cucurbitaceae which lack *ARK2* and *ARK2-LIKE*. This may reflect special symbiotic processes taking place in this particular plant family. Regarding the absence of *ARK2* from non-AM plant genomes, an exception was also found in orchids. *ARK2* but not *ARK1* is present in the genomes of the orchids *Dendrobium officinale* and *Phalaenopsis equestris*. Orchid mycorrhiza is a specialized

type of association orchids develop with non-Glomeromycotina fungi where highly coiled hyphae called pelotons are formed inside orchid parenchyma cells (Dearnaley et al, 2016). These pelotons are ephemeral structures in analogy to AM arbuscules. An RNA-seq study aiming to identify symbiotic genes from the orchid *Bletilla striata* surveyed for the *OsARK1* orthologue. The resulting gene (ID: *DN57616_c4_g2_i16::g.52598::m.52598*), although named *BsAM14*, in fact corresponds to the orthologue of *OsARK2* and is induced during symbiosis with the orchid mycorrhizal fungus *Tulasnella* sp. (Miura et al., 2018). Overall this suggests orchids had lost *ARK1*, as it had happened to other plant clades loosing AM symbiosis competence (Bravo et al., 2016) but *ARK2* was retained in orchids. Some known AM symbiotic genes have been recently shown through phylogenomics approaches to be required for broad intracellular symbioses. These include *CCaMK*, *SYMRK* and *CYCLOPS* (Radhakrishnan et al., 2020) which are, similarly to *ARK2*, present in orchids. In addition, transcript levels of *OsARK2*, but not *OsARK1*, are activated and increased over time in rice roots inoculated with the rice blast fungus *Magnaporthe oryzae*, which develops a biotrophic growth phase in roots (Marcel et al., 2010). Altogether, these observations suggest that although related, ARK1 and ARK2 might not exert exactly the same function with ARK2 likely operating in other root endosymbioses besides the AM association.

ARK1 and *ARK2* are ancient paralogues arising from the duplication of *ARK*, which is present in extant non-flowering plants. The presence of *ARK1* and *ARK2* is a feature of AM competent angiosperms and they conceivably have complementary symbiotic functions which are fulfilled by *ARK* alone in non-flowering plants. By inspecting the kinase domain of *ARK1* and *ARK2* orthologues, there are four highly conserved residues unique to one or the other protein. Three of those residues are in the catalytic and activation loops that are in combination required for catalysis and stabilization of the active form of kinase domains (Nolen et al., 2004). Thus, the ancient duplication and subsequent retention for millions of years of the two paralogues may be explained by differential dynamics in protein phosphorylation. Exploring this exciting research avenue demands prior knowledge on protein targets for phosphorylation which are at the moment not known.

Interestingly, duplication of *ARK2* gave rise to *ARK2-LIKE* in eudicots which likely neo-functionalized to exert an additional function or, alternatively, the same function than

ARK2 in a different fashion. In line with this, ARK2-LIKE invariably has a bulky proline positioned three residues downstream of the gatekeeper residue while in the same position ARK2 has diverse residues but never a proline. In kinase domains, the gatekeeper residue locates at the partition between the two kinase lobes and regulates the architecture of the catalytic cleft by stabilization of the kinase domain regulatory spine (Taylor and Kornev, 2011). The area adjacent to the gatekeeper corresponds to the flexible hinge region and has been postulated to serve as an autoinhibitory molecular brake (Chen et al., 2007). As such, it is conceivable that ARK2 and ARK2-LIKE are both catalytically active but with different degree of stringency or efficiency for their activation. The observation that in dicots there are cases where only *ARK2* or only *ARK2-LIKE* are present suggests they may have overlapping functions.

ARK1, *ARK2* and *ARK2-LIKE* share the same subfamily with *SPARK1*. Unlike the former genes, there is no transcriptional or phylogenomics evidence to propose a symbiotic role for *SPARK1*. However, lack of AM-dependent gene induction does not necessarily reflect symbiotic dispensability. It is also interesting that *SPARK1* loss in eudicots coincided with the duplication of *ARK2* to generate *ARK2-LIKE* and that *SPARK1* was retained in monocots which had lost the ED in *ARK1* and *ARK2*. A symbiotic role for *SPARK1* however, remains highly speculative and the detection of *SPARK1* in the genomes of some non-mycorrhizal monocots (Alismatales) together with the lack of *SPARK1* in some AM-competent monocots such as *B. distachyon* suggest a non-essential or dedicated function, if any, in AM symbiosis. The generation and phenotypic characterization of mutants for this gene would help elucidate a putative AM symbiosis function.

The extracellular regions of members of the subfamilies under study harbour the previously undefined SPARK domain. Importantly, the occurrence of this domain across land plants showed *ARK1* and *ARK2* having coevolved despite their ancient split from *ARK*. A graphical summary of the occurrence of the SPARK domain across RLKs in the Streptophyta is displayed in Fig. 15. The SPARK domain was lost in monocots in both *ARK1* and *ARK2* in independent evolutionary events. This poses the intriguing question of what molecular processes are being orchestrated by the SPARK domain and why evolutionary pressure has prompted its parallel loss.

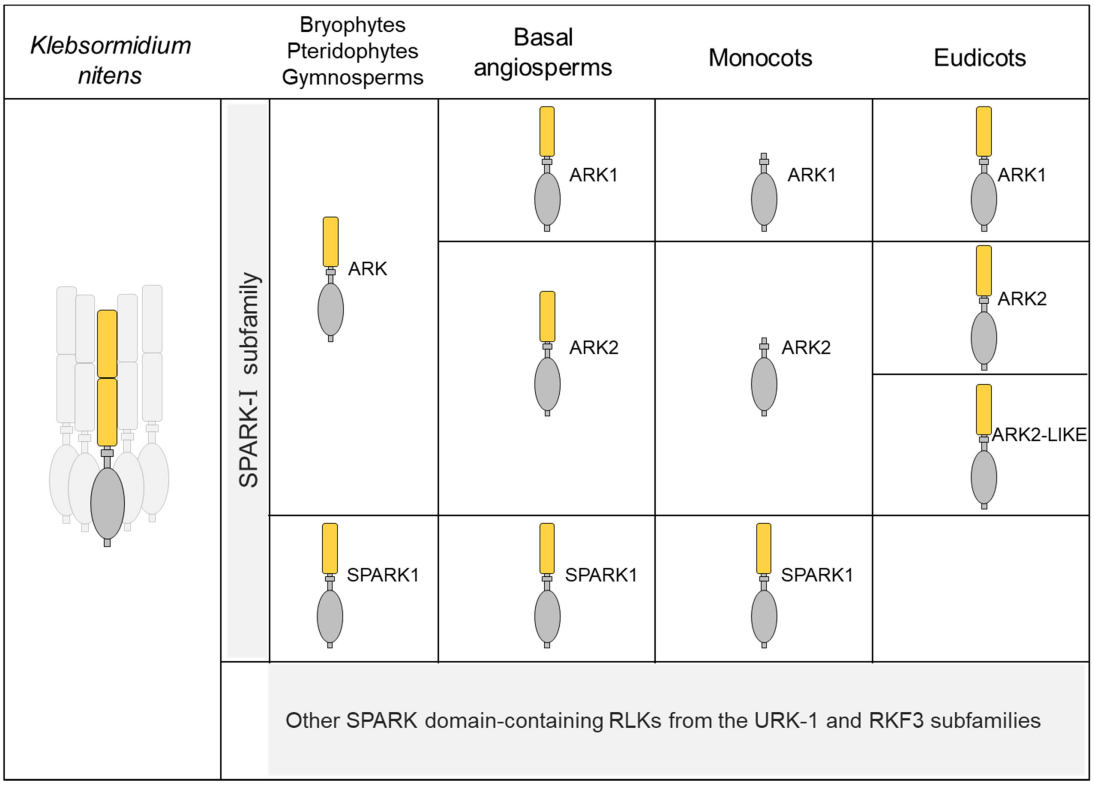

Figure 15. Occurrence of the SPARK domain across receptor-like kinases (RLKs) in the Streptophyta. The SPARK domains are shown in yellow and kinase domains in grey.

The sequence features of the SPARK domain do not resemble any other described domain with known structure and as such, homology modelling could not be performed. Protein alignments showed cysteine residues to be the most conserved feature of the SPARK domain. Cysteines follow a signature arrangement that is fundamentally different than other cysteine-rich EDs such as the ones present in the known Cysteine-rich Receptor-like Kinases (CRKs, Vaattovaara et al., 2019). It may be possible that the SPARK domain corresponds to a protein structure stabilized by disulphide bridges. Recently, an *A. thaliana* LRR RLK, *HYDROGEN PEROXIDE-INDUCED* CA^{2+} *INCREASES 1* (*AtHPCA1*), was described to sense hydrogen peroxide (H_2O_2) through H_2O_2-mediated oxidation of its conserved cysteine pairs in the ED (Wu et al., 2020). Similar dynamics can putatively occur for SPARK domain-containing RLKs. ARK1 in dicots always harbours a SPARK domain. If ARK1 localizes to the PAM in dicots similarly to the rice scenario (Roth et al., 2018), which can be suggested based on

similarities in mutant phenotypes and phylogenomics pattern of conservation among AM-competent plant species (Bravo et al., 2016), then the SPARK domain would face the PAS. The PAS is an apoplastic compartment of known acidic nature (Guttenberger, 2000). Acidification of the PAS is likely caused by proton pumps at the PAM fuelling nutrient exchange as arbuscule development progresses (Krajinski et al., 2014; Wang et al., 2014; Liu et al., 2020). As sulphur bond stability depends on pH, it is a possibility that the acidic environment of the PAS may change the stability of the SPARK domain as arbuscule development or nutrient exchange progresses. It could also be possible that the SPARK domain detaches in such conditions, leaving a protein resembling the ectodomain-less ARK1 present in monocots. If that is the case, ARK1 functioning in monocots would differ in that it lacks SPARK domain-mediated regulation prior to PAS acidification. Alternatively, H_2O_2-mediated mechanisms can also be envisioned for SPARK domain stability as arbuscule collapse involves an important burst of hydrolytic activity and oxidation of plant and fungal membranes (Floss et al., 2017). This would also be in line with the observation of aggregating peroxisomes around collapsing arbuscules (Pumplin and Harrison, 2009).

A publicly available Pfam entry was created for the SPARK domain which will conveniently allow monitoring all proteins containing it as they appear in public databases. While some ancient RLKs subfamilies have been subjected to remarkable expansion in angiosperms such as the LRR-containing RLKs (Man et al., 2020), it is interesting that the SPARK domain is present only in three relatively small RLK subfamilies. The SPARK-I subfamily (previously URK-2) being the focus of this study has normally no more than three members per species. Some species like the model *A. thaliana* is entirely devoid of the subfamily as *ARK1*, *ARK2* and *ARK2-LIKE* have been lost in non-AM plant species and *SPARK1* has been lost in eudicots. The other two RLK subfamilies that have retained the SPARK domain are the URK-1 and the RKF3. Upon its discovery, a gene from the RKF3 subfamily was first found to be expressed in flowers justifying the naming of the subfamily (Takahashi et al., 1998). Besides that, no functional data is available for any member of these two subfamilies. This may appear curious at first as the extensively studied *A. thaliana* has representatives in both subfamilies. However, the absence of distinctive gene expression patterns and the potential genetic redundancy of the few members within the two subfamilies have

likely prevented functional discoveries from both the reverse and forward genetics perspectives.

The surprising finding of the SPARK domain being present in RLKs of the charophyte algae *K. nitens*, mostly in a tandem arrangement indicates the SPARK domain being apt to function as a modular unit. An important representation of SPARK domain-containing RLKs was found in *K. nitens* and only three known domains have been documented to be present in the extracellular regions of RLKs in this species; the LRR, Calcium-dependent Lectin (C-LEC), and Proline-rich/extensin domains (Dievart et al., 2020). This highlights the SPARK domain being one of the ancient domains at the base of RLK evolution predating the appearance of the myriad of domain organizations seen in RLKs of higher plants.

The presence of the SPARK domain in *K. nitens* RLKs also indicates this domain to have originated before the onset of the AM association. A recent time-calibrated phylogeny places the origin of the Glomeromycotina to circa 660 million years ago, around 200 million years earlier than the possible origin of the AM symbiosis (Lutzoni et al., 2018). Although no charophyte-fungal association has been described, some genes from the so-called symbiotic "toolkit" are present in charophytes, including LysM RLKs which first appeared in this group (Delaux et al., 2015). It is also interesting that SPARK domain-containing RLKs were found only in the terrestrial *K. nitens*, which principally inhabits soil crusts but not in the aquatic *Chara braunii*. Whether the occurrence of the SPARK domain is associated with adaptation to terrestrial environments in the sister group of land plants can be explored as more streptophyte algae genomes inhabiting different environments are becoming available (Cheng et al., 2019; Jiao et al., 2020; Liang et al., 2020; Wang et al., 2020b).

In angiosperms, the SPARK domain also occurs in RLPs suggesting the putative signal perception capability the SPARK domain has, can potentially be uncoupled from intracellular kinase domain-mediated signal transduction in a same protein. This also suggests SPARK domain-containing proteins to be able to form protein complexes that would in conjunction complete an extracellular-to-intracellular signal transduction unit. The only SPARK domain-containing protein that has been functionally characterized in rice corresponds to one of these RLPs. OsSPARK9/OsSRL1 participates in maintenance of cell wall formation and several mutant alleles have been described

to have multiple morphological defects including rolled leaves (Xiang et al., 2012; Li et al., 2017). Besides a signal peptide, a GPI anchor site and a SPARK domain, OsSPARK9/OsSRL1 does not appear to have other protein domains or motifs. One of the *srl1* mutant alleles that had been investigated and that phenocopied other alleles corresponds to a point mutation leading to an amino acid substitution in the SPARK domain-coding region (Xiang et al., 2012), indicating the SPARK domain is likely directly involved in the biological processes modulated by OsSPARK9/OsSRL1. In light of these observations in rice and the presence of the SPARK domain in RLKs of *K. nitens*, it can be speculated that the SPARK domain assists in surveillance of cell wall dynamics, a process shared by plants and algae. In AM symbiosis, modulation of cell wall dynamics must be important as plant and AM fungal cell walls are both a barrier to overcome and a possible avenue for symbiont recognition (reviewed in Rich et al., 2014). During the initial stages of arbuscule development the plant needs to loosen its cell wall to allow AM fungal entry and plant cell wall continuity must be reinstated after arbuscule degeneration. Also, the AM fungal cell wall faces the PAS throughout arbuscule development which then collapses and degrades as arbuscules disappear. There is still much to learn about this newly described domain starting from its structural properties and potential ligands. From the AM symbiosis perspective, it would be interesting to link the presence or absence of the SPARK domain in symbiotic RLKs with particular subcellular mechanisms and its effect in overall AM symbiosis functioning.

Chapter 5

Investigating the symbiotic role of *OsARK2*

5.1. Introduction

OsARK1 and *OsARK2* are coevolving genes from the SPARK-I RLK subfamily (Chapter 4). Besides phylogenetic relatedness, OsARK1 and OsARK2 have comparable predicted protein structures, this is, predicted active kinase domains and absence of EDs. These observations suggest part of their functions may overlap. However, there are several features of *OsARK2* that are not shared with *OsARK1* including its comparatively lower AM-dependent transcriptional induction (Güimil et al., 2005; Roth et al., 2018), the lack of signal peptide and the conservation of specific residues in key motifs of the kinase domain (Chapter 4). Besides, the split of *ARK* that generated *ARK1* and *ARK2* is ancient and the two paralogues have retained conserved features across land plants. With few exceptions, all AM angiosperms have *ARK1*. Likewise, all AM angiosperms have *ARK2* and/or *ARK2-LIKE*, suggesting the two paralogues to play important symbiotic roles. As mutation of *ARK1* in rice and *M. truncatula* results in dysfunctional AM symbiosis (Chapter 3, Bravo et al., 2016; Roth et al., 2018), it is clear that ARK2/ARK2-LIKE and ARK1 do not exert a fully redundant function. It is still unclear, however, if OsARK2 partially complements OsARK1 function or whether it operates via entirely different mechanisms of action. Comparatively studying the two paralogues in AM symbiosis would help discern their commonalities and differences and potentially provide an explanation for their coevolution.

While a symbiotic function has been demonstrated for OsARK1 in post-arbuscule development regulation at the PAM (Chapter 3, Roth et al., 2018), no function is known for *OsARK2* or its orthologues. Given that *OsARK2* is transcriptionally induced in arbusculated cells (Roth et al., 2018), it may be possible that it functions in this particular cell type similarly to *OsARK1*.

In this chapter, *OsARK2* symbiotic role was investigated in a comparable fashion to *OsARK1* by employing an insertional mutant of *OsARK2* and by generating a double knockout (DKO). Time course colonization assays allowed establishing that *OsARK2* has a symbiotic role that is not equal to that of *OsARK1*. Post-arbuscule development dynamics in the mutants were further studied using lipid imaging and preliminary results suggested common alterations in arbusculated cells across genotypes. These findings suggest there are common and distinctive mechanisms underlying the regulation the two RLKs exert on the AM association.

5.2. Results

5.2.1. Molecular characterization of a Tos17 insertional *ark2* mutant in rice

A Tos17 insertional mutant allele of *OsARK2* was retrieved from a public collection (ID: NG0028, hereafter referred as *ark2*) (Miyao et al., 2003). PCR genotyping followed by Sanger sequencing of the purified gel electrophoresis band confirmed the presence of the insertion and its specific location in *ark2* (Fig. 16a-b). The Tos17 insertion locates in exon V between the first and second nucleotide of the codon encoding the universal Asp residue from the catalytic loop of the kinase domain (978 bp from first nucleotide of ATG). This mutation would render the protein dysfunctional for kinase activity and structurally compromised as translation would not proceed to generate crucial kinase motifs downstream of the insertion. RNA extraction and RT-PCR were carried out over wild-type and *ark2* mutant plants colonized by *R. irregularis* (10 wpi) to confirm perturbation of the transcript. Oligonucleotides were designed to amplify *OsARK2* cDNA upstream, spanning and downstream of the insertion. There were transcripts detected using primer pairs amplifying the region upstream of the insertion (Fig. 16c). There were no transcripts detected using oligonucleotides spanning the insertion suggesting either *OsARK2* transcription does not proceed beyond the Tos17 element or that it does but the Tos17 element is too long to be amplified by PCR. When using oligonucleotides downstream of the insertion, transcripts were detected suggesting that the Tos17 element may be transcribed or that there are promoter regions inside the

Tos17 element allowing downstream transcription (Fig. 16c). These results indicate that in the *ark2* mutant the Tos17 insertion perturbs *OsARK2* transcription.

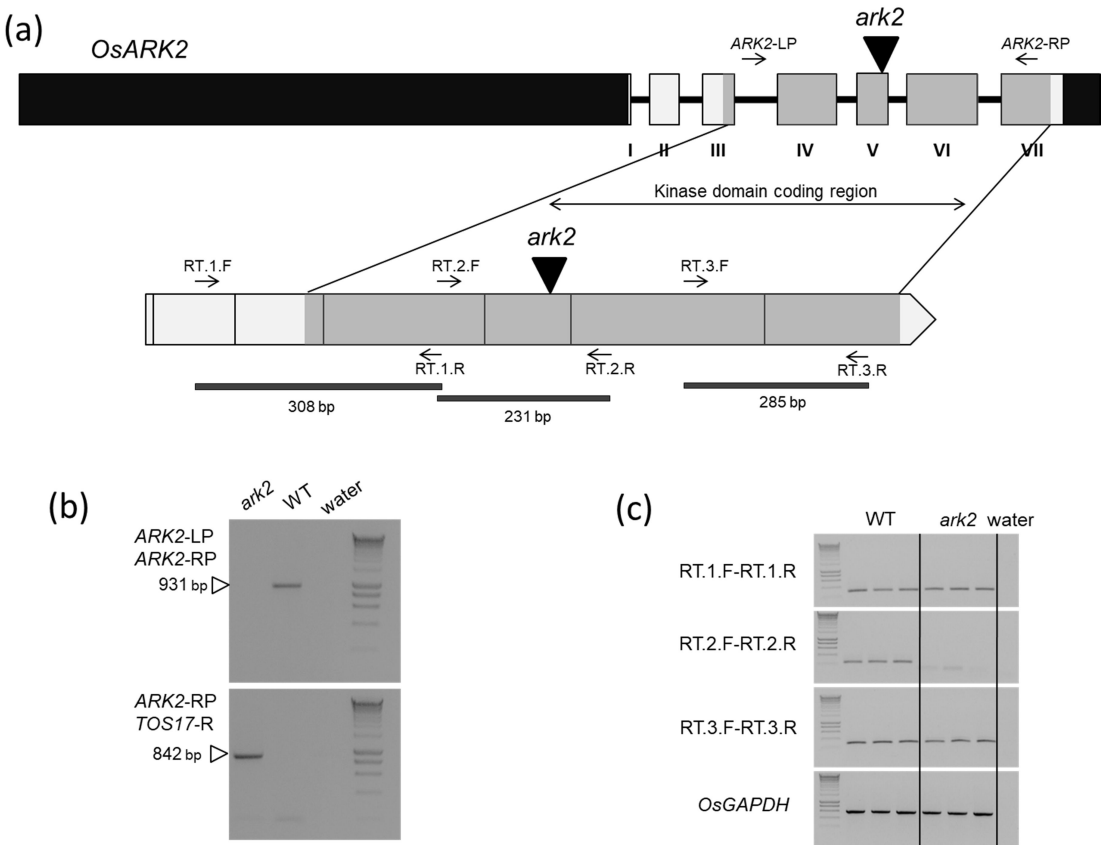

Figure 16. Molecular characterization of an *ark2* mutant. (a) Gene structure schematic of *OsARK2* depicting exons in roman numerals. Site of Tos17 insertion is shown as a triangle. Black boxes correspond to untranslated regions. Arrows correspond to sites of oligonucleotide hybridization for genotyping and RT-PCR. (b) Gel electrophoresis of PCR genotyping over *ark2* mutant. (c) RT-PCR amplifying *OsARK2* cDNA upstream, flanking and downstream of the Tos17 insertion (35 PCR cycles). *GAPDH*, *GLYCERALDEHYDE 3-PHOSPHATE DEHYDROGENASE*, WT, wild-type.

5.2.2. *ark2* has a reduced colonization phenotype

In order to test if *OsARK2* has a symbiotic function and if so, to what extent it is similar to that of *OsARK1*, a comparative *R. irregularis* colonization assay was carried out employing the *ark2* mutant and the *ark1-2* mutant allele (hereafter referred as *ark1* to avoid confusion). High inoculum pressure consisting of 500 *R. irregularis* spores were applied to rice plants growing in cones and colonization levels were evaluated at 4 and 8 wpi. Similar to *ark1*, *ark2* mutant plants did not show defects in plant growth (Fig. 17).

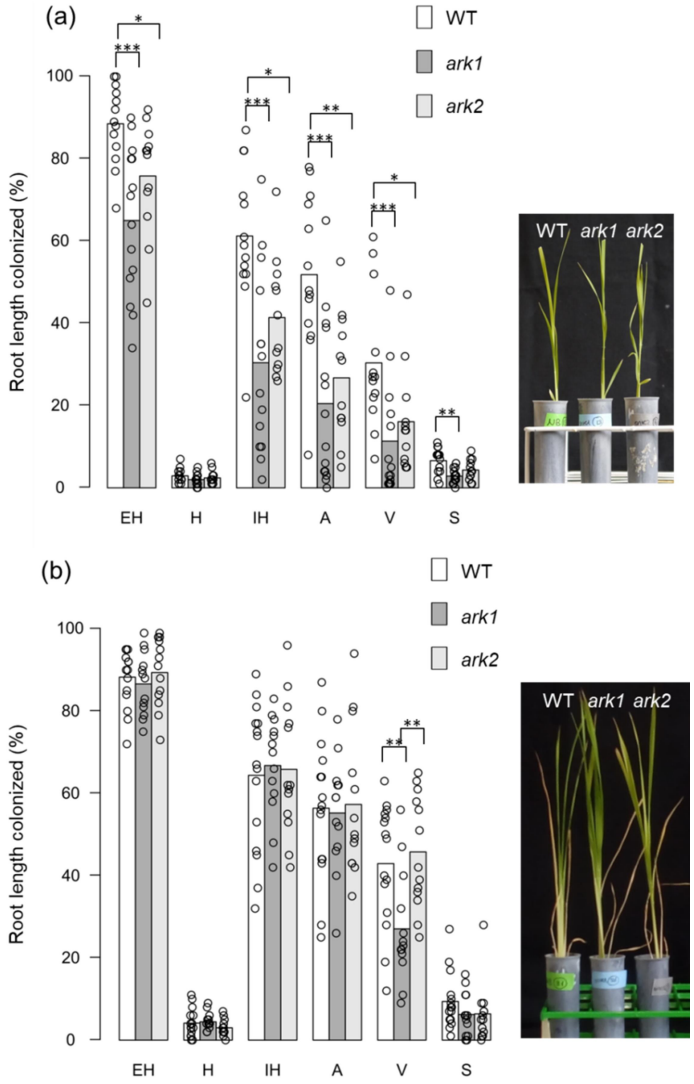

Figure 17. *ark2* AM colonization phenotype with high *R. irregularis* inoculation pressure. Plants were inoculated with 500 *R. irregularis* spores and roots were harvested at four (a) and eight (b) weeks post inoculation. Statistically significant differences in percentages of symbiotic structures are determined by Kruskal-Wallis test with post hoc Dunn test using Benjamini-Hochberg multiple comparison correction (*, $p < 0.05$; **, $p < 0.01$; ***, $p < 0.001$). Bars represent means. Representative pictures at the day of harvesting are given to illustrate equivalent plant growth dynamics in *ark1* and *ark2* mutants compared to the wild-type (WT). EH, extraradical hyphae; H; hyphopodia; IH, intraradical hyphae; A, arbuscules; V, vesicles; S, spores.

At the early time point *ark2* plants had reduced levels of extraradical hyphae, intraradical hyphae, arbuscules and vesicles compared to the wild-type confirming a symbiotic function for *OsARK2* (Fig. 17a). At this stage, the reduced colonization levels of *ark1* and *ark2* were similar. At 8 wpi, *ark2* plants had comparable levels of colonization than the wild-type (Fig. 17b). Interestingly, *ark1* plants also had similar

levels of colonization than the wild-type at the late time point, albeit exhibiting reduced levels of vesicles (Fig. 17b).

To assess the *ark2* phenotype under low inoculum pressure conditions, plants were inoculated with 300 *R. irregularis* spores and grown in black falcon tubes (corresponding to a 20% volume increase of substrate compared to grey cones used in the previous experiment). In these conditions, colonization levels at 5 wpi were marginal in all genotypes, rarely surpassing 5% of arbuscules (not shown). At 10 wpi, arbuscule and vesicle levels were lower in *ark2* compared to the wild-type and higher than those of *ark1* mutants (Fig. 18). Thus, under these conditions mutation of *OsARK1* and *OsARK2* had quantitatively distinct phenotypic consequences, *ark2* exhibiting intermediate reduced colonization levels in relation to the wild-type and *ark1*. In this assay all genotypes exhibited a positive AM growth response (Fig. 18). AM growth responses are normally not observed in the Nipponbare inbreed line in standard conditions (shorter time frames and smaller containers) but was evident here at 10 wpi. This homogeneity across genotypes illustrates differential colonization levels in the mutants are not explained by indirect defects in plant growth.

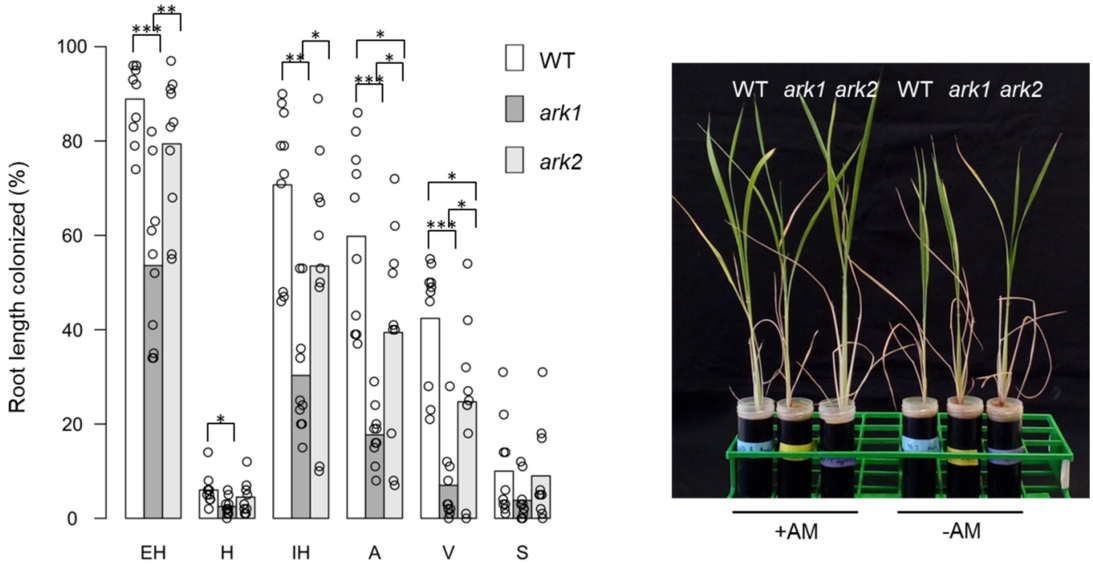

Figure 18. *ark2* AM colonization phenotype with low *R. irregularis* inoculation pressure. Plants were inoculated with 300 *R. irregularis* spores and roots were harvested at ten weeks post inoculation. Statistically significant differences in percentages of symbiotic structures are determined by Kruskal-Wallis test with post hoc Dunn test using Benjamini-Hochberg multiple comparison correction (*, $p < 0.05$; **, $p < 0.01$; ***, $p < 0.001$). Bars represent means. A representative picture of rice plants at the day of harvesting including mock-inoculated (-AM) plants is shown at the right. EH, extraradical hyphae; H; hyphopodia; IH, intraradical hyphae; A, arbuscules; V, vesicles; S, spores; WT, wild-type.

To evaluate potential complementary or redundant functions between *OsARK1* and *OsARK2*, a cross was generated using the two mutant alleles. A colonization experiment was carried out using this DKO along with the single mutants. Plants were inoculated with 300 *R. irregularis* spores and grown using the standard grey cone system for six weeks. Although the pattern of colonization in the single mutants reproduced previous observations, colonization levels across plants were highly variable, especially in the wild-type where percentage of root length colonized by intraradical hyphae ranged between 3 and 86% (Fig. 19). In these conditions, arbuscule levels were still significantly different between the wild-type and *ark1* and the DKO while the *ark2* mutant had intermediate arbuscule levels (averaging 20.8%) that were not statistically significantly different to the other three genotypes. DKO plants were still capable to host AM fungi forming all symbiotic structures and had similar colonization levels than those of *ark1* (Fig. 19).

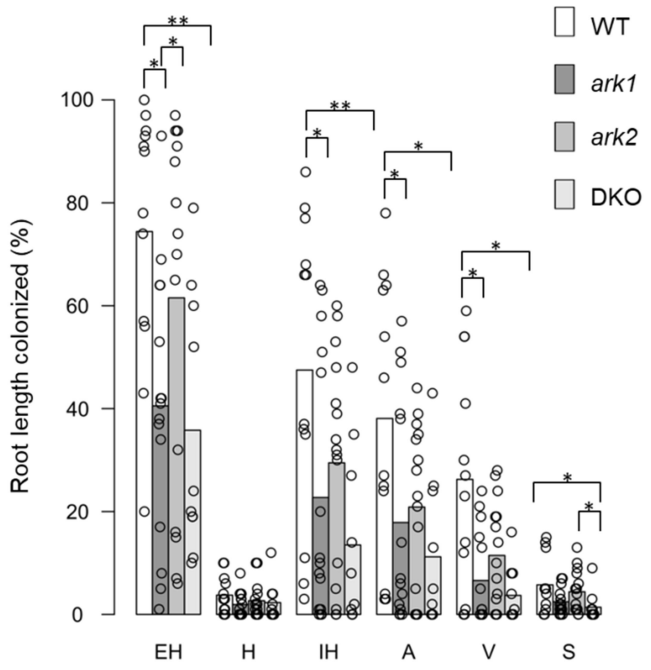

Figure 19. AM colonization phenotype of *ark1*, *ark2* and double knockout (DKO) rice plants. Plants were inoculated with 300 *R. irregularis* spores and roots were harvested at six weeks post inoculation. Statistically significant differences in percentages of symbiotic structures are determined by Kruskal-Wallis test with post hoc Dunn test using Benjamini-Hochberg multiple comparison correction (*, $p < 0.05$; **, $p < 0.01$). Bars represent means. EH, extraradical hyphae; H; hyphopodia; IH, intraradical hyphae; A, arbuscules; V, vesicles; S, spores; WT, wild-type.

5.2.3. Investigating post-arbuscule development dynamics in *ark1* and *ark2* mutants in rice

From work in *ark1* mutants, which have morphologically normal arbuscules and a reduced colonization phenotype that can be rescued by surrounding wild-type nurse plants, it has been established that OsARK1 functions in the post-arbuscule development stage (Chapter 3, Roth et al., 2018). This stage is dominated by nutrient assimilation by the symbiotic partners, arbuscule collapse and fungal vesicle development. In exchange for Pi, the AM fungus receives carbon in the form of sugars and lipids (reviewed in Rich et al., 2017b; Roth and Paszkowski, 2017). A link between arbuscule collapse and lipid dynamics is possible as lipid droplets emerge in arbusculated cells as they collapse (Kobae et al., 2014). As a marked reduction in vesicle abundance in *ark1*, *ark2* and DKO, which are lipid storage structures (Jabaji-Hare et al., 1984) can be seen, it was decided to study post-arbuscule stage dynamics focusing on possible alterations in lipid homeostasis in the different mutant backgrounds.

The fatty acid content from *ark1* and *ark2* roots was measured through HPLC assays. Samples used were from the colonization experiment shown in Fig. 18 and included uninoculated roots. Palmitvaccenic acid ($16:1^{\Delta 11cis}$) is an abundant AM fungal-exclusive fatty acid produced through desaturation of plant supplied palmitic acid (Brands et al., 2020; Cheeld et al., 2020). The levels of $16:1^{\Delta 11cis}$ were higher in wild-type roots compared to the single mutants in line with the previously measured higher colonization levels in the wild-type (Fig. 20a). The levels of plant fatty acids (18:0 to 22:1) were identical in uninoculated roots across genotypes (Fig. 20a). In colonized roots, the fatty acid levels were higher in the wild-type compared to the single mutants (Fig. 20a). However, AM fungi can also have small amounts of fatty acids otherwise mostly found in plants (Wewer et al., 2014). Thus, from this assay it can be concluded that at least in roots not hosting AM fungi, overall fatty acid content is not impaired in *ark1* and *ark2*.

Although lipid storage fungal vesicles are less frequently found in *ark1* and *ark2* mutants, they still occur. In order to test whether vesicles in the mutant genotypes have lower amounts of lipids, roots were treated with the lysochrome Sudan red IV and observed in a light microscope. Although less frequent, patches of vesicles in the

mutants can be found along the root length. Vesicles in *ark1* and *ark2* are of similar size than those in the wild-type and display intense Sudan red IV signal indicating that they are packed with lipids (Fig. 20b). The above observations suggest *ark1* and *ark2* mutant plants are not impaired in the production of lipids and that a proportion of plant derived fatty acids is able to reach AM fungi and accumulate in viable fungal vesicles.

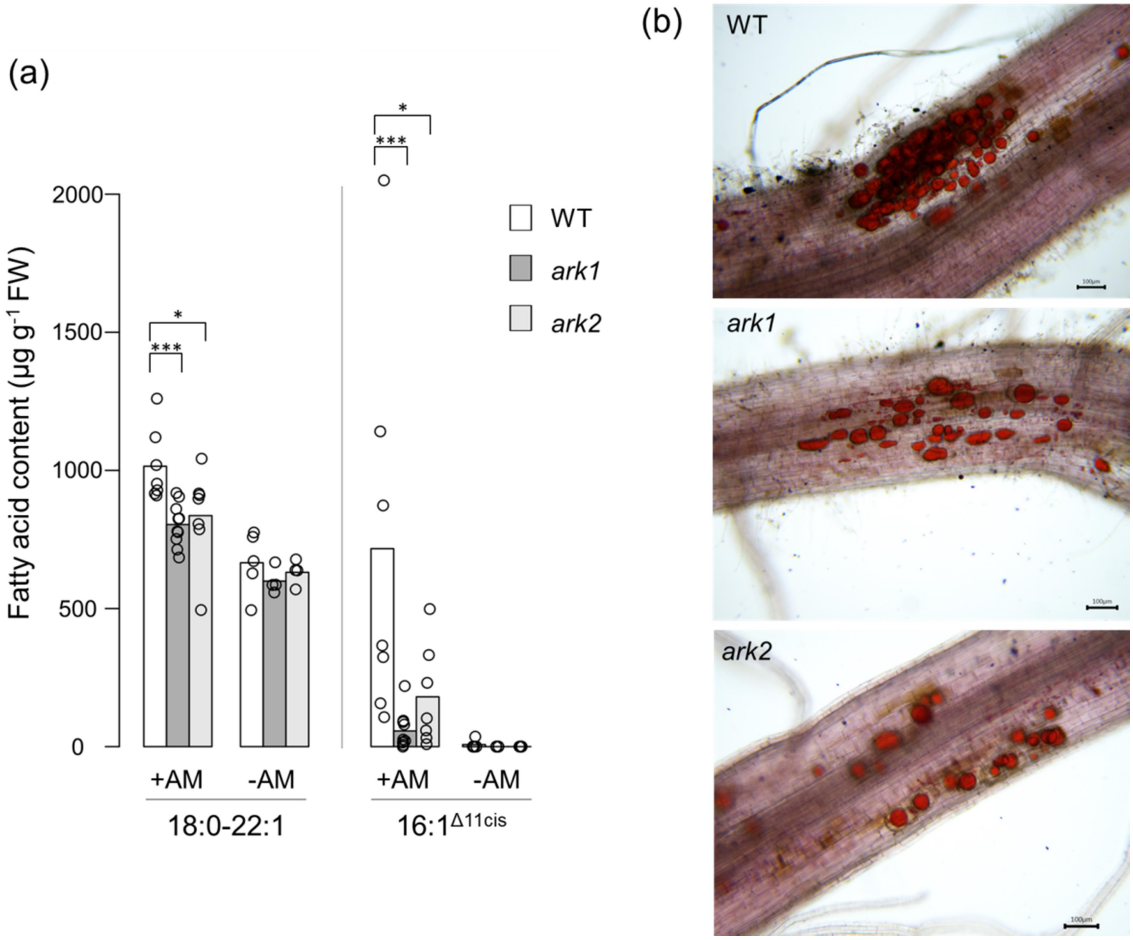

Figure 20. Lipids in roots and in AM fungal vesicles in the single mutants. (a) Fatty acid content in roots of *R. irregularis* colonized (+AM) or non-colonized (-AM) *ark1* and *ark2* mutant roots. $16:1^{\Delta 11cis}$ corresponds to the AM fungal fatty acid palmitvaccenic acid. 18:0-22.1 correspond to the following fatty acids: 18:0, 18:1, 18:2, 18:3, 20:0; 20:1, 20:2, 20:3, 22:0 and 22:1. Statistically significant differences between genotypes are shown (Kruskal–Wallis test, post hoc Dunn test, *, $p < 0.05$; ***, $p < 0.001$). Bars represent means. (b) Sudan red IV staining of AM fungal vesicles. Representative pictures are shown. Scale bar, 100 µm. WT, wild-type.

A blue fluorescent dye, Ac-201, has been recently developed to stain lipids in plant tissues (Kuntam et al., 2015). In order to visualize lipids in arbusculated cells, a new protocol was established employing Ac-201 in conjunction with WGA to visualize

fungal structures. Ac-201 and WGA-Alexa Fluor™ 633 have non-overlapping excitation and emission properties which allowed clear recognition of lipids and fungal chitin in arbusculated cells using confocal microscopy. In wild-type roots, cells hosting fully branched arbuscules exhibited different levels of lipids, as inferred by the intensity of the blue Ac-201 signal (Fig. 21). Regardless of their intensity, the distribution of lipids in arbusculated cells was largely homogeneous but bright spots appeared in cells hosting collapsing arbuscules (Fig. 21). The simultaneous observation of arbusculated cells with different levels of lipids in common root segments suggests lipid distribution dynamically changes through arbuscule development and collapse forming a continuum of largely transient stages (Fig. 22).

Roots of the *ark1* and *ark2* single mutants and the DKO were treated with Ac-201 and visualized as before. Lipids were observed in arbusculated cells of the three mutant genotypes but wild-type plants had an evidently higher representation of arbusculated cells displaying very strong Ac-201 signal (Fig. 23). The intensity of Ac-201 signal was measured on cells hosting fully developed arbuscules in one plant per genotype. There was a higher representation of arbusculated cells with brighter Ac-201 signal in the wild-type and the *ark1* mutant than in the *ark2* mutant and the DKO (Fig. 24a, representative images in Fig. 24b). However, these are preliminary results from one biological replicate per genotype. The screening of more biological replicates will allow performing proper comparisons with statistical basis. Encouragingly, it can be concluded that co-staining AM colonized roots with Ac-201 and WGA-Alexa Fluor™ 633 provides a useful method to visualize lipids in arbusculated cells with potential usefulness in comparative phenotypic inspections of the three mutant genotypes.

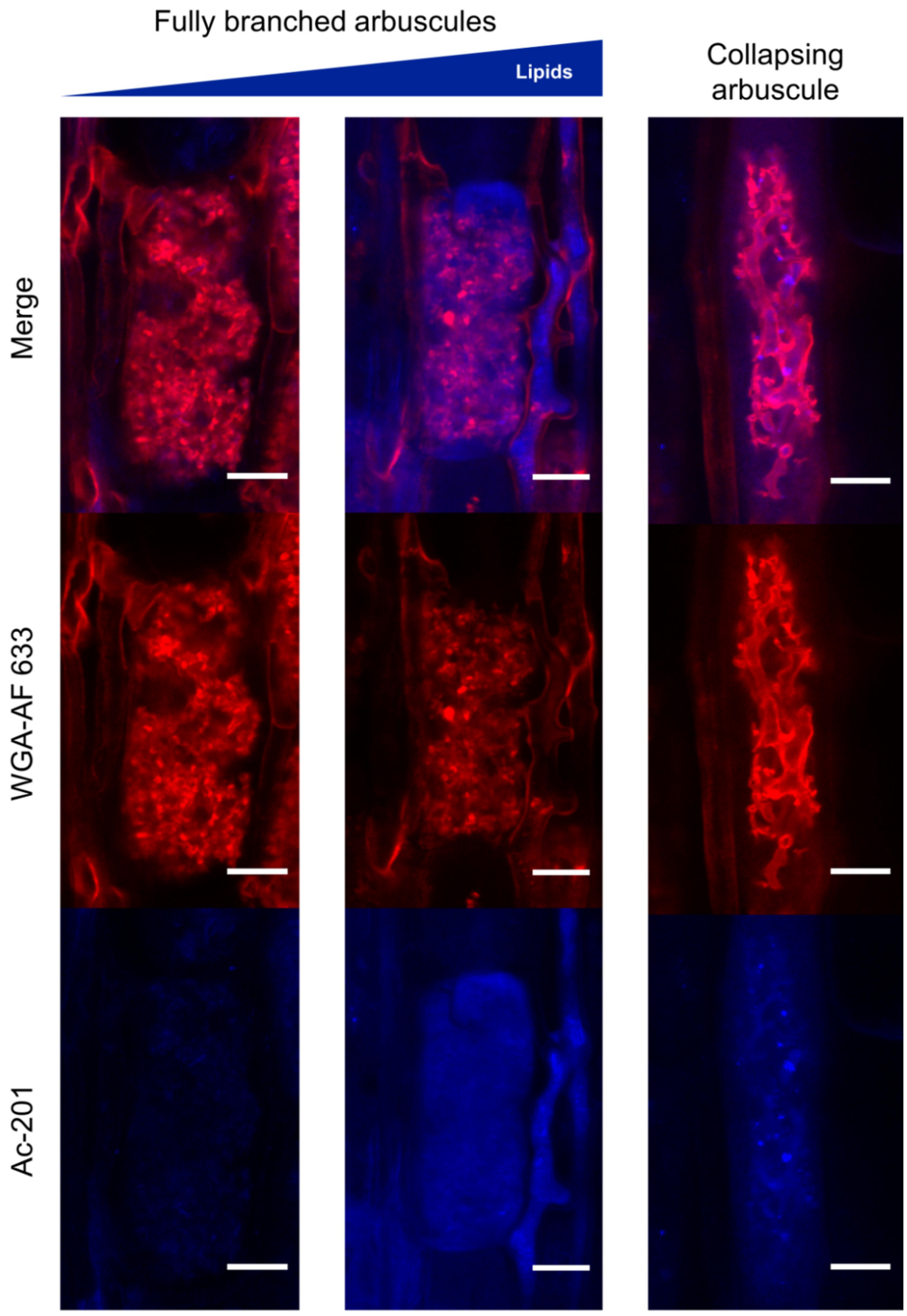

Figure 21. Lipid imaging in arbusculated cells of wild-type (WT) rice roots. Roots from colonization experiment depicted in Fig. 18 were employed (300 *R. irregularis* spore inoculum, ten weeks post inoculation). Representative images of arbusculated cells co-stained with Ac-201 and wheat germ agglutinin (WGA)-Alexa Fluor™ 633 are shown. Scale bar, 10 µm.

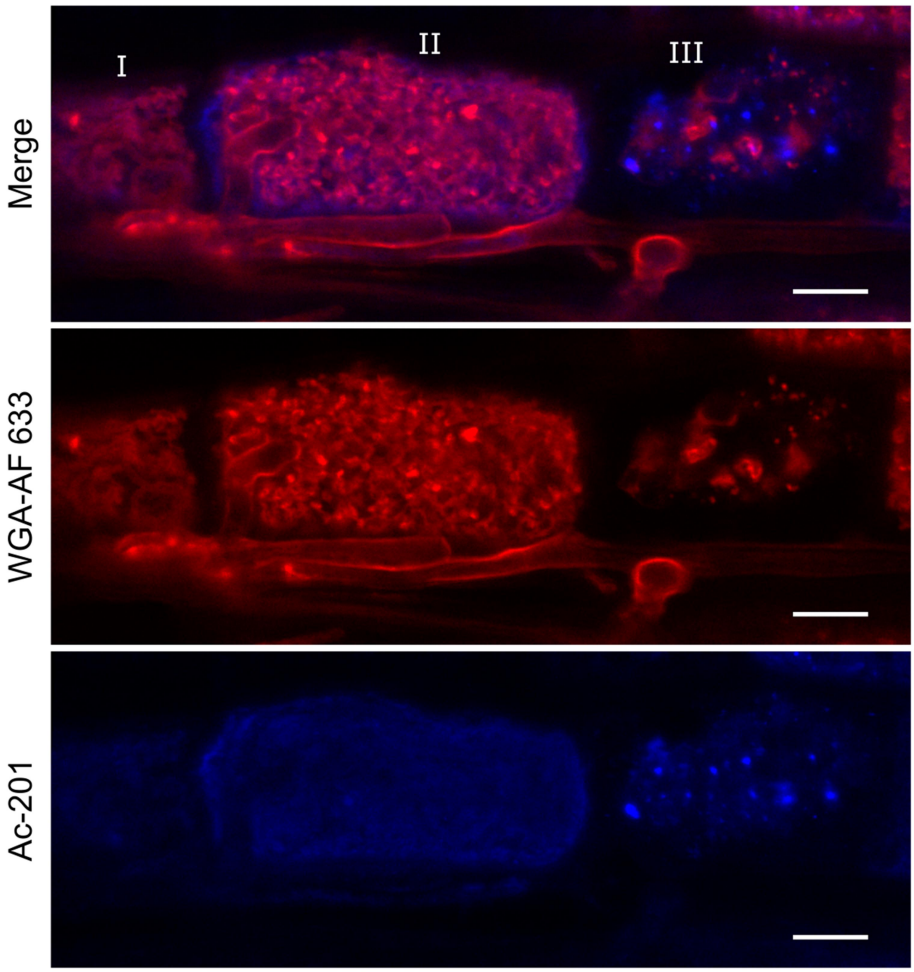

Figure 22. Concurrent patterns of lipid distribution in arbusculated cells of wild-type (WT) rice roots. Roots from colonization experiment depicted in Fig. 18 were employed (300 *R. irregularis* spore inoculum, ten weeks post inoculation). A representative root section co-stained with Ac-201 and wheat germ agglutinin (WGA)-Alexa Fluor™ 633 is shown with three root cortex cells hosting arbuscules of different developmental stages. I, arbusculated cell with faint Ac-201 signal. II, arbusculated cell hosting a mature arbuscule and stronger homogeneous signal. III, arbusculated cell hosting a collapsing arbuscule and displaying bright Ac-201 dye signal in small clusters. Scale bar, 10 µm.

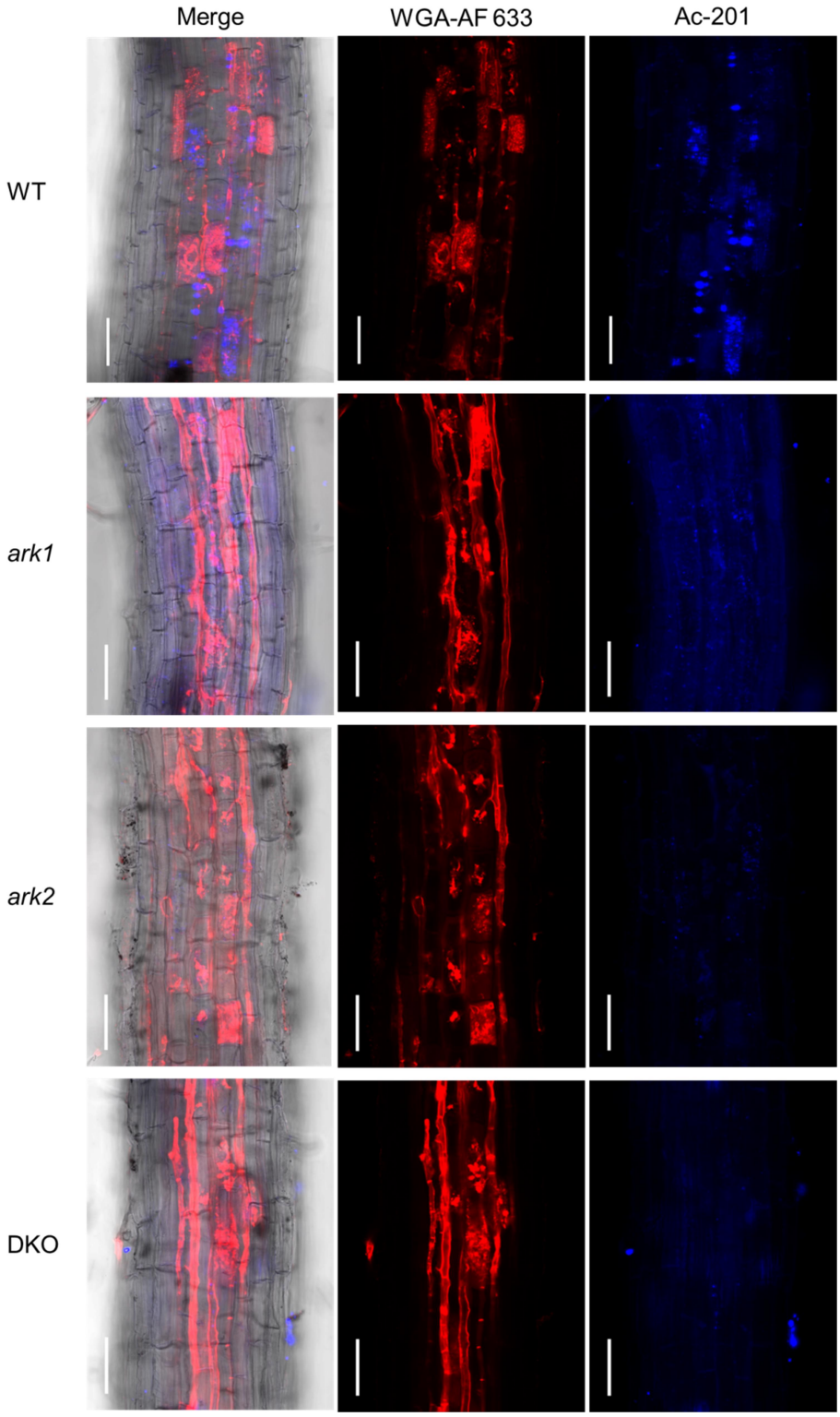

Figure 23. Overview of lipid distribution in roots of wild-type rice, *ark1*, *ark2* and the double knockout (DKO). Roots were co-stained with Ac-201 and wheat germ agglutinin (WGA)-Alexa Fluor™ 633. Roots from colonization experiment depicted in Fig. 19 were employed (300 *R. irregularis* spore inoculum, six weeks post inoculation). Representative root sections are shown. Scale bar, 50 µm.

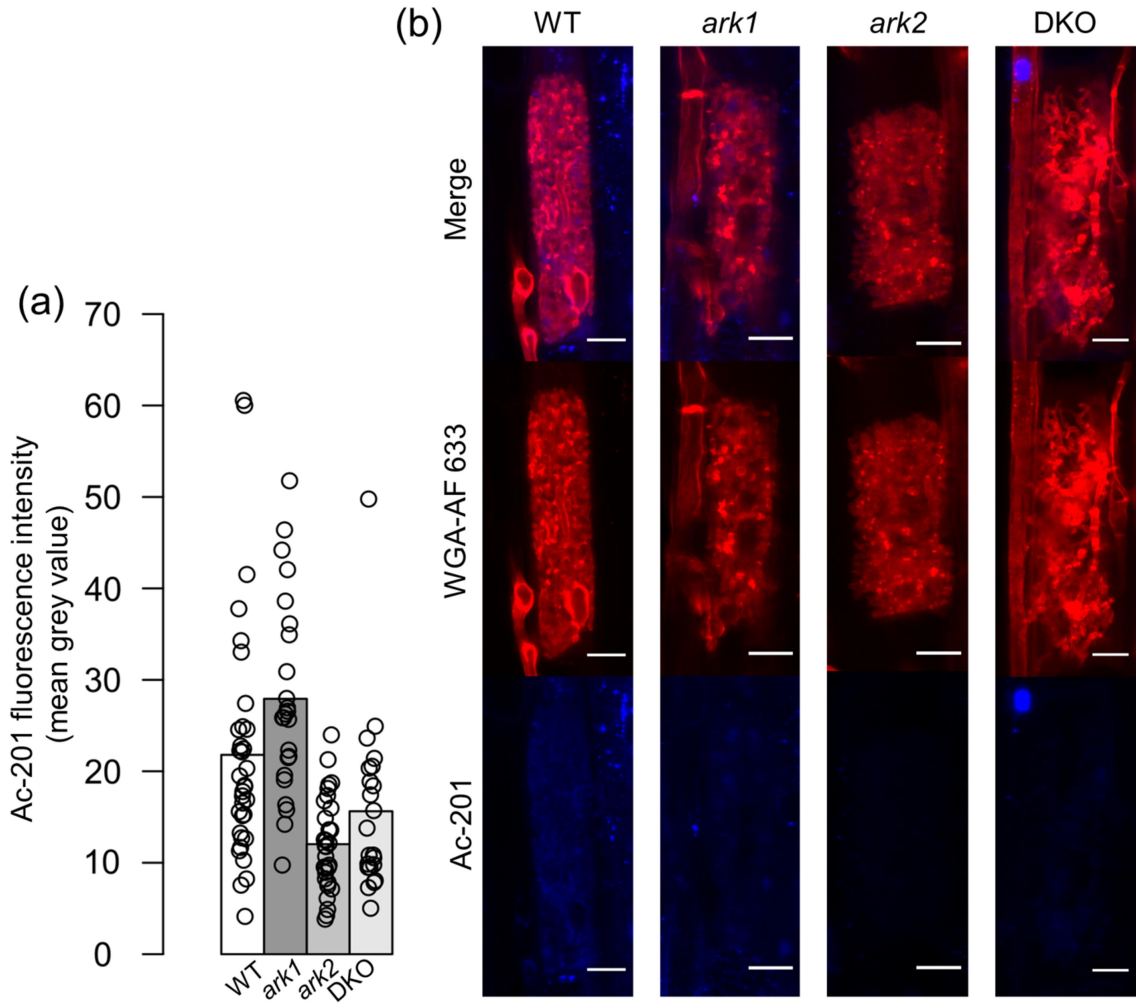

Figure 24. Lipid distribution in arbusculated cells of wild-type rice, *ark1*, *ark2* and the double knockout (DKO). Roots were co-stained with Ac-201 and wheat germ agglutinin (WGA)-Alexa Fluor™ 633. Roots from colonization experiment depicted in Fig. 19 were employed (300 *R. irregularis* spore inoculum, six weeks post inoculation). (a) Quantification of Ac-201 fluorescence intensity in arbusculated cells. One plant (biological replicate) per genotype was used and therefore no statistics are calculated. Bars represent the mean of 22-34 arbusculated cells per plant. (b) Representative images of arbusculated cells. Scale bar, 10 µm.

5.2.4. Preliminary characterization of lipid dynamics in a *Brachypodium distachyon ark1* mutant

The grass model *B. distachyon* has remarkably different interaction dynamics with the AM fungus *R. irregularis* compared to rice by for example favouring the symplastic route for cell-to-cell hyphal spread (Hong et al., 2012). In light of these differences, it was decided to study the lipid distribution in arbusculated cells of a mutant allele of *BdARK1*

(*Bradi4g19550*). This allele (ID: JJ27771, hereafter referred as *ark1*) derives from a *B. distachyon* T-DNA insertional mutant collection (Bragg et al., 2012). The *ark1* mutant was molecularly characterized by PCR genotyping using a gene specific and a T-DNA primer pair followed by purification and Sanger sequencing of the electrophoresis band (Fig. 25a-b). This confirmed the T-DNA insertion occurs in the *BdARK1* kinase domain-coding region upstream of the catalytic loop (2,001 bp from first nucleotide of ATG).

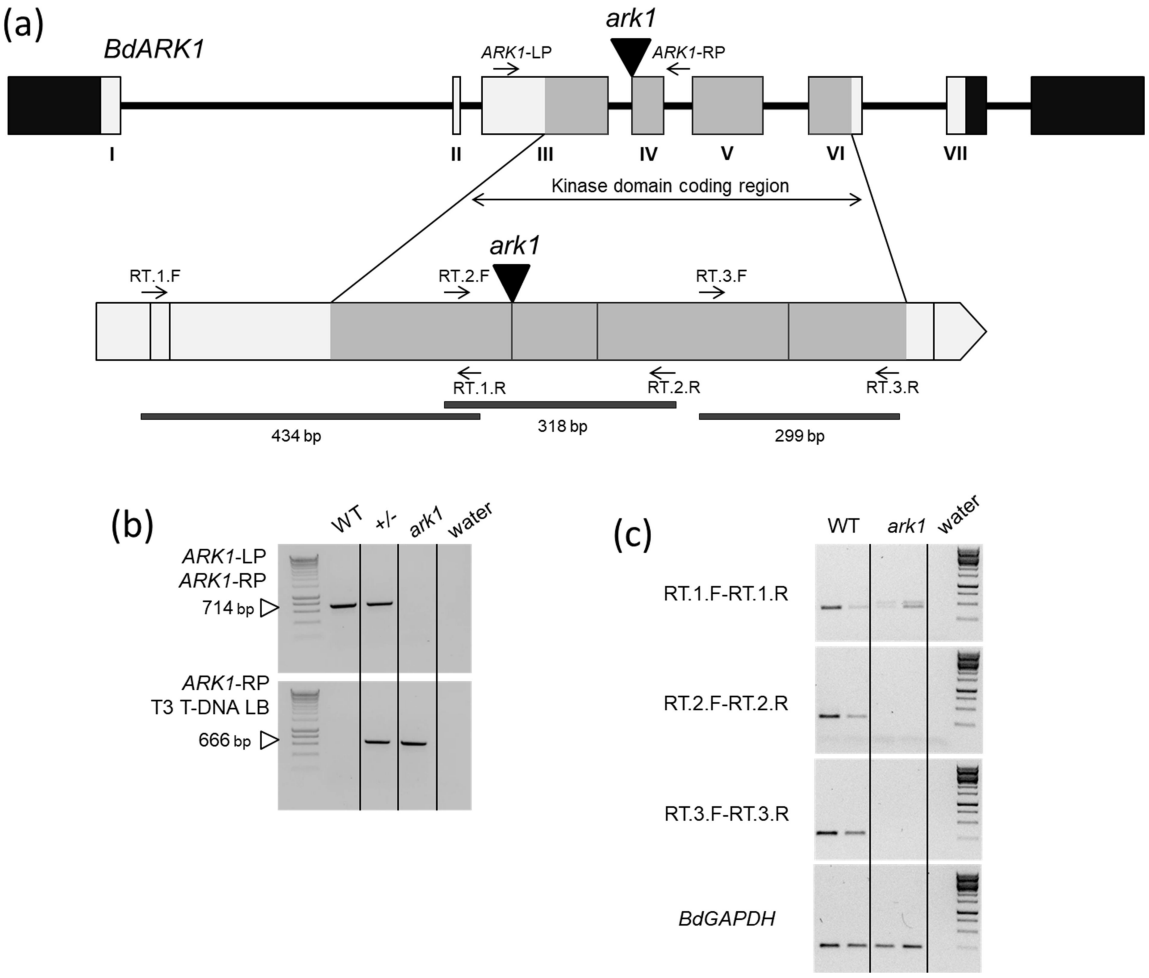

Figure 25. Molecular characterization of a T-DNA insertional mutant of *ARK1* in *B. distachyon*. (a) Gene structure schematic depicting exons in roman numerals. Site of T-DNA insertion is shown as a triangle. Black boxes correspond to untranslated regions. Arrows correspond to sites of oligonucleotide hybridization for genotyping and RT-PCR. (b) Gel electrophoresis of PCR genotyping over *ark1* mutant. (c) RT-PCR amplifying *BdARK1* cDNA upstream, flanking and downstream of the T-DNA insertion (35 PCR cycles). *GAPDH*, *GLYCERALDEHYDE 3-PHOSPHATE DEHYDROGENASE*; WT, wild-type; +/-, heterozygous.

RNA was extracted from wild-type and mutant roots of plants inoculated with 300 *R. irregularis* spores and grown in cones for eight weeks. cDNA was synthesized and RT-PCR assays performed to test for *BdARK1* transcript detection. To this end, oligonucleotides were designed to amplify regions upstream, spanning and downstream of the T-DNA insertion (Fig. 25a). Only electrophoresis bands upstream of the insertion were detected confirming *BdARK1* to be transcriptionally perturbed in the *ark1* mutant (Fig. 25c).

No evident differences in plant growth were detected between the wild-type and the *ark1* mutant in AM colonized or mock-inoculated plants (Fig. 26a-b). Only two homozygous mutant plants were retrieved from the original segregating population obtained. These two plants had lower levels of extraradical hyphae, intraradical hyphae, arbuscules and vesicles compared to wild-type plants (Fig. 26c). Roots were treated with Ac-201 and distribution of lipids in arbusculated cells was observed under the confocal microscope. The intensity of the Ac-201 signal was remarkably lower in arbusculated cells from the two *ark1* mutant plants (Fig. 26d and representative images in Fig. 26e). However, as these are preliminary results from only two biological replicates of the *ark1* mutant, further screenings will be needed to establish whether the differences in colonization and lipid distribution are reproducible. As in rice, Ac-201 and WGA-Alexa Fluor™ 633 co-staining of roots proved a useful method to visualize lipids in arbusculated cells of *B. distachyon*.

Altogether, these preliminary observations from rice and *B. distachyon* suggest that although mutation in *OsARK1*, *OsARK2*, and *BdARK1* results in no evident defects in arbuscule development, arbusculated cells may exhibit alterations in the distribution of lipids.

5.3. Discussion

In this chapter, a symbiotic role of OsARK2 was investigated stimulated by its evolutionary history and close homology to OsARK1 (Chapter 4). OsARK1 has a post-arbuscule development role supported by a mutant phenotype (Chapter 3, Roth et al., 2018). Because of this occurrence of a phenotype in *ark1*, it was expected that OsARK1 and OsARK2 do not function fully redundantly. It was still possible, however, for the

two paralogues to exhibit partial redundancy, hypothetically explaining why the phenotype of *ark1* consisted in partial reduction in the levels of AM colonization.

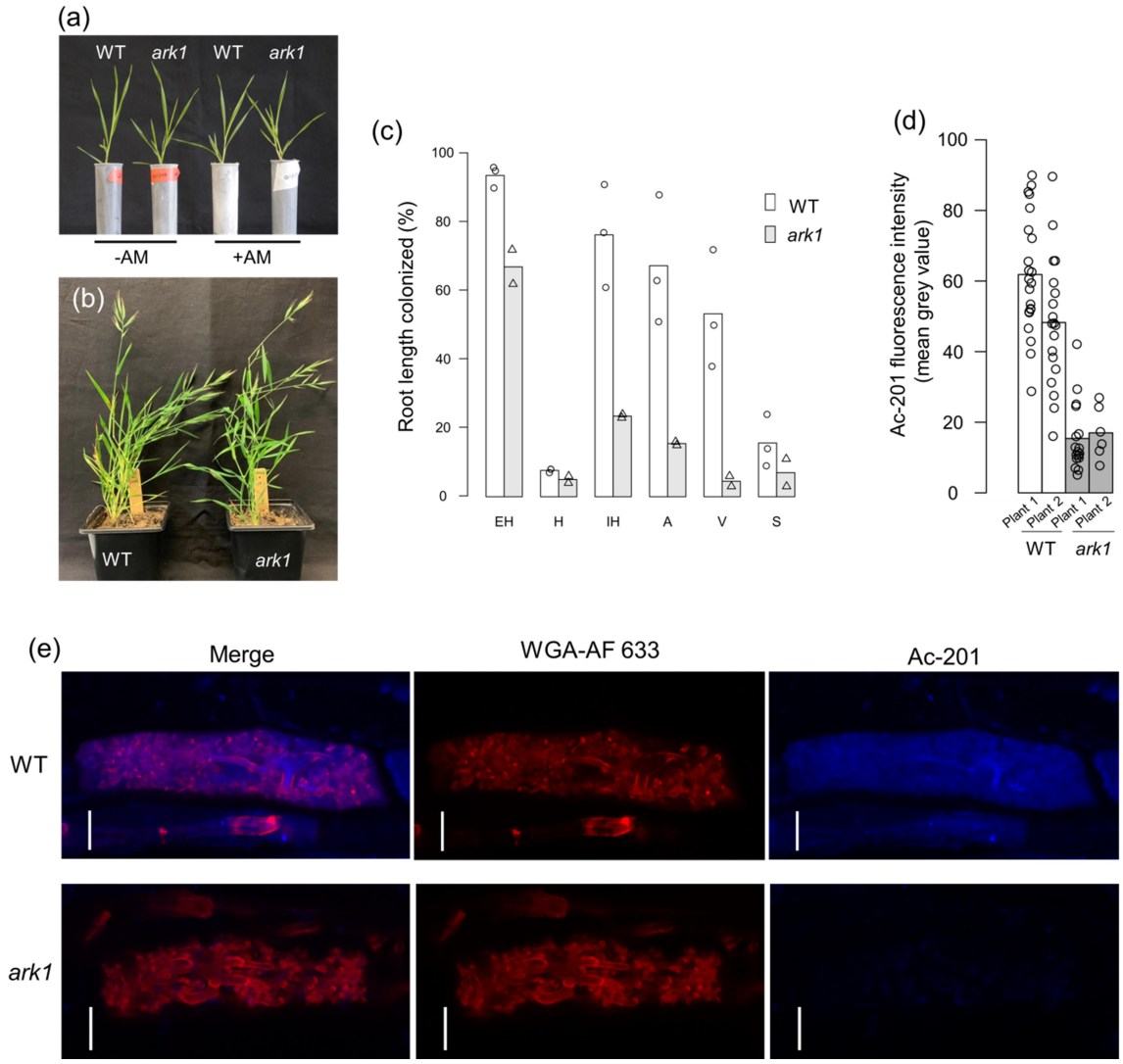

Figure 26. Preliminary AM phenotype of *B. distachyon ark1* mutant. (a) Representative images of four weeks post inoculation plants including mock-inoculated (-AM) plants. (b) Representative images of 2 month-old plants growing in soil pots. (c) Preliminary *ark1* AM colonization phenotype. Plants were inoculated with 300 *R. irregularis* spores and roots were harvested at eight weeks post inoculation. As only two biological replicates of *ark1* were available, no statistics are calculated. Bars represent means. (d) Quantification of Ac-201 fluorescence intensity in arbusculated cells of two plants (biological replicates) per genotype co-stained with Ac-201 and wheat germ agglutinin (WGA)-Alexa Fluor™ 633. As only two biological replicates per genotype were used, no statistics are calculated. Bars represent means. (e) Representative images of arbusculated cells of wild-type *B. distachyon* and *ark1* mutant. Scale bar, 10 µm. EH, extraradical hyphae; H; hyphopodia; IH, intraradical hyphae; A, arbuscules; V, vesicles; S, spores. WT, wild-type.

OsARK1 and OsARK2 have a similar predicted protein structure essentially consisting of an active cytosolic kinase domain with common and distinctive residues across orthologues and an N-terminal transmembrane region (Chapter 4). The *ark2* mutant allele characterized in this study is of similar nature as the two *ark1* alleles previously analysed (Chapter 3, Roth et al., 2018) with the insertion located in the middle of the kinase domain-coding region. As no other protein domains are present in OsARK2, the mutation is likely to fully abolish OsARK2 function.

The colonization phenotype of *ark2* was analysed and contrasted to that of *ark1* in different experiments. In a first experiment, a high amount of spore inoculum was applied to roots grown in a small volume of substrate. When colonization was assessed at an early time point, the levels of extraradical hyphae, intraradical hyphae, arbuscules and vesicles were significantly higher in the wild-type compared to *ark2*. There were no colonization differences between the *ark1* and *ark2* mutants. At a later time point, colonization levels increased in the single mutants reaching wild-type levels. However, the levels of vesicles in the *ark1* mutant, although increased compared to the early time point, remained lower than in the wild-type and *ark2*. On the one hand, the reduction in the levels of colonization in *ark2* at the early time point provides evidence for OsARK2 having a symbiotic role. On the other hand, only *ark1* but not *ark2* had reduced levels of vesicles at the late time point, supporting the notion of OsARK1 and OsARK2 operating differently in AM symbiosis. It is in addition interesting to note that although the *ark1* phenotype reported here confirms OsARK1 being important for the formation of AM fungal vesicles, it did not fully mirror the observations reported in Roth et al., (2018) where colonization levels in the wild-type and *ark1* mutant were similar at an early time point to then considerably drop in the *ark1* mutant at a late time point. It has to be noted, however, that the experimental set up of Roth et al., (2018) was different, mainly in terms of the containers used for plant growth consisting of flat petri dishes. In those conditions, roots could not grow gravitropically and in the absence of drainage, plants and AM fungi likely experienced different exposure to water and nutrients compared to plants grown in cones which may have affected the interaction dynamics between the symbionts. In this experiment using high AM inoculum pressure, colonization defects in *ark1* and *ark2* were evident at the first time point assessed. This suggests OsARK1 and OsARK2 regulate AM symbiosis as early as the first arbuscules appear. Because of

the high amounts of spore inoculum applied, wild-type plants might have had the chance to quickly reach high levels of colonization, effectively evidencing the defects in the mutants. It may also be possible that AM colonization had already reached saturation by the late time point of colonization assessments causing an apparent homogeneity in the levels of fungal structures between genotypes that would not have occurred if less inoculum had been applied or if roots had more space to grow.

In a second experiment, using lower amounts of spore inoculum and growing plants in more voluminous containers, conditions allowed for a slow pace of the colonization process. Indeed, at an early time point arbuscules were just starting to appear. The late time point was harvested at ten wpi. When using regular cones, plants normally start exhibiting symptoms of stress at such prolonged cultivation but as containers in this particular experiment were bigger, plants grew without visible alterations. In fact, at this stage inoculated plants were bigger than uninoculated plants in wild-type and mutant genotypes alike. This illustrates that in the rice Nipponbare inbred line a mycorrhizal-dependent growth response can happen in certain conditions and provides a clear indication that mutation in *OsARK1* or *OsARK2* does not pleiotropically affect overall plant growth. In this second experiment, the arbuscule and vesicle levels in the *ark2* mutant were lower than in the wild-type but in contrast to the previous experiment, the arbuscule and vesicle levels in *ark2* were higher than in *ark1*. These observations confirm OsARK2 to have a role in AM symbiosis which in part might be different than that of OsARK1.

Once a cross between *ark1* and *ark2* was generated, a new colonization experiment was carried out although the limited amounts of seed available in a first instance did not allow for time course observations. Plants grown in standard inoculum levels and containers showed that the development of AM symbiosis can proceed in the absence of *OsARK1* and *OsARK2*. In this experiment, a similar pattern of colonization in the single mutants was observed compared to the previous experiment. This time, however, differences were in some comparisons not statistically significant presumably due to the important variability in colonization levels that occurred in wild-type plants. Performing an additional time course AM colonization experiment using the single and double mutants will be necessary to evaluate to what degree the

defect in AM symbiosis development in the double mutant differs from the single mutants.

Although the *ark1* and *ark2* phenotypes are different, they still have in common that roots are not defective in AM fungal entry and arbuscule formation. Some AM symbiotic mutants such as *d14l* and *nope1* in monocots display almost complete abolishment of AM colonization (Gutjahr et al., 2015a; Nadal et al., 2017) reflecting the involvement of the respective protein products in presymbiotic processes. In other mutants, AM fungal entry and spread occurs but in a delayed fashion, which has for instance been documented for *cerk1* (reviewed in Chiu and Paszkowski, 2020) and *mlo* (Jacott et al., 2020) mutants in several plant species. In these cases, alterations in AM colonization are manifested early, mainly in hyphopodia formation or in the number of infection units but once AM fungal entry occurs, symbiotic structures such as arbuscules and vesicles develop normally and in the long term no quantitative defects are to be observed. The underlying processes impaired in these mutants may also likely relate to presymbiosis. Another group of mutants of genes functioning mainly in arbusculated cells display alterations in arbuscule development such as stunted or not fully branched arbuscules (reviewed in Luginbuehl and Oldroyd, 2017). The phenotypes of *ark1* and *ark2* contrast with the above-mentioned as quantitative alterations are seen at different time points and both *OsARK1* and *OsARK2* are known to be expressed in arbusculated cells (Roth et al., 2018) yet not affecting arbuscule development per se. Although descriptions of phenotypes such as those of *ark1* and *ark2* are novel, it can be expected that several other mutants reported in the literature to lack a symbiotic phenotype in experiments involving only one time point may actually exhibit similar phenotypes to those of *ark1* and *ark2*. Performing multiple experiments in a time course set up is needed for the appropriate documentation of AM symbiotic phenotypes (Montero et al., 2019) and taking this approach was crucial for the characterization of *ark1* and *ark2*.

Once arbuscules develop, OsARK1 appears at the PAM surrounding mature to collapsing arbuscules (Roth et al., 2018). Whether OsARK2 also localizes at the PAM is unknown. As *OsARK2* has a comparatively lower AM-dependent gene induction than *OsARK1* (Güimil et al., 2005; Gutjahr et al., 2015b; Roth et al., 2018), investigating its protein

localization may require genetic tools to increase protein amounts and allow visualization.

Because of the post-arbuscule development role of OsARK1, it was decided to study this stage in the *ark1* and *ark2* mutants. Arbuscule development is a transient process that in rice last only 2-3 days in its active Pi acquiring phase (based on protein dynamics of OsPT11, Kobae and Hata, 2010). This rapid development implies that the AM fungus has a limited time window to handle the resources acquired. Plant Pi transporters retrieving Pi from the PAS can be found at the PAM surrounding developing to mature arbuscules (Harrison et al., 2002; Pumplin and Harrison, 2009; Kobae and Hata, 2010; Tamura et al., 2012). This localization is shared by STR and STR2 (Zhang et al., 2010; Gutjahr et al., 2011) which are thought to be the transporters of fatty acids needed for fungal nourishment (Bravo et al., 2017; Jiang et al., 2017; Keymer et al., 2017; Jiang et al., 2018). When arbuscule collapse commences, septa appear at the branches and trunk of the arbuscule and lipid droplets emerge (Kobae et al., 2014). The means by which arbuscules internalize fatty acids supplied by plants are unclear and it is not known what the fate of the nutritional resources still in the body of a collapsing arbuscule is. They can either be recycled by the plant or supplied to the AM fungus in as-yet-unknown pathways independent of the presence of arbuscules. Lipid dynamics were consequently studied in the mutants from a biochemical and cell biological perspective. The lipid profile was similar in uninoculated roots of *ark1* and *ark2* compared to the wild-type. Although in inoculated wild-type roots there were more lipids detected compared to the single mutants, it is possible than the surplus of lipids in the wild-type corresponded to AM fungal lipids as a reflection of the higher colonization levels in wild-type plants. Adapting a protocol originally developed for staining dark septate fungal endophytes (Barrow and Aaltonen, 2001), proved useful in staining lipids inside AM fungal vesicles which filled them in the wild-type and in the two single mutants. The even lipid profiling in uninoculated roots and presence of lipids in vesicles (which derive form plant supplied fatty acids) across genotypes suggest that no overall disruption in lipid production occurs in the single mutants. Performing these assays in the DKO would help elucidate whether OsARK1 and OsARK2 act redundantly in symbiotic lipid homoeostasis.

If lipid production remains unchanged across genotypes, it was still possible for lipid dynamics to be locally disrupted at the site where *OsARK1* and *OsARK2* are transcriptionally active, the arbusculated cell. To study this, lipids in arbusculated cells were observed employing the lipophilic dye Ac-201, recently developed to stain lipids in plant tissues (Kuntam et al., 2015). Other lipophilic dyes such as Nile red and BODIPY have been used in the past to stain lipids in fungi (see examples in Kobae et al., 2014; Wang et al., 2018). However, Nile red has a broad absorption and emission range hindering co-localization studies. On the other hand, the green fluorescent BODIPY has low photo-stability (Ohsaki et al., 2010). In addition, under confocal microscope, rice roots tend to display high autofluorescence levels in the range of Nile red excitation/emission. In contrast, the blue Ac-201 dye has close to ultraviolet excitation/emission properties allowing for accurate co-staining and visualization of lipids together with the far red WGA-Alexa Fluor™ 633 for chitin staining. The protocol presented here can be usefully adapted to additional purposes by introducing a third green/yellow dye providing its compatibility with the treatment. While lipophilic dyes can easily stain AM spores and extraradical hyphae, their access inside roots tissues is more challenging. In preliminary attempts, Ac-201 was assayed in fresh roots but only AM hyphae in epidermal and upper cortex cell layers were stained. As the focus of this study are arbusculated cells which are usually formed deeper in the root cortex and often neighbouring aerenchymatous tissue in rice (Gutjahr et al., 2009; Vallino et al., 2014), it was decided to work on fixed tissue. Although this prevented the study of temporal dynamics, an advantage of this methodology was to be able to co-localize lipids with clearly WGA-stained arbuscules of different developmental stages. As such, in both rice and *B. distachyon*, it was possible to image lipids in arbusculated cells from wild-type and mutant roots and preliminary observations suggested lipid distribution is impaired in arbusculated cells from the mutant alleles. In the *B. distachyon ark1* mutant, arbusculated cells were almost devoid form Ac-201 signal. If this pattern is confirmed in independent experiments, it would be interesting to study the nature of these differences as rice and *B. distachyon* belong to different subfamilies within the Poaceae which has undergone important diversification (Glémin and Bataillon, 2009).

The range on how lipid dynamics can be altered in arbusculated cells is ample. An AM specific pathway constituted by lipid biosynthesis enzymes and transporters has been

described and proposed to be required for AM fungal lipid nourishment (Bravo et al., 2017; Jiang et al., 2017; Keymer et al., 2017; Luginbuehl et al., 2017; Brands et al., 2018; Jiang et al., 2018; Xue et al., 2018). Disruption of components of this pathway results in lipids not to be transferred to AM fungi but also in alterations in arbuscule morphology. As such, it is at the moment not clear if this pathway is directly involved in fungal nourishment or indirectly, by regulating arbuscule development. The arbuscule morphology defect in the mutant of the fatty acid biosynthesis enzyme-coding gene *MtRAM2* was reported to be rescued by wild-type nurse plants in one study (Luginbuehl et al., 2017), albeit conflicted with the findings in another study which described a partial rescue (Jiang et al., 2017). Also, wild-type nurse plants were not able to rescue the arbuscule development defects of mutants of *LjRAM2*, *LjDIS*, *LjSTR* (Keymer et al., 2017), *OsSTR* (Gutjahr et al., 2012) and *MtFatM* (Jiang et al., 2018). As *ark1*, *ark2* and DKO plants can host fully developed arbuscules, a possible role in lipid dynamics should occur in a pathway parallel or downstream of the above-described and likely functioning in arbusculated cells hosting mature to collapsing arbuscules. The findings in this chapter provide a first glimpse on the role of a new AM symbiosis RLK, OsARK2, and invite to explore further its potential concerted mechanisms of action with OsARK1.

Chapter 6

Transcriptional signatures of mutants of *OsARK1* and *OsARK2*

6.1. Introduction

At the start of signal transduction pathways, RLKs often serve as nodes linking extra- and intracellular environments. Ligands of diverse chemical nature bind to compatible RLK extracellular protein motifs activating the intracellular kinase domains. This often leads to phosphorylation of cytosolic proteins or co-receptors which spreads the transduced signal inside the cell. In all their complexity, signalling cascades culminate in cellular responses to the original sensing event, resulting in physiological consequences at the tissue and organ levels. For the signal transduction pathway(s) that OsARK1 and OsARK2 integrate, the physiological outcomes influence symbiotic AM fungi, as inferred by the phenotypes of the respective mutant alleles (Chapters 3 and 5). Major questions arise on both the mechanistic and broader biological context of OsARK1 and OsARK2 functioning. First, neither OsARK1 nor OsARK2 is likely to be competent for signal perception as the extracellular SPARK domain is broadly absent across monocot orthologues (Chapter 4). This suggests that ligand sensing is performed by unknown receptors other than OsARK1 and OsARK2. Second, no downstream components of the pathway(s) are known for these or other SPARK-I subfamily members in any plant species. In the absence of insights from related proteins, a full range of mechanisms of action is possible for OsARK1 and OsARK2. In the simplest scenario, they may phosphorylate and consequently regulate neighbouring nutrient transporters but complex intracellular signalling cascades leading to activation or repression of transcriptional regulators are also plausible. Third, although the physiological consequences for the plant and the AM fungus upon *OsARK1* impairment

are known to relate to the post-arbuscule development stage and the maintenance of fungal fitness (Chapter 3), there is no evidence at the moment to link these observations with particular molecular pathways. Finally, it is not known how would OsARK1 and OsARK2 position in either the same or parallel symbiotic signalling pathways.

In order to identify putative downstream signalling components depending on OsARK1 and OsARK2, and to interrogate their potentially redundant and/or synergistic functions, an RNA-seq assay was conducted using the corresponding single mutants as well as the DKO. Based on the analysis of transcriptionally induced and repressed genes, general patterns of expression were also look at with the aim of associating the different phenotypes to particular biological processes.

6.2. Results

6.2.1. Global transcriptional responses of *ark1*, *ark2* and double mutants

Mutation in *OsARK1* and *OsARK2* results in different degrees of reduced levels of colonization by the AM fungus *R. irregularis* and, as shown by lipid imaging, potential common alterations in arbusculated cells (Chapter 5). In order to capture the transcriptional landscape of the different mutants during AM symbiosis, an RNA seq experiment was carried out. Aiming to tease out transcriptional responses caused solely by differential colonization levels, it was decided to use root material from the colonization experiment from Chapter 5 depicted in Fig. 19 (samples used for RNA-seq are reproduced in Fig. 27). This experiment in particular had important variations in colonization across biological replicates, especially in the wild-type. For RNA-seq purposes, this variation was considered advantageous as the AM transcriptional signature in the wild-type was expected to vary with colonization allowing for several biological replicates to overlap with those of the often low colonized mutants. Following RNA extraction, ten biological replicates per genotype were selected for RNA-seq analyses based on RNA yield and quality resulting in a total of 40 samples (Fig. 27).

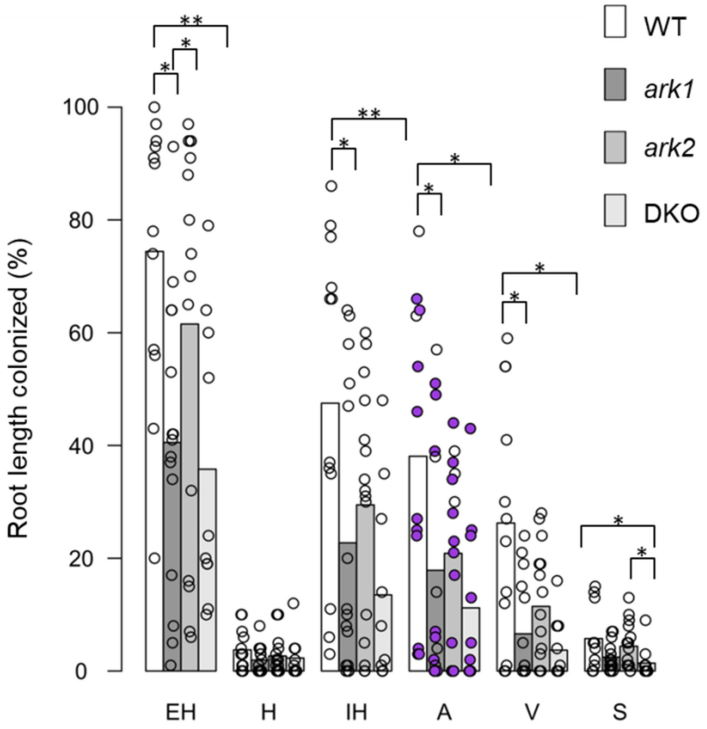

Figure 27. Root colonization of rice plants used for RNA-seq. Colonization graph is reproduced here from experiment depicted in Fig. 19. Plants were inoculated with 300 *R. irregularis* spores and roots were harvested at six weeks post inoculation. Statistically significant differences in percentages of symbiotic structures are determined by Kruskal-Wallis test with post hoc Dunn test using Benjamini-Hochberg multiple comparison correction (*, $p < 0.05$; **, $p < 0.01$). Bars represent means. Arbuscule levels of samples subjected to RNA-seq assays are displayed by purple-colouring the individual samples. EH, extraradical hyphae; H; hyphopodia; IH, intraradical hyphae; A, arbuscules; V, vesicles; S, spores; DKO, double knockout; WT, wild-type.

Once RNA-seq libraries were produced, downstream quality control assessments were performed. This showed homogeneous error rates between samples averaging 0.021% and with an average GC content of 51.7% (Appendix Table 5). Paired-end clean reads were mapped against the rice genome (81.9% average mapping rate) and expression levels calculated as transcripts per million (TPM).

A total of 142 genes were upregulated in any of the three mutant genotypes compared to the wild-type (log2 fold change ≥ 1, FDR adjusted $p \leq 0.05$) while 566 genes were downregulated (log2 fold change ≤ -1, FDR adjusted $p \leq 0.05$, Fig. 28). There was considerable overlap of upregulated genes in the three mutant genotypes in relation to the wild-type. On the other hand, a higher volume of genes appeared as downregulated in *ark1* and the DKO than in the *ark2* mutant (Fig. 28). AM colonization considerably

alters the transcriptional landscape of rice plants (Güimil et al., 2005; Gutjahr et al., 2015b; Fiorilli et al., 2015a) and the overall low colonization levels *ark1* and the DKO had compared to the *ark2* mutant suggests part of the transcriptional response in *ark1* and the DKO may be explained by their low colonization levels rather than by direct effects of the mutation. It was therefore necessary to refine the set of downregulated genes.

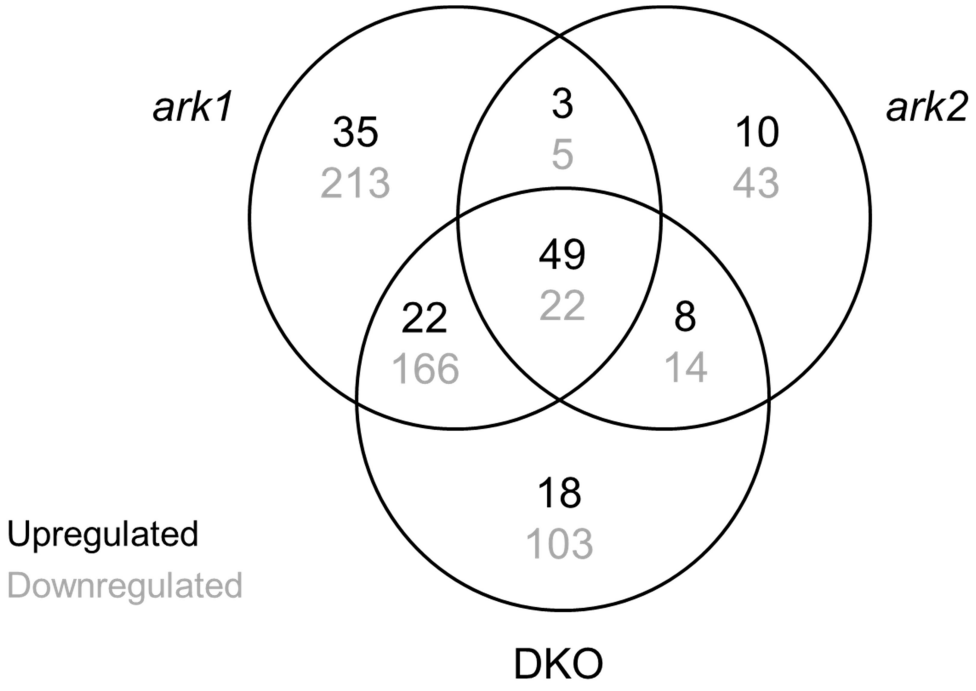

Figure 28. Global transcriptional responses of *ark1*, *ark2* and double knockout (DKO) rice mutants. Venn diagram of upregulated (log2 fold change ≥ 1, FDR adjusted $p \leq 0.05$) and downregulated (log2 fold change ≤ -1, FDR adjusted $p \leq 0.05$) genes in single *ark1*, *ark2* and DKO) in relation to the wild-type. RNA was extracted from roots of plants inoculated with 300 spores of *R. irregularis* and harvested at six weeks post inoculation.

6.2.2. Transcriptionally repressed genes in *ark1*, *ark2* and the DKO during AM symbiosis

In order to minimize the inclusion of genes not regulated by OsARK1 and/or OsARK2 in the dataset of downregulated genes, Spearman correlation analyses were implemented for each gene comparing percentage of arbuscules and expression levels across replicates (Spearman R ≥ 0.631, $p \leq 0.05$). Benefiting from the high number of samples

per genotype (N = 10) and their diverse levels of colonization, it was possible to find around half of the downregulated genes in *ark1* and the DKO (51 and 46% respectively) still positively correlating with arbuscule levels in the mutants. These positively-correlating genes in the mutant backgrounds are unlikely to depend on OsARK1 or OsARK2 for their expression. This exercise also showed that by choosing percentage of arbuscules for the correlation analyses it was possible to clearly individualize those genes that are known to be expressed in arbusculated cells including several important known players of the AM symbiosis such as *OsPT11* (Paszkowski et al., 2002, given as an example in Fig. 29) and *OsSTR* (Gutjahr et al., 2012). In contrast, only 5% of the downregulated genes of *ark2* positively correlated with arbuscule levels in the mutant in line with the higher colonization levels among *ark2* replicates. The downregulated genes reported in this chapter are those filtered after exclusion of genes displaying positive correlation between expression and arbuscule levels in one of the three mutant genotypes (Fig. 30). Exceptions were made when a given gene showed positive correlation in one of the genotypes and negative correlation in another which occurred rarely. This filtering reduced the number of colonization-dependent (and likely OsARK1/OsARK2-independent) genes from 566 to 312 genes (Fig. 30) although it is expected that a fraction of the remaining genes still correlate with colonization but not necessarily with arbuscule abundance. Further excluding the genes that appeared as downregulated in one of the single mutant genotypes but not in the DKO resulted in a final dataset of 165 genes whose transcriptional activity putatively depend on OsARK1 and/or OsARK2 signalling. These genes were assigned to four different transcriptional groups (I – IV) as shown in Fig. 30b.

Although the small volume of downregulated genes in the different transcriptional groups impeded gene ontology (GO) enrichment analyses, GO slims were retrieved for the total set of 165 downregulated genes. Catalytic activity, hydrolase activity and binding were among the most represented molecular function GO slims encountered (Fig. 31). Appendix Table 6 lists GO slims for genes downregulated in the three mutant genotypes in relation to the wild-type (Group I).

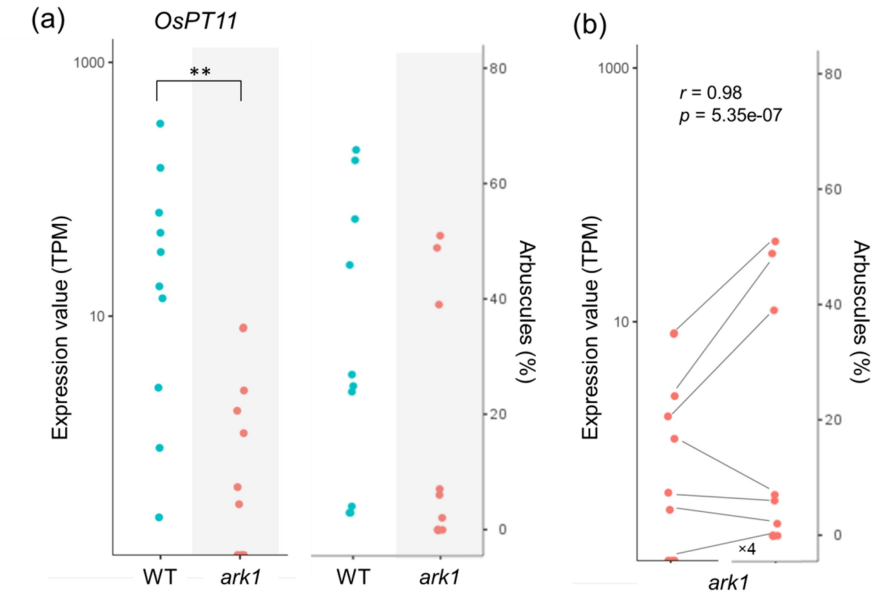

Figure 29. *OsPT11* expression appears as downregulated in the *ark1* mutant as a reflection of lower arbuscule levels. (a) *OsPT11* expression values (measured in transcripts per million ,TPM) of the ten individual replicates are extracted from the RNA-seq dataset and levels of arbuscule colonization are shown. *OsPT11* expression levels are downregulated in *ark1* compared to the wild-type (log2 fold-change = -4.9, $p = 0.003$). (b) *OsPT11* expression levels and arbuscule levels in the *ark1* mutant are shown side by side. Lines connect values from the same biological replicates, reflecting correspondence between *OsPT11* expression and arbuscule levels. Correlation coefficient and *p* value show significant positive correlation. ×4 accounts for four *ark1* replicates that had no observed arbuscules and no *OsPT11* transcripts detected.

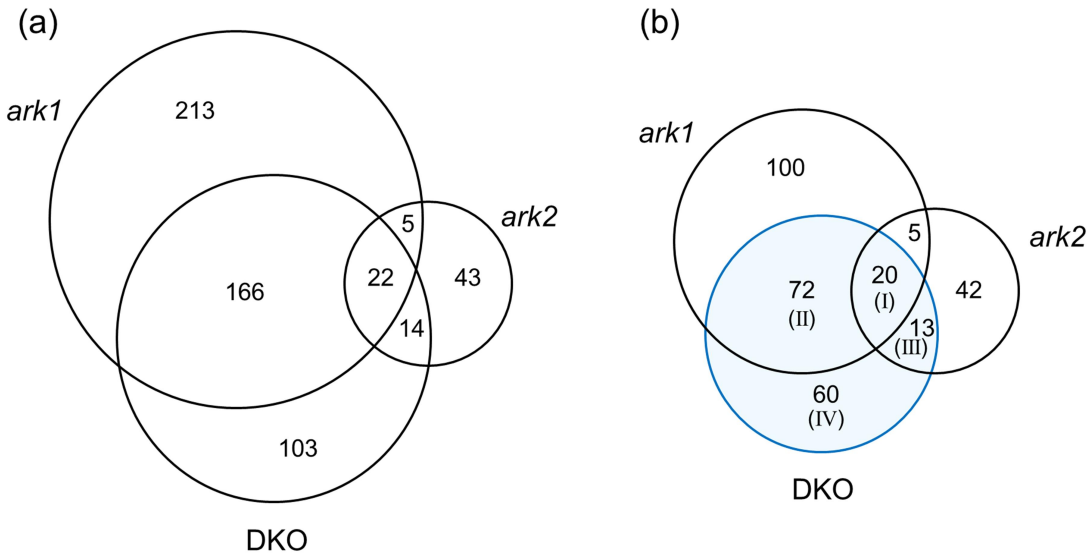

Figure 30. Downregulated genes in *ark1*, *ark2* and DKO in relation to the wild-type. RNA-seq assay was conducted over 10 biological replicates per genotype (inoculated with 300 *R. irregularis* spores, harvested at 6 weeks post inoculation). (a) Venn diagram of total downregulated genes (log2 fold-change ≤ -1, $p \leq 0.05$). (b) Venn diagram of downregulated genes as in (a) but excluding genes that despite being downregulated displayed expression levels positively correlating with arbuscule levels in the respective mutant genotypes (Spearman $R \geq 0.631$, $p \leq 0.05$). Blue circled gene groups of interest (I to IV) are discussed in the text.

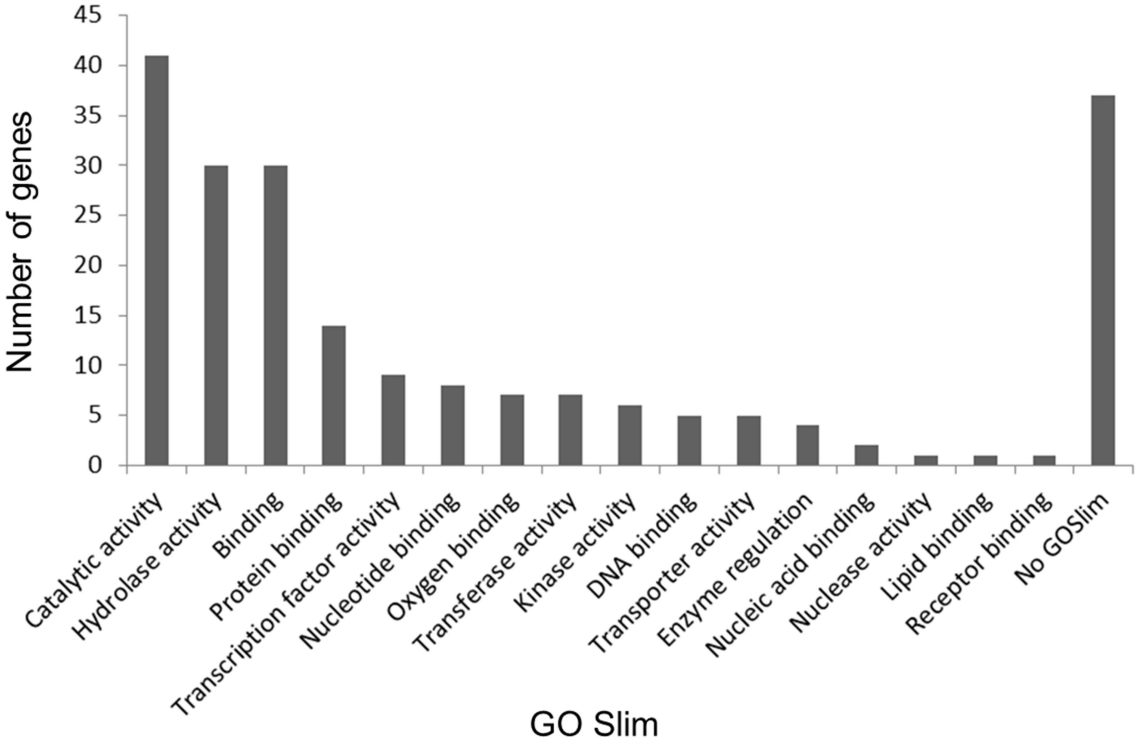

Figure 31. Molecular function GO slim occurrence in Groups I - IV. A given gene can have several associated GO slims.

A set of 20 genes whose expression putatively depends on both OsARK1 and OsARK2 were identified, corresponding to genes downregulated in *ark1*, *ark2* and the DKO (Group I, Table 3). Four of these genes have been functionally annotated including the stress-induced *ABA-STRESS-RIPENING 1* (*OsASR1*, *LOC_Os01g72900*, Philippe et al., 2010; Arenhart et al., 2015), *GLUCANASE 1* (*OsGLN1*, *LOC_Os01g71830*, Akiyama and Pillai, 2001), *OsWRKY8* (*LOC_Os05g50610*, Song et al., 2009) and a member of an ethylene biosynthesis enzyme group, *1-AMINOCYCLOPROPANE-1-CARBOXYLIC ACID OXIDASE 4* (*OsACO4*, *LOC_Os11g08380*, Iwai et al., 2006; Rzewuski and Sauter, 2008) (see Appendix Table 7 for descriptions and references of all functionally annotated genes across datasets). *OsGLN1* encodes an endo-1,3-β-glucanase capable of hydrolysing the cell wall β-glucans of the rice fungal pathogen *Pyricularia oryzae* (Akiyama and Pillai, 2001). In addition, *OsGLN1* is one of the 42 genes previously described to strictly require

the removal of the suppressor of AM signalling *OsSMAX1* for its expression in uninoculated rice roots (Choi et al., 2020, Appendix Table 8).

The most downregulated gene in the three mutant genotypes, *LOC_Os06g11230*, had no transcripts detected in any of the total 30 root samples from the three mutant genotypes. This gene, however, is predicted to encode a short 146 amino acid-long protein with no known domains and with no homology to other proteins outside rice. A phylostratographic study in rice recognized it as one of the more than 1,000 young genes occurring only in the genus *Oryza* (Cui et al., 2015). The second most downregulated gene in the DKO, *LOC_Os01g64850*, had no expression in the *ark1* mutant and in the DKO while its expression levels in the wild-type correlated with arbuscule abundance. It corresponds to the AM-induced gene *OsAM21* (Güimil et al., 2005) and encodes a predicted subtilase from the SBT1.13 clade (Taylor and Qiu, 2017). Besides *LOC_Os06g11230* and *OsAM21*, there were five more genes in this dataset with no expression in the DKO. These eight genes are likely under strict transcriptional dependence of OsARK1 and OsARK2 and with the exception of *OsAM21*, they encode proteins with no predicted known domains, although two of them harbour predicted signal peptides for secretion (see Appendix Table 9 for a full list of genes with no expression in the DKO). Expression level graphs are shown for the five most downregulated Group I genes in the DKO (Fig. 32a-e) which include besides the above-mentioned, a gene encoding a F-box domain-containing protein (*LOC_Os11g36790*) and a putative chitinase conserved in the genomes of AM competent plant clades (*LOC_Os07g19040*, Bravo et al., 2016, see a list of all AM conserved genes in Appendix Table 10). In addition, one gene coding for a predicted LRR-containing protein (*LOC_Os04g55420*) had expression levels positively correlating with arbuscule abundance in the DKO (R = 0.75, p = 0.01) but negatively correlating in the *ark1* mutant (R = -0.74; p = 0.01). Collectively, hydrolase activity and catalytic activity are the two most represented molecular function GO slims in Group I, with four and three genes in these categories respectively (Appendix Table 6).

Table 3. Genes downregulated in *ark1*, *ark2* and the DKO in relation to the wild-type (Group I, log2fc ≤ -1, $p \leq 0.05$). Log2 fold change compared to the WT is displayed with red hue intensity correlating to stronger downregulation. Genes are ordered based on DKO fold change expression. Locus IDs in red correspond to genes with no expression in the DKO (see Appendix Table 9 for details of all genes with no expression in the DKO). Names of the protein products of functionally annotated genes are given. For their functions and references, see Appendix Table 7.

Locus ID	Predicted annotation	Functional annotation	*ark1* log2fc	*ark2* log2fc	DKO log2fc
LOC_Os06g11230	expressed protein	N/A	-9.3	-9.4	-9.3
LOC_Os01g64850	OsSub10 - Putative Subtilisin homologue, expressed	N/A	-5.0	-2.6	-5.0
LOC_Os11g36790	OsFBO6 - F-box and other domain containing protein, expressed	N/A	-3.7	-4.7	-4.0
LOC_Os07g19040	glycosyl hydrolase, putative, expressed	N/A	-3.7	-3.1	-4.0
LOC_Os01g72900	abscisic stress-ripening, putative, expressed	Asr1	-3.0	-2.7	-3.9
LOC_Os11g39850	expressed protein	N/A	-4.3	-4.4	-3.8
LOC_Os04g28330	expressed protein	N/A	-3.0	-2.1	-3.0
LOC_Os05g03700	hypothetical protein	N/A	-2.1	-2.3	-2.1
LOC_Os06g10850	lipase, putative, expressed	N/A	-1.7	-1.8	-1.9
LOC_Os08g26980	expressed protein	N/A	-1.9	-2.0	-1.9
LOC_Os04g04040	expressed protein	N/A	-1.8	-1.9	-1.7
LOC_Os08g10500	expressed protein	N/A	-1.7	-1.1	-1.7
LOC_Os02g39030	transmembrane protein 17, putative, expressed	N/A	-1.2	-2.0	-1.6
LOC_Os04g55420	leucine-rich repeat family protein, putative, expressed	N/A	-1.6	-1.5	-1.6
LOC_Os06g36940	expressed protein	N/A	-1.7	-1.7	-1.6
LOC_Os12g42410	expressed protein	N/A	-1.6	-1.7	-1.6
LOC_Os01g71830	glycosyl hydrolases family 17, putative, expressed	GLN1	-1.1	-1.8	-1.6
LOC_Os04g47720	cis-zeatin O-glucosyltransferase, putative, expressed	N/A	-1.9	-1.3	-1.5
LOC_Os05g50610	WRKY8, expressed	WRKY8	-3.0	-2.5	-1.4
LOC_Os11g08380	1-aminocyclopropane-1-carboxylate oxidase, putative, expressed	ACO4	-1.2	-1.2	-1.2

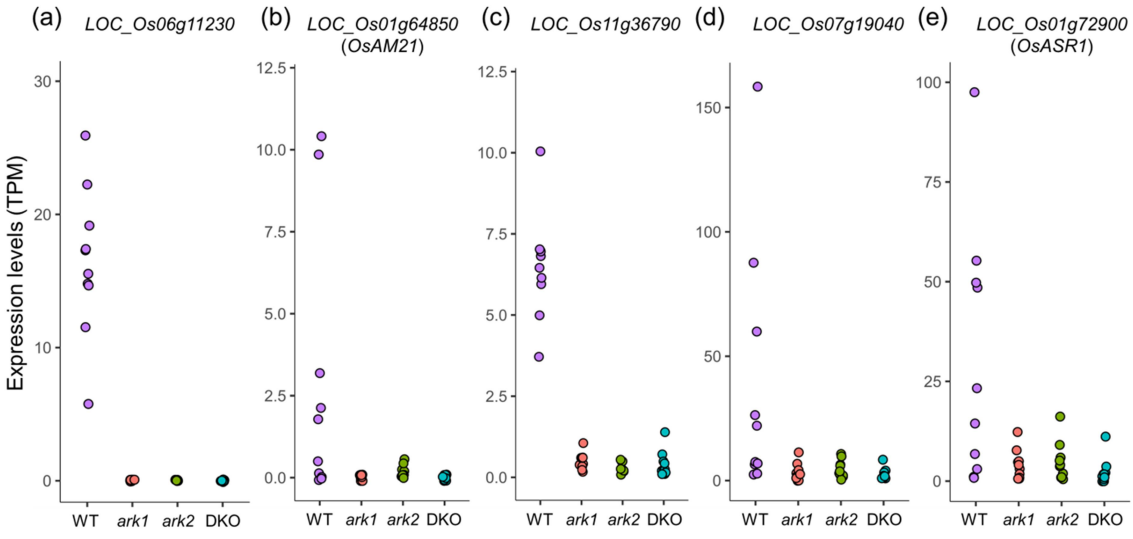

Figure 32. Expression levels of downregulated genes in Group I. The five most downregulated genes in the double knockout (DKO) in relation to the wild-type (WT) are shown. Group I includes genes downregulated in the three mutant genotypes (log2fc ≤ -1, $p \leq 0.05$). Transcripts per million (TPM) expression values of the ten individual replicates per genotype are extracted from the RNA-seq dataset.

72 genes were downregulated in *ark1* and the DKO but not in *ark2* which putatively correspond to OsARK2-independent genes (Group II, Table 4 for the 20 most downregulated genes in the DKO, Appendix Table 11 for the full list). Five of the genes in this dataset had no transcripts detected in *ark1* and the DKO (Appendix Table 9). Nine of the total 72 Group II genes have been functionally annotated (Appendix Table 7) including genes encoding a transcription factor putatively participating in the AM symbiosis (*OsAM18*, *LOC_Os03g40080*, Fiorilli et al., 2015b) and two nutrient transporters; *NITRATE TRANSPORTER 1/PEPTIDE TRANSPORTER FAMILY 2.2* (*OsNPF2.2*, *LOC_Os12g44100*, Li et al., 2015) and *PHOSPHATE TRANSPORTER 4* (*OsPT4*, *LOC_Os04g10750*, Ye et al., 2015; Zhang et al., 2015; Ye et al., 2017). Four of the Group II genes are conserved in AM competent plant genomes (Bravo et al., 2016, Appendix Table 10). These encode a predicted ABC transporter (*LOC_Os04g40570*), a dehydrogenase (*OsDHY1*, *LOC_Os12g43740*), a cytochrome P450 domain-containing protein (*LOC_Os07g33620*) and a subunit of Replication Factor C (*OsRFCb*, *LOC_Os10g42400*). In addition, *DHY1* and *RFCb* had been confirmed to occur in the AM liverwort *M. paleacea* but absent in the non-host *M. polymorpha* (Radhakrishnan et al., 2020). The most downregulated Group II gene in the DKO compared to the wild-type is predicted to encode for a GRAS transcription factor (*LOC_Os11g04590*, see expression graph along with the five most downregulated Group II genes in the DKO in Fig. 33). This gene along with *OsAM18* is the only GRAS transcription factor predicted in this dataset. *LOC_Os11g04590* is one of the nine rice members of the Scarecrow-like 3 (SCL3) clade of GRAS transcription factors while *OsAM18* belongs to the *Lilium longiflorum* Scarecrow-like (LlSCL) clade that has 13 members in rice (Cenci and Rouard, 2017). Other three predicted transcriptions factors from different protein subfamilies are present in this dataset (Appendix Table 12).

Interestingly, more than a quarter of the 42 genes strictly dependent on *OsSMAX1* mutation for their expression in uninoculated rice plants (Choi et al., 2020), can be found in Group II (Appendix Table 8). These include the third most downregulated gene in the DKO, *LOC_Os01g42150*, which encodes a short 95 amino acid-long predicted protein with a signal peptide for secretion. Collectively, catalytic activity, binding and hydrolase activity are the three most represented molecular function GO slims, with the three categories being present in at least 20% of the downregulated genes.

Table 4. Genes downregulated in *ark1* and the DKO but not in *ark2* in relation to the wild-type (Group II, log2fc ≤ -1, $p \leq 0.05$). Only the 20 most downregulated genes in the DKO are displayed from a total of 72 genes in this dataset. For the full list see Appendix Table 11. Log2 fold change compared to the WT is displayed with red hue intensity correlating to stronger downregulation. Genes are ordered based on DKO fold change expression. Locus IDs in red correspond to genes with no expression in the DKO (see Appendix Table 9 for details of all genes with no expression in the DKO). Names of the protein products of functionally annotated genes are given. For their functions and references, see Appendix Table 7.

Locus ID	Predicted annotation	Functional annotation	*ark1* log2fc	DKO log2fc
LOC_Os11g04590	GRAS family transcription factor containing protein, expressed	N/A	-5.6	-6.4
LOC_Os01g58660	LTPL29 - Protease inhibitor/seed storage/LTP family protein precursor, expressed	N/A	-5.5	-6.3
LOC_Os01g42150	MEGL13 - Maternally expressed gene MEG family protein precursor, expressed	N/A	-3.7	-5.3
LOC_Os09g28840	OsSCP43 - Putative Serine Carboxypeptidase homologue, expressed	N/A	-7.2	-4.4
LOC_Os01g72910	abscisic stress-ripening, putative, expressed	Asr2	-5.5	-4.3
LOC_Os10g34760	RIPER3 - Ripening-related family protein precursor, putative, expressed	N/A	-4.8	-3.7
LOC_Os03g38350	expressed protein	N/A	-2.5	-3.4
LOC_Os06g20110	expressed protein	N/A	-5.4	-3.3
LOC_Os06g45240	inactive receptor kinase At2g26730 precursor, putative, expressed	N/A	-3.8	-3.2
LOC_Os05g06814	expressed protein	N/A	-3.2	-3.1
LOC_Os05g48740	expressed protein	N/A	-2.6	-2.7
LOC_Os09g26380	aminotransferase, classes I and II, domain containing protein, expressed	N/A	-2.4	-2.7
LOC_Os11g34740	hypothetical protein	N/A	-2.5	-2.5
LOC_Os01g41810	cytochrome P450 72A1, putative, expressed	N/A	-2.1	-2.5
LOC_Os12g40180	expressed protein	N/A	-2.5	-2.5
LOC_Os03g40080	GRAS family transcription factor containing protein, expressed	AM18	-2.9	-2.4
LOC_Os09g30462	expressed protein	N/A	-3.1	-2.4
LOC_Os06g46020	expressed protein	N/A	-2.4	-2.4
LOC_Os01g35610	expressed protein	N/A	-2.4	-2.3
LOC_Os08g23170	expressed protein	N/A	-2.3	-2.3

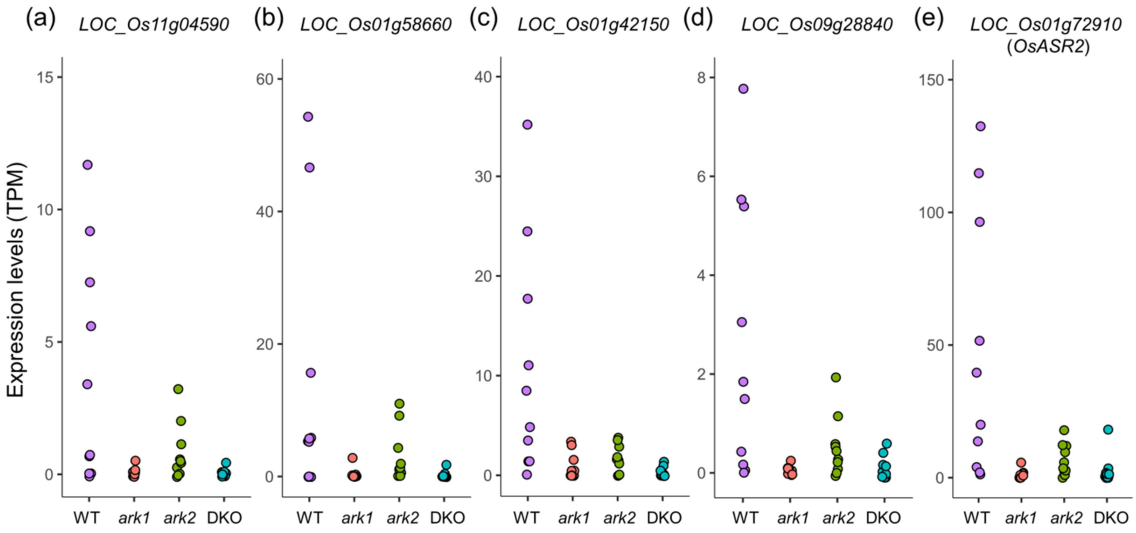

Figure 33. Expression levels of downregulated genes in Group II. The five most downregulated genes in the double knockout (DKO) in relation to the wild-type (WT) are shown. Group II includes genes downregulated in the *ark1* mutant and the DKO (log2fc ≤ -1, $p \leq 0.05$) but not in the *ark2* mutant. Transcripts per million (TPM) expression values of the ten individual replicates per genotype are extracted from the RNA-seq dataset.

A set of 13 genes were downregulated in *ark2* and the DKO but not in *ark1* which putatively correspond to OsARK1-independent genes (Group III, Table 5). Four of these genes have been functionally annotated. These include genes coding for a putative subtilase inhibitor (*OsOCPI1*, *LOC_Os01g42860*, Huang et al., 2007b) and a mannose-binding lectin that has been shown to interact with a *M. oryzae* chitinase (*OsMBL1*, *LOC_Os01g24710*, Claes et al., 1990; Han et al., 2019). *OCPI1* is conserved among AM plant clade genomes (Bravo et al., 2016). The most downregulated gene in this dataset, *LOC_Os06g09400*, is also the only one with no expression in *ark2* and the DKO (Appendix Table 9). *LOC_Os06g09400* is predicted to encode a short 126 amino acid-long protein with no known domains. Expression level graphs are shown for the five most downregulated Group III genes in the DKO (Fig. 34). Catalytic activity and binding are the two most represented molecular function GO terms in this set of genes, with four and three genes in these categories respectively.

Table 5. Genes downregulated in *ark2* and the DKO but not in *ark1* in relation to the wild-type (Group III, log2fc ≤ -1, $p \leq 0.05$). Log2 fold change compared to the WT is displayed with red hue intensity correlating to stronger downregulation. Genes are ordered based on DKO fold change expression. Locus ID in red corresponds to a gene with no expression in *ark2* and the DKO (see Appendix Table 9 for details). Names of the protein products of functionally annotated genes are given. For their functions and references, see Appendix Table 7.

Locus ID	Predicted annotation	Functional annotation	*ark2* log2fc	DKO log2fc
LOC_Os06g09400	hypothetical protein	N/A	-3.0	-2.9
LOC_Os01g42860	inhibitor I family protein, putative, expressed	OCPI1	-2.3	-2.7
LOC_Os01g24710	jacalin-like lectin domain containing protein, expressed	SalT|MBL1	-2.1	-2.1
LOC_Os06g17000	BURP domain containing protein, expressed	N/A	-2.7	-2.1
LOC_Os09g19970	expressed protein	N/A	-2.0	-2.0
LOC_Os12g08700	expressed protein	N/A	-2.0	-1.9
LOC_Os08g31850	expressed protein	N/A	-1.6	-1.9
LOC_Os01g71820	glycosyl hydrolases family 17, putative, expressed	N/A	-2.0	-1.5
LOC_Os10g28360	1,2-dihydroxy-3-keto-5-methylthiopentene dioxygenase protein, putative, expressed	ARD4	-1.0	-1.3
LOC_Os02g04690	cycloartenol synthase, putative, expressed	N/A	-1.5	-1.3
LOC_Os04g16722	uncharacterized protein ycf68, putative, expressed	N/A	-1.6	-1.2
LOC_Os03g12290	glutamine synthetase, catalytic domain containing protein, expressed	GLN1;2|GS1;2	-1.2	-1.1
LOC_Os01g57350	diacylglycerol kinase, putative, expressed	N/A	-1.0	-1.1

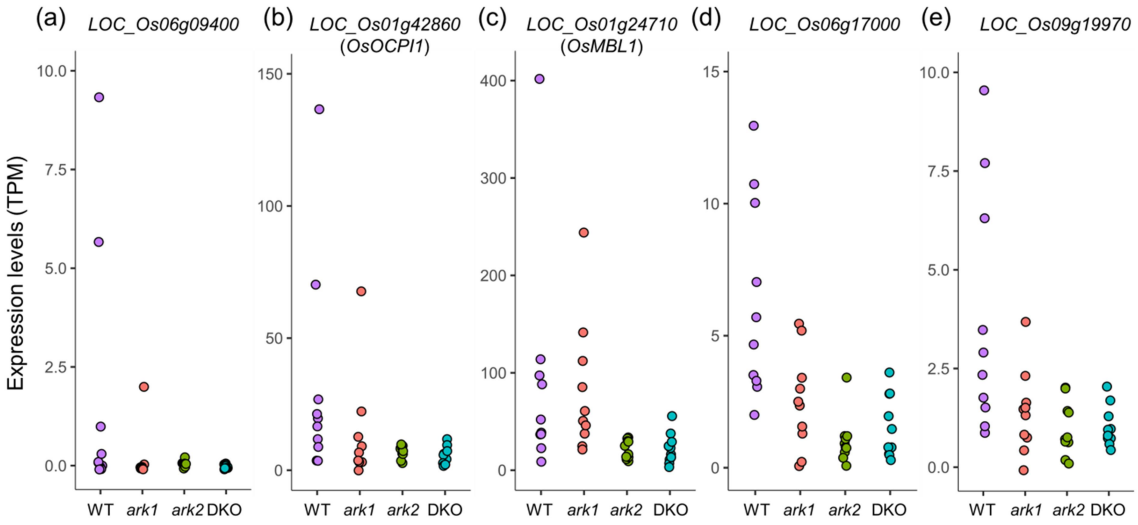

Figure 34. Expression levels of downregulated genes in Group III. The five most downregulated genes in the double knockout (DKO) in relation to the wild-type (WT) are shown. Group III includes genes downregulated in the *ark2* mutant and the DKO (log2fc ≤ -1, $p \leq 0.05$) but not in the *ark1* mutant. Transcripts per million (TPM) expression values of the ten individual replicates per genotype are extracted from the RNA-seq dataset.

60 genes were downregulated only in the DKO, suggesting them to be under redundant regulation by OsARK1 and OsARK2 (Group IV, Table 6 for the 20 most downregulated genes, Appendix Table 13 for the full list). Two of the genes in this dataset had no expression in the DKO (Appendix Table 9). 13 of the Group IV genes have been functionally annotated including the one with the greatest downregulation. This gene corresponds to *HYDROPEROXIDE LYASE 2* (*OsHPL2*, *LOC_Os02g12680*), an enzyme participating in lipid metabolism (Chehab et al., 2006; Gomi et al., 2010, see *OsHPL2* expression level graph along with the five most downregulated Group IV genes in Fig. 35). Among this set of 60 genes, *OsHPL2* is particular in the sense that it corresponds to one of the two genes whose expression negatively correlates with arbuscule levels in the *ark1* mutant (R = -0.67, p = 0.03). The other gene is *LOC_Os01g21970* which corresponds to *OsAM92* (Güimil et al., 2005). *OsAM92* expression negatively correlates with arbuscule abundance in the *ark1* mutant (R = -0.68, p = 0.02) while the correlation is positive in the wild-type (R = 0.71, p = 0.02) and in the *ark2* mutant (R = 0.69, p = 0.02). *OsAM92* is predicted to encode for a receptor-like cytoplasmic kinase from the RLCK-VIII subfamily (Appendix Table 12) and is one of the five genes in Group IV that have been previously shown to be expressed in uninoculated rice upon *OsSMAX1* mutation (Choi et al., 2020, Appendix Table 8). CLE peptides have been described to regulate AM

colonization levels (Müller et al., 2019; Karlo et al., 2020) and a gene encoding a CLE protein, *FON2 SPARE1* (*OsFOS1*, *LOC_Os02g21890*, Suzaki et al., 2009) was downregulated only in the DKO. Collectively, catalytic activity, hydrolase activity and binding are the three most represented molecular function GO terms, resembling the scenario found in the previous gene groups.

In summary, differential transcriptional signatures across mutant genotypes points towards the existence of independent, complementary and redundant functions of OsARK1 and OsARK2, but a possible residual inclusion of colonization-dependent genes in the different datasets prevents a close examination of these patterns. The overall transcriptional repression of hydrolysis-related genes dominates in the different mutant genotypes suggesting OsARK1 and OsARK2 function in the post-arbuscule development stage by regulating arbuscule degeneration pathways. Several putatively relevant signalling components downstream of the RLKs were identified including transcriptional regulators and genes conserved in AM genomes.

Table 6. Genes downregulated only in the DKO in relation to the wild-type (Group IV, log2fc ≤ -1, $p \leq 0.05$). The 20 most downregulated genes are displayed from a total of 60 genes in this dataset. For the full list see Appendix Table 13. Log2 fold change compared to the WT is displayed with red hue intensity correlating to stronger downregulation. Genes are ordered based on fold change expression. Locus IDs in red correspond to genes with no expression in the DKO (see Appendix Table 9 for details of all genes with no expression in the DKO). Names of the protein products of functionally annotated genes are given. For their functions and references, see Appendix Table 7.

Locus ID	Predicted annotation	Functional annotation	DKO log2fc
LOC_Os02g12680	cytochrome P450, putative, expressed	AOS3|HPL2	-3.3
LOC_Os06g05510	expressed protein	N/A	-3.0
LOC_Os09g25060	WRKY76, expressed	WRKY76	-2.7
LOC_Os05g04390	expressed protein	N/A	-2.6
LOC_Os03g57520	VQ domain containing protein, putative, expressed	N/A	-2.6
LOC_Os02g10550	expressed protein	N/A	-2.5
LOC_Os06g44160	heat shock protein DnaJ, putative, expressed	N/A	-2.5
LOC_Os06g12090	miro, putative, expressed	Sar1d	-2.4
LOC_Os10g18870	dirigent, putative, expressed	N/A	-2.3
LOC_Os03g38800	AAA family ATPase, putative, expressed	N/A	-2.3
LOC_Os04g45590	glyoxalase family protein, putative, expressed	N/A	-2.3
LOC_Os03g60560	ZOS3-21 - C2H2 zinc finger protein, expressed	ZFP182|ZOS3-21	-2.2
LOC_Os12g25090	expressed protein	Sci1|PR6	-2.2
LOC_Os03g21500	expressed protein	N/A	-2.2
LOC_Os03g06210	expressed protein	N/A	-2.1
LOC_Os11g47530	glycosyl hydrolase, putative, expressed	N/A	-2.0
LOC_Os11g47600	glycosyl hydrolase, putative, expressed	N/A	-2.0
LOC_Os08g02700	fructose-bisphospate aldolase isozyme, putative, expressed	N/A	-2.0
LOC_Os10g34910	secretory protein, putative, expressed	N/A	-2.0
LOC_Os01g64470	harpin-induced protein 1 domain containing protein, expressed	N/A	-1.9

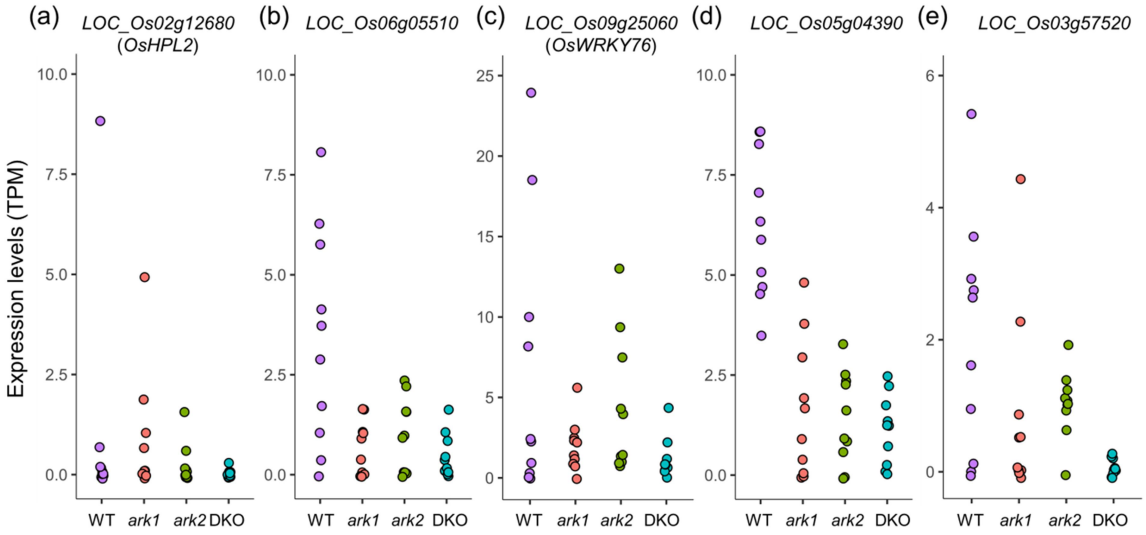

Figure 35. Expression levels of downregulated genes in Group IV. The five most downregulated genes in the double knockout (DKO) in relation to the wild-type (WT) are shown. Group IV includes genes downregulated in the DKO only (log2fc ≤ -1, p ≤ 0.05). Transcripts per million (TPM) expression values of the ten individual replicates per genotype are extracted from the RNA-seq dataset.

6.2.3. Transcriptionally induced genes in *ark1*, *ark2* and the DKO during AM symbiosis

From the total 142 genes transcriptionally induced in any of the mutant genotypes in relation to the wild-type, a subset of 97 genes of interest was identified after excluding genes upregulated in any of the single mutants but not in the DKO. These genes were assigned to four different transcriptional groups (V – VIII, Fig. 36). Half of these genes of interest were upregulated in all mutant genotypes (Group V). Protein binding, catalytic activity and nucleotide binding were among the most represented molecular function GO slims encountered (Fig. 37). GO slims for Group V genes can be found in Appendix Table 6.

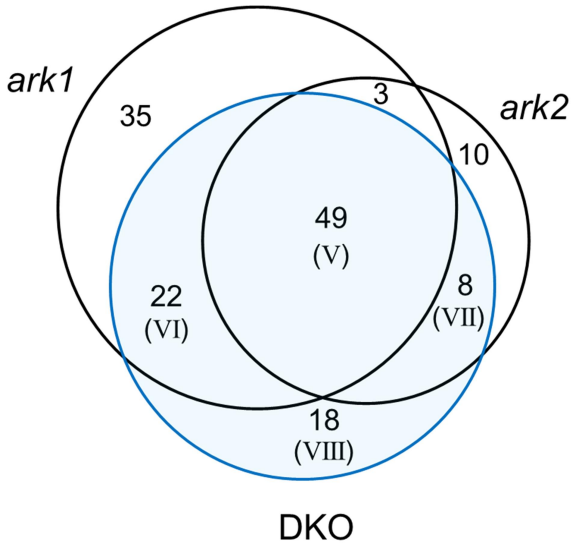

Figure 36. Upregulated genes in *ark1*, *ark2* and DKO in relation to the wild-type (log2 fold change ≥ 1, $p \leq 0.05$). RNA-seq assay was conducted over 10 biological replicates per genotype (inoculated with 300 *R. irregularis* spores, harvested at 6 weeks post inoculation). Blue circled gene groups of interest (V to VIII) are discussed in the text.

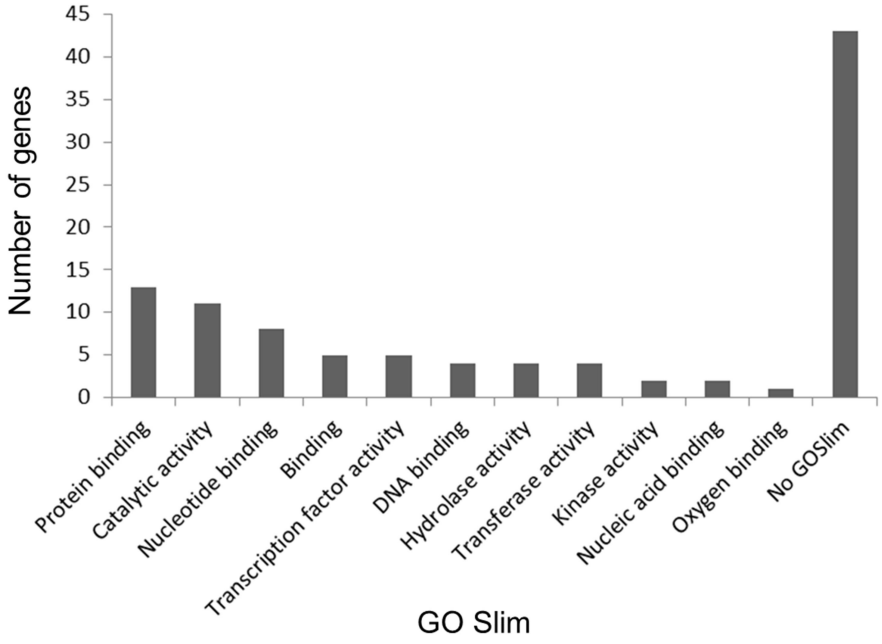

Figure 37. Molecular function GO slim occurrence in groups V – VIII. A given gene can have several associated GO slims.

A total of 49 genes were upregulated in *ark1*, *ark2* and DKO (Group V, Table 7 for the 20 most upregulated genes in the DKO, Appendix Table 14 for the full list). The most upregulated gene in the three mutant genotypes, *LOC_Os03g02470*, encodes a 407

amino acid-long protein harbouring a DUF3778 domain and a transmembrane domain at the C terminal region. No other known protein domains are predicted to occur in the next three most upregulated genes, with the exception of *LOC_Os08g27870*, encoding an Early flowering 4 (Elf4) domain-containing protein. The fifth most upregulated gene in the DKO is also one of the five Group V genes that have been functionally annotated (Appendix Table 7) corresponding to *PECTIN METHYL ESTERASE 1* (*OsPME1*, *LOC_Os03g19610*) which putatively mediates cell wall mechanical properties and pollen development (Kanneganti and Gupta, 2009). *OsPME1* is also transcriptionally induced in uninoculated *smax1* rice roots (Choi et al., 2020, Appendix Table 8). Expression graphs of the above mentioned genes can be found in Fig. 38. Two Group V genes code for predicted transcription factors (Appendix Table 12) including the functionally annotated *RICE PROLAMIN-BOX BINDING FACTOR* (*OsRPBF*, *LOC_Os02g15350*) which is a transcriptional activator of rice seed storage protein genes (Yamamoto et al., 2006). Catalytic activity was the only molecular function GO slim present in more than 10% of the genes in this dataset.

A total of 22 genes were upregulated in *ark1* and the DKO but not in *ark2* (Group VI, Table 8). From the five most upregulated genes in the DKO in this dataset (see Fig. 39 for expression graphs) one codes for a protein harbouring a predicted known domain. This corresponds to *LOC_Os02g49640*, encoding a short 113 amino acid-long protein harbouring a Mediator complex Med11 domain. No molecular function GO term was evidently overrepresented in this dataset. Protein binding was the most represented being associated with three genes.

Eight putatively *OsARK1*-independent genes were upregulated in *ark2* and the DKO but not in *ark1* (Group VII, Table 9). The most upregulated gene in this dataset, *LOC_Os03g31560*, encodes a DNA helicase Pif1-like domain-containing protein. While the second most upregulated gene does not harbour known domains, the third most upregulated gene, *LOC_Os02g52730*, encodes a nitrite/sulphite reductase domain-containing protein. The fourth and fifth most upregulated Group VII genes, *LOC_Os07g10580* and, *LOC_Os07g40690*, encode a predicted cysteine-rich Gliadin-containing protein and a member of the NAD dependent epimerase/dehydratase family respectively (see Fig. 40 for expression graphs of the five most upregulated Group VII genes in the DKO). No gene in this dataset was found to be functionally annotated. The

molecular function GO slims catalytic activity and protein binding were associated with two genes.

Table 7. Genes upregulated in *ark1*, *ark2* and the DKO in relation to the wild-type (Group V, log2fc > 1, $p \leq 0.05$). Only the 20 most upregulated genes are displayed from a total of 49 genes in this dataset. For the full list see Appendix Table 14. Log2 fold change compared to the WT is displayed with blue hue intensity correlating to stronger upregulation. Genes are ordered based on DKO fold change expression. Names of the protein products of functionally annotated genes are given. For their functions and references, see Appendix Table 7.

Locus ID	Predicted annotation	Functional annotation	*ark1* log2fc	*ark2* log2fc	DKO log2fc
LOC_Os03g02470	expressed protein	N/A	12.6	12.6	12.3
LOC_Os03g43100	expressed protein	N/A	10.9	11.0	10.9
LOC_Os08g27870	EARLY flowering protein, putative, expressed	N/A	11.4	10.7	10.7
LOC_Os02g53240	expressed protein	N/A	9.8	9.5	9.7
LOC_Os03g19610	pectinesterase, putative, expressed	PME1	9.3	8.1	8.7
LOC_Os05g50390	expressed protein	N/A	7.0	8.2	8.6
LOC_Os06g11240	12-oxophytodienoate reductase, putative, expressed	N/A	8.4	8.7	8.5
LOC_Os12g05220	expressed protein	N/A	8.4	8.3	8.3
LOC_Os07g01960	hypothetical protein	N/A	8.7	8.1	8.2
LOC_Os08g10612	expressed protein	N/A	8.7	8.7	8.2
LOC_Os09g38104	hypothetical protein	N/A	6.6	8.2	8.1
LOC_Os05g34490	expressed protein	N/A	8.0	8.2	7.8
LOC_Os02g15350	dof zinc finger domain containing protein, putative, expressed	RPBF|Dof3	8.4	8.4	7.8
LOC_Os09g22160	expressed protein	N/A	7.3	8.2	7.6
LOC_Os04g32080	11-beta-hydroxysteroid dehydrogenase, putative, expressed	N/A	7.5	6.8	7.5
LOC_Os04g52790	expressed protein	N/A	7.1	7.0	7.1
LOC_Os08g10870	hypothetical protein	N/A	5.5	6.9	7.0
LOC_Os12g01250	csAtPR5, putative, expressed	N/A	6.3	6.2	6.9
LOC_Os01g35330	circumsporozoite protein precursor, putative, expressed	N/A	5.3	6.7	6.4
LOC_Os06g04930	expressed protein	N/A	6.5	6.1	6.0

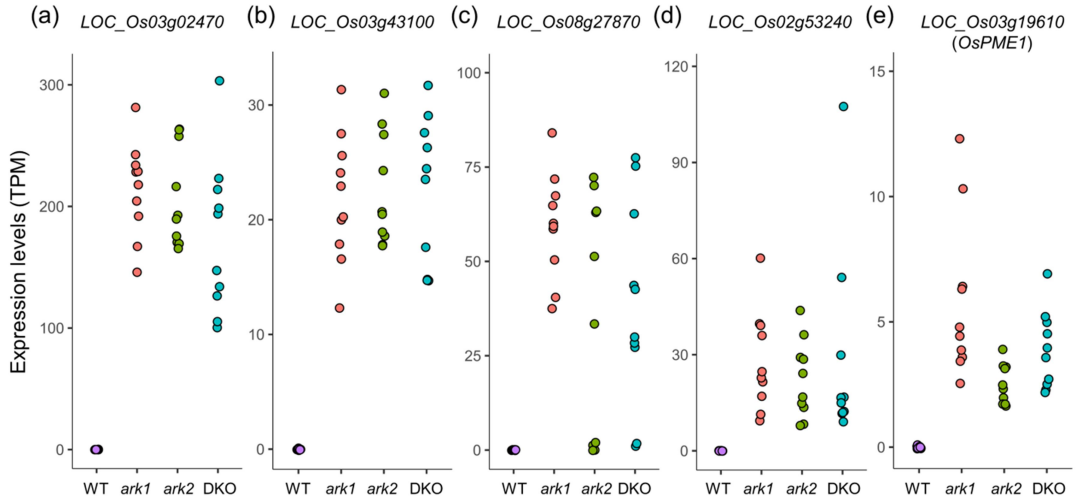

Figure 38. Expression levels of upregulated genes in Group V. The five most upregulated genes in the double knockout (DKO) in relation to the wild-type (WT) are shown. Group V includes genes upregulated in the three mutant genotypes (log2fc ≥ 1, $p \leq 0.05$). Transcripts per million (TPM) expression values of the ten individual replicates per genotype are extracted from the RNA-seq dataset.

Table 8. Genes upregulated in *ark1* and the DKO but not in *ark2* in relation to the wild-type (Group VI, log2fc > 1, $p \leq 0.05$). Log2 fold change compared to the WT is displayed with blue hue intensity correlating to stronger upregulation. Genes are ordered based on DKO fold change expression.

Locus ID	Predicted annotation	Functional annotation	*ark1* log2fc	DKO log2fc
LOC_Os04g02490	expressed protein	N/A	11.1	10.0
LOC_Os02g49640	expressed protein	N/A	10.7	9.8
LOC_Os07g26100	expressed protein	N/A	9.9	8.9
LOC_Os11g24890	expressed protein	N/A	8.8	8.8
LOC_Os11g31630	expressed protein	N/A	7.9	8.4
LOC_Os12g02140	hypothetical protein	N/A	6.3	6.9
LOC_Os08g40520	expressed protein	N/A	5.6	5.5
LOC_Os01g11170	expressed protein	N/A	7.2	5.1
LOC_Os08g17390	expressed protein	N/A	5.1	4.6
LOC_Os07g39240	expressed protein	N/A	3.4	2.5
LOC_Os11g39190	NB-ARC domain containing protein, putative, expressed	N/A	2.2	2.3
LOC_Os11g45090	NB-ARC domain containing protein, expressed	N/A	1.9	2.1
LOC_Os10g36670	expressed protein	N/A	2.1	1.9
LOC_Os12g08025	expressed protein	N/A	1.6	1.8
LOC_Os07g32630	UDP-glucoronosyl and UDP-glucosyl transferase domain containing protein, expressed	N/A	2.0	1.8
LOC_Os06g39070	UDP-glucoronosyl and UDP-glucosyl transferase, putative, expressed	N/A	1.6	1.4
LOC_Os12g08020	expressed protein	N/A	1.4	1.3
LOC_Os02g19470	expressed protein	N/A	1.3	1.2
LOC_Os11g45050	NBS-LRR disease resistance protein, putative, expressed	N/A	1.2	1.2
LOC_Os01g43110	expressed protein	N/A	1.1	1.1
LOC_Os01g36610	expressed protein	N/A	1.3	1.1
LOC_Os02g13600	expressed protein	N/A	1.2	1.1

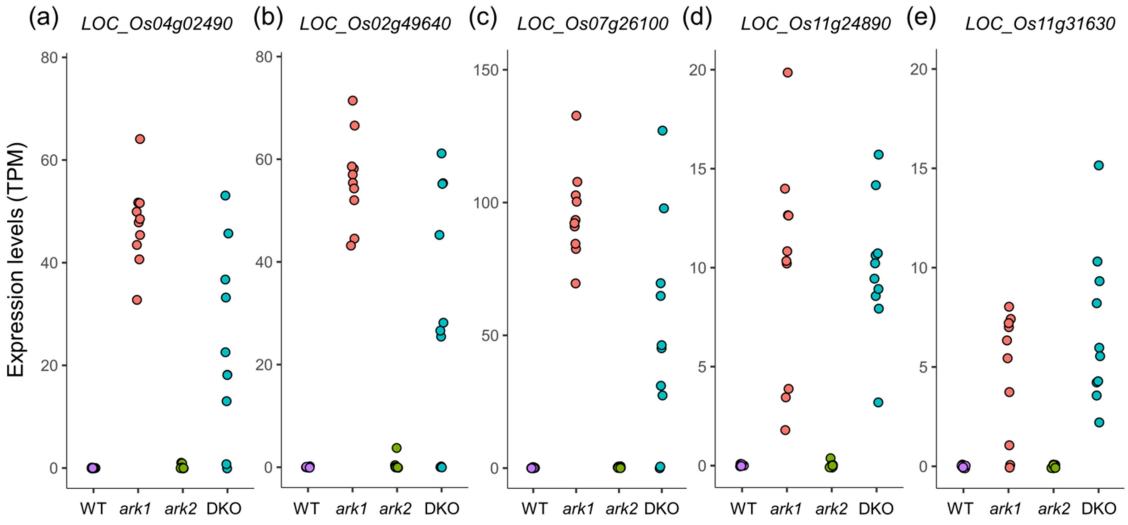

Figure 39. Expression levels of upregulated genes in Group VI. The five most upregulated genes in the double knockout (DKO) in relation to the wild-type (WT) are shown. Group VI includes genes upregulated in the *ark1* mutant and the DKO (log2fc ≥ 1, $p \leq 0.05$) but not in the *ark2* mutant. Transcripts per million (TPM) expression values of the ten individual replicates per genotype are extracted from the RNA-seq dataset.

Table 9. Genes upregulated in *ark2* and the DKO but not in *ark1* in relation to the wild-type (Group VII, log2fc > 1, $p \leq 0.05$). Log2 fold change compared to the WT is displayed with blue hue intensity correlating to stronger upregulation. Genes are ordered based on DKO fold change expression.

Locus ID	Predicted annotation	Functional annotation	*ark2* log2fc	DKO log2fc
LOC_Os03g31560	retrotransposon protein, putative, unclassified, expressed	N/A	8.6	6.3
LOC_Os04g32800	basic proline-rich protein, putative, expressed	N/A	7.4	5.7
LOC_Os02g52730	ferredoxin--nitrite reductase, putative, expressed	N/A	5.0	4.7
LOC_Os07g10580	PROLM26 - Prolamin precursor, expressed	N/A	3.5	3.3
LOC_Os07g40690	NAD dependent epimerase/dehydratase family protein, putative, expressed	N/A	2.5	2.1
LOC_Os11g24140	plastocyanin-like domain containing protein, putative, expressed	N/A	1.9	1.9
LOC_Os05g39870	CAMK_KIN1/SNF1/Nim1_like.24, expressed	N/A	1.6	1.3
LOC_Os08g06330	zinc finger C-x8-C-x5-C-x3-H type family protein, expressed	N/A	1.4	1.2

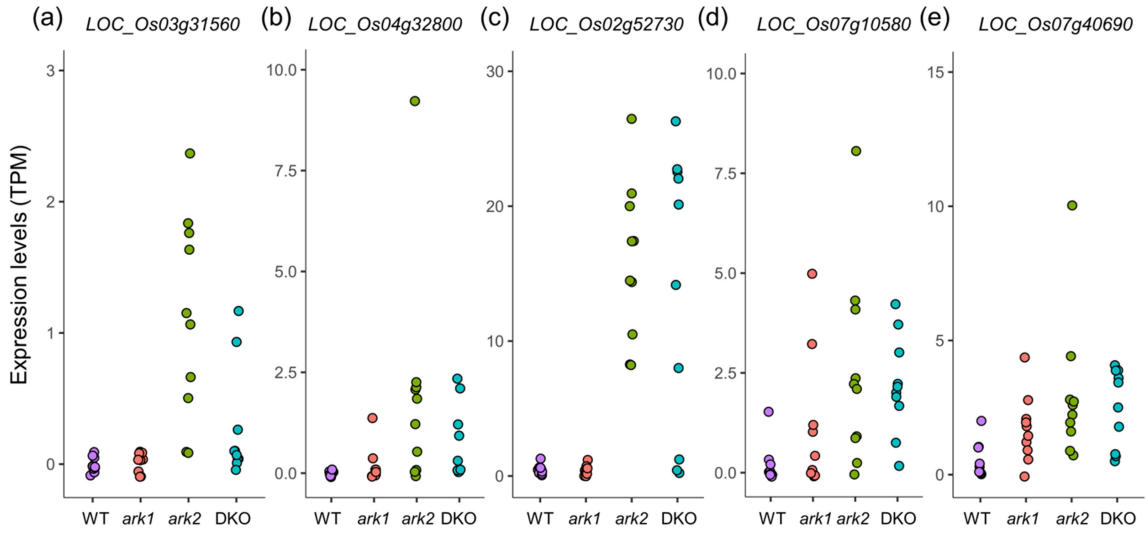

Figure 40. Expression levels of upregulated genes in Group VII. The five most upregulated genes in the double knockout (DKO) in relation to the wild-type (WT) are shown. Group VII includes genes upregulated in the *ark2* mutant and the DKO (log2fc ≥ 1, $p \leq 0.05$) but not in the *ark1* mutant. Transcripts per million (TPM) expression values of the ten individual replicates per genotype are extracted from the RNA-seq dataset.

A set of 18 genes were upregulated only in the DKO which are potentially under redundant regulation by *OsARK1* and *OsARK2* (Group VIII, Table 10). Three of these genes have been functionally annotated including the one with the greatest fold change, *S-ADENOSYL-l-METHIONINE SYNTHETASE 3* (*OsSAMS3*, *LOC_Os01g18860*), which is part of an enzyme group synthesising a cofactor essential for various methylation reactions (Li et al., 2011). The other two functionally annotated genes correspond to *AUXIN RESPONSE FACTOR 11* (*OsARF11*, *LOC_Os04g56850*, Liu et al., 2018) and *FLOURY ENDOSPERM 10* (*OsFLO10*, *LOC_Os03g07220*) which participates in endosperm development (Wu et al., 2019). Besides *OsSAMS3*, the five most upregulated

genes in this list include one encoding a cytochrome P450 domain-containing protein (*LOC_Os02g09330*), a short 86 amino acid-long protein with signal peptide (*LOC_Os07g25060*) and two genes encoding LRR domain-containing proteins (*LOC_Os02g57960* and *LOC_Os04g26350*). The gene product of *LOC_Os04g26350* is also predicted to harbour a NB-ARC domain (see Fig. 41 for expression graphs of the five most upregulated genes). In line with the other upregulated gene datasets, the predominant molecular function GO slims encountered were protein binding and catalytic activity, being associated with four and three genes from this dataset respectively.

In general, mutation of *OsARK1* and *OsARK2* renders a much more convergent response in terms of upregulated genes. While the overall slight overrepresentation of genes related with binding and catalytic activity does not reveal much about the nature of this response, the upregulation of genes related with seed nutrient process and cell wall remodelling may reflect an effort to adjust to a scenario in which arbuscule degeneration and nutrient dynamics are disrupted in the mutants.

Table 10. Genes upregulated in the DKO only in relation to the wild-type (Group VIII, log2fc > 1, $p \leq 0.05$). Log2 fold change compared to the WT is displayed with blue hue intensity correlating to stronger upregulation. Names of the protein products of functionally annotated genes are given. For their functions and references, see Appendix Table 7.

Locus ID	Predicted annotation	Functional annotation	DKO log2fc
LOC_Os01g18860	S-adenosylmethionine synthetase, putative, expressed	SAMS3	5.4
LOC_Os02g57960	Leucine Rich Repeat family protein, expressed	N/A	3.6
LOC_Os02g09330	cytochrome P450, putative, expressed	N/A	2.5
LOC_Os04g26350	Leucine Rich Repeat family protein, expressed	N/A	2.3
LOC_Os07g25060	thionin-like peptide, putative, expressed	N/A	2.1
LOC_Os06g16160	expressed protein	N/A	1.5
LOC_Os04g56850	auxin response factor, putative, expressed	ARF11	1.3
LOC_Os02g36600	aldose 1-epimerase, putative, expressed	N/A	1.3
LOC_Os03g52180	4-hydroxy-3-methylbut-2-enyl diphosphate reductase, putative, expressed	N/A	1.2
LOC_Os08g36390	ZOS8-07 - C2H2 zinc finger protein, expressed	N/A	1.2
LOC_Os10g41838	F-box protein interaction domain containing protein, expressed	N/A	1.2
LOC_Os03g60639	expressed protein	N/A	1.1
LOC_Os12g14699	protein kinase domain containing protein, expressed	N/A	1.1
LOC_Os11g30040	esterase PIR7, putative	N/A	1.1
LOC_Os08g06500	PPR repeat domain containing protein, putative, expressed	N/A	1.0
LOC_Os09g36850	expressed protein	N/A	1.0
LOC_Os03g07220	PPR repeat domain containing protein, putative, expressed	FLO10	1.0
LOC_Os11g23930	expressed protein	N/A	1.0

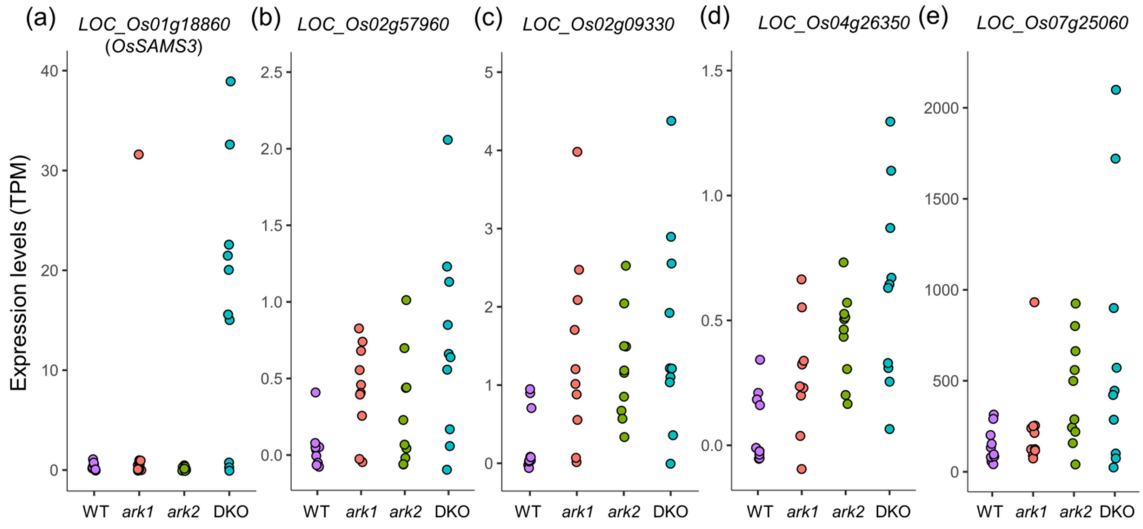

Figure 41. Expression levels of upregulated genes in Group VIII. The five most upregulated genes in the double knockout (DKO) in relation to the wild-type (WT) are shown. Group VIII includes genes upregulated in the DKO only (log2fc ≥ 1, $p \leq 0.05$). Transcripts per million (TPM) expression values of the ten individual replicates per genotype are extracted from the RNA-seq dataset.

6.2.4. Preliminary characterization of an overexpression line of *OsARK1*

OsARK1 expression is limited to arbusculated cells and its protein localization at the PAM surrounding mature to collapsing arbuscules suggests this expression may be confined to the late stages of arbuscule development (Roth et al., 2018). In order to validate the transcriptional signatures in the *ark1* mutant, an overexpression line was generated through Golden Gate cloning where *OsARK1* expression is driven by the constitutive rice ubiquitin promoter. The construct also harbours a N-terminal GFP tag (pOsUbi:OsARK1-GFP) which allowed for confocal microscopy evaluations of the first batch of T1 generation plants. Imaging on coleoptiles of germinated seedlings showed GFP signal at the cell boundaries and also perinuclear signal in plants deriving from 11 independent transformants (Fig. 42a). This indicates the ubiquitin promoter being able to drive *OsARK1* expression ectopically. In addition, a line transformed with the pOsPT11:OsARK1-GFP construct was generated. The *OsPT11* promoter likely drives the expression of genes earlier than the native *OsARK1* promoter, but still restricted to the arbusculated cell. Localization of proteins to the PAM is likely mediated by transient reorientation of secretion during arbuscule development and the promoter of the

orthologue of *OsPT11* in *M. truncatula* has been used to drive the expression of several genes for PAM localization (Pumplin et al., 2012). As many hydrolase-coding genes seem to be under transcriptional dependency of OsARK1, the pOsPT11:OsARK1-GFP line will be useful to test if hydrolases can be prematurely activated in arbusculated cells and assess if this has consequences in the lifespan of arbuscules. In T1 plants derived from five independent transformants, clear and specific GFP signal was observed in arbusculated cells (Fig. 42b). Although the purpose of these initial screenings was to preliminary evaluate the usefulness of a large number of independent transformants rather than to carefully document localization dynamics, it was still possible for the pOsPT11:OsARK1-GFP line to image some arbusculated cells where GFP signal appears to localize to the branch domain of the PAM but not to the trunk domain (Fig. 42b). This shows the *OsPT11* promoter being able to drive expression of *OsARK1* to the PAM. Gene expression and colonization assays are now needed to evaluate the effects of these spatial and temporal changes in *OsARK1* expression in both, the gene expression of the genes that putatively depend on OsARK1 and also in the overall maintenance of the AM association.

6.3. Discussion

Given that OsARK1 and OsARK2 are RLKs, which are usually placed at the start of signal transduction cascades, their symbiotic function is most likely to be indirectly exerted by downstream components under their regulation. The molecular events unfolding from a putative OsARK1/OsARK2-mediated signal perception to the metabolic processes leading to AM fungal fitness maintenance are unknown. As mechanistic insights for members of the SPARK-I subfamily are inexistent, drawing parallels is thus not possible. This prompted the development of the transcriptional survey presented here as a way to advance the understanding on the molecular machinery operating under OsARK1 and OsARK2 regulation. The dataset generated is the first for SPARK-I subfamily members.

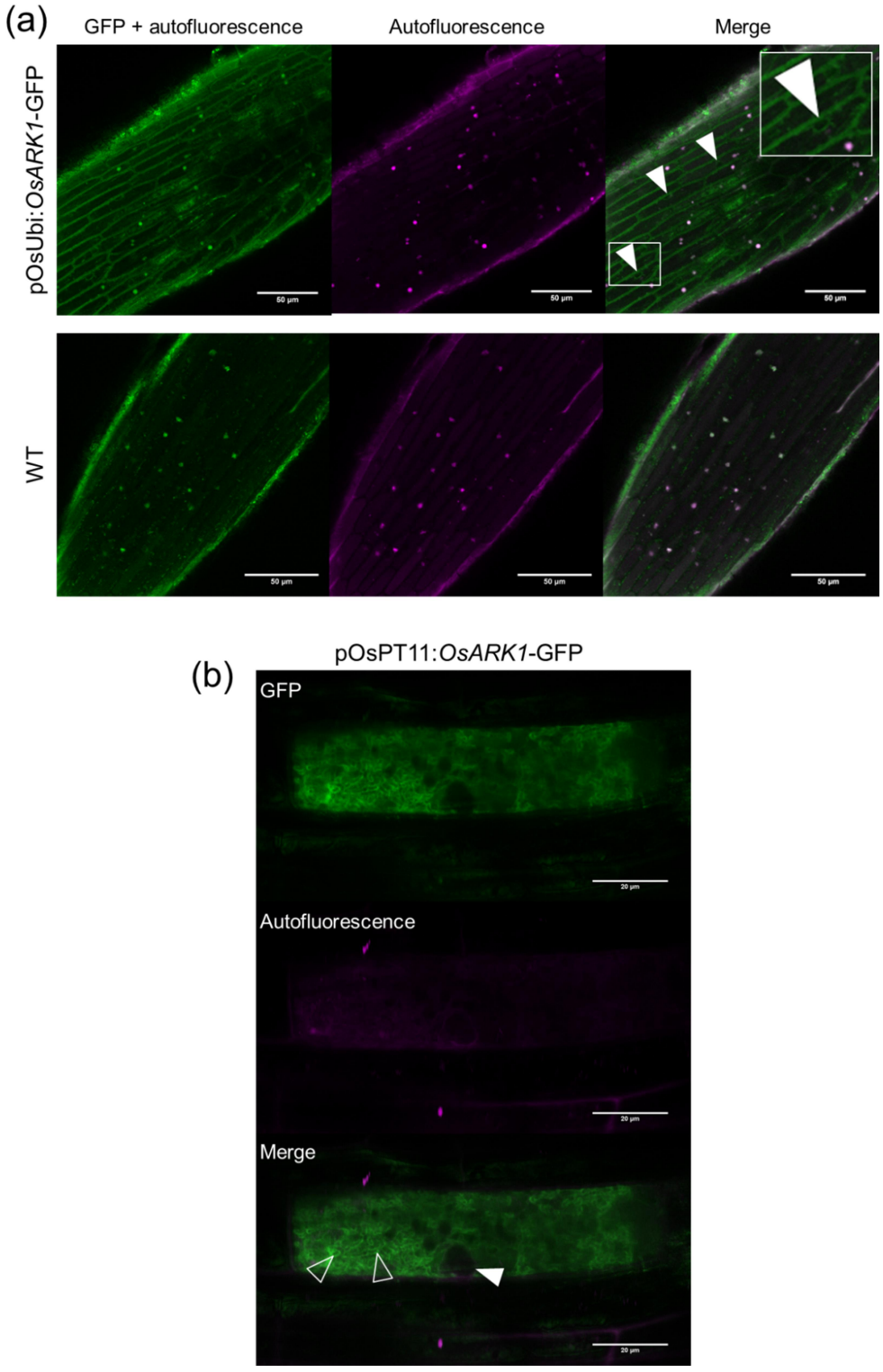

Figure 42. Live cell imaging of *OsARK1*-GFP driven by a constitutive or AM specific promoter. (a) GFP signal in coleoptiles of three-day-old rice seedlings. One representative coleoptile per genotype is shown. Arrowheads point to perinuclear signal in coleoptile cells. Inset shows in more detail the perinuclear signal. (b) Representative arbusculated cell of a pOsPT11:OsARK1-GFP plant (six weeks post inoculation). Open arrowheads indicate arbuscule branches and solid arrowhead shows the arbuscule trunk.

Transcriptional responses were measured over plants colonized with the AM fungus *R. irregularis*. The *ark1* and *ark2* single mutants and the DKO were used aiming to interrogate possible differences in the responses regulated by the two coevolving RLKs. The strategy undertaken consisted in employing a high number of biological replicates from an experiment with varying levels of colonization followed by correlation analyses to distinguish colonization-dependent genes. An alternative design using a small number of samples with homogeneous colonization levels within genotypes would lead to global transcriptional responses reflecting the overall higher colonization of the wild-type and lower in the mutants rather than OsARK1/OsARK2-dependent mechanisms. Still, many more genes appeared downregulated in the *ark1* and the DKO than in *ark2*. The volume of downregulated genes in *ark1* was even higher than that of the DKO likely as a reflection of the greater number of biological replicates in the *ark1* mutant that had very low levels of colonization in this particular experiment. The expression levels of many of these downregulated genes positively correlated with arbuscule abundance in the mutants and were considered unlikely to depend on OsARK1/OsARK2. These included known transcriptional markers of colonization levels such as *OsAM1* (*LOC_Os04g04750*), *OsPT11* and *OsSTR* (Gutjahr et al, 2008). Also, most of the components of a proposed AM-specific lipid biosynthesis pathway (Bravo et al., 2017; Jiang et al., 2017; Keymer et al., 2017; Luginbuehl et al., 2017; Brands et al., 2018; Jiang et al., 2018) including the rice orthologues of *WRI5* (*LOC_Os05g45954*), *FatM* (*LOC_Os01g31760*) and *RAM2* (*LOC_Os03g52570*) were downregulated in *ark1* and the DKO but positively correlated with colonization in the mutants.

Although the downregulated gene-filtered dataset importantly reduced the volume of colonization-dependent genes, it is expected that several genes that do not fully correlate with arbuscule levels in a biological context (but whose expression is for instance associated to the abundance of other symbiotic structures) remained in the dataset despite not being under regulation by OsARK1 and/or OsARK2. This can be inferred as the volume of downregulated transcripts in *ark1* and the DKO, although reduced to half after filtering, was still bigger than that of *ark2*. As such, unequivocally individualizing responses exclusively dependent of one of the two RLKs was not possible but general conclusions could be drawn. In addition, several individual components putatively operating under OsARK1 and OsARK2 regulation were identified

and some genes could be stringently associated to the RLKs' function as no expression was detected in any of the high number of individual mutant biological replicates despite varying levels of AM colonization. It will be important to validate in independent experiments the results here presented by assessing the transcriptional changes of selected genes in the different mutant backgrounds.

As several genes were downregulated in the single mutants and others did only in the DKO, it can be inferred that the two RLKs can complementary and redundantly influence gene expression in pathways that may overlap or crosstalk. From the many genes that displayed reduced but not abolished expression in any of the mutant genotypes, one cannot rule out that *OsSPARK1*, the only other member of this subfamily in rice, may at some extent redundantly regulate their expression.

Notably, several genes coding for predicted hydrolases were downregulated across all transcriptional groups. Among them, an endo-1,3-β-glucanase, OsGLN1, has been described to hydrolyse fungal β-glucans (Akiyama and Pillai, 2001) which are the most abundant fungal cell wall polysaccharides (Fesel and Zuccaro, 2016). Another hydrolase-coding gene downregulated in the three mutant genotypes, *LOC_Os07g19040*, is conserved in AM competent plant clades (Bravo et al., 2016) and belongs to the Glycoside Hydrolase 18 (GH18) family which is mostly comprised by chitinases (Lombard et al., 2014; Chen et al., 2020). Arbuscules are ephemeral structures and hydrolases are important components of the arbuscule degeneration program (Floss et al., 2017). In a *M. truncatula* mutant of the *OsPT11* orthologue, *MtPT4*, that displays prematurely degenerating arbuscules (Javot et al., 2007), global transcriptomics has shown genes coding for hydrolases to be transcriptionally induced including the orthologue of *LOC_Os07g19040*, *Medtr5g043550* (Floss et al., 2017). A MYB-like transcription factor, MtMYB1, was able to regulate the expression of some selected hydrolase-coding genes, these being downregulated in a *myb1* mutant that had no phenotypic alterations in symbiosis development and upregulated in an *MtMYB1* overexpression line, which had a *pt4*-like phenotype (Floss et al., 2017). MtMYB1 was hypothesised to regulate arbuscule degeneration in association with MtNSP1 and MtDELLA (Floss et al., 2017) whose rice orthologues had no alterations in transcript levels in any of the mutant phenotypes. *MtMYB1* orthologues are present in angiosperm but not in monocots (Floss et al., 2017). As arbuscule degeneration is a process

occurring in all AM competent plants, including bryophytes, pteridophytes and gymnosperms, MYB1 is unlikely to be the only transcription factor deploying this function. One MYB transcription factor-coding gene, *LOC_Os01g64360*, was downregulated in *ark1* and the DKO although it was the least transcriptionally repressed gene among the 72 Group II genes (log2 fold-change -1.2 and -1.0 in *ark1* and the DKO respectively, $p \leq 0.05$). *LOC_Os01g64360* is one of the 116 members of a MYB subclade in rice, which is different to the MYB-like clade in *M. truncatula* containing *MtMYB1* (Zheng et al., 2016). Thus, if an arbuscule degeneration program orchestrated by OsARK1 and/or OsARK2 exists, it is most likely to be different to the pathway described in Floss et al., (2017).

The second most downregulated gene in Group I, corresponded to the AM-induced gene *OsAM21* (Güimil et al., 2005) and is predicted to encode for a subtilase. Subtilases are serine proteases that function mainly in extracellular proteolysis and post-translational modification of other proteins (reviewed in Schaller et al., 2018). *OsAM21* is one of the three genes in rice belonging to the SBT1.13 clade. The others, *LOC_Os01g64860* (contiguous to *OsAM21*) and *LOC_Os05g36010* are not transcriptionally induced in AM conditions and do not show altered gene expression in the mutant genotypes. From a total of 33 subtilase clades, the SBT1.13, SBT1.10 and SBT4.16 are the three plant subtilase gene lineages known to mediate symbiotic interactions (Taylor and Qiu, 2017). These subtilase clades are interestingly not present in the AM non-host *A. thaliana* (Taylor and Qiu, 2017). In other plant species, members of the SBT1.13 are expressed in response to LCOs from *Sinorhizobium meliloti* in *M. truncatula* (Van Zeijl et al., 2015), nodulation with *Frankia* sp. in actinorhizal plants (Ribeiro et al., 1995; Laplaze et al., 2000; Svistoonoff et al., 2003; Hocher et al., 2006), pathogenesis with an oomycete in potato (Gao et al., 2013) and herbivory in tomato (Meyer et al., 2016). Two apoplastic *L. japonicus* subtilases, SbtM1 and SbtM3 have been shown to function in AM symbiosis with the respective mutants exhibiting reduced colonization levels and arbuscule formation (Takeda et al., 2009). However, these two subtilases belong to the SBT1.10 clade that has ten members in rice according to a recent phylogeny by Li et al., (2020) and that has diverged from the *OsAM21* SBT1.13 clade early in the evolution of angiosperms (Taylor and Qiu, 2017). Because there are no mechanistic insights on the subtilases described to function in AM symbiosis or in the other biotic interactions

mentioned above, it is not straightforward to assign a function for OsAM21. As subtilases function in the apoplast, OsAM21 may operate at the PAS by modulating cell wall dynamics, degrading fungal proteins or post-translationally modifying PAS proteins from fungal or plant origin. A plausible but, at this stage, also speculative scenario would be that extracellular subtilases along with the rest of hydrolases collectively facilitate the degradation and recycling of arbuscule-derived material during arbuscule collapse. If *ark1* and *ark2* are defective in this process, delayed arbuscule degeneration would be expected to occur. Although comparatively studying such dynamics *in vivo* would be challenging, the altered distribution of lipids observed in arbusculated cells of the mutants (Chapter 5) may reflect alterations during arbuscule degeneration in line with the observed correlation between arbuscule collapse and emergence of lipid droplets (Kobae et al., 2014).

An involvement of OsARK1 and OsARK2 in the arbuscule degeneration program would be in line with the post-arbuscule development role described for OsARK1 (Chapter 3, Roth et al., 2018). As the *ark1* mutant has reduced colonization levels that can be recovered by the presence of wild-type nurse plants, this would suggest that defective arbuscule degeneration in the mutant results in disruption of nutrient homeostasis leading to reduced fungal fitness. As surrounding wild-type plants are able to nourish the fungus and support its reproduction, the phenotype in mutant plants may likely recover by constant rounds of colonization by wild-type supported fungi, a process that can occur in the *ark1* mutant with no obstacles as OsARK1 does not regulate initial AM fungal invasion and arbuscule formation. As it is currently unknown why arbuscules degenerate at all, a link between arbuscule degeneration and sustained AM symbiosis is an exciting avenue to explore.

If OsARK1 or OsARK2 operate in standard signal transduction pathways, a potential regulation of arbuscule degeneration programs should occur through the intermediate activation of transcriptional regulators, similar to the *M. truncatula* hydrolases regulated by MtMYB1 (Floss et al., 2017). *LOC_Os11g04590*, the most downregulated gene in Group II (including genes downregulated in *ark1* and the DKO) is predicted to encode a GRAS transcription factor. In several plant species including *L. japonicus*, *Petunia hybrida* and tomato, the number of GRAS genes induced during AM colonization is the highest relative to other transcription factor families (Xue et al., 2015; Rich et al., 2017a;

Ho Plágaro et al., 2019). Several members of the GRAS family of transcription factors participate in regulating AM symbiosis (reviewed in Pimprikar and Gutjahr, 2018). *LOC_Os11g04590* is a member of the SCL3 clade of GRAS transcription factors which is different to the clades harbouring GRAS members known to function in the AM symbiosis such as RAM1, NSP1, NSP2, DIP1 RAD1, DELLA and MIG1 (Cenci and Rouard, 2017). In a time course expression experiment, two members of the SCL3 clade in tomato, *SlGRAS11* and *SlGRAS18* showed progressively increased expression during the interaction with *R. irregularis* peaking in the last time point at eight wpi (Ho Plágaro et al., 2019). In addition, promoter GUS assays showed *SlGRAS18* to be expressed in arbusculated cells (Ho Plágaro et al., 2019). Similarly, arbusculated cell-specific promoter activity has been demonstrated for one of the seven SCL3 members in *M. truncatula*, *MtGras1* (Hartmann et al., 2019). In addition, yeast two-hybrid (Y2H) assays showed that the *M. truncatula* GRAS transcription factor MtRAM1 can interact with MtGras1 (termed MtTF80, Park et al., 2015). The only member of the AM non-host *A. thaliana* that belongs to this GRAS clade, *AtSCL3*, is described to antagonize DELLA in controlling GA responses (Zhang et al., 2011). The null *scl3* mutant had reduced GA responses and enhanced expression of GA biosynthetic genes (Zhang et al., 2011). In AM plant species, the collective evidence suggests that GA levels increase in colonized roots but inhibits colonization or arbuscule development when applied exogenously, likely as a reflection of DELLA acting in different stages of symbiosis development (reviewed in Fonouni-Farde et al., 2016; Das and Gutjahr, 2019). As DELLA controls in part the arbuscule degeneration program in *M. truncatula* (Floss et al., 2017), it would be interesting to investigate if the downregulation of the GRAS gene *LOC_Os11g04590* in *ark1* and the DKO reflects an involvement of OsARK1 in GA signalling in the post-arbuscule development stage.

The only other GRAS gene downregulated in the dataset, *OsAM18*, and potentially under transcriptional dependency by OsARK1 belongs to the LlSCL clade of GRAS transcription factors (Cenci and Rouard, 2017). The phenotype of a Tos17 insertional mutant of *OsAM18* was analysed by Fiorilli et al., (2015b). In that study, reduced colonization levels in *am18* were reported at a single time point. However, they were accompanied by a reduction of root biomass (Fiorilli et al., 2015b). As such, a direct involvement of *OsAM18* in the AM symbiosis is yet to be demonstrated. There were

seven other predicted transcription factors from diverse families that were downregulated in any of the three mutant genotypes (including the above-mentioned MYB gene) but on the basis of fold change expression, the GRAS gene *LOC_Os11g04590* is the only strong transcription factor candidate to operate in an OsARK1-dependent symbiotic signalling pathway mechanism. It has to be noted, however, that transcription factors are diverse and many of the highly downregulated genes reported here may be cryptic transcriptional regulators not assigned to any established protein family.

Several other downregulated genes coding for diverse types of proteins are of potential interest. A member of an ethylene biosynthesis enzyme group, *OsACO4* (Iwai et al., 2006; Rzewuski and Sauter, 2008), was downregulated in the three mutant genotypes. Expression of *OsACO4* is also downregulated in rice roots challenged with the rice blast fungus *M. oryzae* (Marcel et al., 2010) perhaps reflecting that mutant host plants may not perceive the AM fungus as a symbiont. Genes coding for a nitrate transporter, OsNPF.2.2, and a phosphate transporter, OsPT4, which are both involved in nutrient homeostasis (Li et al., 2015; Ye et al., 2015), where downregulated in *ark1* and the DKO whose altered expression may occur as a response to unbalanced symbiotic nutrient exchanges. Genes coding for OsOCPI1, a putative subtilase inhibitor that is also conserved in AM genomes (Huang et al., 2007b; Bravo et al., 2016) and OsMBL1, a chitinase-interacting lectin (Claes et al., 1990; Han et al., 2019) were downregulated in *ark2* and DKO but not in *ark1* which may point towards an additional role for OsARK2 in fine-tuning hydrolase activity.

The most downregulated gene in the DKO, but not in the single mutants, and potentially under redundant regulation by OsARK1 and OsARK2 is *OsHPL2*, coding for a fatty acid-cleaving hydroperoxide lyase (Chehab et al., 2006; Gomi et al., 2010). It would be interesting to test biochemically if some lipid dynamics are affected only in the DKO as the lipid assays reported in this dissertation (Chapter 5) were conducted only on the single mutants when the DKO was still not available. Other interesting genes under potential redundant regulation by the two RLKs include one of the few transcription factor-coding genes in the whole dataset, OsWRKY76, which is a transcriptional repressor of biosynthetic fungal pathogen defence-related metabolites (Yokotani et al., 2013; Liu et al., 2016; Liang et al., 2017) and one of the five kinases found to be

downregulated in this study, OsAM92. Also, a CLE protein-coding gene, *OsFOS1*, was downregulated only in the DKO. The CLE peptide MtCLE53 was recently found to regulate SL production through a root-to-shoot-to-root signalling pathway involving the LRR RLK SUPER NUMERIC NODULES (MtSUNN) (Müller et al., 2019; Karlo et al., 2020). OsFOS1 regulates floral meristem maintenance in conjunction with the CLE peptide FLORAL ORGAN NUMBER 2 (OsFON2) whose receptor is the LRR RLK OsFON1, the rice orthologue of MtSUNN (Suzaki et al., 2009). A redundant regulation by OsARK1 and OsARK2 of a CLE-mediated AM signalling mechanism is thus possible to occur although considering the high volume of CLE protein-coding genes in plant genomes, OsFOS1 might operate in signalling pathways different than the one described in Müller et al., (2019) and Karlo et al., (2020).

Interestingly nearly half of the 42 genes previously shown to require the removal of the suppressor of AM signalling, OsSMAX1, for their expression (Choi et al, 2020) were downregulated in any of the three mutant genotypes. The expression of *OsSMAX1* itself was not affected in the different mutant backgrounds. Genes encoding the hydrolase OsGLN1 and the kinase OsAM92 belong to this group of downregulated genes. OsSMAX1 is part of a signalling pathway that allows AM colonization upon perception of a currently unknown butenolide compound by the karrikin receptor OsD14L (Gutjahr et al., 2015a). OsD14L mediates OsSMAX1 removal, allowing activation of downstream AM signalling pathways (Choi et al., 2020). OsSMAX1 was proposed to negatively regulate several AM conserved genes including *OsARK2* (Choi et al., 2020). These observations suggest the OsD14L signalling pathway to operate in different stages of symbiosis development and to exert influence over the OsARK1/OsARK2 signalling pathway.

Many genes were importantly induced in the three mutant genotypes surpassing in volume of genes the other upregulated transcriptional groups. *OsPMI*, a cell wall remodelling-related gene (Kanneganti and Gupta, 2009) was in this group as well as *OsRPBF*, the gene encoding a transcriptional regulator of seed storage protein genes (Yamamoto et al., 2006). A limited number of genes were upregulated with independence of one of the single RLKs. Although differential regulation by OsARK1 or OsARK2 in upregulated genes is possible, the small subset of candidates and their lack of predicted protein domains and GO terms do not allow to associate these genes with particular molecular processes. The exclusive upregulation of several genes in the DKO,

again suggest the existence of complementary and redundant functions for the two RLKs. As before, endosperm development was represented by an annotated gene, *OsFLO10* (Wu et al., 2019). The upregulation of these genes described to function in seed nutrient dynamics together with the auxin response factor *OsARF11* (Liu et al., 2018) and a DNA methylation-related gene (*OsSAMS3*, Li et al., 2011) point towards a general reprograming of metabolic pathways. This probably takes place as a way of adjusting to the nutrient unbalances caused by hosting a microbe where symbiosis homeostasis is lost. However, as no evident alterations in plant growth are perceived in either the single or double mutants (Chapter 5), these putative metabolic changes may result in localized effects.

In summary, this first survey on the transcriptional responses of mutants of members of the SPARK-I subfamily in rice revealed several putatively important elements constituent of an OsARK1 and OsARK2 signalling circuit. On the basis of level of downregulation in different transcriptional groups, previous functional gene annotations, links to other AM signalling pathways and ancient conservation in AM plant genomes, a subset of genes was identified to prioritize in further studies. For those genes downregulated in *ark1* it may be useful to test for transcriptional changes employing the overexpression line of *OsARK1* generated in this study. Importantly the findings of this chapter suggest an involvement of OsARK1 and OsARK2 in the arbuscule degeneration program and an unexplored link between this program and the maintenance of AM fungal fitness.

Chapter 7

Conclusions and perspectives

7.1. Main contributions of this dissertation

AM symbiosis development is a finely orchestrated succession of profound changes in the morphology and physiology of the organisms involved. Ancient and widespread signalling pathways, as the association itself, are expected to control the molecular events that lead to a successful mutualism. Inherent in the AM association, is the rapid development and collapse of arbuscules, around which a complex symbiotic interface forms to facilitate inter-organismic communication and nutrient exchange. The means by which plants and AM fungi perceive each other in arbusculated cells are not known. In this dissertation, a combination of genetics, cell biology and phylogenetics was used to understand the symbiotic role of a PAM-localized RLK, OsARK1. This work led to the recognition of a new symbiotic functional phase, the post-arbuscule development stage, which is required for AM symbiosis maintenance and depends on OsARK1. A new RLK with an AM symbiotic role was identified, OsARK2. The parallel evolutionary dynamics of the two RLKs led to the discovery of the SPARK domain, a previously uncharacterized protein domain of ancient origins. Transcriptomics on *OsARK1* and *OsARK2* mutants revealed the two RLKs have complementary and redundant functions and several putative components of the signalling pathways they integrate were identified.

7.1.1. A RLK functioning at the post-arbuscule development stage

RLKs perceive environmental signals and the finding of one, OsARK1, been localized to the PAM represented a first molecular component putatively perceiving signals from the PAS. Phenotypes of mutants of genes encoding proteins localized to the

arbusculated cell normally display alterations in arbuscule morphology symptomatic of a function in arbuscule development. In contrast, OsARK1 functions in the post-arbuscule development stage. The *ark1* mutant phenotype consists in a decrease in AM fungal abundance that could be rescued by nutrients or signals derived from a wild-type common mycorrhizal network. This indicated that OsARK1 regulates AM symbiosis maintenance in arbusculated cells. These cells hosted fully developed arbuscules implying that OsARK1-mediated processes occurring during arbuscule maturity or degeneration are important to sustain AM fungal fitness and consequently AM symbiosis stability over time.

7.1.2. The SPARK domain defines a new class of RLKs

A phylogenetic analysis showed *OsARK1* having a paralogue, here named *OsARK2*. The early diverging AM liverwort *M. paleacea* has one *ARK* homologue with equivalent similarity to *OsARK1* and *OsARK2*, which all belong to an unknown RLK subfamily. *ARK1* and *ARK2* orthologues exhibited a parallel evolutionary pattern or retention or loss of their ED-coding region. Constituting this ED, a new protein domain was discovered and named SPARK. The SPARK domain has a unique cysteine arrangement and is present in a significant proportion of the RLKs from the charophyte algae *K. nitens*. In land plants, the SPARK domain is present in ARK, ARK1, ARK2, ARK2-LIKE and SPARK1 orthologues identified in this dissertation, which form the SPARK-I subfamily. The SPARK domain is also present in two other undefined RLK subfamilies and in angiosperm-specific RLPs. Thus, it can be suggested that a sulphide bridge-stabilized protein domain partnered with an intracellular kinase domain early in the evolution of the Viridiplantae for perception of as-yet-unknown ligand(s) and a group of SPARK domain-containing RLKs then dedicated to foster AM symbiosis. These findings contribute to the understanding of AM and RLK evolution.

7.1.3. OsARK2, a new RLK functioning in the AM symbiosis

Stimulated by the finding of OsARK2 coevolving with OsARK1, a phenotypic characterization of an *ark2* allele was carried out. This revealed a reduced colonization

phenotype whose degree or timing of the alterations did not mirror those of the *ark1* mutant indicating the two RLKs modulating AM symbiosis in related yet different ways. As in the case of *ark1*, neither *ark2* nor the double mutant had visible alterations in arbuscule development. Lipid distribution in arbusculated cells, however, seemed altered in the mutant backgrounds. Although these patterns need confirmation, the new method to stain lipids in arbusculated cells for confocal microscopy imaging proved useful for an otherwise challenging cell type to access and represents a technical advance for AM research, with potential applications in other systems.

7.1.4. A putative link between arbuscule degeneration and AM symbiosis maintenance

Transcriptomics analyses of the single and double *ark1 ark2* mutants identified a number of genes potentially regulated by one or both RLKs. Genes encoding hydrolytic enzymes were especially well represented among genes downregulated in all mutant backgrounds. It is proposed that these hydrolytic enzymes assist in the arbuscule degeneration process. The ephemeral nature of arbuscules has for long perplexed researchers as much energy investment must take place to power the profound cellular changes associated with arbuscule formation. For the most studied RLK in this dissertation, OsARK1, a link between arbuscule collapse and AM fungal fitness can be proposed which is in line with its localization at the PAM surrounding mature to collapsing arbuscules, its mutant phenotype affected in the post-arbuscule development stage, and its hydrolase activity-related transcriptional signature.

7.2. Future perspectives

The characterization of these new AM RLKs inaugurate the study of an ancient signalling pathway whose complexity is yet to be disclosed. Extracellular signal perception requires an ED, which is missing from OsARK1 and OsARK2. The involvement in signal perception of OsSPARK1, which has an extracellular SPARK domain, in concert with OsARK1 and/or OsARK2 as co-receptors is a possibility to explore. Alternatively, it is also conceivable for the two RLKs to complex with members

of other RLK subfamilies. If this is the case, candidates may be identified by large scale interaction screenings or by selecting candidates based on their phylogenomics pattern. A similar approach would be useful to identify interactions with other kinds of proteins such as intracellular kinases or membrane proteins that can influence RLK functioning or turnover. For downstream components of the OsARK1/OsARK2 pathway(s), the transcriptomics analysis performed in this dissertation provides several candidates to further test for their involvement in the AM symbiosis.

In addition to use rice or other AM angiosperms as model systems, the study of this ancient pathway can be greatly benefited by employing *M. paleacea* as in this AM liverwort there is only one member of the SPARK-I subfamily, *MpARK*. Following the recent availability of the *M. paleacea* genome (Radhakrishnan et al., 2020), and mirroring parallel efforts in the development of *M. polymorpha* as a model system for plant molecular biology, it is expected that transformation and mutagenesis protocols will soon be available for *M. paleacea*. In addition, *MpARK* harbours a SPARK domain which in this dissertation was cloned into a vector compatible for crystallography work and pull down assays which in the future may help elucidate the function of this newly characterized protein domain.

A possible role of OsARK1 in arbuscule degeneration can be studied using the transgenic lines generated in this study through Golden Gate cloning. The overexpression line of *OsARK1* as well as *OsARK1* driven by the *OsPT11* promoter can potentially alter both the default spatial and temporal dynamics of OsARK1, evidencing via phenotypic or transcriptomics inspections a role in arbuscule degeneration. The study of lipid dynamics, both analytical and through the imaging technique developed in this dissertation can be used to complement AM phenotypic inspections. Beyond the particular RLKs analysed, the results generated in this dissertation invites to explore the fate of the plant and AM fungal-derived materials produced during arbuscule degeneration and rethink the role of arbuscule turnover as a potential driver of interspecies signalling and nourishment that results in a sustained AM symbiosis.

Appendix

Appendix Table 1. Level 0 modules for Golden Gate cloning used in this study.

Name	Code	Antibiotic selection	Type of module	Origin
***OsARK1* (genomic)**	EC85087_pL0M_S_OsARK1_85087	Kanamycin	S (Level 0)	Hector Montero
***OsUBIQUITIN* promoter**	EC15328_pL0M-PU-pOsUBI3-intron-15328	Spectinomycin	PU (Level 0)	Feike et al., 2019
***OsPT11* promoter**	pL0M-PU_OsPt11_85017 EC85017	Spectinomycin	PU (Level 0)	Ronelle Roth
TagGFP	pL0M-C-TagGFP2-85022 EC85022	Spectinomycin	C (Level 0)	Ronelle Roth
Actin terminator	EC44300 - pL0M-T-Act2-1	Spectinomycin	T (Level 0)	Weber et al., 2011
Level 1 backbone	EC47732_pL1V-F1	Ampicillin	Cloning vector (Level 1)	Weber et al., 2011
Level 2 backbone	EC60606_pL2V-GW	Kanamycin	Cloning vector (Level 2)	Andy Breakspear
End linker	EC41722_ELE1	Spectinomycin	End linker (Level 1)	Weber et al., 2011

Appendix Table 2. List and sequences of oligonucleotides

Oligonucleotide name	Sequence (5'-3')
Genotyping	
Tos17 R	GACAACACCGGAGCTATACAAATCG
T3-TDNA-LB	AGCTGTTTCCTGTGTGAAATTG
NF1782 LP	GAGGTGATCAACAGGTGGTCAGG
NF1782 RP	GATAACTTGGGCTCCATGCTCTCT
NF4582 LP	GGGATTGTGCATCTGTCTTGAGG
NF4582 RP	CCGCAATTTTCAATATCAACACGA
OsARK2-LP	AACGGGTTATTTCTTGCCCT
OsARK2-RP	CACGTTGCCTTCTCTGATGA
BdARK1-LP	CTGGCCATCGTAATCCTCAAA
BdARK1-RP	GGTAAGAACACGAAAGGCAAAC
RT-PCR	
OsGAPDH-RT-F	AGGTTCTTCCTGATTTGAATGG
OsGAPDH-RT-R	CAACTGCACTGGACGGCTTA
OsARK1.RT-1-F	GGATGGCTTTGATTATGGTAAC
OsARK1.RT-1-R	GCGTAGTTTATCGCCTTCT
OsARK1.RT-2-F	ATCAAGCACATCCACAAGTCGG
OsARK1.RT-2-R	AGCCAATGGTCCCTCTCACATC
OsARK1.RT-3-F	CTTACTGACAGAGAGCATGGAG
OsARK1.RT-3-R	AGCCCCGTTGCATACTGATACT
OsARK2-RT-1-F	ACCTGAAACGATCCAAGAAAGA
OsARK2-RT-1-R	CTCCTGCCCATCGCAATAA
OsARK2-RT-2-F	ATGGGCAGGAGGAATGTTT
OsARK2-RT-2-R	CCGACAATTTGGGTTCCATATC
OsARK2-RT-3-F	GGGATGTCTACAGCTTTGGTATG
OsARK2-RT-3-R	TGGAGATCTTTAGGGCCTTCT
BdGAPDH-RT-F	TTGCTCTCCAGAGCGATGAC
BdGAPDH-RT-R	CTCCACGACATAATCGGCAC
BdARK1-RT-1-F	CACAGAAGGGCAGTACATCAA
BdARK1-RT-1-R	CGTCGCAGTACCCAAAGAG
BdARK1-RT-2-F	CAACCTCGTCTGCCTCTTT
BdARK1-RT-2-R	CTCACATCCGTGAACACCTT
BdARK1-RT-3-F	CACATTCCAAGCTCACTTGTTC
BdARK1-RT-3-R	TGCTTTGTCCATCTCCTCATAC
Cloning SPARK domain	
MpARK-F	GAAGAAGGGGTATCTTTGGATAAAAGAGCCGGATGTCCACTCGACTTTT
MpARK-R	TATCGAATTCCTGCAGATATACCCATGGAGTCTTCCTCTTCCTGTGTCC
HM.pET-20b(+).MpARK.LP	GGAGATATACATATGGGATGTCCACTCGACTTTTCG
HM.pET-20b(+).MpARK.RP	GTGGTGGTGCTCGAGATCTGGAAGGTCAGACCTCTT

Appendix Table 3. Plant genomes used to retrieve sequences for SPARK domain searches (one species per genus over plant genomes available) and phylogenetic analyses (one species per order, species name in green). If squares are coloured, orthologues of the respective protein are present in the genome. Blue squares, presence of SPARK domain. Pink squares, absence of SPARK domain. Numbers inside coloured boxes indicate multiple copies of the respective gene in the genome.

Broad classification	Order	Species	SPARK1	ARK	ARK1	ARK2	ARK2-like	Source protein sequence (if not iTAK)
Anthocerotophyta	Anthocerotales	*Anthoceros agrestis*						Li et al., 2020
Marchantiophyta	Marchantiales	*Marchantia polymorpha*						
Marchantiophyta	Marchantiales	*Marchantia palacea*						Radhakrishnan et al., 2020
Bryophyta	Funariales	*Physcomitrella patens*						
Bryophyta	Sphagnales	*Sphagnum fallax*						
Lycophytes	Selaginellales	*Selaginella moellendorffii*						NCBI (all)
Ferns	Salviniales	*Salvinia cucullata*						
Ferns	Salviniales	*Azolla filiculoides*						FernBase
Gymnosperms	Ginkgoales	*Ginkgo biloba*						
Gymnosperms	Pinales	*Pinus lambertiana*	x2					
Gymnosperms	Pinales	*Picea abies*	x2					
ANA grade	Amborellales	*Amborella trichopoda*						NCBI (ARK1)
Magnoliids	Laurales	*Cinnamomum micranthum*						NCBI (all)
Monocots	Alismatales	*Spirodela polyrhiza*						
Monocots	Alismatales	*Lemna minor*						
Monocots	Alismatales	*Zostera marina*						
Monocots	Pandanales	*Xerophyta viscosa*						
Monocots	Asparagales	*Dendrobium officinale*						
Monocots	Asparagales	*Phalaenopsis equestris*						
Monocots	Arecales	*Phoenix dactylifera*						NCBI (all)
Monocots	Poales	*Ananas comosus*						NCBI (ARK1)
Monocots	Poales	*Leersia perrieri*						
Monocots	Poales	*Oryza sativa*						NCBI (ARK2)
Monocots	Poales	*Phyllostachys heterocycla*						
Monocots	Poales	*Brachypodium distachyon*						Phytozome (ARK2)
Monocots	Poales	*Aegilops tauschii*						Uniprot (ARK1), NCBI (ARK2)
Monocots	Poales	*Hordeum vulgare*						
Monocots	Poales	*Triticum urartu*						
Monocots	Poales	*Lolium perenne*						
Monocots	Poales	*Panicum hallii*						
Monocots	Poales	*Setaria viridis*						
Monocots	Poales	*Dichanthelium oligosanthes*						
Monocots	Poales	*Echinochloa crus-galli*	x2					
Monocots	Poales	*Sorghum bicolor*			X2			
Monocots	Poales	*Zea mays*						NCBI (ARK2)
Monocots	Poales	*Eragrostis tef*			X2	X2		
Monocots	Poales	*Oropetium thomaeum*						
Monocots	Poales	*Zoysia pacifica*						
Monocots	Zingiberales	*Musa acuminata*						
Basal Eudicots	Ranunculales	*Aquilegia coerulea*						
Basal Eudicots	Ranunculales	*Macleaya cordata*						
Core Eudicots (superrosids)	Saxifragales	*Kalanchoe laxifora*			x2	X2		
Core Eudicots (superrosids)	Saxifragales	*Rhodiola crenulata*						
Core Eudicots (rosids)	Vitales	*Vitis vinifera*						NCBI (ARK1, ARK2)
Core Eudicots (rosids)	Oxalidales	*Cephalotus follicularis*						
Core Eudicots (rosids)	Malpighiales	*Manihot esculenta*						
Core Eudicots (rosids)	Malpighiales	*Ricinus communis*						
Core Eudicots (rosids)	Malpighiales	*Linum usitatissimum*			x2			
Core Eudicots (rosids)	Malpighiales	*Populus trichocarpa*			x2			
Core Eudicots (rosids)	Malpighiales	*Salix purpurea*						

Appendix Table 3. (continuation)

Broad classification	Order	Species	SPARK1	ARK	ARK1	ARK2	ARK2-like	Source protein sequence (if not iTAK)
Core Eudicots (rosids)	Fabales	*Ammopiptanthus nanus*						
Core Eudicots (rosids)	Fabales	*Arachis duranensis*						
Core Eudicots (rosids)	Fabales	*Glycine max*			x2			
Core Eudicots (rosids)	Fabales	*Cajanus cajan*						
Core Eudicots (rosids)	Fabales	*Phaseolus vulgaris*						
Core Eudicots (rosids)	Fabales	*Vigna angularis*						
Core Eudicots (rosids)	Fabales	*Lotus japonicus*						
Core Eudicots (rosids)	Fabales	*Medicago truncatula*						
Core Eudicots (rosids)	Fabales	*Trifolium subterraneum*						
Core Eudicots (rosids)	Fabales	*Cicer arietinum*						NCBI (ARK2-LIKE)
Core Eudicots (rosids)	Fabales	*Glycyrrhiza uralensis*					X2	
Core Eudicots (rosids)	Rosales	*Ficus carica*						
Core Eudicots (rosids)	Rosales	*Artocarpus camansi*			x2			
Core Eudicots (rosids)	Rosales	*Fragaria vesca*						
Core Eudicots (rosids)	Rosales	*Malus domestica*			x2		X4	
Core Eudicots (rosids)	Rosales	*Prunus persica*						
Core Eudicots (rosids)	Rosales	*Rosa chinensis*						
Core Eudicots (rosids)	Rosales	*Pyrus bretschneideri*			x2			
Core Eudicots (rosids)	Cucurbitales	*Citrullus lanatus*						
Core Eudicots (rosids)	Cucurbitales	*Cucumis sativus*						
Core Eudicots (rosids)	Cucurbitales	*Cucurbita maxima*						NCBI (ARK1)
Core Eudicots (rosids)	Cucurbitales	*Momordica charantia*						
Core Eudicots (rosids)	Cucurbitales	*Lagenaria siceraria*						
Core Eudicots (rosids)	Fagales	*Fagus sylvatica*						
Core Eudicots (rosids)	Fagales	*Quercus lobata*						
Core Eudicots (rosids)	Fagales	*Juglans regia*			x2		x2	
Core Eudicots (rosids)	Fagales	*Betula pendula*						
Core Eudicots (rosids)	Myrtales	*Eucalyptus grandis*						NCBI (ARK1)
Core Eudicots (rosids)	Myrtales	*Punica granatum*						
Core Eudicots (rosids)	Sapindales	*Citrus grandis*						
Core Eudicots (rosids)	Sapindales	*Atalantia buxifola*				X2		
Core Eudicots (rosids)	Sapindales	*Azadirachta indica*					X2	
Core Eudicots (rosids)	Sapindales	*Dimocarpus longan*						
Core Eudicots (rosids)	Malvales	*Theobroma cacao*			x2			
Core Eudicots (rosids)	Malvales	*Gossypium arboreum*						
Core Eudicots (rosids)	Malvales	*Corchorus capsularis*			X2			
Core Eudicots (rosids)	Brassicales	*Carica papaya*						
Core Eudicots (rosids)	Brassicales	*Arabidopsis thaliana*						
Core Eudicots (rosids)	Brassicales	*Barbarea vulgaris*						
Core Eudicots (rosids)	Brassicales	*Boechera stricta*						
Core Eudicots (rosids)	Brassicales	*Brassica rapa*						
Core Eudicots (rosids)	Brassicales	*Camelina sativa*						
Core Eudicots (rosids)	Brassicales	*Capsella grandiflora*						
Core Eudicots (rosids)	Brassicales	*Cardamine hirsuta*						
Core Eudicots (rosids)	Brassicales	*Eutrema salsugineum*						
Core Eudicots (rosids)	Brassicales	*Lepidium meyenii*						
Core Eudicots (rosids)	Brassicales	*Raphanus sativus*						
Core Eudicots (rosids)	Brassicales	*Thellungiella parvula*						
Core Eudicots (superasterids)	Caryophyllales	*Fagopyrum esculentum*						
Core Eudicots (superasterids)	Caryophyllales	*Beta vulgaris*						
Core Eudicots (superasterids)	Caryophyllales	*Spinacia oleracea*						
Core Eudicots (superasterids)	Caryophyllales	*Amaranthus hypochondriacus*						
Core Eudicots (superasterids)	Caryophyllales	*Chenopodium quinoa*						
Core Eudicots (asterids)	Cornales	*Camptotheca acuminate*			x2			
Core Eudicots (asterids)	Ericales	*Camellia sinensis*						NCBI (all)
Core Eudicots (asterids)	Ericales	*Rhododendron delavayi*						
Core Eudicots (asterids)	Ericales	*Actinidia chinensis*						
Core Eudicots (asterids)	Solanales	*Ipomoea trifida*						
Core Eudicots (asterids)	Solanales	*Petunia inflata*			X2		X2	
Core Eudicots (asterids)	Solanales	*Solanum lycopersicum*						
Core Eudicots (asterids)	Solanales	*Capsicum annuum*				X2		
Core Eudicots (asterids)	Solanales	*Nicotiana attenuata*						
Core Eudicots (asterids)	Gentianales	*Coffea canephora*						
Core Eudicots (asterids)	Gentianales	*Calotropis gigantea*						
Core Eudicots (asterids)	Lamiales	*Handroanthus impetiginosus*				x2		
Core Eudicots (asterids)	Lamiales	*Fraxinus excelsior*			X2			
Core Eudicots (asterids)	Lamiales	*Olea europaea*			X3		X2	
Core Eudicots (asterids)	Lamiales	*Mimulus guttatus*			X3			
Core Eudicots (asterids)	Lamiales	*Salvia splendis*			X2			
Core Eudicots (asterids)	Lamiales	*Mentha longifolia*						
Core Eudicots (asterids)	Asterales	*Helianthus annuus*						
Core Eudicots (asterids)	Asterales	*Cynara cardunculus*						
Core Eudicots (asterids)	Asterales	*Lactuca sativa*				X2		
Core Eudicots (asterids)	Asterales	*Erigeron breviscapus*						
Core Eudicots (asterids)	Apiales	*Daucus carota*					x2	
Core Eudicots (asterids)	Apiales	*Panax notoginseng*						

Appendix Table 4. Plant transcriptomes used to retrieve sequences for SPARK domain searches (one species per genus over plant genomes available) and phylogenetic analyses (one species per order, species name in green). If squares are coloured, orthologues of the respective protein are present in the transcriptome. Blue squares, presence of SPARK domain. Pink squares, absence of SPARK domain. Numbers inside coloured boxes indicate multiple copies of the respective gene in the transcriptome.

Broad classification	Order	Species	SPARK1	ARK	ARK1	ARK2	ARK2-like	Source protein sequence (if not iTAK)
Anthocerotophyta	Notothyladales	*Phaeoceros carolinianus*						1KP
Anthocerotophyta	Notothyladales	*Paraphymatoceros hallii*						1KP
Lycophytes	Isoetales	*Isoetes sp*						1KP
Ferns	Ophioglossales	*Sceptridium dissectum*						1KP
Ferns	Osmundales	*Osmunda sp*						1KP
Ferns	Schizaeales	*Anemia tomentosa*						1KP
Ferns	Polypodiales	*Polypodium hesperium*						1KP
Cycadophyta	Cycadales	*Encephalartos barteri*						1KP
Gymnosperms	Cupressales	*Sciadopitys verticillata*						1KP
Gymnosperms	Cupressales	*Taxus baccata*						1KP
Gymnosperms	Cupressales	*Neocallitropsis pancheri*		x2				1KP
Gymnosperms	Cupressales	*Acmopyle pancheri*						1KP
ANA grade	Austrobaileyales	*Illicium floridanum*						1KP
Magnoliids	Canellales	*Drimys winteri*						1KP
Magnoliids	Magnoliales	*Myristica fragrans*						1KP
Magnoliids	Piperales	*Saruma henryi*						1KP
Basal Core Eudicots	Dilleniales	*Hibbertia grossulariifolia*						1KP

Appendix Table 5. Details for quality control assessments of 40 samples used in RNA-seq analysis. Raw reads: the original sequencing reads counts; Clean reads: number of reads after filtering; Raw data: raw reads number multiply by read length, saved in G unit; Clean data: clean reads number multiply by read length, saved in G unit. Error rate: average sequencing error rate, which is calculated by Qphred=-10log10(e); Q20: percentages of bases whose correct base recognition rates are greater than 99% in total bases; Q30: percentages of bases whose correct base recognition rates are greater than 99.9% in total bases. GC content: percentages of guanine and cytosine in total bases.

Sample	Raw reads	Clean reads	Raw data(G)	Clean data(G)	Error rate(%)	Q20(%)	Q30(%)	GC content(%)	rRNA_rate(%)
WT 1	27050529	26065716	8.1	7.8	0.02	98.24	94.87	51.23	1.9
WT 2	25547207	24482687	7.7	7.3	0.02	98.34	95.16	51.98	5.27
WT 3	24821098	23669803	7.4	7.1	0.02	98.13	94.59	50.33	8.01
WT 4	22865325	21895497	6.9	6.6	0.02	98.19	94.74	50.93	2.19
WT 5	24856700	23849479	7.5	7.2	0.02	98.62	95.9	52.11	1.92
WT 6	26790461	26046274	8	7.8	0.02	98.4	95.28	53.57	1.36
WT 7	31491384	30362609	9.4	9.1	0.03	97.98	94.17	49.46	1.72
WT 8	26841933	25068765	8.1	7.5	0.03	97.86	93.97	49.31	35.34
WT 9	21853470	20950815	6.6	6.3	0.02	98.02	94.25	50.85	1.26
WT 10	27818187	26964534	8.3	8.1	0.02	98.08	94.47	52.8	1.12
ark1 1	34224347	33304345	10.3	10	0.02	98.02	94.32	51.12	1.8
ark1 2	23898733	23263208	7.2	7	0.02	98.11	94.56	50.18	1.25
ark1 3	30614813	29383899	9.2	8.8	0.03	97.74	93.75	51.66	7.77
ark1 4	33272589	32341290	10	9.7	0.03	97.94	94.11	51.93	1.26
ark1 5	31041198	29883696	9.3	9	0.02	98.01	94.29	52.21	1.28
ark1 6	24980210	24337594	7.5	7.3	0.02	98.27	94.84	52.65	0.86
ark1 7	22028469	21409532	6.6	6.4	0.02	98.25	94.82	51.56	1.34
ark1 8	25100527	24191442	7.5	7.3	0.02	98.23	94.75	52.42	1.02
ark1 9	22965577	22065773	6.9	6.6	0.02	98.26	94.81	51.88	2.2
ark1 10	26307003	25802896	7.9	7.7	0.02	98.24	94.76	52.05	1.8
ark2 1	27591684	26978410	8.3	8.1	0.02	98.12	94.43	51.8	0.96
ark2 2	25577944	24999498	7.7	7.5	0.02	98.36	95.02	51.89	0.76
ark2 3	25795113	25313641	7.7	7.6	0.02	98.39	95.11	52.56	2.12
ark2 4	26619486	25915372	8	7.8	0.02	98.28	94.83	52.92	2.33
ark2 5	28422166	27532870	8.5	8.3	0.02	98.28	94.91	52.31	2.67
ark2 6	24390965	23847147	7.3	7.2	0.02	98.26	94.78	52.41	1.01
ark2 7	31552938	30899022	9.5	9.3	0.02	98.14	94.6	53.34	2.11
ark2 8	24498019	24009784	7.3	7.2	0.02	98.34	95.04	53.15	1.39
ark2 9	27041604	26164132	8.1	7.8	0.02	98.17	94.59	51.08	1.37
ark2 10	24027858	23532554	7.2	7.1	0.02	98.27	94.87	52.86	1.02
DKO 1	25542058	24809820	7.7	7.4	0.02	98.29	94.88	51.39	0.98
DKO 2	24843494	24395863	7.5	7.3	0.02	98.29	94.89	51.48	0.97
DKO 3	21496101	21162443	6.4	6.3	0.02	98.31	94.94	52.74	0.75
DKO 4	29397692	28616943	8.8	8.6	0.02	98.26	94.81	51.04	0.97
DKO 5	28015991	27486257	8.4	8.2	0.02	98.15	94.5	51.98	3.78
DKO 6	22599356	22062924	6.8	6.6	0.02	98.24	94.73	49.16	1.12
DKO 7	24695270	24005319	7.4	7.2	0.02	98.26	94.78	52.03	1.34
DKO 8	25673046	25013424	7.7	7.5	0.02	98.28	94.89	52.02	2.54
DKO 9	21017739	20476626	6.3	6.1	0.02	98.28	94.9	52.66	15.82
DKO 10	22368639	21719653	6.7	6.5	0.02	98.34	94.99	51.5	2.03

Appendix Table 6. GO slims for genes downregulated (Group I, log2fc ≤ -1, $p \leq 0.05$) and upregulated (Group V, log2fc ≥ 1, $p \leq 0.05$) in the three mutant genotypes in relation to the wild-type. C, cellular component; F, molecular function; P, biological process.

Group I				
Model	Putative Function	GOSlim ID	GO Name	Type
LOC_Os01g64850.1	OsSub10 - Putative Subtilisin homologue, expressed	GO:0005623	cell	C
		GO:0016787	hydrolase activity	F
		GO:0019538	protein metabolic process	P
		GO:0008152	metabolic process	P
		GO:0005618	cell wall	C
		GO:0005515	protein binding	F
LOC_Os11g36790.1	OsFBO6 - F-box and other domain containing protein, expressed	GO:0003677	DNA binding	F
		GO:0009791	post-embryonic development	P
		GO:0005829	cytosol	C
LOC_Os07g19040.1	glycosyl hydrolase, putative, expressed	GO:0006950	response to stress	P
		GO:0008152	metabolic process	P
		GO:0009628	response to abiotic stimulus	P
		GO:0003824	catalytic activity	F
		GO:0005623	cell	C
		GO:0005488	binding	F
		GO:0016787	hydrolase activity	F
		GO:0009991	response to extracellular stimulus	P
		GO:0007154	cell communication	P
LOC_Os06g10850.1	lipase, putative, expressed	GO:0005575	cellular_component	C
		GO:0016787	hydrolase activity	F
		GO:0006629	lipid metabolic process	P
LOC_Os02g39030.2	transmembrane protein 17, putative, expressed	GO:0008152	metabolic process	P
		GO:0009987	cellular process	P
		GO:0030234	enzyme regulator activity	F
		GO:0005634	nucleus	C
LOC_Os04g55420.1	leucine-rich repeat family protein, putative, expressed	GO:0007165	signal transduction	P
LOC_Os01g71830.1	glycosyl hydrolases family 17, putative, expressed	GO:0006950	response to stress	P
		GO:0009607	response to biotic stimulus	P
		GO:0008152	metabolic process	P
		GO:0003824	catalytic activity	F
		GO:0016020	membrane	C
		GO:0005773	vacuole	C
		GO:0016787	hydrolase activity	F
		GO:0005488	binding	F
		GO:0005618	cell wall	C
		GO:0009628	response to abiotic stimulus	P
LOC_Os04g47720.1	cis-zeatin O-glucosyltransferase, putative, expressed	GO:0016740	transferase activity	F
		GO:0008152	metabolic process	P
		GO:0005829	cytosol	C
		GO:0009607	response to biotic stimulus	P
LOC_Os05g50610.1	WRKY8, expressed	GO:0009058	biosynthetic process	P
		GO:0006139	nucleobase, nucleoside, nucleotide and nucleic acid metabolic process	P
		GO:0003700	sequence-specific DNA binding transcription factor activity	F
LOC_Os11g08380.1	1-aminocyclopropane-1-carboxylate oxidase, putative, expressed	GO:0009058	biosynthetic process	P
		GO:0009987	cellular process	P
		GO:0005575	cellular_component	C
		GO:0003824	catalytic activity	F
		GO:0008152	metabolic process	P

Appendix Table 6. (continuation)

Group V				
Model	Putative Function	GOSlim ID	GO Name	Type
LOC_Os08g27870.1	EARLY flowering protein, putative, expressed	GO:0003674	molecular_function	F
		GO:0009628	response to abiotic stimulus	P
		GO:0008150	biological_process	P
LOC_Os03g19610.1	pectinesterase, putative, expressed	GO:0005618	cell wall	C
		GO:0008152	metabolic process	P
		GO:0016787	hydrolase activity	F
		GO:0008150	biological_process	P
LOC_Os06g11240.1	12-oxophytodienoate reductase, putative, expressed	GO:0006950	response to stress	P
		GO:0003824	catalytic activity	F
		GO:0008152	metabolic process	P
LOC_Os02g15350.1	dof zinc finger domain containing protein, putative, expressed	GO:0003677	DNA binding	F
		GO:0009058	biosynthetic process	P
		GO:0006139	nucleobase, nucleoside, nucleotide and nucleic acid metabolic process	P
		GO:0003700	sequence-specific DNA binding transcription factor activity	F
		GO:0009536	plastid	C
LOC_Os04g32080.1	11-beta-hydroxysteroid dehydrogenase, putative, expressed	GO:0009719	response to endogenous stimulus	P
		GO:0003824	catalytic activity	F
		GO:0008152	metabolic process	P
		GO:0006629	lipid metabolic process	P
		GO:0005623	cell	C
LOC_Os11g39160.1	NBS-LRR disease resistance protein, putative, expressed	GO:0005623	cell	C
		GO:0000166	nucleotide binding	F
		GO:0006950	response to stress	P
LOC_Os05g01330.1	expressed protein	GO:0003674	molecular_function	F
		GO:0005739	mitochondrion	C
		GO:0008150	biological_process	P
LOC_Os07g05450.1	sulfotransferase domain containing protein, expressed	GO:0005575	cellular_component	C
		GO:0008152	metabolic process	P
		GO:0016740	transferase activity	F
		GO:0009719	response to endogenous stimulus	P
LOC_Os11g43700.1	RGH1A, putative, expressed	GO:0000166	nucleotide binding	F
		GO:0006950	response to stress	P
		GO:0005886	plasma membrane	C
LOC_Os03g02180.1	cytochrome P450, putative, expressed	GO:0005783	endoplasmic reticulum	C
		GO:0009058	biosynthetic process	P
		GO:0009987	cellular process	P
		GO:0019748	secondary metabolic process	P
		GO:0003824	catalytic activity	F
		GO:0008152	metabolic process	P
		GO:0009628	response to abiotic stimulus	P
LOC_Os01g45760.1	YUC4, putative, expressed	GO:0007275	multicellular organismal development	P
		GO:0000003	reproduction	P
		GO:0009791	post-embryonic development	P
		GO:0009790	embryo development	P
		GO:0005488	binding	F
		GO:0008152	metabolic process	P
		GO:0009058	biosynthetic process	P
		GO:0009987	cellular process	P
		GO:0009653	anatomical structure morphogenesis	P
		GO:0009908	flower development	P
		GO:0000166	nucleotide binding	F
		GO:0003824	catalytic activity	F
LOC_Os01g37650.1	esterase, putative, expressed	GO:0005575	cellular_component	C
		GO:0016787	hydrolase activity	F
		GO:0008152	metabolic process	P
LOC_Os11g12340.2	disease resistance protein RPM1, putative, expressed	GO:0006950	response to stress	P
		GO:0008219	cell death	P
		GO:0005515	protein binding	F
		GO:0000166	nucleotide binding	F
		GO:0005886	plasma membrane	C
LOC_Os01g07170.1	HORMA domain containing protein, putative, expressed	GO:0016043	cellular component organization	P
		GO:0007049	cell cycle	P
		GO:0003677	DNA binding	F
		GO:0005634	nucleus	C
LOC_Os05g04410.1	peroxidase precursor, putative, expressed	GO:0006950	response to stress	P
		GO:0005576	extracellular region	C
		GO:0005515	protein binding	F
		GO:0005618	cell wall	C
		GO:0003824	catalytic activity	F
		GO:0005829	cytosol	C
		GO:0008152	metabolic process	P
LOC_Os11g44990.1	NB-ARC domain containing protein, expressed	GO:0005515	protein binding	F
		GO:0006950	response to stress	P
LOC_Os11g45180.1	NBS-LRR disease resistance protein, putative, expressed	GO:0005515	protein binding	F
		GO:0006950	response to stress	P
LOC_Os03g55720.2	cytochrome b6f complex subunit, putative, expressed	GO:0003824	catalytic activity	F
		GO:0016020	membrane	C
		GO:0009536	plastid	C
		GO:0009579	thylakoid	C
		GO:0008152	metabolic process	P
LOC_Os07g44250.1	dirigent, putative, expressed	GO:0005623	cell	C
		GO:0003674	molecular_function	F
		GO:0006950	response to stress	P
		GO:0009058	biosynthetic process	P
		GO:0009987	cellular process	P
		GO:0019748	secondary metabolic process	P

Appendix Table 7. Functionally annotated genes. Functional annotations were retrieved from the dataset of Yao et al., (2018). Log2 fold change compared to the WT is displayed with red and blue hue intensity correlating to stronger down- and upregulation respectively. Genes are ordered based on DKO fold change expression in different transcriptional groups.

				Downregulated in		
Locus ID	Protein product	Function	References	*ark1*	*ark2*	DKO
LOC_Os01g72900	Asr1	Member of ABA-stress-ripening transcription factor familiy. Regulates aluminum responsive genes.	Philippe et al., 2010; Arenhart et al., 2015	-3.0	-2.7	-3.9
LOC_Os01g71830	GLN1	Endo-1,3-β-glucanase. Induced by drought stress and ABA. recombinant protein hydrolyzed the cell wall β-glucans of a fungal pathogen.	Akiyama and Pillai, 2001	-1.1	-1.8	-1.6
LOC_Os05g50610	WRKY8	Putative regulator of ABA-independent signaling pathways during abiotic stress.	Song et al., 2009	-3.0	-2.5	-1.4
LOC_Os11g08380	ACO4	1-aminocyclopropane-1-carboxylic acid oxidase. Member of an ethylene biosynthesis enzyme group.	Iwai et al., 2006; Rzewuski and Sauter, 2008	-1.2	-1.2	-1.2
LOC_Os01g72910	Asr2	Member of ABA-stress-ripening transcription factor familiy.	Philippe et al., 2010	-5.5		-4.3
LOC_Os03g40080	AM18	AM-induced GRAS protein mediating success of AM colonization.	Fiorilli et al., 2015	-2.9		-2.4
LOC_Os07g48010	POX8.1|prx110	Peroxidase induced during infection by *Xanthomonas oryzae.*	Chittoor et al., 1997; Passardi et al., 2004	-2.0		-2.3
LOC_Os12g44100	NPF2.2	Nitrate transporter. Unloads nitrate from the xylem for root-to-shoot nitrate transport.	Li et al., 2015	-2.3		-1.9
LOC_Os03g61829	HAD1	Haloacid dehalogenase-like hydrolase. Has acid phosphatase and phytase activities. Enhances phosphate accumulation.	Pandey et al., 2017	-1.7		-1.6
LOC_Os05g10650	PPi-PFK	Pyrophosphate-dependent phosphofructo-1-kinase induced by hypoxia stress.	Pandey and Kim, 2012	-1.8		-1.5
LOC_Os09g37120	ODCa	Ornithine decarboxylase involved in putrescine synthesis and in salt stress responses.	Quinet et al., 2010	-1.2		-1.1
LOC_Os04g10750	Pht1;4|PT4	Phosphate-influx transporter. Facilitates acquisition and mobilization of phosphate and arsenate.	Ye et al., 2015; Zhang et al., 2015; Ye et al., 2017	-1.2		-1.1
LOC_Os04g01520	Nope1	N-acetylglucosamine transporter required for early signalling in AM symbiosis	Nadal et al., 2017	-1.3		-1.1
LOC_Os01g42860	OCPI1	Chymotrypsin inhibitor-like. Induced by drought stress and ABA.	Huang et al., 2007b		-2.3	-2.7
LOC_Os01g24710	SalT|MBL1	Jacalin-related mannose-binding lectin. Induced by *Magnaporthe oryzae* infection, salt stress and drought. Interacts with a *M. oryzae* chitinase.	Claes et al., 1990; Han et al., 2019		-2.1	-2.1
LOC_Os10g28360	ARD4	Acireductone dioxygenase modulating root growth in a upland rice genotype.	Ramanathan et al., 2018		-1.0	-1.3
LOC_Os03g12290	GLN1;2|GS1;2	Cytosolic Glutamine synthetase. Assimilates ammonium in roots.	Funayama et al., 2013; Yamaya and Kusano, 2014		-1.2	-1.1
LOC_Os02g12680	AOS3|HPL2	Hydroperoxide lyase. Catalyzes the cleavage of fatty acid hydroperoxides produced by lipoxygenase into aldehydes and oxoacids.	Chehab et al., 2006; Gomi et al., 2010			-3.3
LOC_Os09g25060	WRKY76	Transcriptional represor of biosynthetic fungal pathogen defense-related metabolites. Has a role in cold tolerance.	Yokotani et al., 2013; Liu et al., 2016; Liang et al., 2017			-2.7
LOC_Os06g12090	Sar1d	Small GTPase. Part of coat protein complex II (COPII) which mediates protein export from the ER to the Golgi apparatus.	Tian et al., 2013			-2.4
LOC_Os03g60560	ZFP182|ZOS3-21	C_2H_2-type zinc finger protein. Required for ABA-induced antioxidant defense. Involved in abiotic stress responses.	Huang et al., 2007a; Huang et al 2012; Zhang et al., 2012			-2.2
LOC_Os12g25090	Sci1|PR6	Subtilisin-chymotrypsin inhibitor. Induced during pathogen infection.	Gómez-Ariza et al., 2007			-2.2

Appendix Table 7. (Continuation)

Locus ID	Protein product	Function	References	Downregulated in *ark1*	Downregulated in *ark2*	Downregulated in DKO
LOC_Os03g46060	LP|PR-5	Salt stress-induced osmotin-like protein involved in salt stress tolerance.	Ren et al., 2006			-1.8
LOC_Os09g29200	GSTU17	Tau class glutathione transferase. Regulates responses to abiotic stresses.	Yang et al., 2009			-1.3
LOC_Os06g11290	OPR1	12-oxophytodienoic acid reductase. Suggested to be involved in defense and stress responses in a JA-dependent fashion.	Agrawal et al., 2003; Sobajima et al., 2007			-1.3
LOC_Os03g01320	qLTG3-1	Protein of unknown function required for the expression of defense response genes in low-temperature germinability.	Fujino et al., 2008; Fujino and Matsuda, 2010; Shim et al., 2020			-1.1
LOC_Os02g21890	FOS1	CLAVATA3/embryo surrounding region-related protein functioning in floral meristem maintenance.	Suzaki et al., 2009			-1.0
LOC_Os07g11380	RAG2	α-amylase/trypsin inhibitor regulating grain weight and seed quality.	Zhou et al., 2017b			-1.0
LOC_Os05g51570	VPE4	Member of a vacuolar processing enzyme family regulating vacuole-mediated programmed cell death.	Deng et al., 2011			-1.0
LOC_Os07g39270	GGPPS1	Plastidic geranylgeranyl diphosphate synthase. Provides precursors for chlorophyll, carotenoid and GA biosynthesis pathways.	Zhou et al., 2017a			-1.0

Locus ID	Name	Function	References	Upregulated in *ark1*	Upregulated in *ark2*	Upregulated in DKO
LOC_Os03g19610	PME1	Pectin methyl esterase putatively mediating mechanical properties of cell wall and pollen development.	Kanneganti and Gupta, 2009	9.3	8.1	8.7
LOC_Os02g15350	RPBF|Dof3	Prolamin box binding factor. GA-responsive transcriptional activator of seed storage protein genes.	Washio, 2001; Washio, 2003; Yamamoto et al., 2006; Kawakatsu et al., 2009; Schmidt et al., 2014	8.4	8.4	7.8
LOC_Os03g02180	F5HL2	Ferulate 5-hydroxylase. Cytochrome P450-dependent monooxygenase involved in the phenylpropanoid pathway.	Kim et al., 2006	3.4	3.9	3.2
LOC_Os01g45760	YUCCA1|YUC1	Involved in tryptophan-dependent auxin biosynthesis.	Yamamoto et al., 2007	2.4	2.5	2.5
LOC_Os11g12340	RPR1	Probenazole-responsive disease resistance protein.	Sakamoto et al., 1999	1.9	2.2	1.7
LOC_Os01g18860	SAMS3	S-Adenosyl-l-methionine synthetase. Participates in histone and DNA methylation to regulate gene expression during flowering.	Li et al., 2011			5.4
LOC_Os04g56850	ARF11	Auxin response factor. Transcriptional regulator of plant height and leaf angle.	Liu et al., 2018			1.3
LOC_Os03g07220	FLO10	P-type pentatricopeptide repeat protein. Participates in maintenance of mitochondrial function and endosperm development.	Wu et al., 2019			1.0

Appendix Table 8. Genes from Groups I – VIII that were upregulated in *smax1* mock plants (Choi et al., 2020). Genes in green were not expressed in wild-type plants from Choi et al., (2020) study and are therefore part of the genes strictly requiring removal of *OsSMAX1* for their expression. Log2 fold change compared to the WT is displayed with red and blue hue intensity correlating to stronger down- and upregulation respectively. Genes are ordered based on DKO fold change expression in different transcriptional groups. When available, functional annotations are given (see Appendix Table 7 for descriptions).

			Down/Upregulated in			
Locus ID	Predicted annotation	Functional annotation	*ark1*	*ark2*	DKO	
LOC_Os01g71830	glycosyl hydrolases family 17, putative, expressed	GLN1	-1.1	-1.8	-1.6	
LOC_Os01g42150	MEGL13 - Maternally expressed gene MEG family protein precursor, expressed	N/A	-3.7		-5.3	
LOC_Os05g06814	expressed protein	N/A	-3.2		-3.1	
LOC_Os09g26380	aminotransferase, classes I and II, domain containing protein, expressed	N/A	-2.4		-2.7	
LOC_Os01g41810	cytochrome P450 72A1, putative, expressed	N/A	-2.1		-2.5	
LOC_Os07g38750	AP2 domain containing protein, expressed	N/A	-2.3		-1.9	
LOC_Os10g23160	ent-kaurenoic acid oxidase 1, putative, expressed	N/A	-1.7		-1.9	
LOC_Os04g40570	ABC transporter, ATP-binding protein, putative, expressed	N/A	-2.4		-1.8	
LOC_Os04g43390	Os4bglu16 - monolignol beta-glucoside homologue, expressed	N/A	-2.3		-1.7	
LOC_Os01g50590	cytochrome P450, putative, expressed	N/A	-1.6		-1.7	
LOC_Os05g12400	BURP domain containing protein, expressed	N/A	-2.5		-1.6	
LOC_Os07g33620	cytochrome P450 domain containing protein, expressed	N/A	-1.6		-1.3	
LOC_Os07g05380	ATPase BadF/BadG/BcrA/BcrD type, putative, expressed	N/A	-1.2		-1.2	
LOC_Os08g06190	berberine and berberine like domain containing protein, expressed	N/A	-1.4		-1.2	
LOC_Os04g49500	U-box domain-containing protein, putative, expressed	N/A	-1.6		-1.2	
LOC_Os03g24730	expressed protein	N/A			-1.6	
LOC_Os01g21970	protein kinase, putative, expressed	N/A			-1.1	
LOC_Os11g14040	glutathione S-transferase, N-terminal domain containing protein, expressed	N/A			-1.0	
LOC_Os12g12590	NADP-dependent oxidoreductase, putative, expressed	N/A			-1.0	
LOC_Os07g39270	polyprenyl synthetase, putative, expressed	GGPPS1			-1.0	
LOC_Os03g02470	expressed protein	N/A	12.6	12.6	12.3	
LOC_Os03g43100	expressed protein	N/A	10.9	11.0	10.9	
LOC_Os02g53240	expressed protein	N/A	9.8	9.5	9.7	
LOC_Os03g19610	pectinesterase, putative, expressed	PME1	9.3	8.1	8.7	
LOC_Os05g50390	expressed protein	N/A	7.0	8.2	8.6	
LOC_Os12g05220	expressed protein	N/A	8.4	8.3	8.3	
LOC_Os08g10612	expressed protein	N/A	8.7	8.7	8.2	
LOC_Os09g22160	expressed protein	N/A	7.3	8.2	7.6	
LOC_Os04g52790	expressed protein	N/A	7.1	7.0	7.1	
LOC_Os10g35160	expressed protein	N/A	3.7	2.9	3.9	
LOC_Os11g45180	NBS-LRR disease resistance protein, putative, expressed	N/A	1.3	1.2	1.3	
LOC_Os11g45090	NB-ARC domain containing protein, expressed	N/A	1.9		2.1	

Appendix Table 9. Genes that had no expression in any of the 10 biological replicates of the DKO (TPM < 0.3). When likewise none of the 10 biological replicates in the single mutants had transcripts detected, cells are coloured black. Log2 fold change compared to the WT is displayed with red intensity correlating to stronger downregulation. Genes are ordered based on DKO fold change expression in different transcriptional groups.

					Downregulated in			No transcripts detected in		
Locus ID	Predicted function	Signal peptide	Pfam	GO term	*ark1*	*ark2*	DKO	*ark1*	*ark2*	DKO
LOC_Os06g11230	Expressed protein	No	N/A	N/A	-9.3	-9.4	-9.3			
LOC_Os01g64850	OsSub10 - Putative Subtilisin homologue, expressed	Yes	Subtilase family (PF00082); Peptidase inhibitor I9 (PF05922); Fibronectin type-III domain (PF17766)	Proteolysis (GO:0006508); Serine-type endopeptidase activity (GO:0004252)	-5.0	-2.6	-5.0			
LOC_Os04g28330	Expressed protein	Yes	N/A	N/A	-3.0	-2.1	-3.0			
LOC_Os05g03700	Hypothetical protein	No	N/A	N/A	-2.1	-2.3	-2.1			
LOC_Os08g26980	Expressed protein	No	N/A	N/A	-1.9	-2.0	-1.9			
LOC_Os04g04040	Expressed protein	Yes	N/A	N/A	-1.8	-1.9	-1.7			
LOC_Os12g42410	Expressed protein	No	N/A	N/A	-1.6	-1.7	-1.6			
LOC_Os11g34740	Hypothetical protein	No	N/A	N/A	-2.5		-2.5			
LOC_Os06g46020	Expressed protein	Yes	N/A	N/A	-2.4		-2.4			
LOC_Os01g35610	Expressed protein	No	N/A	N/A	-2.4		-2.3			
LOC_Os08g23170	Expressed protein	Yes	N/A	N/A	-2.3		-2.3			
LOC_Os06g14640	Zinc finger, C3HC4 type domain containing protein, expressed	No	Ring finger domain (PF13639)	N/A	-2.0		-1.9			
LOC_Os06g09400	Hypothetical protein	No	N/A	N/A		-3.0	-2.9			
LOC_Os03g21500	Expressed protein	No	N/A	N/A			-2.2			
LOC_Os03g06210	Expressed protein	No	N/A	N/A			-2.1			

Appendix Table 10. AM conserved genes. Genes were identified in Bravo et al., (2016) and rice orthologues for *DHY1*, *RFCb* and *OCPI1* were identified in Radhakrishnan et al., (2020). For the other genes, rice orthologues were identified in Choi et al., (2020). Log2 fold change compared to the WT is displayed with red intensity correlating to stronger downregulation.

				Downregulated in		
Locus ID *Oryza sativa*	Locus ID *Medicago truncatula*	Name	Putative function	*ark1*	*ark2*	DKO
LOC_Os07g19040	Medtr5g043550	N/A	Glycosyl hydrolase. Chitinase	-3.7	-3.1	-4.0
LOC_Os04g40570	Medtr3g086430	N/A	ABC transporter, ATP-binding protein,	-2.4		-1.8
LOC_Os12g43740	Medtr4g097510	DHY1	Short-chain dehydrogenase/reductase	-1.7		-1.4
LOC_Os07g33620	Medtr5g092150	N/A	cytochrome P450 domain containing protein	-1.6		-1.3
LOC_Os10g42400	Medtr3g118160	RFCb	Replication factor C subunit	-1.7		-1.3
LOC_Os01g42860	Medtr3g020970	OCPI1	Chymotrypsin inhibitor-like. Subtilisin inhibitor		-2.3	-2.7

Appendix Table 11. Genes downregulated in *ark1* and the DKO but not in *ark2* in relation to the wild-type (Group II, log2fc ≤ -1, $p \leq 0.05$, related to Table 4). Log2 fold change compared to the WT is displayed with red hue intensity correlating to stronger downregulation. Genes are ordered based on DKO fold change expression. Locus IDs in red correspond to genes with no expression in the DKO (see Appendix Table 9 for details of all genes with no expression in the DKO). Names of the protein products of functionally annotated genes are given. For their functions and references, see Appendix Table 7.

Locus ID	Predicted annotation	Functional annotation	*ark1* log2fc	DKO log2fc
LOC_Os11g04590	GRAS family transcription factor containing protein, expressed	N/A	-5.6	-6.4
LOC_Os01g58660	LTPL29 - Protease inhibitor/seed storage/LTP family protein precursor, expressed	N/A	-5.5	-6.3
LOC_Os01g42150	MEGL13 - Maternally expressed gene MEG family protein precursor, expressed	N/A	-3.7	-5.3
LOC_Os09g28840	OsSCP43 - Putative Serine Carboxypeptidase homologue, expressed	N/A	-7.2	-4.4
LOC_Os01g72910	abscisic stress-ripening, putative, expressed	Asr2	-5.5	-4.3
LOC_Os10g34760	RIPER3 - Ripening-related family protein precursor, putative, expressed	N/A	-4.8	-3.7
LOC_Os03g38350	expressed protein	N/A	-2.5	-3.4
LOC_Os06g20110	expressed protein	N/A	-5.4	-3.3
LOC_Os06g45240	inactive receptor kinase At2g26730 precursor, putative, expressed	N/A	-3.8	-3.2
LOC_Os05g06814	expressed protein	N/A	-3.2	-3.1
LOC_Os05g48740	expressed protein	N/A	-2.6	-2.7
LOC_Os09g26380	aminotransferase, classes I and II, domain containing protein, expressed	N/A	-2.4	-2.7
LOC_Os11g34740	hypothetical protein	N/A	-2.5	-2.5
LOC_Os01g41810	cytochrome P450 72A1, putative, expressed	N/A	-2.1	-2.5
LOC_Os12g40180	expressed protein	N/A	-2.5	-2.5
LOC_Os03g40080	GRAS family transcription factor containing protein, expressed	AM18	-2.9	-2.4
LOC_Os09g30462	expressed protein	N/A	-3.1	-2.4
LOC_Os06g46020	expressed protein	N/A	-2.4	-2.4
LOC_Os01g35610	expressed protein	N/A	-2.4	-2.3
LOC_Os08g23170	expressed protein	N/A	-2.3	-2.3
LOC_Os03g25360	peroxidase precursor, putative, expressed	N/A	-3.0	-2.3
LOC_Os03g25010	GDSL-like lipase/acylhydrolase, putative, expressed	N/A	-1.9	-2.3
LOC_Os03g17870	metallothionein, putative, expressed	N/A	-1.8	-2.3
LOC_Os07g48010	peroxidase precursor, putative, expressed	POX8.1|prx110	-2.0	-2.3
LOC_Os01g10440	xylosyltransferase, putative, expressed	N/A	-2.8	-2.2
LOC_Os01g64100	glycosyl hydrolase, putative, expressed	N/A	-2.2	-2.2
LOC_Os01g03130	expressed protein	N/A	-2.1	-2.0
LOC_Os02g10520	OsSub12 - Putative Subtilisin homologue, expressed	N/A	-2.3	-2.0
LOC_Os05g04660	thioesterase family protein, putative, expressed	N/A	-2.4	-2.0
LOC_Os06g14640	zinc finger, C3HC4 type domain containing protein, expressed	N/A	-2.0	-1.9
LOC_Os02g07730	haloacid dehalogenase-like hydrolase domain-containing protein 3, putative, expressed	N/A	-1.4	-1.9
LOC_Os07g34050	harpin-induced protein 1 domain containing protein, expressed	N/A	-2.2	-1.9
LOC_Os07g38750	AP2 domain containing protein, expressed	N/A	-2.3	-1.9
LOC_Os12g44100	peptide transporter PTR2, putative, expressed	NPF2.2	-2.3	-1.9
LOC_Os01g70870	ZOS1-23 - C2H2 zinc finger protein, expressed	N/A	-2.2	-1.9
LOC_Os10g23160	ent-kaurenoic acid oxidase 1, putative, expressed	N/A	-1.7	-1.9
LOC_Os04g40570	ABC transporter, ATP-binding protein, putative, expressed	N/A	-2.4	-1.8
LOC_Os07g26110	membrane associated DUF588 domain containing protein, putative, expressed	N/A	-1.8	-1.8
LOC_Os01g50100	ABC transporter, ATP-binding protein, putative, expressed	N/A	-1.9	-1.8
LOC_Os04g43390	Os4bglu16 - monolignol beta-glucoside homologue, expressed	N/A	-2.3	-1.7
LOC_Os01g50590	cytochrome P450, putative, expressed	N/A	-1.6	-1.7
LOC_Os05g12400	BURP domain containing protein, expressed	N/A	-2.5	-1.6
LOC_Os03g61829	haloacid dehalogenase-like hydrolase family protein, putative, expressed	HAD1	-1.7	-1.6
LOC_Os05g10650	6-phosphofructokinase, putative, expressed	PPi-PFK	-1.8	-1.5

Appendix Table 11. (continuation)

Locus ID	Predicted annotation	Functional annotation	*ark1* log2fc	DKO log2fc
LOC_Os04g41960	NADP-dependent oxidoreductase, putative, expressed	N/A	-1.7	-1.5
LOC_Os06g05430	expressed protein	N/A	-1.8	-1.4
LOC_Os06g47130	C2 domain containing protein, expressed	N/A	-1.3	-1.4
LOC_Os12g43740	oxidoreductase, short chain dehydrogenase/reductase family, putative, expressed	N/A	-1.7	-1.4
LOC_Os08g31910	expressed protein	N/A	-1.6	-1.4
LOC_Os08g31410	sulfate transporter, putative, expressed	N/A	-1.6	-1.4
LOC_Os10g32700	hypersensitive-induced response protein, putative, expressed	N/A	-1.4	-1.4
LOC_Os05g04490	peroxidase precursor, putative, expressed	N/A	-1.6	-1.3
LOC_Os07g33620	cytochrome P450 domain containing protein, expressed	N/A	-1.6	-1.3
LOC_Os10g42400	expressed protein	N/A	-1.7	-1.3
LOC_Os02g03210	FAD-binding and arabino-lactone oxidase domains containing protein, putative, expressed	N/A	-1.5	-1.2
LOC_Os07g05380	ATPase BadF/BadG/BcrA/BcrD type, putative, expressed	N/A	-1.2	-1.2
LOC_Os08g42590	mtN19, putative, expressed	N/A	-1.3	-1.2
LOC_Os10g11200	aminotransferase, classes I and II, domain containing protein, expressed	N/A	-1.2	-1.2
LOC_Os08g06190	berberine and berberine like domain containing protein, expressed	N/A	-1.4	-1.2
LOC_Os07g44140	cytochrome P450 72A1, putative, expressed	N/A	-1.0	-1.2
LOC_Os10g33210	peptide transporter PTR3-A, putative, expressed	N/A	-1.0	-1.2
LOC_Os04g49500	U-box domain-containing protein, putative, expressed	N/A	-1.6	-1.2
LOC_Os06g39230	aldehyde dehydrogenase, putative, expressed	N/A	-1.0	-1.2
LOC_Os12g05180	avr9/Cf-9 rapidly elicited protein, putative, expressed	N/A	-1.2	-1.1
LOC_Os09g37120	pyridoxal-dependent decarboxylase protein, putative, expressed	ODCa	-1.2	-1.1
LOC_Os02g57560	tyrosine protein kinase domain containing protein, putative, expressed	N/A	-1.1	-1.1
LOC_Os10g34170	glutaredoxin domain containing protein, putative, expressed	N/A	-1.3	-1.1
LOC_Os05g06970	peroxidase precursor, putative, expressed	N/A	-1.1	-1.1
LOC_Os04g10750	inorganic phosphate transporter, putative, expressed	Pht1;4|PT4	-1.2	-1.1
LOC_Os04g01520	expressed protein	Nope1	-1.3	-1.1
LOC_Os10g38090	cytochrome P450, putative, expressed	N/A	-1.2	-1.1
LOC_Os01g64360	MYB family transcription factor, putative, expressed	N/A	-1.2	-1.0

Appendix Table 12. Transcription factors and kinases. Protein subfamilies are assigned according to the iTAK Plant Transcription factor and Protein Kinase Identifier and Classifier (Zheng et al., 2016). Log2 fold change compared to the WT is displayed with red and blue hue intensity correlating to stronger down- and upregulation respectively. Genes are ordered based on DKO fold change expression in different transcriptional groups. When available, functional annotations are given (see Appendix Table 7 for descriptions).

				Down/Upregulated in		
Locus ID	Predicted annotation	Functional annotation	Protein subfamily	*ark1*	*ark2*	DKO
Transcription factors						
LOC_Os05g50610	WRKY8, expressed	WRKY8	WRKY	-3.0	-2.5	-1.4
LOC_Os11g04590	GRAS family transcription factor containing protein, expressed	N/A	GRAS	-5.6		-6.4
LOC_Os03g40080	GRAS family transcription factor containing protein, expressed	AM18	GRAS	-2.9		-2.4
LOC_Os07g38750	AP2 domain containing protein, expressed	N/A	AP2/ERF-ERF	-2.3		-1.9
LOC_Os01g70870	ZOS1-23 - C2H2 zinc finger protein, expressed	N/A	C2H2	-2.2		-1.9
LOC_Os01g64360	MYB family transcription factor, putative, expressed	N/A	MYB	-1.2		-1.0
LOC_Os09g25060	WRKY76, expressed	WRKY76	WRKY			-2.7
LOC_Os03g60560	ZOS3-21 - C2H2 zinc finger protein, expressed	ZFP182|ZOS3-21	C2H2			-2.2
LOC_Os02g56600	no apical meristem protein, putative, expressed	N/A	NAC			-1.1
LOC_Os02g15350	dof zinc finger domain containing protein, putative, expressed	RPBF|Dof3	C2C2-Dof	8.4	8.4	7.8
LOC_Os05g36990	ATOFP18/OFP18, putative, expressed	N/A	OFP	2.5	5.3	4.7
LOC_Os08g06330	zinc finger C-x8-C-x5-C-x3-H type family protein, expressed	N/A	C3H		1.4	1.2
LOC_Os04g56850	auxin response factor, putative, expressed	ARF11	B3-ARF			1.3
LOC_Os08g36390	ZOS8-07 - C2H2 zinc finger protein, expressed	N/A	C2H2			1.2
Protein kinases						
LOC_Os06g45240	inactive receptor kinase At2g26730 precursor, putative, expressed	N/A	RLK-Pelle LRR-III	-3.8		-3.2
LOC_Os02g57560	tyrosine protein kinase domain containing protein, putative, expressed	N/A	RLK-Pelle RLCK-IV	-1.1		-1.1
LOC_Os01g21970	protein kinase, putative, expressed	N/A	RLK-Pelle RLCK-VIII			-1.1
LOC_Os05g39870	CAMK_KIN1/SNF1/Nim1_like.24, expressed	N/A	CAMK CAMKL-CHK1		1.6	1.3
LOC_Os12g14699	protein kinase domain containing protein, expressed	N/A	RLK-Pelle DLSV			1.1

Appendix Table 13. Genes downregulated in the DKO only in relation to the wild-type (Group IV, log2fc ≤ -1, $p \leq 0.05$, related to Table 6). Log2 fold change compared to the WT is displayed with red hue intensity correlating to stronger downregulation. Genes are ordered based on fold change expression. Locus IDs in red correspond to genes with no expression in the DKO (see Appendix Table 9 for details of all genes with no expression in the DKO). Names of the protein products of functionally annotated genes are given. For their functions and references, see Appendix Table 7.

Locus ID	Predicted annotation	Functional annotation	DKO log2fc
LOC_Os02g12680	cytochrome P450, putative, expressed	AOS3|HPL2	-3.3
LOC_Os06g05510	expressed protein	N/A	-3.0
LOC_Os09g25060	WRKY76, expressed	WRKY76	-2.7
LOC_Os05g04390	expressed protein	N/A	-2.6
LOC_Os03g57520	VQ domain containing protein, putative, expressed	N/A	-2.6
LOC_Os02g10550	expressed protein	N/A	-2.5
LOC_Os06g44160	heat shock protein DnaJ, putative, expressed	N/A	-2.5
LOC_Os06g12090	miro, putative, expressed	Sar1d	-2.4
LOC_Os10g18870	dirigent, putative, expressed	N/A	-2.3
LOC_Os03g38800	AAA family ATPase, putative, expressed	N/A	-2.3
LOC_Os04g45590	glyoxalase family protein, putative, expressed	N/A	-2.3
LOC_Os03g60560	ZOS3-21 - C2H2 zinc finger protein, expressed	ZFP182|ZOS3-21	-2.2
LOC_Os12g25090	expressed protein	Sci1|PR6	-2.2
LOC_Os03g21500	expressed protein	N/A	-2.2
LOC_Os03g06210	expressed protein	N/A	-2.1
LOC_Os11g47530	glycosyl hydrolase, putative, expressed	N/A	-2.0
LOC_Os11g47600	glycosyl hydrolase, putative, expressed	N/A	-2.0
LOC_Os08g02700	fructose-bisphospate aldolase isozyme, putative, expressed	N/A	-2.0
LOC_Os10g34910	secretory protein, putative, expressed	N/A	-2.0
LOC_Os01g64470	harpin-induced protein 1 domain containing protein, expressed	N/A	-1.9
LOC_Os03g46060	thaumatin family domain containing protein, expressed	LP|PR-5	-1.8
LOC_Os01g11600	expressed protein	N/A	-1.8
LOC_Os03g30050	protein kinase family protein, putative, expressed	N/A	-1.7
LOC_Os01g55510	dynein light chain type 1 domain containing protein, expressed	N/A	-1.7
LOC_Os02g21290	expressed protein	N/A	-1.7
LOC_Os03g10440	glycosyl hydrolase family 10 protein, putative, expressed	N/A	-1.7
LOC_Os03g24730	expressed protein	N/A	-1.6
LOC_Os05g19570	expansin precursor, putative, expressed	N/A	-1.5
LOC_Os01g40580	hypersensitive-induced response protein, putative, expressed	N/A	-1.4
LOC_Os10g39300	aspartic proteinase nepenthesin, putative, expressed	N/A	-1.4
LOC_Os01g65490	DNA binding protein, putative, expressed	N/A	-1.4
LOC_Os09g29200	glutathione S-transferase, putative, expressed	GSTU17	-1.3
LOC_Os01g27240	12-oxophytodienoate reductase, putative, expressed	N/A	-1.3
LOC_Os01g45250	DUF1645 domain containing protein, putative, expressed	N/A	-1.3
LOC_Os01g13780	expressed protein	N/A	-1.3
LOC_Os06g11290	12-oxophytodienoate reductase, putative, expressed	OPR1	-1.3
LOC_Os03g56860	expressed protein	N/A	-1.3
LOC_Os07g43670	ribonuclease T2 family domain containing protein, expressed	N/A	-1.2
LOC_Os06g23114	copper methylamine oxidase precursor, putative, expressed	N/A	-1.2
LOC_Os03g52370	PIII4 - Proteinase inhibitor II family protein precursor, expressed	N/A	-1.2
LOC_Os02g52450	regulator of ribonuclease, putative, expressed	N/A	-1.1
LOC_Os02g56600	no apical meristem protein, putative, expressed	N/A	-1.1
LOC_Os03g52380	PIII5 - Proteinase inhibitor II family protein precursor, expressed	N/A	-1.1
LOC_Os01g66700	beta-hexosaminidase precursor, putative, expressed	N/A	-1.1

Appendix Table 13. (continuation)

Locus ID	Predicted annotation	Functional annotation	DKO log2fc
LOC_Os01g21970	protein kinase, putative, expressed	N/A	-1.1
LOC_Os07g06830	gibberellin receptor GID1L2, putative, expressed	N/A	-1.1
LOC_Os11g04010	ICE-like protease p20 domain containing protein, putative, expressed	N/A	-1.1
LOC_Os12g16220	nmrA-like family domain containing protein, expressed	N/A	-1.1
LOC_Os03g01320	LTPL116 - Protease inhibitor/seed storage/LTP family protein precursor, expressed	qLTG3-1	-1.1
LOC_Os11g14040	glutathione S-transferase, N-terminal domain containing protein, expressed	N/A	-1.0
LOC_Os12g12590	NADP-dependent oxidoreductase, putative, expressed	N/A	-1.0
LOC_Os03g58580	nodulin, putative, expressed	N/A	-1.0
LOC_Os02g21890	expressed protein	FOS1	-1.0
LOC_Os01g51360	lipase, putative, expressed	N/A	-1.0
LOC_Os10g40030	short chain dehydrogenase/reductase protein, putative, expressed	N/A	-1.0
LOC_Os05g50100	expressed protein	N/A	-1.0
LOC_Os07g11380	RAL4 - Seed allergenic protein RA5/RA14/RA17 precursor, expressed	RAG2	-1.0
LOC_Os02g37330	heavy metal associated domain containing protein, expressed	N/A	-1.0
LOC_Os05g51570	vacuolar-processing enzyme precursor, putative, expressed	VPE4	-1.0
LOC_Os07g39270	polyprenyl synthetase, putative, expressed	GGPPS1	-1.0

Appendix Table 14. Genes upregulated in *ark1*, *ark2* and the DKO in relation to the wild-type (Group V, log2fc > 1, $p \leq 0.05$, related to Table 7). Log2 fold change compared to the WT is displayed with blue hue intensity correlating to stronger upregulation. Genes are ordered based on DKO fold change expression. Names of the protein products of functionally annotated genes are given. For their functions and references, see Appendix Table 7.

Locus ID	Predicted annotation	Functional annotation	*ark1* log2fc	*ark2* log2fc	DKO log2fc
LOC_Os03g02470	expressed protein	N/A	12.6	12.6	12.3
LOC_Os03g43100	expressed protein	N/A	10.9	11.0	10.9
LOC_Os08g27870	EARLY flowering protein, putative, expressed	N/A	11.4	10.7	10.7
LOC_Os02g53240	expressed protein	N/A	9.8	9.5	9.7
LOC_Os03g19610	pectinesterase, putative, expressed	PME1	9.3	8.1	8.7
LOC_Os05g50390	expressed protein	N/A	7.0	8.2	8.6
LOC_Os06g11240	12-oxophytodienoate reductase, putative, expressed	N/A	8.4	8.7	8.5
LOC_Os12g05220	expressed protein	N/A	8.4	8.3	8.3
LOC_Os07g01960	hypothetical protein	N/A	8.7	8.1	8.2
LOC_Os08g10612	expressed protein	N/A	8.7	8.7	8.2
LOC_Os09g38104	hypothetical protein	N/A	6.6	8.2	8.1
LOC_Os05g34490	expressed protein	N/A	8.0	8.2	7.8
LOC_Os02g15350	dof zinc finger domain containing protein, putative, expressed	RPBF|Dof3	8.4	8.4	7.8
LOC_Os09g22160	expressed protein	N/A	7.3	8.2	7.6
LOC_Os04g32080	11-beta-hydroxysteroid dehydrogenase, putative, expressed	N/A	7.5	6.8	7.5
LOC_Os04g52790	expressed protein	N/A	7.1	7.0	7.1
LOC_Os08g10870	hypothetical protein	N/A	5.5	6.9	7.0
LOC_Os12g01250	csAtPR5, putative, expressed	N/A	6.3	6.2	6.9
LOC_Os01g35330	circumsporozoite protein precursor, putative, expressed	N/A	5.3	6.7	6.4
LOC_Os06g04930	expressed protein	N/A	6.5	6.1	6.0
LOC_Os02g58370	expressed protein	N/A	5.3	5.7	4.8
LOC_Os05g36990	ATOFP18/OFP18, putative, expressed	N/A	2.5	5.3	4.7
LOC_Os09g10660	expressed protein	N/A	4.3	4.9	4.6
LOC_Os11g39160	NBS-LRR disease resistance protein, putative, expressed	N/A	4.6	2.5	4.6
LOC_Os04g09450	expressed protein	N/A	4.8	3.9	4.1
LOC_Os05g01330	expressed protein	N/A	5.3	3.6	4.1
LOC_Os07g05450	sulfotransferase domain containing protein, expressed	N/A	4.5	4.2	4.0
LOC_Os10g35160	expressed protein	N/A	3.7	2.9	3.9
LOC_Os07g15340	hAT dimerisation domain-containing protein, putative, expressed	N/A	3.7	2.9	3.7
LOC_Os05g42160	expressed protein	N/A	2.9	3.6	3.7
LOC_Os11g43700	RGH1A, putative, expressed	N/A	3.3	3.2	3.4
LOC_Os06g11830	hAT dimerisation domain-containing protein, putative, expressed	N/A	3.4	2.6	3.3
LOC_Os03g02180	cytochrome P450, putative, expressed	F5HL2	3.4	3.9	3.2
LOC_Os01g36064	hAT dimerisation domain-containing protein, putative, expressed	N/A	3.3	2.7	3.2
LOC_Os01g45760	YUC4, putative, expressed	YUCCA1|YUC1	2.4	2.5	2.5
LOC_Os02g29774	expressed protein	N/A	2.5	2.4	2.5
LOC_Os11g45040	expressed protein	N/A	2.5	2.0	2.3
LOC_Os07g25800	OsFBDUF37 - F-box and DUF domain containing protein, expressed	N/A	1.6	1.8	2.1
LOC_Os03g01520	expressed protein	N/A	2.4	2.1	2.0
LOC_Os07g01904	expressed protein	N/A	1.8	1.9	1.9
LOC_Os01g37650	esterase, putative, expressed	N/A	1.8	2.1	1.8
LOC_Os11g12340	disease resistance protein RPM1, putative, expressed	RPR1	1.9	2.2	1.7
LOC_Os01g07170	HORMA domain containing protein, putative, expressed	N/A	1.4	1.2	1.4
LOC_Os05g04410	peroxidase precursor, putative, expressed	N/A	1.4	1.6	1.4
LOC_Os11g44990	NB-ARC domain containing protein, expressed	N/A	1.4	1.1	1.3
LOC_Os11g45180	NBS-LRR disease resistance protein, putative, expressed	N/A	1.3	1.2	1.3
LOC_Os07g27350	atuA, putative, expressed	N/A	1.0	1.1	1.2
LOC_Os03g55720	cytochrome b6f complex subunit, putative, expressed	N/A	1.2	1.4	1.2
LOC_Os07g44250	dirigent, putative, expressed	N/A	1.0	1.6	1.1

References

Agrawal, G. K., Jwa, N. S., Shibato, J., Han, O., Iwahashi, H., & Rakwal, R. (2003). Diverse environmental cues transiently regulate OsOPR1 of the "octadecanoid pathway" revealing its importance in rice defense/stress and development. *Biochemical and biophysical research communications*, *310*(4), 1073-1082.

Akiyama, K., Matsuzaki, K. I., & Hayashi, H. (2005). Plant sesquiterpenes induce hyphal branching in arbuscular mycorrhizal fungi. *Nature*, *435*(7043), 824-827.

Akiyama, T., & Pillai, M. A. (2001). Molecular cloning, characterization and in vitro expression of a novel endo-1, 3-β-glucanase up-regulated by ABA and drought stress in rice (Oryza sativa L.). *Plant Science*, *161*(6), 1089-1098.

An, J., Zeng, T., Ji, C., de Graaf, S., Zheng, Z., Xiao, T. T., ... & Pan, Z. (2019). A Medicago truncatula SWEET transporter implicated in arbuscule maintenance during arbuscular mycorrhizal symbiosis. *New Phytologist*, *224*(1), 396-408.

Ané, J. M., Kiss, G. B., Riely, B. K., Penmetsa, R. V., Oldroyd, G. E., Ayax, C., ... & Rosenberg, C. (2004). Medicago truncatula DMI1 required for bacterial and fungal symbioses in legumes. *Science*, *303*(5662), 1364-1367.

Antolín-Llovera, M., Ried, M. K., & Parniske, M. (2014). Cleavage of the SYMBIOSIS RECEPTOR-LIKE KINASE ectodomain promotes complex formation with Nod factor receptor 5. *Current Biology*, *24*(4), 422-427.

Arenhart, R. A., Schunemann, M., Bucker Neto, L., Margis, R., Wang, Z. Y., & Margis-Pinheiro, M. (2016). Rice ASR1 and ASR5 are complementary transcription factors regulating aluminium responsive genes. *Plant, cell & environment*, *39*(3), 645-651.

Ashburner, M., Ball, C. A., Blake, J. A., Botstein, D., Butler, H., Cherry, J. M., ... & Harris, M. A. (2000). Gene ontology: tool for the unification of biology. *Nature genetics*, *25*(1), 25-29.

Bago, B., Pfeffer, P. E., & Shachar-Hill, Y. (2000). Carbon metabolism and transport in arbuscular mycorrhizas. *Plant physiology*, *124*(3), 949-958.

Baier, M. C., Keck, M., Gödde, V., Niehaus, K., Küster, H., & Hohnjec, N. (2010). Knockdown of the symbiotic sucrose synthase MtSucS1 affects arbuscule maturation and maintenance in mycorrhizal roots of Medicago truncatula. *Plant physiology*, *152*(2), 1000-1014.

Balestrini, R., Berta, G., & Bonfante, P. (1992). The plant nucleus in mycorrhizal roots: positional and structural modifications. *Biology of the Cell*, *75*(3), 235-243.

Banasiak, J., Borghi, L., Stec, N., Martinoia, E., & Jasiński, M. (2020). The full-size ABCG transporter of Medicago truncatula is involved in strigolactone secretion, affecting arbuscular mycorrhiza. *Frontiers in plant science*, *11*.

Barrow, J., & Aaltonen, R. (2001). Evaluation of the internal colonization of Atriplex canescens (Pursh) Nutt. roots by dark septate fungi and the influence of host physiological activity. *Mycorrhiza*, *11*(4), 199-205.

Bécard, G., Douds, D. D., & Pfeffer, P. E. (1992). Extensive in vitro hyphal growth of vesicular-arbuscular mycorrhizal fungi in the presence of CO2 and flavonols. *Appl. Environ. Microbiol.*, *58*(3), 821-825.

Bécard, G., & Fortin, J. A. (1988). Early events of vesicular–arbuscular mycorrhiza formation on Ri T-DNA transformed roots. *New Phytologist*, *108*(2), 211-218.

Begum, N., Qin, C., Ahanger, M. A., Raza, S., Khan, M. I., Ahmed, N., ... & Zhang, L. (2019). Role of Arbuscular Mycorrhizal Fungi in Plant Growth Regulation: Implications in Abiotic Stress Tolerance. *Frontiers in plant science*, *10*, 1068.

Berendzen, K., Searle, I., Ravenscroft, D., Koncz, C., Batschauer, A., Coupland, G., ... & Ülker, B. (2005). A rapid and versatile combined DNA/RNA extraction protocol and its application to the analysis of a novel DNA marker set polymorphic between Arabidopsis thaliana ecotypes Col-0 and Landsberg erecta. *Plant Methods*, *1*(1), 4.

Besserer, A., Puech-Pagès, V., Kiefer, P., Gomez-Roldan, V., Jauneau, A., Roy, S., ... & Séjalon-Delmas, N. (2006). Strigolactones stimulate arbuscular mycorrhizal fungi by activating mitochondria. *PLoS biology*, *4*(7).

Blancaflor, E. B., Zhao, L., & Harrison, M. J. (2001). Microtubule organization in root cells of Medicago truncatula during development of an arbuscular mycorrhizal symbiosis with Glomus versiforme. *Protoplasma*, *217*(4), 154-165.

Bonfante-Fasolo, P. (1984). Anatomy and morphology of VA mycorrhizae. *VA mycorrhizae*, *57*, 5-33.

Bonfante, P., & Genre, A. (2015). Arbuscular mycorrhizal dialogues: do you speak 'plantish'or 'fungish'?. *Trends in plant science*, *20*(3), 150-154.

Bragg, J. N., Wu, J., Gordon, S. P., Guttman, M. E., Thilmony, R., Lazo, G. R., ... & Vogel, J. P. (2012). Generation and characterization of the Western Regional Research Center Brachypodium T-DNA insertional mutant collection. *PLoS One*, *7*(9).

Brands, M., Wewer, V., Keymer, A., Gutjahr, C., & Dörmann, P. (2018). The Lotus japonicus acyl-acyl carrier protein thioesterase FatM is required for mycorrhiza formation and lipid accumulation of Rhizophagus irregularis. *The Plant Journal*, *95*(2), 219-232.

Brands, M., Cahoon, E., & Doermann, P. (2020). Palmitvaccenic acid (Δ11-cis-hexadecenoic acid) is synthesized by an OLE1-like desaturase in the arbuscular mycorrhiza fungus Rhizophagus irregularis. *bioRxiv*.

Bravo, A., York, T., Pumplin, N., Mueller, L. A., & Harrison, M. J. (2016). Genes conserved for arbuscular mycorrhizal symbiosis identified through phylogenomics. *Nature Plants*, *2*(2), 1-6.

Bravo, A., Brands, M., Wewer, V., Dörmann, P., & Harrison, M. J. (2017). Arbuscular mycorrhiza-specific enzymes FatM and RAM 2 fine-tune lipid biosynthesis to promote development of arbuscular mycorrhiza. *New Phytologist*, *214*(4), 1631-1645.

Breuillin-Sessoms, F., Floss, D. S., Gomez, S. K., Pumplin, N., Ding, Y., Levesque-Tremblay, V., ... & Benedito, V. A. (2015). Suppression of arbuscule degeneration in Medicago truncatula phosphate transporter4 mutants is dependent on the ammonium transporter 2 family protein AMT2; 3. *The Plant Cell*, *27*(4), 1352-1366.

Brundrett, M. C. (2002). Coevolution of roots and mycorrhizas of land plants. *New phytologist*, *154*(2), 275-304.

Brundrett, M. C., & Tedersoo, L. (2018). Evolutionary history of mycorrhizal symbioses and global host plant diversity. *New Phytologist*, *220*(4), 1108-1115.

Buendia, L., Wang, T., Girardin, A., & Lefebvre, B. (2016). The LysM receptor-like kinase Sl LYK 10 regulates the arbuscular mycorrhizal symbiosis in tomato. *New Phytologist*, *210*(1), 184-195.

Buendia, L., Girardin, A., Wang, T., Cottret, L., & Lefebvre, B. (2018). LysM receptor-like kinase and LysM receptor-like protein families: an update on phylogeny and functional characterization. *Frontiers in plant science*, *9*, 1531.

Cameron, D. D., Neal, A. L., van Wees, S. C., & Ton, J. (2013). Mycorrhiza-induced resistance: more than the sum of its parts?. *Trends in plant science*, *18*(10), 539-545.

Carotenuto, G., Chabaud, M., Miyata, K., Capozzi, M., Takeda, N., Kaku, H., ... & Genre, A. (2017). The rice LysM receptor-like kinase Os CERK 1 is required for the perception of short-chain chitin oligomers in arbuscular mycorrhizal signaling. *New Phytologist*, *214*(4), 1440-1446.

Carotenuto, G., Volpe, V., Russo, G., Politi, M., Sciascia, I., de Almeida-Engler, J., & Genre, A. (2019). Local endoreduplication as a feature of intracellular fungal accommodation in arbuscular mycorrhizas. *New Phytologist*, *223*(1), 430-446.

Cao, Y., Halane, M. K., Gassmann, W., & Stacey, G. (2017). The role of plant innate immunity in the legume-rhizobium symbiosis. *Annual review of plant biology*, *68*, 535-561.

Cavagnaro, T. R., Bender, S. F., Asghari, H. R., & van der Heijden, M. G. (2015). The role of arbuscular mycorrhizas in reducing soil nutrient loss. Trends in Plant Science, 20(5), 283-290.

Cenci, A., & Rouard, M. (2017). Evolutionary analyses of GRAS transcription factors in angiosperms. *Frontiers in plant science*, *8*, 273.

Cheeld, H., Bhutada, G., Beaudoin, F., & Eastmond, P. J. (2020). DES2 is a fatty acid Δ11 desaturase capable of synthesizing palmitvaccenic acid in the arbuscular mycorrhizal fungus Rhizophagus irregularis. *FEBS letters*.

Chehab, E. W., Raman, G., Walley, J. W., Perea, J. V., Banu, G., Theg, S., & Dehesh, K. (2006). Rice HYDROPEROXIDE LYASES with unique expression patterns generate distinct aldehyde signatures in Arabidopsis. *Plant physiology*, *141*(1), 121-134.

Chen, H., Ma, J., Li, W., Eliseenkova, A. V., Xu, C., Neubert, T. A., ... & Mohammadi, M. (2007). A molecular brake in the kinase hinge region regulates the activity of receptor tyrosine kinases. *Molecular cell*, *27*(5), 717-730.

Chen, L. Q., Cheung, L. S., Feng, L., Tanner, W., & Frommer, W. B. (2015). Transport of sugars. *Annual Review of Biochemistry*, *84*.

Chen, M., Arato, M., Borghi, L., Nouri, E., & Reinhardt, D. (2018). Beneficial services of arbuscular mycorrhizal fungi–from ecology to application. *Frontiers in plant science*, *9*, 1270.

Chen, W., Jiang, X., & Yang, Q. (2020). Glycoside hydrolase family 18 chitinases: The known and the unknown. *Biotechnology Advances*, 107553.

Cheng, S., Xian, W., Fu, Y., Marin, B., Keller, J., Wu, T., ... & Wittek, S. (2019). Genomes of subaerial Zygnematophyceae provide insights into land plant evolution. *Cell*, *179*(5), 1057-1067.

Chittoor, J. M., Leach, J. E., & White, F. F. (1997). Differential induction of a peroxidase gene family during infection of rice by Xanthomonas oryzae pv. oryzae. *Molecular Plant-Microbe Interactions*, 10(7), 861-871.

Chiu, C. H., & Paszkowski, U. (2019). Mechanisms and impact of symbiotic phosphate acquisition. *Cold Spring Harbor perspectives in biology*, *11*(6), a034603.

Chiu, C. H., & Paszkowski, U. (2020). Receptor-like kinases sustain symbiotic scrutiny. *Plant Physiology*, *182*(4), 1597-1612.

Choi, J., Lee, T., Cho, J., Servante, E. K., Pucker, B., Summers, W., ... & Paszkowski, U. (2020). The negative regulator SMAX1 controls mycorrhizal symbiosis and strigolactone biosynthesis in rice. *Nature Communications*, *11*(1), 1-13.

Claes, B., Dekeyser, R., Villarroel, R., Van den Bulcke, M., Bauw, G., Van Montagu, M., & Caplan, A. (1990). Characterization of a rice gene showing organ-specific expression in response to salt stress and drought. *The Plant Cell*, *2*(1), 19-27.

Crooks, G. E., Hon, G., Chandonia, J. M., & Brenner, S. E. (2004). WebLogo: a sequence logo generator. *Genome research*, *14*(6), 1188-1190.

Couzigou, J. M., Lauressergues, D., André, O., Gutjahr, C., Guillotin, B., Bécard, G., & Combier, J. P. (2017). Positive gene regulation by a natural protective miRNA enables arbuscular mycorrhizal symbiosis. *Cell host & microbe*, *21*(1), 106-112.

Cui, X., Lv, Y., Chen, M., Nikoloski, Z., Twell, D., & Zhang, D. (2015). Young genes out of the male: an insight from evolutionary age analysis of the pollen transcriptome. *Molecular plant*, *8*(6), 935-945.

Das, D., & Gutjahr, C. (2019). Role of phytohormones in arbuscular mycorrhiza development. *The model legume Medicago truncatula*, 485-500

De Castro, E., Sigrist, C. J., Gattiker, A., Bulliard, V., Langendijk-Genevaux, P. S., Gasteiger, E., ... & Hulo, N. (2006). ScanProsite: detection of PROSITE signature matches and ProRule-associated functional and structural residues in proteins. *Nucleic acids research*, *34*(suppl_2), W362-W365.

Dearnaley, J., Perotto, S., & Selosse, M. A. (2016). Structure and development of orchid mycorrhizas. *Molecular mycorrhizal symbiosis*, 63-86.

Delaux, P. M., Bécard, G., & Combier, J. P. (2013). NSP 1 is a component of the Myc signaling pathway. *New Phytologist*, *199*(1), 59-65.

Delaux, P. M., Radhakrishnan, G. V., Jayaraman, D., Cheema, J., Malbreil, M., Volkening, J. D., ... & Rothfels, C. J. (2015). Algal ancestor of land plants was preadapted for symbiosis. *Proceedings of the National Academy of Sciences*, *112*(43), 13390-13395.

Deng, M., Bian, H., Xie, Y., Kim, Y., Wang, W., Lin, E., ... & Wang, J. (2011). Bcl-2 suppresses hydrogen peroxide-induced programmed cell death via OsVPE2 and OsVPE3, but not via OsVPE1 and OsVPE4, in rice. *The FEBS journal*, *278*(24), 4797-4810.

Desaki, Y., Kouzai, Y., Ninomiya, Y., Iwase, R., Shimizu, Y., Seko, K., ... & Nishizawa, Y. (2018). Os CERK 1 plays a crucial role in the lipopolysaccharide-induced immune response of rice. *new phytologist*, *217*(3), 1042-1049.

Dievart, A., Gottin, C., Périn, C., Ranwez, V., & Chantret, N. (2020). Origin and Diversity of Plant Receptor-Like Kinases. *Annual Review of Plant Biology*, *71*.

Dobin, A., Davis, C. A., Schlesinger, F., Drenkow, J., Zaleski, C., Jha, S., ... & Gingeras, T. R. (2013). STAR: ultrafast universal RNA-seq aligner. *Bioinformatics*, *29*(1), 15-21.

Edgar, R. C. (2004). MUSCLE: multiple sequence alignment with high accuracy and high throughput. *Nucleic acids research*, *32*(5), 1792-1797.

El-Gebali, S., Mistry, J., Bateman, A., Eddy, S. R., Luciani, A., Potter, S. C., ... & Finn, R. D. (2019). The Pfam protein families database in 2019. *Nucleic acids research*, *47*(D1), D427-D432.

Endre, G., Kereszt, A., Kevei, Z., Mihacea, S., Kaló, P., & Kiss, G. B. (2002). A receptor kinase gene regulating symbiotic nodule development. *Nature*, *417*(6892), 962-966.

Engler, C., Gruetzner, R., Kandzia, R., & Marillonnet, S. (2009). Golden gate shuffling: a one-pot DNA shuffling method based on type IIs restriction enzymes. *PloS one*, *4*(5).

Eom, J. S., Chen, L. Q., Sosso, D., Julius, B. T., Lin, I. W., Qu, X. Q., ... & Frommer, W. B. (2015). SWEETs, transporters for intracellular and intercellular sugar translocation. *Current Opinion in Plant Biology*, *25*, 53-62.

Feike, D., Korolev, A. V., Soumpourou, E., Murakami, E., Reid, D., Breakspear, A., ... & Miller, J. B. (2019). Characterizing standard genetic parts and establishing common principles for engineering legume and cereal roots. *Plant biotechnology journal*, *17*(12), 2234-2245.

Feng, F., Sun, J., Radhakrishnan, G. V., Lee, T., Bozsóki, Z., Fort, S., ... & Oldroyd, G. E. D. (2019). A combination of chitooligosaccharide and lipochitooligosaccharide recognition promotes arbuscular mycorrhizal associations in Medicago truncatula. *Nature communications*, *10*(1), 1-12.

Fernández, I., Cosme, M., Stringlis, I. A., Yu, K., de Jonge, R., van Wees, S. M., ... & Van der Heijden, M. G. (2019). Molecular dialogue between arbuscular mycorrhizal fungi and the nonhost plant Arabidopsis thaliana switches from initial detection to antagonism. *New Phytologist*, *223*(2), 867-881.

Ferrol, N., Azcón-Aguilar, C., & Pérez-Tienda, J. (2019). Arbuscular mycorrhizas as key players in sustainable plant phosphorus acquisition: An overview on the mechanisms involved. *Plant science*, *280*, 441-447.

Fesel, P. H., & Zuccaro, A. (2016). β-glucan: Crucial component of the fungal cell wall and elusive MAMP in plants. *Fungal Genetics and Biology*, *90*, 53-60.

Fiorilli, V., Vallino, M., Biselli, C., Faccio, A., Bagnaresi, P., & Bonfante, P. (2015a). Host and non-host roots in rice: cellular and molecular approaches reveal differential responses to arbuscular mycorrhizal fungi. *Frontiers in plant science*, *6*, 636.

Fiorilli, V., Volpe, V., Zanini, S., Vallino, M., Abbà, S., & Bonfante, P. (2015b). A Rice GRAS Gene Has an Impact on the Success of Arbuscular Mycorrhizal Colonization. *American Journal of Plant Sciences*, *6*, 1905-1915.

Floss, D. S., Gomez, S. K., Park, H. J., MacLean, A. M., Müller, L. M., Bhattarai, K. K., ... & Harrison, M. J. (2017). A transcriptional program for arbuscule degeneration during AM symbiosis is regulated by MYB1. *Current Biology*, *27*(8), 1206-1212.

Fujino, K., Sekiguchi, H., Matsuda, Y., Sugimoto, K., Ono, K., & Yano, M. (2008). Molecular identification of a major quantitative trait locus, qLTG3–1, controlling low-temperature

germinability in rice. *Proceedings of the National Academy of Sciences*, *105*(34), 12623-12628.

Fujino, K., & Matsuda, Y. (2010). Genome-wide analysis of genes targeted by qLTG3-1 controlling low-temperature germinability in rice. *Plant molecular biology*, *72*(1-2), 137.

Funayama, K., Kojima, S., Tabuchi-Kobayashi, M., Sawa, Y., Nakayama, Y., Hayakawa, T., & Yamaya, T. (2013). Cytosolic glutamine synthetase1; 2 is responsible for the primary assimilation of ammonium in rice roots. *Plant and cell physiology, 54*(6), 934-943.

Gao, L., Tu, Z. J., Millett, B. P., & Bradeen, J. M. (2013). Insights into organ-specific pathogen defense responses in plants: RNA-seq analysis of potato tuber-Phytophthora infestans interactions. *BMC genomics*, *14*(1), 340.

Genre, A., Chabaud, M., Timmers, T., Bonfante, P., & Barker, D. G. (2005). Arbuscular mycorrhizal fungi elicit a novel intracellular apparatus in Medicago truncatula root epidermal cells before infection. *The Plant Cell*, *17*(12), 3489-3499.

Genre, A., Chabaud, M., Faccio, A., Barker, D. G., & Bonfante, P. (2008). Prepenetration apparatus assembly precedes and predicts the colonization patterns of arbuscular mycorrhizal fungi within the root cortex of both Medicago truncatula and Daucus carota. *The Plant Cell*, *20*(5), 1407-1420.

Giovannetti, M., Avio, L., & Sbrana, C. (2015). Functional significance of anastomosis in arbuscular mycorrhizal networks. In *Mycorrhizal networks* (pp. 41-67). Springer, Dordrecht.

Girardin, A., Wang, T., Ding, Y., Keller, J., Buendia, L., Gaston, M., ... & Lefebvre, B. (2019). LCO receptors involved in arbuscular mycorrhiza are functional for rhizobia perception in legumes. *Current Biology*, *29*(24), 4249-4259.

Glémin, S., & Bataillon, T. (2009). A comparative view of the evolution of grasses under domestication. *New phytologist*, *183*(2), 273-290.

Gobbato, E., Marsh, J. F., Vernié, T., Wang, E., Maillet, F., Kim, J., ... & Mysore, K. S. (2012). A GRAS-type transcription factor with a specific function in mycorrhizal signaling. *Current Biology*, *22*(23), 2236-2241.

Göhre, V., & Paszkowski, U. (2006). Contribution of the arbuscular mycorrhizal symbiosis to heavy metal phytoremediation. Planta, 223(6), 1115-1122.

Gómez-Ariza, J., Campo, S., Rufat, M., Estopà, M., Messeguer, J., Segundo, B. S., & Coca, M. (2007). Sucrose-mediated priming of plant defense responses and broad-spectrum disease resistance by overexpression of the maize pathogenesis-related PRms protein in rice plants. *Molecular Plant-Microbe Interactions*, *20*(7), 832-842.

Gomi, K., Satoh, M., Ozawa, R., Shinonaga, Y., Sanada, S., Sasaki, K., ... & Takabayashi, J. (2010). Role of hydroperoxide lyase in white-backed planthopper (Sogatella furcifera Horváth)-induced resistance to bacterial blight in rice, Oryza sativa L. *The Plant Journal*, *61*(1), 46-57.

Gou, X., & Li, J. (2020). Paired receptor and coreceptor kinases perceive extracellular signals to control plant development. *Plant Physiology*, *182*(4), 1667-1681.

Gough, C., & Cullimore, J. (2011). Lipo-chitooligosaccharide signaling in endosymbiotic plant-microbe interactions. *Molecular Plant-Microbe Interactions*, 24(8), 867-878.

Gross, M. (2017). Where is all the phosphorus?. *Current Biology*, *27*(21), R1141-R1144.

Groth, M., Takeda, N., Perry, J., Uchida, H., Dräxl, S., Brachmann, A., ... & Parniske, M. (2010). NENA, a Lotus japonicus homolog of Sec13, is required for rhizodermal infection by arbuscular mycorrhiza fungi and rhizobia but dispensable for cortical endosymbiotic development. *The Plant Cell*, *22*(7), 2509-2526.

Güimil, S., Chang, H. S., Zhu, T., Sesma, A., Osbourn, A., Roux, C., ... & Paszkowski, U. (2005). Comparative transcriptomics of rice reveals an ancient pattern of response to microbial colonization. *Proceedings of the National Academy of Sciences*, *102*(22), 8066-8070.

Gutjahr, C., Banba, M., Croset, V., An, K., Miyao, A., An, G., ... & Paszkowski, U. (2008). Arbuscular mycorrhiza–specific signaling in rice transcends the common symbiosis signaling pathway. *The Plant Cell*, *20*(11), 2989-3005.

Gutjahr, C., Casieri, L., & Paszkowski, U. (2009). Glomus intraradices induces changes in root system architecture of rice independently of common symbiosis signaling. *New phytologist*, *182*(4), 829-837.

Gutjahr, C., Radovanovic, D., Geoffroy, J., Zhang, Q., Siegler, H., Chiapello, M., ... & Paszkowski, U. (2012). The half-size ABC transporters STR1 and STR2 are indispensable for mycorrhizal arbuscule formation in rice. *The Plant Journal*, *69*(5), 906-920.

Gutjahr, C., & Parniske, M. (2013). Cell and developmental biology of arbuscular mycorrhiza symbiosis. *Annual review of cell and developmental biology*, *29*.

Gutjahr, C., Gobbato, E., Choi, J., Riemann, M., Johnston, M. G., Summers, W., ... & Paszkowski, U. (2015a). Rice perception of symbiotic arbuscular mycorrhizal fungi requires the karrikin receptor complex. *Science*, *350*(6267), 1521-1524.

Gutjahr, C., Sawers, R. J., Marti, G., Andrés-Hernández, L., Yang, S. Y., Casieri, L., ... & Paszkowski, U. (2015b). Transcriptome diversity among rice root types during asymbiosis and interaction with arbuscular mycorrhizal fungi. *Proceedings of the National Academy of Sciences*, *112*(21), 6754-6759.

Guttenberger, M. (2000). Arbuscules of vesicular-arbuscular mycorrhizal fungi inhabit an acidic compartment within plant roots. *Planta*, *211*(3), 299-304.

Han, Y., Song, L., Peng, C., Liu, X., Liu, L., Zhang, Y., ... & Wang, Z. (2019). A Magnaporthe chitinase interacts with a rice Jacalin-related lectin to promote host colonization. *Plant physiology*, *179*(4), 1416-1430.

Hanks, S. K., & Hunter, T. (1995). Protein kinases 6. The eukaryotic protein kinase superfamily: kinase (catalytic) domain structure and classification. *The FASEB journal*, *9*(8), 576-596.

Harrison, M. J., Dewbre, G. R., & Liu, J. (2002). A phosphate transporter from Medicago truncatula involved in the acquisition of phosphate released by arbuscular mycorrhizal fungi. *The Plant Cell*, *14*(10), 2413-2429.

Harrison, M. J., & Ivanov, S. (2017). Exocytosis for endosymbiosis: membrane trafficking pathways for development of symbiotic membrane compartments. *Current opinion in plant biology*, *38*, 101-108.

Hartmann, R. M., Schaepe, S., Nübel, D., Petersen, A. C., Bertolini, M., Vasilev, J., ... & Hohnjec, N. (2019). Insights into the complex role of GRAS transcription factors in the arbuscular mycorrhiza symbiosis. *Scientific reports*, *9*(1), 1-15.

He, J., Zhang, C., Dai, H., Liu, H., Zhang, X., Yang, J., ... & Wang, E. (2019). A LysM receptor heteromer mediates perception of arbuscular mycorrhizal symbiotic signal in rice. *Molecular plant*, *12*(12), 1561-1576.

Heck, C., Kuhn, H., Heidt, S., Walter, S., Rieger, N., & Requena, N. (2016). Symbiotic fungi control plant root cortex development through the novel GRAS transcription factor MIG1. *Current Biology*, *26*(20), 2770-2778.

Helber, N., Wippel, K., Sauer, N., Schaarschmidt, S., Hause, B., & Requena, N. (2011). A versatile monosaccharide transporter that operates in the arbuscular mycorrhizal fungus Glomus sp is crucial for the symbiotic relationship with plants. *The Plant Cell*, *23*(10), 3812-3823.

Ho Plágaro, T., Molinero Rosales, N., Fariña Flores, D., Villena Díaz, M., & García-Garrido, J. M. (2019). Identification and expression analysis of GRAS transcription factor genes involved in the control of arbuscular mycorrhizal development in tomato. *Frontiers in Plant Science*, *10*, 268.

Hocher, V., Auguy, F., Argout, X., Laplaze, L., Franche, C., & Bogusz, D. (2006). Expressed sequence-tag analysis in Casuarina glauca actinorhizal nodule and root. *New Phytologist*, *169*(4), 681-688.

Hogekamp, C., & Küster, H. (2013). A roadmap of cell-type specific gene expression during sequential stages of the arbuscular mycorrhiza symbiosis. BMC genomics, 14(1), 306.

Hong, J. J., Park, Y. S., Bravo, A., Bhattarai, K. K., Daniels, D. A., & Harrison, M. J. (2012). Diversity of morphology and function in arbuscular mycorrhizal symbioses in Brachypodium distachyon. *Planta*, *236*(3), 851-865.

Horváth, B., Yeun, L. H., Domonkos, Á., Halász, G., Gobbato, E., Ayaydin, F., ... & Ratet, P. (2011). Medicago truncatula IPD3 is a member of the common symbiotic signaling pathway required for rhizobial and mycorrhizal symbioses. *Molecular plant-microbe interactions*, *24*(11), 1345-1358.

Huang, J., Yang, X., Wang, M. M., Tang, H. J., Ding, L. Y., Shen, Y., & Zhang, H. S. (2007a). A novel rice C2H2-type zinc finger protein lacking DLN-box/EAR-motif plays a role in salt tolerance. *Biochimica et Biophysica Acta (BBA)-Gene Structure and Expression*, *1769*(4), 220-227.

Huang, J., Sun, S., Xu, D., Lan, H., Sun, H., Wang, Z., ... & Zhang, H. (2012). A TFIIIA-type zinc finger protein confers multiple abiotic stress tolerances in transgenic rice (Oryza sativa L.). *Plant molecular biology*, *80*(3), 337-350.

Huang, Y., Xiao, B., & Xiong, L. (2007b). Characterization of a stress responsive proteinase inhibitor gene with positive effect in improving drought resistance in rice. *Planta*, *226*(1), 73-85.

Hubbard, C., Singleton, D., Rauch, M., Jayasinghe, S., Cafiso, D., & Castle, D. (2000). The secretory carrier membrane protein family: structure and membrane topology. *Molecular Biology of the Cell*, *11*(9), 2933-2947.

Humphreys, C. P., Franks, P. J., Rees, M., Bidartondo, M. I., Leake, J. R., & Beerling, D. J. (2010). Mutualistic mycorrhiza-like symbiosis in the most ancient group of land plants. *Nature communications*, *1*(1), 1-7.

Imaizumi-Anraku, H., Takeda, N., Charpentier, M., Perry, J., Miwa, H., Umehara, Y., ... & Pike, J. (2005). Plastid proteins crucial for symbiotic fungal and bacterial entry into plant roots. *Nature*, *433*(7025), 527-531.

Ivanov, S., Austin, J., Berg, R. H., & Harrison, M. J. (2019). Extensive membrane systems at the host–arbuscular mycorrhizal fungus interface. *Nature plants*, *5*(2), 194-203.

Iwai, T., Miyasaka, A., Seo, S., & Ohashi, Y. (2006). Contribution of ethylene biosynthesis for resistance to blast fungus infection in young rice plants. *Plant physiology*, *142*(3), 1202-1215.

Jabaji-Hare, S., Deschene, A., & Kendrick, B. (1984). Lipid content and composition of vesicles of a vesicular-arbuscular mycorrhizal fungus. *Mycologia*, *76*(6), 1024-1030.

Jacott, C. N., Charpentier, M., Murray, J. D., & Ridout, C. J. (2020). Mildew Locus O facilitates colonization by arbuscular mycorrhizal fungi in angiosperms. *New Phytologist*.

Jaillais, Y., & Ott, T. (2020). The nanoscale organization of the plasma membrane and its importance in signaling: A proteolipid perspective. *Plant Physiology*, *182*(4), 1682-1696.

Javot, H., Penmetsa, R. V., Terzaghi, N., Cook, D. R., & Harrison, M. J. (2007). A Medicago truncatula phosphate transporter indispensable for the arbuscular mycorrhizal symbiosis. *Proceedings of the National Academy of Sciences*, *104*(5), 1720-1725.

Javot, H., Penmetsa, R. V., Breuillin, F., Bhattarai, K. K., Noar, R. D., Gomez, S. K., ... & Harrison, M. J. (2011). Medicago truncatula mtpt4 mutants reveal a role for nitrogen in the regulation of arbuscule degeneration in arbuscular mycorrhizal symbiosis. *The Plant Journal*, *68*(6), 954-965.

Jayne, B., & Quigley, M. (2014). Influence of arbuscular mycorrhiza on growth and reproductive response of plants under water deficit: a meta-analysis. Mycorrhiza, 24(2), 109-119.

Jiang, Y., Wang, W., Xie, Q., Liu, N., Liu, L., Wang, D., ... & Wang, E. (2017). Plants transfer lipids to sustain colonization by mutualistic mycorrhizal and parasitic fungi. *Science*, *356*(6343), 1172-1175.

Jiang, Y., Xie, Q., Wang, W., Yang, J., Zhang, X., Yu, N., ... & Wang, E. (2018). Medicago AP2-domain transcription factor WRI5a is a master regulator of lipid biosynthesis and transfer during mycorrhizal symbiosis. *Molecular plant*, *11*(11), 1344-1359.

Jiao, C., Sørensen, I., Sun, X., Sun, H., Behar, H., Alseekh, S., ... & Jeon, S. (2020). The Penium margaritaceum Genome: Hallmarks of the Origins of Land Plants. *Cell*.

Jin, Y., Chen, Z., Yang, J., Mysore, K. S., Wen, J., Huang, J., ... & Wang, E. (2018). IPD3 and IPD3L function redundantly in rhizobial and mycorrhizal symbioses. *Frontiers in Plant Science*, *9*, 267.

Jones, D. T., Taylor, W. R., & Thornton, J. M. (1992). The rapid generation of mutation data matrices from protein sequences. *Bioinformatics*, *8*(3), 275-282.

Käll, L., Krogh, A., & Sonnhammer, E. L. (2004). A combined transmembrane topology and signal peptide prediction method. *Journal of molecular biology*, *338*(5), 1027-1036.

Kanamori, N., Madsen, L. H., Radutoiu, S., Frantescu, M., Quistgaard, E. M., Miwa, H., ... & Jensen, T. H. (2006). A nucleoporin is required for induction of Ca2+ spiking in legume nodule development and essential for rhizobial and fungal symbiosis. *Proceedings of the National Academy of Sciences*, *103*(2), 359-364.

Kanehisa, M., & Goto, S. (2000). KEGG: kyoto encyclopedia of genes and genomes. *Nucleic acids research*, *28*(1), 27-30.

Kanneganti, V., & Gupta, A. K. (2009). Isolation and Expression analysis of OsPME1, encoding for a putative Pectin Methyl Esterase from Oryza sativa (subsp. indica). *Physiology and Molecular Biology of Plants*, *15*(2), 123-131.

Karlo, M., Boschiero, C., Landerslev, K. G., Blanco, G. S., Wen, J., Mysore, K. S., ... & de Bang, T. C. (2020). The CLE53-SUNN genetic pathway negatively regulates arbuscular mycorrhiza root colonization in Medicago truncatula. *Journal of Experimental Botany*.

Kawahara, Y., de la Bastide, M., Hamilton, J. P., Kanamori, H., McCombie, W. R., Ouyang, S., ... & Childs, K. L. (2013). Improvement of the Oryza sativa Nipponbare reference genome using next generation sequence and optical map data. *Rice*, *6*(1), 4.

Kawakatsu, T., Yamamoto, M. P., Touno, S. M., Yasuda, H., & Takaiwa, F. (2009). Compensation and interaction between RISBZ1 and RPBF during grain filling in rice. *The Plant Journal*, *59*(6), 908-920.

Keymer, A., Pimprikar, P., Wewer, V., Huber, C., Brands, M., Bucerius, S. L., ... & Gutjahr, C. (2017). Lipid transfer from plants to arbuscular mycorrhiza fungi. *Elife*, *6*, e29107.

Keymer, A., & Gutjahr, C. (2018). Cross-kingdom lipid transfer in arbuscular mycorrhiza symbiosis and beyond. *Current opinion in plant biology*, *44*, 137-144.

Kim, J. H., Yang, D. H., Kim, J. S., Baek, M. H., Park, Y. M., Wi, S. G., ... & Chung, B. Y. (2006). Cloning, characterization, and expression of two cDNA clones for a rice ferulate-5-hydroxylase gene, a cytochrome P450-dependent monooxygenase. *Journal of Plant Biology*, *49*(3), 200.

Kim, S., Zeng, W., Bernard, S., Liao, J., Venkateshwaran, M., Ane, J. M., & Jiang, Y. (2019). Ca 2+-regulated Ca 2+ channels with an RCK gating ring control plant symbiotic associations. *Nature communications*, *10*(1), 1-12.

Kistner, C., Winzer, T., Pitzschke, A., Mulder, L., Sato, S., Kaneko, T., ... & Szczyglowski, K. (2005). Seven Lotus japonicus genes required for transcriptional reprogramming of the root during fungal and bacterial symbiosis. *The Plant Cell*, *17*(8), 2217-2229.

Khade, S. W., Rodrigues, B. F., & Sharma, P. K. (2010). Arbuscular mycorrhizal status and root phosphatase activities in vegetative Carica papaya L. varieties. *Acta physiologiae plantarum*, *32*(3), 565-574.

Kobae, Y., & Hata, S. (2010). Dynamics of periarbuscular membranes visualized with a fluorescent phosphate transporter in arbuscular mycorrhizal roots of rice. *Plant and Cell Physiology*, *51*(3), 341-353.

Kobae, Y., Tamura, Y., Takai, S., Banba, M., & Hata, S. (2010). Localized expression of arbuscular mycorrhiza-inducible ammonium transporters in soybean. *Plant and Cell Physiology*, *51*(9), 1411-1415.

Kobae, Y., Gutjahr, C., Paszkowski, U., Kojima, T., Fujiwara, T., & Hata, S. (2014). Lipid droplets of arbuscular mycorrhizal fungi emerge in concert with arbuscule collapse. *Plant and Cell Physiology*, *55*(11), 1945-1953.

Kobae, Y., & Fujiwara, T. (2014). Earliest colonization events of *Rhizophagus irregularis* in rice roots occur preferentially in previously uncolonized cells. *Plant and Cell Physiology*, *55*(8), 1497-1510.

Kobae, Y., Kawachi, M., Saito, K., Kikuchi, Y., Ezawa, T., Maeshima, M., ... & Fujiwara, T. (2015). Up-regulation of genes involved in N-acetylglucosamine uptake and metabolism suggests a recycling mode of chitin in intraradical mycelium of arbuscular mycorrhizal fungi. *Mycorrhiza*, *25*(5), 411-417.

Kobae, Y. (2019). Dynamic phosphate uptake in arbuscular mycorrhizal roots under field conditions. *Frontiers in Environmental Science*, *6*, 159.

Koegel, S., Lahmidi, N. A., Arnould, C., Chatagnier, O., Walder, F., Ineichen, K., ... & Courty, P. E. (2013). The family of ammonium transporters (AMT) in Sorghum bicolor: two AMT members are induced locally, but not systemically in roots colonized by arbuscular mycorrhizal fungi. *New Phytologist*, *198*(3), 853-865.

Kokkoris, V., Stefani, F., Dalpé, Y., Dettman, J., & Corradi, N. (2020). Nuclear Dynamics in the Arbuscular Mycorrhizal Fungi. *Trends in Plant Science*.

Kosuta, S., Chabaud, M., Lougnon, G., Gough, C., Dénarié, J., Barker, D. G., & Bécard, G. (2003). A Diffusible Factor from Arbuscular Mycorrhizal Fungi Induces Symbiosis-Specific MtENOD11 Expression in Roots ofMedicago truncatula. *Plant physiology*, *131*(3), 952-962.

Krajinski, F., Courty, P. E., Sieh, D., Franken, P., Zhang, H., Bucher, M., ... & Hause, B. (2014). The H+-ATPase HA1 of Medicago truncatula is essential for phosphate transport and plant growth during arbuscular mycorrhizal symbiosis. *The Plant Cell*, *26*(4), 1808-1817.

Kretzschmar, T., Kohlen, W., Sasse, J., Borghi, L., Schlegel, M., Bachelier, J. B., ... & Martinoia, E. (2012). A petunia ABC protein controls strigolactone-dependent symbiotic signalling and branching. *Nature*, *483*(7389), 341-344.

Krings, M., Taylor, T. N., Taylor, E. L., Dotzler, N., & Walker, C. (2011). Arbuscular mycorrhizal-like fungi in Carboniferous arborescent lycopsids. *New Phytologist*, *191*(2), 311-314.

Kumar, S., Stecher, G., Li, M., Knyaz, C., & Tamura, K. (2018). MEGA X: molecular evolutionary genetics analysis across computing platforms. *Molecular biology and evolution*, *35*(6), 1547-1549.

Kuntam, S., Puskás, L. G., & Ayaydin, F. (2015). Characterization of a new class of blue-fluorescent lipid droplet markers for live-cell imaging in plants. *Plant cell reports*, *34*(4), 655-665.

Lambers, H., & Teste, F. P. (2013). Interactions between arbuscular mycorrhizal and non-mycorrhizal plants: do non-mycorrhizal species at both extremes of nutrient availability play the same game. *Plant Cell Environ*, *36*(11), 1911-1915.

Lanfranco, L., Fiorilli, V., & Gutjahr, C. (2018). Partner communication and role of nutrients in the arbuscular mycorrhizal symbiosis. *New Phytologist*, *220*(4), 1031-1046.

Laplaze, L., Ribeiro, A., Franche, C., Duhoux, E., Auguy, F., Bogusz, D., & Pawlowski, K. (2000). Characterization of a Casuarina glauca nodule-specific subtilisin-like protease gene, a homolog of Alnus glutinosa ag12. *Molecular plant-microbe interactions*, *13*(1), 113-117.

Leebens-Mack, J. H., Barker, M. S., Carpenter, E. J., Deyholos, M. K., Gitzendanner, M. A., ... & Wong, G. K. S. (2019). One thousand plant transcriptomes and the phylogenomics of green plants. *Nature*, 574(7780), 679.

Lehti-Shiu, M. D., & Shiu, S. H. (2012). Diversity, classification and function of the plant protein kinase superfamily. *Philosophical Transactions of the Royal Society B: Biological Sciences*, *367*(1602), 2619-2639.

Lévy, J., Bres, C., Geurts, R., Chalhoub, B., Kulikova, O., Duc, G., ... & Dénarié, J. (2004). A putative Ca2+ and calmodulin-dependent protein kinase required for bacterial and fungal symbioses. *Science*, *303*(5662), 1361-1364.

Li, F. W., Nishiyama, T., Waller, M., Frangedakis, E., Keller, J., Li, Z., ... & Cheng, S. (2020). Anthoceros genomes illuminate the origin of land plants and the unique biology of hornworts. *Nature Plants*, *6*(3), 259-272.

Li, W., Han, Y., Tao, F., & Chong, K. (2011). Knockdown of SAMS genes encoding S-adenosyl-l-methionine synthetases causes methylation alterations of DNAs and histones and leads to late flowering in rice. *Journal of plant physiology*, *168*(15), 1837-1843.

Li, W. Q., Zhang, M. J., Gan, P. F., Qiao, L., Yang, S. Q., Miao, H., ... & Shi, C. H. (2017). CLD 1/SRL 1 modulates leaf rolling by affecting cell wall formation, epidermis integrity and water homeostasis in rice. *The Plant Journal*, *92*(5), 904-923.

Li, Y., Ouyang, J., Wang, Y. Y., Hu, R., Xia, K., Duan, J., ... & Zhang, M. (2015). Disruption of the rice nitrate transporter OsNPF2.2 hinders root-to-shoot nitrate transport and vascular development. *Scientific reports*, *5*(1), 1-10.

Liang, X., Chen, X., Li, C., Fan, J., & Guo, Z. (2017). Metabolic and transcriptional alternations for defense by interfering OsWRKY62 and OsWRKY76 transcriptions in rice. *Scientific reports*, *7*(1), 1-15.

Liang, Z., Geng, Y., Ji, C., Du, H., Wong, C. E., Zhang, Q., ... & Ding, Y. (2020). Mesostigma viride genome and transcriptome provide insights into the origin and evolution of streptophyta. *Advanced Science*, *7*(1), 1901850.

Liao, Y., Smyth, G. K., & Shi, W. (2014). featureCounts: an efficient general purpose program for assigning sequence reads to genomic features. *Bioinformatics*, *30*(7), 923-930.

Ligrone, R., Carafa, A., Lumini, E., Bianciotto, V., Bonfante, P., & Duckett, J. G. (2007). Glomeromycotean associations in liverworts: a molecular, cellular, and taxonomic analysis. *American Journal of Botany*, *94*(11), 1756-1777.

Lindsay, P. L., Williams, B. N., MacLean, A., & Harrison, M. J. (2019). A Phosphate-Dependent Requirement for Transcription Factors IPD3 and IPD3L During Arbuscular Mycorrhizal Symbiosis in Medicago truncatula. *Molecular Plant-Microbe Interactions*, *32*(10), 1277-1290.

Liu, J., Chen, X., Liang, X., Zhou, X., Yang, F., Liu, J., ... & Guo, Z. (2016). Alternative splicing of rice WRKY62 and WRKY76 transcription factor genes in pathogen defense. *Plant Physiology*, *171*(2), 1427-1442.

Liu, J., Liu, J., Liu, J., Cui, M., Huang, Y., Tian, Y., ... & Xu, G. (2019). The potassium transporter SlHAK10 is involved in mycorrhizal potassium uptake. *Plant physiology*, *180*(1), 465-479.

Liu, J., Chen, J., Xie, K., Tian, Y., Yan, A., Liu, J., ... & Xu, G. (2020). A mycorrhiza-specific H+-ATPase is essential for arbuscule development and symbiotic phosphate and nitrogen uptake. *Plant, Cell & Environment*.

Liu, S., Wang, J., Han, Z., Gong, X., Zhang, H., & Chai, J. (2016). Molecular mechanism for fungal cell wall recognition by rice chitin receptor OsCEBiP. *Structure*, *24*(7), 1192-1200.

Liu, W., Kohlen, W., Lillo, A., den Camp, R. O., Ivanov, S., Hartog, M., ... & Yang, W. C. (2011). Strigolactone biosynthesis in Medicago truncatula and rice requires the symbiotic GRAS-type transcription factors NSP1 and NSP2. *The Plant Cell*, *23*(10), 3853-3865.

Liu, X., Yang, C. Y., Miao, R., Zhou, C. L., Cao, P. H., Lan, J., ... & Tian, Y. L. (2018). DS1/OsEMF1 interacts with OsARF11 to control rice architecture by regulation of brassinosteroid signaling. *Rice*, *11*(1), 46.

Lohse, S., Schliemann, W., Ammer, C., Kopka, J., Strack, D., & Fester, T. (2005). Organization and metabolism of plastids and mitochondria in arbuscular mycorrhizal roots of Medicago truncatula. *Plant Physiology*, *139*(1), 329-340.

Lombard, V., Golaconda Ramulu, H., Drula, E., Coutinho, P. M., & Henrissat, B. (2014). The carbohydrate-active enzymes database (CAZy) in 2013. *Nucleic acids research*, *42*(D1), D490-D495.

Love, M. I., Huber, W., & Anders, S. (2014). Moderated estimation of fold change and dispersion for RNA-seq data with DESeq2. *Genome biology*, *15*(12), 550.

Luginbuehl, L. H., Menard, G. N., Kurup, S., Van Erp, H., Radhakrishnan, G. V., Breakspear, A., ... & Eastmond, P. J. (2017). Fatty acids in arbuscular mycorrhizal fungi are synthesized by the host plant. *Science*, *356*(6343), 1175-1178.

Luginbuehl, L. H., & Oldroyd, G. E. (2017). Understanding the arbuscule at the heart of endomycorrhizal symbioses in plants. *Current Biology*, *27*(17), R952-R963.

Lutzoni, F., Nowak, M. D., Alfaro, M. E., Reeb, V., Miadlikowska, J., Krug, M., ... & Hilu, K. (2018). Contemporaneous radiations of fungi and plants linked to symbiosis. *Nature communications*, *9*(1), 1-11.

Maillet, F., Poinsot, V., André, O., Puech-Pagès, V., Haouy, A., Gueunier, M., ... & Martinez, E. A. (2011). Fungal lipochitooligosaccharide symbiotic signals in arbuscular mycorrhiza. *Nature*, *469*(7328), 58-63.

Man, J., Gallagher, J. P., & Bartlett, M. (2020). Structural evolution drives diversification of the large LRR-RLK gene family. *New Phytologist*.

Marcel, S., Sawers, R., Oakeley, E., Angliker, H., & Paszkowski, U. (2010). Tissue-adapted invasion strategies of the rice blast fungus Magnaporthe oryzae. *The Plant Cell*, *22*(9), 3177-3187.

Mardhiah, U., Caruso, T., Gurnell, A., & Rillig, M. C. (2016). Arbuscular mycorrhizal fungal hyphae reduce soil erosion by surface water flow in a greenhouse experiment. *Applied Soil Ecology*, *99*, 137-140.

Martin, F. M., Uroz, S., & Barker, D. G. (2017). Ancestral alliances: plant mutualistic symbioses with fungi and bacteria. *Science*, *356*(6340), eaad4501.

Martínez-Medina, A., Pescador, L., Fernández, I., Rodríguez-Serrano, M., García, J. M., Romero-Puertas, M. C., & Pozo, M. J. (2019). Nitric oxide and phytoglobin PHYTOGB1 are regulatory elements in the Solanum lycopersicum–Rhizophagus irregularis mycorrhizal symbiosis. *New Phytologist*, *223*(3), 1560-1574.

Mélida, H., Sopeña-Torres, S., Bacete, L., Garrido-Arandia, M., Jordá, L., López, G., ... & Molina, A. (2018). Non-branched β-1, 3-glucan oligosaccharides trigger immune responses in Arabidopsis. *The Plant Journal*, *93*(1), 34-49.

Merckx, V. S. (2013). Mycoheterotrophy: an introduction. In *Mycoheterotrophy* (pp. 1-17). Springer, New York, NY.

Meyer, M., Huttenlocher, F., Cedzich, A., Procopio, S., Stroeder, J., Pau-Roblot, C., ... & Schaller, A. (2016). The subtilisin-like protease SBT3 contributes to insect resistance in tomato. *Journal of experimental botany*, *67*(14), 4325-4338.

Mi, H., Muruganujan, A., Ebert, D., Huang, X., & Thomas, P. D. (2019). PANTHER version 14: more genomes, a new PANTHER GO-slim and improvements in enrichment analysis tools. *Nucleic acids research*, *47*(D1), D419-D426.

Miura, C., Yamaguchi, K., Miyahara, R., Yamamoto, T., Fuji, M., Yagame, T., ... & Kaminaka, H. (2018). The mycoheterotrophic symbiosis between orchids and mycorrhizal fungi possesses major components shared with mutualistic plant-mycorrhizal symbioses. *Molecular Plant-Microbe Interactions*, *31*(10), 1032-1047.

Miyao, A., Tanaka, K., Murata, K., Sawaki, H., Takeda, S., Abe, K., ... & Hirochika, H. (2003). Target site specificity of the Tos17 retrotransposon shows a preference for insertion within genes and against insertion in retrotransposon-rich regions of the genome. *The Plant Cell*, *15*(8), 1771-1780.

Montero, H., Choi, J., & Paszkowski, U. (2019). Arbuscular mycorrhizal phenotyping: the dos and don'ts. *The New phytologist*, *221*(3), 1182.

Morin, E., Miyauchi, S., San Clemente, H., Chen, E. C., Pelin, A., de la Providencia, I., ... & Kuo, A. (2019). Comparative genomics of Rhizophagus irregularis, R. cerebriforme, R. diaphanus and Gigaspora rosea highlights specific genetic features in Glomeromycotina. *New Phytologist*, *222*(3), 1584-1598.

Müller, L. M., Flokova, K., Schnabel, E., Sun, X., Fei, Z., Frugoli, J., ... & Harrison, M. J. (2019). A CLE–SUNN module regulates strigolactone content and fungal colonization in arbuscular mycorrhiza. *Nature plants*, *5*(9), 933-939.

Nadal, M., & Paszkowski, U. (2013). Polyphony in the rhizosphere: presymbiotic communication in arbuscular mycorrhizal symbiosis. *Current opinion in plant biology*, *16*(4), 473-479.

Nadal, M., Sawers, R., Naseem, S., Bassin, B., Kulicke, C., Sharman, A., ... & Paszkowski, U. (2017). An N-acetylglucosamine transporter required for arbuscular mycorrhizal symbioses in rice and maize. *Nature plants*, *3*(6), 17073.

Nagahashi, G., & Douds Jr, D. D. (2011). The effects of hydroxy fatty acids on the hyphal branching of germinated spores of AM fungi. *Fungal biology*, *115*(4-5), 351-358.

Nolen, B., Taylor, S., & Ghosh, G. (2004). Regulation of protein kinases: controlling activity through activation segment conformation. *Molecular cell*, *15*(5), 661-675.

Ohsaki, Y., Shinohara, Y., Suzuki, M., & Fujimoto, T. (2010). A pitfall in using BODIPY dyes to label lipid droplets for fluorescence microscopy. *Histochemistry and cell biology*, *133*(4), 477-480.

Op den Camp, R. O., Streng, A., De Mita, S., Cao, Q., Polone, E., Liu, W., ... & Bisseling, T. (2011). LysM-type mycorrhizal receptor recruited for rhizobium symbiosis in nonlegume Parasponia. *Science*, *331*(6019), 909-912.

Pandey, B. K., Mehra, P., Verma, L., Bhadouria, J., & Giri, J. (2017). OsHAD1, a haloacid dehalogenase-like apase, enhances phosphate accumulation. *Plant physiology*, *174*(4), 2316-2332.

Pandey, D. M., & Kim, S. R. (2012). Identification and expression analysis of hypoxia stress inducible CCCH-type zinc finger protein genes in rice. *Journal of Plant Biology*, *55*(6), 489-497.

Park, H. J., Floss, D. S., Levesque-Tremblay, V., Bravo, A., & Harrison, M. J. (2015). Hyphal branching during arbuscule development requires Reduced Arbuscular Mycorrhiza1. *Plant Physiology*, *169*(4), 2774-2788.

Parniske, M. (2008). Arbuscular mycorrhiza: the mother of plant root endosymbioses. *Nature Reviews Microbiology*, *6*(10), 763-775.

Passardi, F., Longet, D., Penel, C., & Dunand, C. (2004). The class III peroxidase multigenic family in rice and its evolution in land plants. *Phytochemistry*, *65*(13), 1879-1893.

Paszkowski, U., Kroken, S., Roux, C., & Briggs, S. P. (2002). Rice phosphate transporters include an evolutionarily divergent gene specifically activated in arbuscular mycorrhizal symbiosis. *Proceedings of the National Academy of Sciences*, *99*(20), 13324-13329.

Philippe, R., Courtois, B., McNally, K. L., Mournet, P., El-Malki, R., Le Paslier, M. C., ... & This, D. (2010). Structure, allelic diversity and selection of Asr genes, candidate for drought tolerance, in Oryza sativa L. and wild relatives. *Theoretical and applied genetics*, *121*(4), 769-787.

Pierleoni, A., Martelli, P. L., & Casadio, R. (2008). PredGPI: a GPI-anchor predictor. *BMC bioinformatics*, *9*(1), 392.

Pimprikar, P., Carbonnel, S., Paries, M., Katzer, K., Klingl, V., Bohmer, M. J., ... & Gutjahr, C. (2016). A CCaMK-CYCLOPS-DELLA complex activates transcription of RAM1 to regulate arbuscule branching. *Current Biology*, *26*(8), 987-998.

Pimprikar, P., & Gutjahr, C. (2018). Transcriptional regulation of arbuscular mycorrhiza development. *Plant and Cell Physiology*, *59*(4), 678-695.

Plassard, C., Becquer, A., & Garcia, K. (2019). Phosphorus Transport in Mycorrhiza: How Far Are We?. *Trends in plant science*.

Pucker, B., & Brockington, S. F. (2018). Genome-wide analyses supported by RNA-Seq reveal non-canonical splice sites in plant genomes. *BMC genomics*, *19*(1), 980.

Pumplin, N., & Harrison, M. J. (2009). Live-cell imaging reveals periarbuscular membrane domains and organelle location in Medicago truncatula roots during arbuscular mycorrhizal symbiosis. *Plant physiology*, *151*(2), 809-819.

Pumplin, N., Zhang, X., Noar, R. D., & Harrison, M. J. (2012). Polar localization of a symbiosis-specific phosphate transporter is mediated by a transient reorientation of secretion. *Proceedings of the National Academy of Sciences*, *109*(11), E665-E672.

Quinet, M., Ndayiragije, A., Lefevre, I., Lambillotte, B., Dupont-Gillain, C. C., & Lutts, S. (2010). Putrescine differently influences the effect of salt stress on polyamine metabolism and ethylene synthesis in rice cultivars differing in salt resistance. *Journal of Experimental Botany*, *61*(10), 2719-2733.

Radhakrishnan, G. V., Keller, J., Rich, M. K., Vernié, T., Mbadinga, D. L. M., Vigneron, N., ... & Delaux, P. M. (2020). An ancestral signalling pathway is conserved in intracellular symbioses-forming plant lineages. *Nature Plants*, 1-10.

Ramanathan, V., Rahman, H., Subramanian, S., Nallathambi, J., Kaliyaperumal, A., Manickam, S., ... & Muthurajan, R. (2018). OsARD4 encoding an acireductone dioxygenase improves root architecture in rice by promoting development of secondary roots. *Scientific reports*, *8*(1), 1-15.

Ribeiro, A., Akkermans, A. D., van Kammen, A., Bisseling, T., & Pawlowski, K. (1995). A nodule-specific gene encoding a subtilisin-like protease is expressed in early stages of actinorhizal nodule development. *The Plant Cell*, *7*(6), 785-794.

Rich, M. K., Schorderet, M., & Reinhardt, D. (2014). The role of the cell wall compartment in mutualistic symbioses of plants. *Frontiers in Plant Science*, *5*, 238.

Rich, M. K., Schorderet, M., Bapaume, L., Falquet, L., Morel, P., Vandenbussche, M., & Reinhardt, D. (2015). The petunia GRAS transcription factor ATA/RAM1 regulates symbiotic gene expression and fungal morphogenesis in arbuscular mycorrhiza. *Plant physiology*, *168*(3), 788-797.

Rich, M. K., Courty, P. E., Roux, C., & Reinhardt, D. (2017a). Role of the GRAS transcription factor ATA/RAM1 in the transcriptional reprogramming of arbuscular mycorrhiza in Petunia hybrida. *BMC genomics*, *18*(1), 589.

Rich, M. K., Nouri, E., Courty, P. E., & Reinhardt, D. (2017b). Diet of arbuscular mycorrhizal fungi: bread and butter?. *Trends in Plant Science*, *22*(8), 652-660.

Remy, W., Taylor, T. N., Hass, H., & Kerp, H. (1994). Four hundred-million-year-old vesicular arbuscular mycorrhizae. *Proceedings of the National Academy of Sciences*, *91*(25), 11841-11843.

Ren, H., Gu, G., Longa, J., Yin, Q., Wu, T., Song, T., ... & Dong, H. (2006). Combinative effects of a bacterial type-III effector and a biocontrol bacterium on rice growth and disease resistance. *Journal of biosciences*, *31*(5), 617-627.

Rensing, S. A. (2018). Great moments in evolution: the conquest of land by plants. *Current opinion in plant biology*, *42*, 49-54.

Ried, M. K., Antolín-Llovera, M., & Parniske, M. (2014). Spontaneous symbiotic reprogramming of plant roots triggered by receptor-like kinases. *Elife*, *3*, e03891.

Rillig, M. C., Wright, S. F., Nichols, K. A., Schmidt, W. F., & Torn, M. S. (2001). Large contribution of arbuscular mycorrhizal fungi to soil carbon pools in tropical forest soils. *Plant and Soil*, *233*(2), 167-177.

Robinson, M. D., McCarthy, D. J., & Smyth, G. K. (2010). edgeR: a Bioconductor package for differential expression analysis of digital gene expression data. *Bioinformatics*, *26*(1), 139-140.

Roth, R., & Paszkowski, U. (2017). Plant carbon nourishment of arbuscular mycorrhizal fungi. *Current opinion in plant biology*, *39*, 50-56.

Roth, R., Chiapello, M., Montero, H., Gehrig, P., Grossmann, J., O'Holleran, K., ... & Paszkowski, U. (2018). A rice Serine/Threonine receptor-like kinase regulates arbuscular mycorrhizal symbiosis at the peri-arbuscular membrane. *Nature communications*, *9*(1), 1-12.

Roth, R., Hillmer, S., Funaya, C., Chiapello, M., Schumacher, K., Presti, L. L., ... & Paszkowski, U. (2019). Arbuscular cell invasion coincides with extracellular vesicles and membrane tubules. *Nature plants*, *5*(2), 204-211.

Russo, G., Carotenuto, G., Fiorilli, V., Volpe, V., Faccio, A., Bonfante, P., ... & Genre, A. (2019). TPLATE recruitment reveals endocytic dynamics at sites of symbiotic interface assembly in arbuscular mycorrhizal interactions. *Frontiers in Plant Science*, *10*, 1628.

Rzewuski, G., & Sauter, M. (2008). Ethylene biosynthesis and signaling in rice. Plant science, 175(1-2), 32-42.

Saito, K., Yoshikawa, M., Yano, K., Miwa, H., Uchida, H., Asamizu, E., ... & Kouchi, H. (2007). NUCLEOPORIN85 is required for calcium spiking, fungal and bacterial symbioses, and seed production in Lotus japonicus. *The Plant Cell*, *19*(2), 610-624.

Sakamoto, K., Tada, Y., Yokozeki, Y., Akagi, H., Hayashi, N., Fujimura, T., & Ichikawa, N. (1999). Chemical induction of disease resistance in rice is correlated with the expression of a gene encoding a nucleotide binding site and leucine-rich repeats. *Plant molecular biology*, *40*(5), 847-855.

Schaller, A., Stintzi, A., Rivas, S., Serrano, I., Chichkova, N. V., Vartapetian, A. B., ... & Ramírez, V. (2018). From structure to function–a family portrait of plant subtilases. *New Phytologist*, *218*(3), 901-915.

Schindelin, J., Arganda-Carreras, I., Frise, E., Kaynig, V., Longair, M., Pietzsch, T., ... & Tinevez, J. Y. (2012). Fiji: an open-source platform for biological-image analysis. Nature methods, 9(7), 676-682.

Schmidt, R., Schippers, J. H., Mieulet, D., Watanabe, M., Hoefgen, R., Guiderdoni, E., & Mueller-Roeber, B. (2014). SALT-RESPONSIVE ERF1 is a negative regulator of grain filling and gibberellin-mediated seedling establishment in rice. *Molecular plant*, *7*(2), 404-421.

Shim, K. C., Kim, S. H., Lee, H. S., Adeva, C., Jeon, Y. A., Luong, N. H., ... & Ahn, S. N. (2020). Characterization of a New qLTG3–1 Allele for Low-temperature Germinability in Rice from the Wild Species Oryza rufipogon. *Rice*, *13*(1), 10.

Simard, S. W., Beiler, K. J., Bingham, M. A., Deslippe, J. R., Philip, L. J., & Teste, F. P. (2012). Mycorrhizal networks: mechanisms, ecology and modelling. *Fungal Biology Reviews*, *26*(1), 39-60.

Singh, S., Katzer, K., Lambert, J., Cerri, M., & Parniske, M. (2014). CYCLOPS, a DNA-binding transcriptional activator, orchestrates symbiotic root nodule development. *Cell host & microbe*, *15*(2), 139-152.

Smith, S. E., & Read, D. J. (2008). *Mycorrhizal symbiosis*. Academic press.

Sobajima, H., Tani, T., Chujo, T., Okada, K., Suzuki, K., Mori, S., ... & Yamane, H. (2007). Identification of a jasmonic acid-responsive region in the promoter of the rice 12-oxophytodienoic acid reductase 1 gene OsOPR1. *Bioscience, biotechnology, and biochemistry*, 0711020634-0711020634.

Song, Y., Jing, S., & Yu, D. (2009). Overexpression of the stress-induced OsWRKY08 improves osmotic stress tolerance in Arabidopsis. *Chinese Science Bulletin*, *54*(24), 4671-4678.

Soudzilovskaia, N. A., Vaessen, S., Barcelo, M., He, J., Rahimlou, S., Abarenkov, K., ... & Tedersoo, L. (2020). FungalRoot: global online database of plant mycorrhizal associations. *bioRxiv*, 717488.

Stracke, S., Kistner, C., Yoshida, S., Mulder, L., Sato, S., Kaneko, T., ... & Parniske, M. (2002). A plant receptor-like kinase required for both bacterial and fungal symbiosis. *Nature*, *417*(6892), 959-962.

Strullu-Derrien, C., Rioult, J. P., & Strullu, D. G. (2009). Mycorrhizas in Upper Carboniferous Radiculites-type cordaitalean rootlets. *The New Phytologist*, *182*(3), 561-564.

Strullu-Derrien, C., Kenrick, P., Pressel, S., Duckett, J. G., Rioult, J. P., & Strullu, D. G. (2014). Fungal associations in Horneophyton ligneri from the Rhynie Chert (c. 407 million year old) closely resemble those in extant lower land plants: novel insights into ancestral plant–fungus symbioses. *New Phytologist*, *203*(3), 964-979.

Strullu-Derrien, C., Selosse, M. A., Kenrick, P., & Martin, F. M. (2018). The origin and evolution of mycorrhizal symbioses: from palaeomycology to phylogenomics. *New Phytologist*, *220*(4), 1012-1030.

Sun, J., Miller, J. B., Granqvist, E., Wiley-Kalil, A., Gobbato, E., Maillet, F., ... & Morris, R. J. (2015). Activation of symbiosis signaling by arbuscular mycorrhizal fungi in legumes and rice. *The Plant Cell*, *27*(3), 823-838.

Suzaki, T., Ohneda, M., Toriba, T., Yoshida, A., & Hirano, H. Y. (2009). FON2 SPARE1 redundantly regulates floral meristem maintenance with FLORAL ORGAN NUMBER2 in rice. *PLoS genetics*, *5*(10).

Suzaki, T., Takeda, N., Nishida, H., Hoshino, M., Ito, M., Misawa, F., ... & Kawaguchi, M. (2019). LACK OF SYMBIONT ACCOMMODATION controls intracellular symbiont accommodation in root nodule and arbuscular mycorrhizal symbiosis in Lotus japonicus. *PLoS genetics*, *15*(1).

Svistoonoff, S., Laplaze, L., Auguy, F., Runions, J., Duponnois, R., Haseloff, J., ... & Bogusz, D. (2003). cg12 expression is specifically linked to infection of root hairs and cortical cells during Casuarina glauca and Allocasuarina verticillata actinorhizal nodule development. *Molecular plant-microbe interactions*, *16*(7), 600-607.

Takahashi, T., Mu, J. H., Gasch, A., & Chua, N. H. (1998). Identification by PCR of receptor-like protein kinases from Arabidopsis flowers. *Plant molecular biology*, *37*(4), 587-596.

Takeda, N., Sato, S., Asamizu, E., Tabata, S., & Parniske, M. (2009). Apoplastic plant subtilases support arbuscular mycorrhiza development in Lotus japonicus. *The Plant Journal*, *58*(5), 766-777.

Takeda, N., Tsuzuki, S., Suzaki, T., Parniske, M., & Kawaguchi, M. (2013). CERBERUS and NSP1 of Lotus japonicus are common symbiosis genes that modulate arbuscular mycorrhiza development. *Plant and cell physiology*, *54*(10), 1711-1723.

Tamura, Y., Kobae, Y., Mizuno, T., & Hata, S. (2012). Identification and expression analysis of arbuscular mycorrhiza-inducible phosphate transporter genes of soybean. *Bioscience, biotechnology, and biochemistry*, *76*(2), 309-313.

Taylor, A., & Qiu, Y. L. (2017). Evolutionary history of subtilases in land plants and their involvement in symbiotic interactions. *Molecular Plant-Microbe Interactions*, *30*(6), 489-501.

Taylor, S. S., & Kornev, A. P. (2011). Protein kinases: evolution of dynamic regulatory proteins. *Trends in biochemical sciences*, *36*(2), 65-77.

Taylor, W. R. (1997). Residual colours: a proposal for aminochromography. *Protein engineering*, *10*(7), 743-746.

Tian, L., Dai, L. L., Yin, Z. J., Fukuda, M., Kumamaru, T., Dong, X. B., ... & Qu, L. Q. (2013). Small GTPase Sar1 is crucial for proglutelin and α-globulin export from the endoplasmic reticulum in rice endosperm. *Journal of experimental botany*, *64*(10), 2831-2845.

Tsuzuki, S., Handa, Y., Takeda, N., & Kawaguchi, M. (2016). Strigolactone-induced putative secreted protein 1 is required for the establishment of symbiosis by the arbuscular mycorrhizal fungus Rhizophagus irregularis. *Molecular Plant-Microbe Interactions*, *29*(4), 277-286.

Vaattovaara, A., Brandt, B., Rajaraman, S., Safronov, O., Veidenberg, A., Luklová, M., ... & Wrzaczek, M. (2019). Mechanistic insights into the evolution of DUF26-containing proteins in land plants. *Communications biology*, *2*(1), 1-18.

Vallino, M., Fiorilli, V., & Bonfante, P. (2014). Rice flooding negatively impacts root branching and arbuscular mycorrhizal colonization, but not fungal viability. *Plant, Cell & Environment*, *37*(3), 557-572.

Van Der Heijden, M. G., Klironomos, J. N., Ursic, M., Moutoglis, P., Streitwolf-Engel, R., Boller, T., ... & Sanders, I. R. (1998). Mycorrhizal fungal diversity determines plant biodiversity, ecosystem variability and productivity. *Nature*, *396*(6706), 69-72.

Van Zeijl, A., den Camp, R. H. O., Deinum, E. E., Charnikhova, T., Franssen, H., den Camp, H. J. O., ... & Geurts, R. (2015). Rhizobium lipo-chitooligosaccharide signaling triggers accumulation of cytokinins in Medicago truncatula roots. *Molecular plant*, *8*(8), 1213-1226.

Veiga, R. S., Faccio, A., Genre, A., Pieterse, C. M., Bonfante, P., & Van Der Heijden, M. G. (2013). Arbuscular mycorrhizal fungi reduce growth and infect roots of the non-host plant Arabidopsis thaliana. *Plant, Cell & Environment*, *36*(11), 1926-1937.

Vij, S., Giri, J., Dansana, P. K., Kapoor, S., & Tyagi, A. K. (2008). The receptor-like cytoplasmic kinase (OsRLCK) gene family in rice: organization, phylogenetic relationship, and expression during development and stress. *Molecular Plant*, *1*(5), 732-750.

Wang, E., Yu, N., Bano, S. A., Liu, C., Miller, A. J., Cousins, D., ... & Downie, J. A. (2014). A H+-ATPase that energizes nutrient uptake during mycorrhizal symbioses in rice and Medicago truncatula. *The Plant Cell*, *26*(4), 1818-1830.

Wang, J., Guo, X., Li, L., Qiu, H., Zhang, Z., Wang, Y., & Sun, G. (2018). Application of the Fluorescent Dye BODIPY in the Study of Lipid Dynamics of the Rice Blast Fungus Magnaporthe oryzae. *Molecules*, *23*(7), 1594.

Wang, S., Chen, A., Xie, K., Yang, X., Luo, Z., Chen, J., ... & Feng, H. (2020a). Functional analysis of the OsNPF4. 5 nitrate transporter reveals a conserved mycorrhizal pathway of nitrogen acquisition in plants. *Proceedings of the National Academy of Sciences*.

Wang, S., Li, L., Li, H., Sahu, S. K., Wang, H., Xu, Y., ... & Chang, Y. (2020b). Genomes of early-diverging streptophyte algae shed light on plant terrestrialization. *Nature Plants*, *6*(2), 95-106.

Wang, W., Shi, J., Xie, Q., Jiang, Y., Yu, N., & Wang, E. (2017). Nutrient exchange and regulation in arbuscular mycorrhizal symbiosis. *Molecular Plant*, *10*(9), 1147-1158.

Washio, K. (2001). Identification of Dof proteins with implication in the gibberellin-regulated expression of a peptidase gene following the germination of rice grains. *Biochimica et Biophysica Acta (BBA)-Gene Structure and Expression*, *1520*(1), 54-62.

Washio, K. (2003). Functional dissections between GAMYB and Dof transcription factors suggest a role for protein-protein associations in the gibberellin-mediated expression of the RAmy1A gene in the rice aleurone. *Plant physiology*, *133*(2), 850-863.

Waterhouse, A. M., Procter, J. B., Martin, D. M., Clamp, M., & Barton, G. J. (2009). Jalview Version 2—a multiple sequence alignment editor and analysis workbench. *Bioinformatics*, *25*(9), 1189-1191.

Weber, E., Engler, C., Gruetzner, R., Werner, S., & Marillonnet, S. (2011). A modular cloning system for standardized assembly of multigene constructs. *PloS one*, *6*(2).

Wewer, V., Brands, M., & Dörmann, P. (2014). Fatty acid synthesis and lipid metabolism in the obligate biotrophic fungus R hizophagus irregularis during mycorrhization of Lotus japonicus. *The Plant Journal*, *79*(3), 398-412.

Whiteside, M. D., Werner, G. D., Caldas, V. E., van't Padje, A., Dupin, S. E., Elbers, B., ... & Postma, M. (2019). Mycorrhizal fungi respond to resource inequality by moving phosphorus from rich to poor patches across networks. *Current Biology*, *29*(12), 2043-2050.

Wu, M., Ren, Y., Cai, M., Wang, Y., Zhu, S., Zhu, J., ... & Zhang, H. (2019). Rice FLOURY ENDOSPERM 10 encodes a pentatricopeptide repeat protein that is essential for the trans-splicing of mitochondrial nad1 intron 1 and endosperm development. *New Phytologist*, *223*(2), 736-750.

Wu, F., Chi, Y., Jiang, Z., Xu, Y., Xie, L., Huang, F., ... & Zhang, Y. (2020). Hydrogen peroxide sensor HPCA1 is an LRR receptor kinase in Arabidopsis. *Nature*, 1-5.

Xiang, J. J., Zhang, G. H., Qian, Q., & Xue, H. W. (2012). Semi-rolled leaf1 encodes a putative glycosylphosphatidylinositol-anchored protein and modulates rice leaf rolling by regulating the formation of bulliform cells. *Plant physiology*, *159*(4), 1488-1500.

Xie, X., Huang, W., Liu, F., Tang, N., Liu, Y., Lin, H., & Zhao, B. (2013). Functional analysis of the novel mycorrhiza-specific phosphate transporter AsPT1 and PHT1 family from Astragalus sinicus during the arbuscular mycorrhizal symbiosis. *New Phytologist*, *198*(3), 836-852.

Xue, L., Cui, H., Buer, B., Vijayakumar, V., Delaux, P. M., Junkermann, S., & Bucher, M. (2015). Network of GRAS transcription factors involved in the control of arbuscule development in Lotus japonicus. *Plant Physiology*, *167*(3), 854-871.

Xue, L., Klinnawee, L., Zhou, Y., Saridis, G., Vijayakumar, V., Brands, M., ... & Bucher, M. (2018). AP2 transcription factor CBX1 with a specific function in symbiotic exchange of nutrients in mycorrhizal Lotus japonicus. *Proceedings of the National Academy of Sciences*, *115*(39), E9239-E9246.

Yamamoto, M. P., Onodera, Y., Touno, S. M., & Takaiwa, F. (2006). Synergism between RPBF Dof and RISBZ1 bZIP activators in the regulation of rice seed expression genes. *Plant Physiology*, *141*(4), 1694-1707.

Yamamoto, Y., Kamiya, N., Morinaka, Y., Matsuoka, M., & Sazuka, T. (2007). Auxin biosynthesis by the YUCCA genes in rice. *Plant physiology*, *143*(3), 1362-1371.

Yamaya, T., & Kusano, M. (2014). Evidence supporting distinct functions of three cytosolic glutamine synthetases and two NADH-glutamate synthases in rice. *Journal of Experimental Botany, 65*(19), 5519-5525.

Yang, S. Y., & Paszkowski, U. (2011). Phosphate import at the arbuscule: just a nutrient?. *Molecular plant-microbe interactions*, *24*(11), 1296-1299.

Yang, S. Y., Grønlund, M., Jakobsen, I., Grotemeyer, M. S., Rentsch, D., Miyao, A., ... & Paszkowski, U. (2012). Nonredundant regulation of rice arbuscular mycorrhizal symbiosis by two members of the PHOSPHATE TRANSPORTER1 gene family. *The Plant Cell*, *24*(10), 4236-4251.

Yang, X., Sun, W., Liu, J. P., Liu, Y. J., & Zeng, Q. Y. (2009). Biochemical and physiological characterization of a tau class glutathione transferase from rice (Oryza sativa). *Plant Physiology and Biochemistry*, *47*(11-12), 1061-1068.

Yano, K., Yoshida, S., Müller, J., Singh, S., Banba, M., Vickers, K., ... & Asamizu, E. (2008). CYCLOPS, a mediator of symbiotic intracellular accommodation. *Proceedings of the National Academy of Sciences*, *105*(51), 20540-20545.

Yao, W., Li, G., Yu, Y., & Ouyang, Y. (2018). funRiceGenes dataset for comprehensive understanding and application of rice functional genes. *Gigascience*, *7*(1), gix119.

Ye, Y., Yuan, J., Chang, X., Yang, M., Zhang, L., Lu, K., & Lian, X. (2015). The phosphate transporter gene OsPht1; 4 is involved in phosphate homeostasis in rice. PLoS One, 10(5).

Ye, Y., Li, P., Xu, T., Zeng, L., Cheng, D., Yang, M., ... & Lian, X. (2017). OsPT4 contributes to arsenate uptake and transport in rice. *Frontiers in plant science*, *8*, 2197.

Yokotani, N., Sato, Y., Tanabe, S., Chujo, T., Shimizu, T., Okada, K., ... & Kaku, H. (2013). WRKY76 is a rice transcriptional repressor playing opposite roles in blast disease resistance and cold stress tolerance. *Journal of experimental botany*, *64*(16), 5085-5097.

Yoneyama, K., Xie, X., Kusumoto, D., Sekimoto, H., Sugimoto, Y., Takeuchi, Y., & Yoneyama, K. (2007). Nitrogen deficiency as well as phosphorus deficiency in sorghum promotes the production and exudation of 5-deoxystrigol, the host recognition signal for arbuscular mycorrhizal fungi and root parasites. *Planta*, *227*(1), 125-132.

Yu, N., Luo, D., Zhang, X., Liu, J., Wang, W., Jin, Y., ... & Zeng, L. (2014). A DELLA protein complex controls the arbuscular mycorrhizal symbiosis in plants. *Cell research*, *24*(1), 130-133.

Zhang, F., Sun, Y., Pei, W., Jain, A., Sun, R., Cao, Y., ... & Chen, A. (2015). Involvement of OsPht1;4 in phosphate acquisition and mobilization facilitates embryo development in rice. *The Plant Journal*, *82*(4), 556-569.

Zhang, H., Ni, L., Liu, Y., Wang, Y., Zhang, A., Tan, M., & Jiang, M. (2012). The C2H2-type Zinc Finger Protein ZFP182 is involved in abscisic acid-induced antioxidant defense in rice F. *Journal of Integrative Plant Biology*, *54*(7), 500-510.

Zhang, Q., Blaylock, L. A., & Harrison, M. J. (2010). Two Medicago truncatula half-ABC transporters are essential for arbuscule development in arbuscular mycorrhizal symbiosis. *The Plant Cell*, *22*(5), 1483-1497.

Zheng, Y., Jiao, C., Sun, H., Rosli, H. G., Pombo, M. A., Zhang, P., ... & Zhao, P. X. (2016). iTAK: a program for genome-wide prediction and classification of plant transcription factors, transcriptional regulators, and protein kinases. *Molecular plant*, *9*(12), 1667-1670.

Zhou, F., Wang, C. Y., Gutensohn, M., Jiang, L., Zhang, P., Zhang, D., ... & Lu, S. (2017a). A recruiting protein of geranylgeranyl diphosphate synthase controls metabolic flux toward chlorophyll biosynthesis in rice. *Proceedings of the National Academy of Sciences*, *114*(26), 6866-6871.

Zhou, W., Wang, X., Zhou, D., Ouyang, Y., & Yao, J. (2017b). Overexpression of the 16-kD a α-amylase/trypsin inhibitor RAG 2 improves grain yield and quality of rice. *Plant biotechnology journal*, *15*(5), 568-580.

Zipfel, C., & Oldroyd, G. E. (2017). Plant signalling in symbiosis and immunity. *Nature*, *543*(7645), 328-336.